



HAL
open science

Enhancing the roll stability of heavy vehicles by using an active anti-roll bar system

van Tan Vu

► **To cite this version:**

van Tan Vu. Enhancing the roll stability of heavy vehicles by using an active anti-roll bar system. Automatic. Communauté Université Grenoble Alpes, 2017. English. NNT: . tel-01628011v1

HAL Id: tel-01628011

<https://hal.science/tel-01628011v1>

Submitted on 2 Nov 2017 (v1), last revised 9 Mar 2018 (v2)

HAL is a multi-disciplinary open access archive for the deposit and dissemination of scientific research documents, whether they are published or not. The documents may come from teaching and research institutions in France or abroad, or from public or private research centers.

L'archive ouverte pluridisciplinaire **HAL**, est destinée au dépôt et à la diffusion de documents scientifiques de niveau recherche, publiés ou non, émanant des établissements d'enseignement et de recherche français ou étrangers, des laboratoires publics ou privés.

THÈSE

pour obtenir le grade de

**DOCTEUR DE LA COMMUNAUTE
UNIVERSITE GRENOBLE ALPES**

Spécialité : **Automatique-Productique**

Arrêté ministériel : 7 août 2006

Présentée par **Van Tan VU**

Thèse dirigée par **Olivier SENAME** et
codirigée par **Luc DUGARD**

préparée au sein du **GIPSA-Lab**
dans **Electronique, Electrotechnique, Automatique,**
Traitement du Signal (EEATS)

Enhancing the roll stability of heavy vehicles by using an active anti-roll bar system

Thèse soutenue publiquement le **26 Octobre 2017**,
devant le jury composé de:

M. Xavier MOREAU

Professeur, Université de Bordeaux, Président

M. Didier REMOND

Professeur, INSA de Lyon, Rapporteur

M. Thierry Marie GUERRA

Professeur, Université de Valenciennes et du Hainaut-Cambrésis,
Rapporteur

M. Peter GÁSPÁR

Directeur de Recherche, Académie des Sciences, Hongrie, Examineur

M. Olivier SENAME

Professeur, Grenoble INP, Directeur de thèse

M. Luc DUGARD

Directeur de recherche, CNRS Grenoble, Co-Directeur de thèse



*Dedicated to my wife Thi Lan Anh HOANG
and our daughters Hoang Lan VU, Hoang Yen VU,
with all my love.*

Acknowledgements

I would like to thank my supervisors, Professors Olivier SENAME and Luc DUGARD, for their scientific understanding and for their precious support during my PhD studies. I have been so lucky to work with them, they have been always available and have provided me with the best conditions for me to carry out my research. I have also learnt a lot from them concerning working relationships between students and Professors as well as the balance and harmony between research and real life, I look forward to continuing our collaboration in the future.

This research has been made possible by the financial assistance of the Ministry of Education and Training of Vietnam; for that, I am very grateful. Additionally, I would like to thank my colleagues in the Department of automotive mechanical engineering at the University of Transport and Communications in Vietnam, especially Professors Manh Hung DAO and Van Bang NGUYEN. They helped me a lot in preparing for my PhD studies, and I am looking forward to continue working with them, once I have completed by studies, to develop the Department of automotive mechanical engineering.

I would like to thank Professor Xavier MOREAU for being the president of my doctoral committee; Professor Didier RÉMOND and Professor Thierry Marie GUERRA for their time to review my PhD thesis.

I would also like to thank Professor Peter GÁSPÁR for his suggestions on my topic, participating in my doctoral committee and, especially, allowing me to join his research team at Budapest University of Economics and Technology and the Hungarian Academy of Sciences in November 2016. There, under his supervision, I had the chance to exchange my scientific knowledge with Professor Szabó Zoltán, Dr. Balázs Németh and Mr. András Mihály, thank you all very much.

I would like to thank Mr Tony, Mr Mike, Mr Edmond for helping me learn English. Thank you for your enthusiasm and patience over the whole period of my studies. In particular, I am very grateful to Mr Tony, who has spent a considerable amount of time to help me consolidate my English.

I have spent many happy and unforgettable moments with my dear friends in GIPSA-Lab: Quan, Trung, Tri, Canh, Linh, Phong, Kazusa, Donatien, Rachid, Bojan, Nassim, Lara... Without your companionship, my three years of studies must have been so boring and difficult. I am also grateful to Marielle, Patricia, Gabriel... and all members of the staff of GIPSA-Lab. Without them, my work might have not run smoothly.

I must offer a big thank you to my parents, my parents-in-law, my brother and other members of my family. They have over many years supported and encouraged me so much on the long road of my studies.

Finally, I can not forget to thank my wife and daughters, for their patience and understanding during this endeavour. They have provided me with comfort, solace, and endless love during both challenging and exciting times.

Sincerely,

Van Tan Vu

Contents

Acknowledgements	iii
Résumé des contributions (in French)	xv
Table of Acronyms	xliii
Thesis framework and Publications	1
0.1 Thesis framework	1
0.2 General introduction and problem statement of the thesis	2
0.3 Structure of the thesis	2
0.3.1 Part I: Thesis background and preliminary results	3
0.3.2 Part II: Active anti-roll bar control: LTI approach	3
0.3.3 Part III: Active anti-roll bar control: LPV approach	4
0.3.4 Part IV: Future direction and general conclusions	4
0.4 Publication list	6
I Thesis background and preliminary results	7
1 Introduction	9
1.1 Rollover of heavy vehicles	9
1.1.1 Different categories of vehicle rollover accidents	10
1.1.2 Primary reasons for vehicle rollover	11
1.2 The mechanics of vehicle rollover	13
1.2.1 Vehicle rollover threshold	13
1.2.2 The simplified roll model	14
1.2.3 Rollover of the rigid vehicle	15

1.2.4	The vehicle with compliant tyres	16
1.2.5	The vehicle with roll-compliant suspension	17
1.3	Review of previous research	20
1.3.1	Different models of heavy vehicles	20
1.3.1.1	The Roll model	21
1.3.1.2	The Yaw-Roll model	21
1.3.2	Control methods for the active anti-roll bar system on heavy vehicles . .	21
1.3.2.1	Optimal control	21
1.3.2.2	Neural network control	22
1.3.2.3	Robust control (<i>LPV</i>)	22
1.4	Control objectives	24
1.5	Perspectives	24
1.5.1	Some open research topics and potential extensions:	24
1.5.2	Perspectives "explored" in this thesis:	25
2	Vehicle Modeling	27
2.1	Introduction	27
2.2	An electronic servo-valve hydraulic actuator model	29
2.2.1	The electronic servo-valve model	29
2.2.2	The hydraulic cylinder model	32
2.3	The Yaw-Roll model of a single unit heavy vehicle	34
2.4	The integrated model of a single unit heavy vehicle	37
2.4.1	The fully integrated model	37
2.4.2	The control-oriented integrated model	39
2.4.3	The variables of interest	41
2.5	The design of a passive anti-roll bar system	42

2.5.1	The design of the passive anti-roll bar by using the <i>SAE</i> spring design manual	42
2.5.2	The effectiveness of the passive anti-roll bar on vehicle roll stability . . .	44
2.5.2.1	The effectiveness of the passive anti-roll bar in the frequency domain	45
2.5.2.2	The effectiveness of the passive anti-roll bar in the time domain	45
2.6	Conclusion	46
3	Background on control theory and optimization	49
3.1	Introduction	49
3.2	Dynamical systems	50
3.2.1	Nonlinear dynamical systems	50
3.2.2	LTI dynamical systems	51
3.2.3	LPV dynamical systems	52
3.2.3.1	LPV systems	52
3.2.3.2	Stability of the LPV systems	53
3.3	Signal and system norms	54
3.3.1	Signal norms	54
3.3.2	System norms	54
3.4	Robustness analysis of dynamical systems	55
3.5	Linear Quadratic Regulator control	58
3.6	<i>LTI</i> / H_∞ control problem and design	59
3.6.1	H_∞ optimal control problem	59
3.6.2	<i>LTI</i> / H_∞ control design	60
3.7	<i>LPV</i> / H_∞ control problem and design	62
3.7.1	General problem formulation	62
3.7.2	<i>LPV</i> / H_∞ control synthesis	64
3.7.3	Grid-based LPV approach	66

3.7.4	The LPVTools TM toolbox	67
3.8	Multi-objective optimization by using genetic algorithms	68
3.8.1	Multi-criteria optimization and Pareto-optimal solutions	69
3.8.2	Genetic algorithms	70
3.9	Conclusion	72
II Active anti-roll bar control: LTI approach		73
4	Enhancing the roll stability of heavy vehicles by using LQR active anti-roll bar control	77
4.1	Introduction	77
4.2	The active anti-roll bar <i>LQR</i> control	79
4.3	Simulation results analysis	80
4.3.1	Analysis in the frequency domain	80
4.3.1.1	First case: the effect of ρ_2 and ρ_3 on the transfer functions $\frac{R_{f,r}}{\delta_f}$ and $\frac{u_{f,r}}{\delta_f}$	80
4.3.1.2	Second case: the effect of R_{uf} and R_{ur} on the transfer functions $\frac{R_{f,r}}{\delta_f}$ and $\frac{u_{f,r}}{\delta_f}$	82
4.3.2	Analysis in the time domain	83
4.3.2.1	Performance criteria	84
4.3.2.2	Analysis of the roll stability and the ESVH actuator	84
4.4	Analysis of the effect of the forward velocity on the closed-loop system	86
4.4.1	The effect of the forward velocity on vehicle roll stability	86
4.4.2	The effect of the forward velocity on the physical constraints of the ESVH actuator	88
4.4.2.1	The electronic servo-valve: spool valve displacement and input current limitations	88
4.4.2.2	The hydraulic actuator: load flow and force limitations	89
4.5	Analysis of the handling performance	91

4.5.1	Selecting the criteria to evaluate the handling performance	91
4.5.2	The handling performance analysis	91
4.6	Conclusion	93
5	H_∞ robust control for active anti-roll bar system to prevent vehicle rollover	95
5.1	Introduction	95
5.2	H_∞ robust control synthesis to prevent vehicle rollover	97
5.2.1	H_∞ control synthesis for an active anti-roll bar system	97
5.2.2	Simulation results analysis with the nominal value	99
5.2.2.1	Analysis in the frequency domain	99
5.2.2.2	Analysis in the time domain	101
5.3	Optimal selection of the weighting functions for the H_∞ active anti-roll bar control	102
5.3.1	Multi-criteria optimization (MCO) of the active anti-roll bar control	103
5.3.1.1	The MCO for the H_∞ active anti-roll bar control	103
5.3.1.2	Form of the weighting functions for the H_∞ control synthesis	104
5.3.2	Using genetic algorithms for the MCO problem in the H_∞ active anti-roll bar control	105
5.3.2.1	Solving multi-criteria optimization by genetic algorithms	105
5.3.2.2	Optimization results	107
5.3.3	Evaluation of the optimization results	108
5.3.3.1	Evaluation of optimization results in the frequency domain	108
5.3.3.2	Evaluation of the optimization results in the time domain	109
5.4	Robustness analysis in the frequency domain using the μ -tool	112
5.4.1	Robustness analysis configuration	112
5.4.1.1	Robust performance analysis according to the forward velocity	114
5.4.1.2	Robust performance analysis according to the sprung mass	114
5.4.2	Effect of the forward velocity uncertainties on the closed-loop system	115

5.4.2.1	Effect of the forward velocity uncertainties in the frequency domain	115
5.4.2.2	Effect of the forward velocity uncertainties in the time domain	117
5.5	Comparison between the LQR control and the H_∞ control for the active anti-roll bar system	119
5.6	Conclusion	121
6	Validation of the H_∞ active anti-roll bar control by using TruckSim[®] software	123
6.1	Introduction	124
6.2	Performance criteria	126
6.3	Simulation scenario	127
6.4	Validation with the tour bus	128
6.4.1	Parameters of the tour bus (s-s, 4×2)	129
6.4.2	Simulation results in the case of the unloaded tour bus (Circular road test)	130
6.4.3	Simulation results in the case of the fully loaded tour bus (Cornering manoeuvre)	133
6.5	Validation with the LCF truck	136
6.5.1	Parameters of the LCF truck (s-s, 4×2)	136
6.5.2	Simulation results in the case of the unloaded LCF truck (Sine wave steering)	137
6.5.3	Simulation results in the case of the fully loaded LCF truck (Double lane change)	140
6.6	Conclusion	143
III	Active anti-roll bar control: LPV approach	145
7	Multivariable H_∞/LPV control for active anti-roll bar system	147
7.1	Introduction	147
7.2	An LPV control-oriented model of a single unit heavy vehicle	148

7.3	Formulation of the H_∞/LPV control problem	150
7.3.1	Performance criteria	150
7.3.2	Performance specifications for the H_∞/LPV control design	150
7.3.3	The LPV generalized plant	151
7.4	Grid-based LPV approach for the active anti-roll bar system	152
7.5	Simulation results analysis	153
7.5.1	Analysis in the frequency domain	153
7.5.1.1	The 1 st case: $\rho_1 = v = [40km/h, 130km/h]$ (10 grid points) . .	154
7.5.1.2	The 2 nd case: $\rho_{2,3} = [0, 1]$ (5 grid points)	155
7.5.2	Analysis in the time domain	155
7.6	Validation of the H_∞/LPV active anti-roll bar control by using the TruckSim [®] simulation software	157
7.6.1	Validation with the tour bus (double lane change)	158
7.6.2	Validation with the LCF truck (sine wave steering)	160
7.7	Conclusion	162
8	Effect of oil leakage inside the servo-valve on the performance of an active anti-roll bar system	163
8.1	Introduction	163
8.2	Internal leakage inside the electronic servo-valve	165
8.3	An LPV fully integrated model of a single unit heavy vehicle	167
8.4	Effect of the internal leakage inside the electronic servo-valve on the open-loop system	168
8.4.1	Neutral position of the spool valve	168
8.4.2	Effect of the internal leakage on the open-loop system	170
8.4.2.1	Effect of the internal leakage inside the servo-valve in the fre- quency domain	170
8.4.2.2	Effect of the internal leakage inside the servo-valve in the time domain	171

8.5	Effect of the internal leakage inside the electronic servo-valve on the closed-loop system	174
8.5.1	H_∞/LPV control design for the fully integrated model	174
8.5.2	Simulation results analysis with the nominal value of the total flow pressure coefficient	176
8.5.2.1	Analysis in the frequency domain	176
8.5.2.2	Analysis in the time domain	178
8.5.3	Effect of the internal leakage on the performance of the H_∞/LPV active anti-roll bar control system	181
8.5.3.1	Analysis in the frequency domain	182
8.5.3.2	Analysis in the time domain	183
8.6	Conclusion	185
IV	Future direction and General conclusions	187
9	Future direction to prevent vehicle rollover by using active braking system	189
9.1	Introduction	189
9.2	The LPV model of a single unit heavy vehicle using an active braking system	191
9.3	The H_∞/LPV synthesis for an active braking system	193
9.3.1	The H_∞/LPV control design	193
9.3.2	The solution of the H_∞/LPV control problem	194
9.3.3	Simulation results analysis in the frequency domain	194
9.3.3.1	1 st case: the varying parameters $\rho_1 = v$ vary from 40 km/h to 130 km/h and $\rho_2 = 0.8$	194
9.3.3.2	2 nd case: the varying parameters $\rho_2 = [0, 0.8, 1]$ vary and $\rho_1 = v = 80$ km/h	195
9.4	Analysis in the time domain	197
9.4.1	Braking monitor	197
9.4.2	Simulation results analysis in the time domain	199

9.5	Conclusion	202
10	General conclusions and Perspectives	203
10.1	General conclusions	203
10.2	Perspectives	205
A	Matrices of the fully integrated model	207
B	Characteristics of the ESVH actuators in the fully integrated model	209
C	Matrices of the control-oriented integrated model	213
D	Matrices \mathcal{Q}, \mathcal{R} of the performance index J	215

Résumé des contributions (in French)

Ce texte synthétise les résultats d'un travail de thèse d'une durée de trois années (de janvier 2015 à octobre 2017) effectué dans l'équipe SLR (Systèmes Linéaires et Robustesse) du Département Contrôle des Systèmes au GIPSA-Lab. Le sujet porte sur le renforcement de la stabilité vis-à-vis du roulis des poids lourds par l'usage d'un système de barres anti-roulis actif. Cette thèse a été effectuée sous la direction de M. Olivier SENAME (Professeur à Grenoble INP) et de M. Luc DUGARD (Directeur de Recherche au CNRS). Ce travail a été soutenu par le projet 911 du Ministère de l'Éducation et de la Formation du Vietnam.

Cette thèse se concentre principalement sur le système de barres anti-roulis actif en cherchant à améliorer la stabilité des poids lourds vis-à-vis du roulis. C'est la première étude sur le phénomène de déséquilibre vis-à-vis du roulis des poids lourds dans l'équipe SLR. Cependant, certains apports de la théorie du contrôle et de la génération d'algorithmes mentionnés dans cette thèse sont basés sur de précédentes thèses effectuées dans la même équipe SLR, comme [Poussot-Vassal 2008], [Aubouet 2010], [Do 2011], [Nwesaty 2015], [Nguyen 2016].

Cette thèse est également proche des travaux du Professeur Peter GÁSPÁR et de ses collègues à l'Académie Hongroise des Sciences [Gaspar, Bokor, and Szaszi 2004], [Gaspar, Szabo, and Bokor 2005b]. Dans ces études, les auteurs synthétisent un contrôleur LPV pour le système de barres anti-roulis actif et le système de freinage actif, basés sur le modèle lacet-roulis d'un poids lourd sans remorque. Le système de barres anti-roulis actif fonctionne continuellement, alors que le système de freinage actif est activé seulement en situation critique de déséquilibre.

Durant les trois années de recherche, j'ai toujours entretenu une collaboration fructueuse avec le Professeur Peter GÁSPÁR et plus particulièrement en novembre 2016, quand j'ai participé effectivement à un travail en commun sur place à l'Université d'Économie et de Technologie de Budapest et à l'Académie Hongroise des Sciences. Là, j'ai utilisé le logiciel TruckSim[®] pour évaluer les méthodes de contrôle proposées pour le système de barres anti-roulis actif. De plus, le Professeur Szabó Zoltán m'a présenté les particularités du système LPV et le Docteur Balázs Németh m'a précisé les conditions d'usage de la boîte à outils LPVToolsTM.

Retournement des poids lourds

Les poids lourds sont définis comme des véhicules de marchandise ayant un poids maximum autorisé (véhicule et charge utile) de plus de 3,5 tonnes et incluent également les camions et les bus. L'utilisation des poids lourds comme moyen de transport est d'une grande importance économique dans la plupart des régions du monde. Aux Etats-Unis par exemple, le secteur du transport commercial par camion emploie près de 10 millions de personnes et génère un revenu annuel de plus de 500 milliards de dollars US. Chaque année, les camions transportent plus de 11 milliards de tonnes de marchandises, dont 60% pour un usage domestique. Les bus

longues distances quant à eux, transportent environ 860 millions de passagers par an, soit plus que par avion et par train.

Nous devons reconnaître le rôle des poids lourds dans le développement économique. Néanmoins, du fait de leur masse importante, ils peuvent avoir de graves conséquences pour les autres usagers en cas d'accidents. Les accidents impliquant des poids lourds posent des problèmes complexes dans les pays en voie de développement, ainsi que dans les pays développés comme les USA et l'Europe. Le phénomène de retournement est un des accidents les plus dangereux pour ce type de véhicules. Bien que les retournements soient relativement rares, ils peuvent être mortels. La perte de stabilité du roulis en est la cause principale. Selon la NHTSA (Federal National Highway Traffic Safety Administration), 333 000 poids lourds ont été impliqués dans des accidents de la route en 2012. 3 921 personnes ont été tuées dans des cas de retournements et 104 000 blessées (en augmentation de 18% depuis 2011). En 2013, plus de 4500 personnes ont été tuées dans des accidents de la route impliquant des poids lourds en UE, soit près de 18% des victimes de la route. Bien que les véhicules poids lourds ne représentent qu'une faible part du parc automobile européen, ils sont plus souvent impliqués dans les accidents de la route graves, d'où un important besoin de comprendre les caractéristiques physiques et mécaniques de ce type de véhicule. Cette figure montre deux exemples du phénomène de retournement.



(a)



(b)

Retournement d'un camion (a) avec une remorque solidaire, (b) avec plusieurs remorques.

Différentes catégories d'accidents par retournement

Le retournement pose un problème de sécurité majeur, qui peut entraîner d'importantes conséquences financières et environnementales. Ces accidents sont classés en quatre catégories:

- **Évitable** : le conducteur aurait pu éviter l'accident si un équipement d'alerte avait été installé sur le véhicule. Ceci est étroitement lié au concept TTR (Time-To-Rollover). Les études montrent que cela concerne près de 3,3% du total des accidents par retournement.

- **Potentiellement évitable** : ces accidents auraient pu être évités, selon les compétences du conducteur et la fiabilité de l'équipement d'alerte. Ceux-ci représentent 38,4% du total des accidents par retournement.
- **Non-évitable** : quelles que soient les compétences du conducteur ou la fiabilité du système d'alerte, le retournement du véhicule aurait eu lieu. Ce groupe concerne 49,7% du total des accidents par retournement.
- **Cause inconnue** : cette catégorie représente 8,6% du total des accidents par retournement.

Il est généralement difficile pour un conducteur de sentir si le véhicule est effectivement en train de se retourner. Des études ont montré que seulement une minorité des accidents aurait pu être évitée avec un dispositif d'alerte, potentiellement avec un conducteur plus expérimenté, mais la moitié des accidents de retournement peuvent être évités par l'action seule du conducteur. La raison principale de ce type d'accidents dans lesquels des poids lourds sont impliqués est la perte de stabilité du roulis, quand la force de contact pneu-route d'un côté d'une roue devient nulle. La stabilité du roulis correspond à la capacité du véhicule à supporter des moments de bascule générés durant une prise de virage ou un changement de voie. En effet, les poids lourds ont un centre de masse relativement haut et peuvent perdre la stabilité du roulis malgré de faibles niveaux d'accélération latérale.

Raisons principales d'un retournement de véhicule

Il y a de nombreuses raisons pouvant provoquer un retournement de véhicule ; celles-ci comprennent des facteurs subjectifs tels que la maîtrise du conducteur et la qualité technique du véhicule. Les principales raisons pour un retournement de véhicule sont les suivantes :

- **Mauvaises conditions météorologiques** : des bourrasques de vent latéral sont une des plus évidentes conditions météo pouvant induire un retournement. Des études ont montré que, pour un véhicule avec un centre de gravité haut, la probabilité de retournement augmente. D'autres conditions météorologiques peuvent aussi affecter la surface de la route, telle que la neige, la pluie, le verglas, etc. Toutes ces conditions peuvent contribuer à des retournements car le contact entre le pneu et la surface de la route est réduit.
- **Mancœuvres de freinage brusque** : tout conducteur souhaite avoir un maximum de contrôle sur son véhicule; de ce fait il est très important que le système de freinage fonctionne correctement. Cependant, avec un système de freinage mécanique conventionnel, il y a souvent une force de freinage différente sur chaque roue. Ainsi parfois en cas d'urgence, le système de freinage, en particulier celui des poids lourds, peut entraîner un retournement. Pour contrer les désavantages d'un système de freinage passif, l'ABS (Anti-lock Braking Systems), l'EBS (Electronic Braking Systems) et le correcteur électronique de trajectoire (en anglais ESP ou Electronic Stability Programs) sont utilisés

pour aider à la prévention des retournements, parce qu'ils peuvent ajuster automatiquement les forces de freinage sur chaque roue, donnant un plus grand contrôle du véhicule dans des conditions de conduite difficiles.

- **Contournement d'un obstacle** : lorsqu'un conducteur essaie d'éviter un obstacle sur son chemin, le réflexe est de tourner brutalement, ce qui peut conduire à un retournement du véhicule. Ceci est généralement causé par une sur-réaction par rapport à la situation initiale, ce qui conduit à un phénomène d'oscillations, qui peut augmenter ou diminuer si le véhicule continue en ligne droite ou non. Pour des véhicules avec un haut centre de gravité, comme des bus, les camions-citernes, etc., ce phénomène d'oscillations est souvent répété et amplifié, ce qui augmente le risque de retournement.
- **Erreur du conducteur** : trois-quarts des retournements sont de la responsabilité du conducteur. Dans plus de 90% des cas, le retournement n'est pas le déclencheur, en d'autres termes, d'autres événements dangereux sont survenus avant. Le manque d'attention, la somnolence, la distraction ou la mauvaise évaluation des trajectoires, tout cela peut entraîner une prise de conscience soudaine du danger et donc créer une réaction disproportionnée pour l'éviter. Une conduite attentive peut éviter la plupart des accidents de retournement.
- **Excès de vitesse** : la vitesse du véhicule est toujours l'un des plus importants facteurs dans le phénomène de retournement. La position et la vitesse angulaires du volant, ainsi que la vitesse du véhicule sont les trois facteurs qui influencent grandement la stabilité en roulis des véhicules. Le respect de la vitesse limite maximale autorisée est toujours une priorité absolue et également obligatoire pour tous les conducteurs.



“Jack-knifing” d'un véhicule articulé dérapant.

- **Le “Jack-knifing”** : il s'agit d'un terme commun, dans les accidents impliquant un camion, qui se réfère à une situation dangereuse lorsqu'un véhicule articulé dérape, faisant basculer la remorque d'un côté formant un angle qui ressemble à l'angle formé par la lame d'un canif comme dans la Figure qui précède. La raison principale du dérapage est la défaillance de l'équipement, le blocage des roues dû à un freinage brutal et une mauvaise adhérence en cas de conditions de conduite défavorables. Selon la vitesse du véhicule, le dérapage peut entraîner un retournement du véhicule.

- **La charge** : la majorité des accidents de retournement se produit en raison de facteurs associés à la charge. Cela peut être dû au fait que la charge est insuffisamment sécurisée ou mal rangée. La charge joue un rôle évident : la probabilité de se retourner est deux fois plus importante en cas de surcharge. La variation de charge entraînera un changement de la hauteur du centre de gravité, modifiant ainsi le seuil de retournement.
- **Conception de la route** : la conception de la route peut également contribuer de manière significative au retournement du véhicule. Les ronds-points, les bretelles, les changements de voie et les doubles virages peuvent tous jouer un rôle. Par conséquent, les normes de conception pour les routes et les véhicules doivent assurer une sécurité maximale.
- **Systèmes de suspension** : il existe de nombreux types de systèmes de suspension sur les véhicules. Il est extrêmement important d'adapter les réglages de suspension appropriés aux différentes situations. La probabilité de retournement du véhicule augmente avec un mauvais réglage de la hauteur de caisse, de mauvaises conditions et pressions pour les systèmes de suspension pneumatique, et un défaut de réinitialisation de la soupape de commande de hauteur de caisse après le chargement/déchargement. La suspension contrôlée a été envisagée dans le but d'améliorer la stabilité au roulis du véhicule. Pour les poids lourds, cette approche est limitée par une trop grande consommation d'énergie. Cependant, elle s'est avérée très efficace pour les voitures.

En plus des causes principales énumérées ci-dessus, il y en a beaucoup d'autres qui peuvent mener au retournement du véhicule. Déterminer les causes et proposer des solutions alternatives pour réduire le phénomène de retournement des véhicules sont des tâches extrêmement importantes, mais elles comportent également de nombreuses difficultés. Cela dépend du type de véhicule et de ses conditions de fonctionnement spécifiques. À ce jour, il n'existe pas de solution parfaite.

Motivation et objectifs

Les véhicules automobiles sont maintenant équipés de nombreuses technologies modernes, de sous-systèmes intelligents, dans différents champs de l'ingénierie comme la mécanique, l'électronique, la communication, le contrôle automatique. Ce contexte permet à l'industrie automobile de répondre aux exigences des clients qui souhaitent simultanément des véhicules sûrs et confortables avec une faible consommation de carburant. Cependant, les technologies récentes relatives aux véhicules automobiles sont généralement étudiées et appliquées surtout pour les voitures, beaucoup moins pour les poids lourds. Pourtant, le nombre de poids lourds représente une part significative du nombre total de véhicules utilisés pour le transport et leur rôle dans le développement économique est extrêmement important.

Les poids lourds interviennent souvent dans une large proportion du total des accidents, et les accidents causés par un déséquilibre sont les plus dangereux et les plus sérieux. Par conséquent, il est nécessaire et urgent d'étudier des systèmes d'assistance pour le conducteur de manière

à réduire le phénomène de déséquilibre. Les systèmes de contrôle actifs de la stabilité ont été étudiés pendant environ deux décennies, parmi lesquels le système de freinage actif, le système de suspension actif, le système de direction actif, et le système de barres anti-roulis actif. Parmi ces solutions, le système de barres anti-roulis actif s'est révélé être la solution la plus efficace. En changeant le moment entre le châssis et les masses non suspendues, la stabilité des véhicules vis-à-vis du roulis est améliorée en réponse à différentes sollicitations. Cette thèse se concentre essentiellement sur l'étude des systèmes de barres anti-roulis actifs sur les poids lourds. Les contributions portent principalement sur trois points :

- les actionneurs électroniques à servo-valve hydraulique (ESVH), le modèle intégré inclut ces actionneurs associés au modèle lacet-roulis d'un poids lourd sans remorque ;
- des méthodes avancées de contrôle sont utilisées pour ce système, telles que LQR, le contrôle robuste H_∞ , LPV ;
- la confirmation de l'efficacité du système par l'utilisation du logiciel TruckSim[®].

Le problème à objectifs multiples est toujours considéré comme devant satisfaire simultanément deux objectifs contradictoires : la stabilité transversale et la consommation d'énergie. L'approche par les algorithmes génétiques est aussi utilisée pour optimiser les fonctions de pondération dans la synthèse de la commande H_∞ . L'étude des effets d'une fuite interne dans la servo-valve électronique sur la performance du système de barres anti-roulis actif est aussi détaillée. La partie finale constitue une première étude de la manière dont le système de freinage actif peut être utilisé pour prévenir l'instabilité du véhicule.

Résumé des contributions

Dans cette thèse, les contributions principales seront présentées dans l'ordre suivant :

- **Partie I** : Contexte de la thèse et résultats préliminaires ;
- **Partie II** : Contrôle de barres anti-roulis actif: approche LTI ;
- **Partie III** : Contrôle de barres anti-roulis actif: approche LPV ;
- **Partie IV** : Orientations pour le futur et Conclusions générales.

La première partie apporte quelques idées générales, sur la modélisation de véhicule et sur la théorie du contrôle, qui permettent de faciliter la lecture de la thèse. Cette partie est composée des chapitres suivants :

- **Chapitre 1** : *Introduction*

Le chapitre 1 est une introduction générale portant essentiellement sur le phénomène

d'instabilité d'un véhicule. Les mécanismes de l'instabilité d'un véhicule et une revue des recherches antérieures concernant les systèmes de barres anti-roulis actifs sont aussi présentés. En fin de chapitre, les objectifs de contrôle abordés tout au long de la thèse sont développés.

		Vehicle model (Single unit heavy vehicle)			
		Roll model	Yaw-roll model	Integrated model (ESVH actuators + Yaw-roll)	TruckSim® (ESVH actuators + TruckSim)
Control methods	LQR			+	
	H _c			+	+
	LPV			+	+

Résumé des contributions de thèse sur le système anti-roulis actif.

- **Chapitre 2 : Modélisation du véhicule**

Le chapitre 2 a pour objectif de modéliser l'actionneur ESVH, dont l'entrée de commande est le courant électrique et dont la sortie est la force qui agit sur le châssis. Un modèle intégré est proposé, qui combine le modèle lacet-roulis d'un poids lourd sans remorque avec celui des actionneurs. Ce modèle peut prendre deux formes selon que le système est piloté ou non. Comparativement aux études précédentes, le modèle développé dans ce chapitre apporte une amélioration majeure, en termes de modèle d'actionneur, dans l'étude du système de barres anti-roulis actif pour les poids lourds. Un système de barres anti-roulis passif est également développé sur les bases du manuel SAE pour la synthèse des suspensions.

Les équations différentielles du modèle lacet-roulis d'un véhicule lourd sont les suivantes :

$$\left\{ \begin{array}{l} mv(\dot{\beta} + \dot{\psi}) - m_s h \ddot{\phi} = F_{yf} + F_{yr} \\ -I_{xz} \ddot{\phi} + I_{zz} \ddot{\psi} = F_{yf} l_f - F_{yr} l_r \\ (I_{xx} + m_s h^2) \ddot{\phi} - I_{xz} \ddot{\psi} = m_s g h \phi + m_s v h (\dot{\beta} + \dot{\psi}) - k_f (\phi - \phi_{uf}) \\ \quad - b_f (\dot{\phi} - \dot{\phi}_{uf}) + M_{ARf} + T_f - k_r (\phi - \phi_{ur}) - b_r (\dot{\phi} - \dot{\phi}_{ur}) + M_{ARr} + T_r \\ -r F_{yf} = m_{uf} v (r - h_{uf}) (\dot{\beta} + \dot{\psi}) + m_{uf} g h_{uf} \phi_{uf} - k_{tf} \phi_{uf} \\ \quad + k_f (\phi - \phi_{uf}) + b_f (\dot{\phi} - \dot{\phi}_{uf}) + M_{ARf} + T_f \\ -r F_{yr} = m_{ur} v (r - h_{ur}) (\dot{\beta} + \dot{\psi}) - m_{ur} g h_{ur} \phi_{ur} - k_{tr} \phi_{ur} \\ \quad + k_r (\phi - \phi_{ur}) + b_r (\dot{\phi} - \dot{\phi}_{ur}) + M_{ARr} + T_r \end{array} \right.$$

Les équations dynamiques de l'actionneur ESVH sont résumées comme suit :

$$\begin{cases} F_{act} = A_P \Delta P \\ \frac{V_t}{4\beta_e} \frac{d\Delta P}{dt} + (K_P + C_{tp}) \Delta P - K_x X_v + A_P \frac{dy_a}{dt} = 0 \\ \frac{dX_v}{dt} + \frac{1}{\tau} X_v - \frac{K_v}{\tau} u = 0 \end{cases}$$

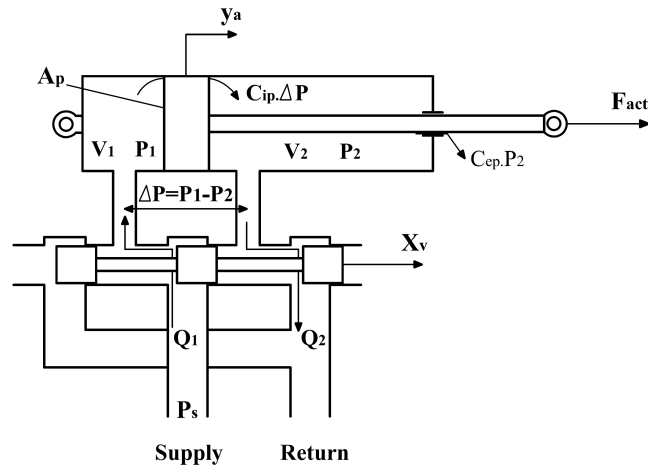
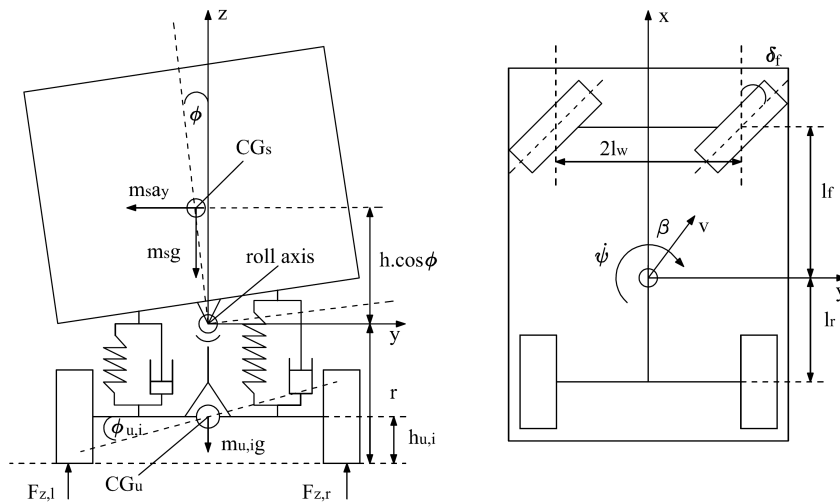


Schéma de l'actionneur ESVH.

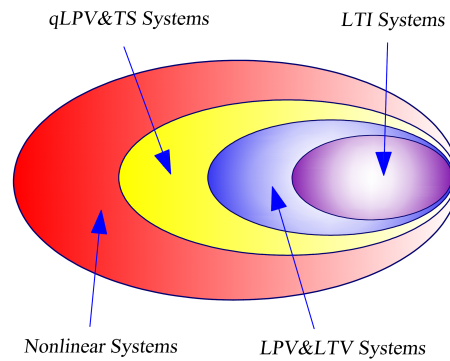


Le modèle lacet-roulis d'un véhicule lourd.

- **Chapitre 3 : Rappels théoriques sur les notions de commande et d'optimisation**

Le chapitre 3 présente des rappels sur la théorie du contrôle et des éléments nécessaires utilisés dans cette thèse pour le développement de la conception du contrôle de la dynamique des véhicules. Pour cela, quelques définitions bien connues, lemmes et

théorèmes sont rappelés pour les systèmes LTI, les systèmes LPV, les commandes LQR, \mathcal{H}_∞ , $\mathcal{H}_\infty/$ LPV utilisant une approche LPV basée sur un maillage pour le retour d'état et le retour dynamique de sortie. L'optimisation multi-objectifs, en utilisant les algorithmes génétiques, est aussi mentionnée comme un point fort de cette thèse. Il convient aussi de noter que certains contenus visant à saisir l'essence de l'étude seront aussi présentés selon les besoins.



Relation entre les différentes classes de systèmes.

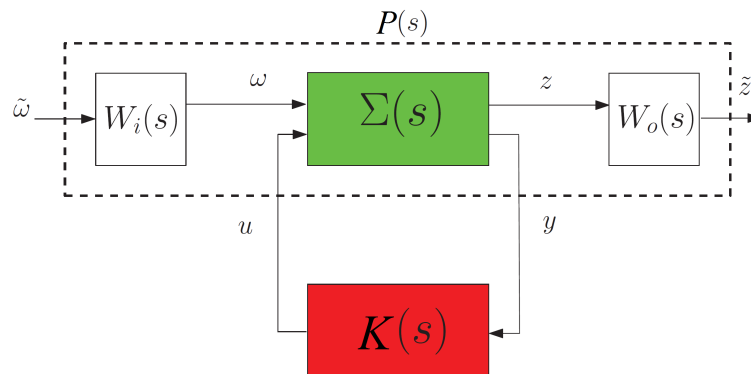


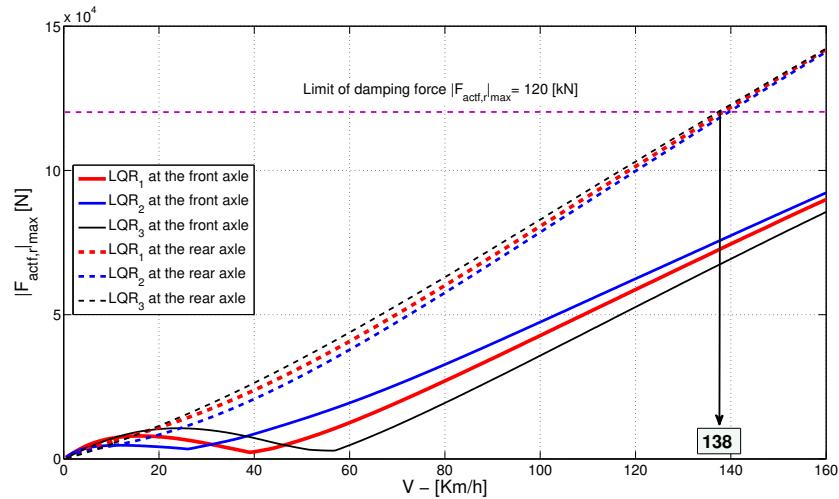
Schéma de contrôle H_∞ généralisé.

La **seconde partie** est consacrée à une des contributions essentielles de cette thèse qui traite de l'approche LTI pour le contrôle de barres anti-roulis actif :

- **Chapitre 4** : *Amélioration de la stabilité en roulis des poids lourds en appliquant une commande LQR active sur les barres anti-roulis*

Le chapitre 4 présente les résultats initiaux de l'évaluation du modèle intégré proposé dans le chapitre 2. Un contrôle de barres anti-roulis actif a été développé selon l'approche LQR, prenant en compte le transfert de charge normalisé et les limitations du courant d'entrée. Les résultats obtenus dans les domaines fréquentiel et temporel montrent l'efficacité de l'approche LQR appliquée au contrôle de barres anti-roulis actif pour améliorer la stabilité vis-à-vis du roulis, et ainsi, éviter le phénomène de renversement

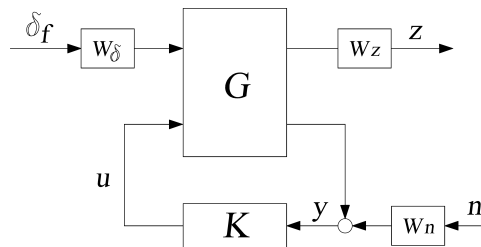
des poids lourds. La vitesse longitudinale maximale admissible obtenue pour un poids lourd est de 138 km/h . Elle garantit que l'actionneur ESVH intervient à l'intérieur de ses limites opérationnelles admissibles (forces, pressions de flux, déplacement de la valve dans son bobinage et courants induits). Il est possible de conclure que l'actionneur ESVH, contrôlé par le courant, est complètement justifié pour un système de barres anti-roulis actif sur les poids lourds.



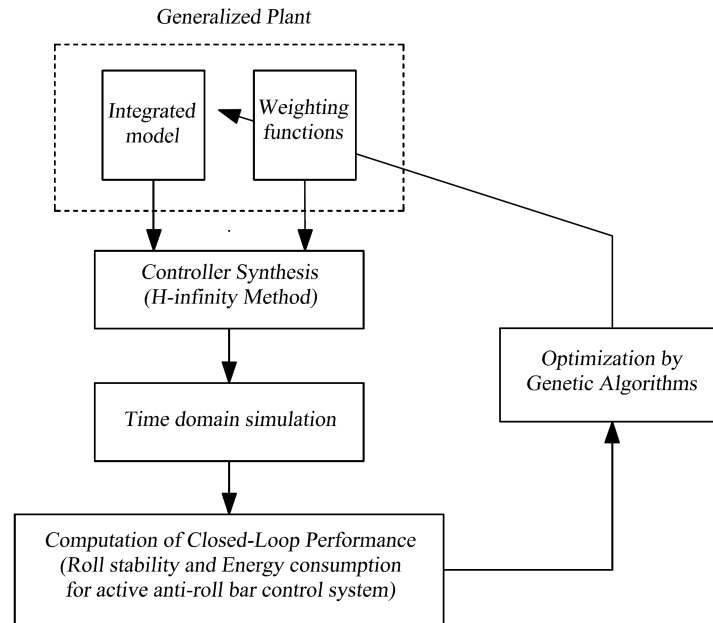
Influence de la vitesse véhicule sur la valeur absolue maximale des forces.

- **Chapitre 5 :** *Commande H_∞ robuste pour les systèmes de barres anti-roulis actifs afin d'éviter le renversement du véhicule*

Le chapitre 5 se concentre sur le problème du contrôle de barres anti-roulis actif utilisant l'approche H_∞ . L'analyse de la robustesse dans le domaine des fréquences est effectuée en utilisant l'outil de la μ -analyse, la vitesse longitudinale et la masse du véhicule étant considérées comme les deux paramètres incertains. Une procédure d'optimisation des fonctions de pondération par les algorithmes génétiques pour le contrôle H_∞ a aussi été proposée. Les objectifs contradictoires entre le transfert de charge normalisé et les courants à l'entrée sont gérés en utilisant seulement un paramètre de haut niveau, ce qui présente un grand avantage pour résoudre le problème de contrôle multi-objectifs.



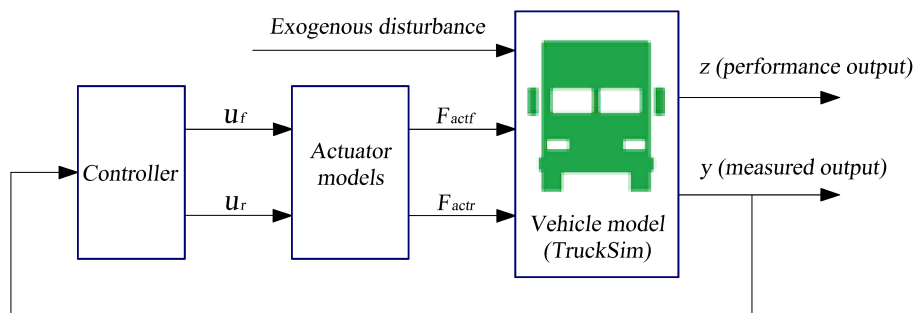
La structure en boucle fermée de la commande H_∞ de la barre anti-roulis active.



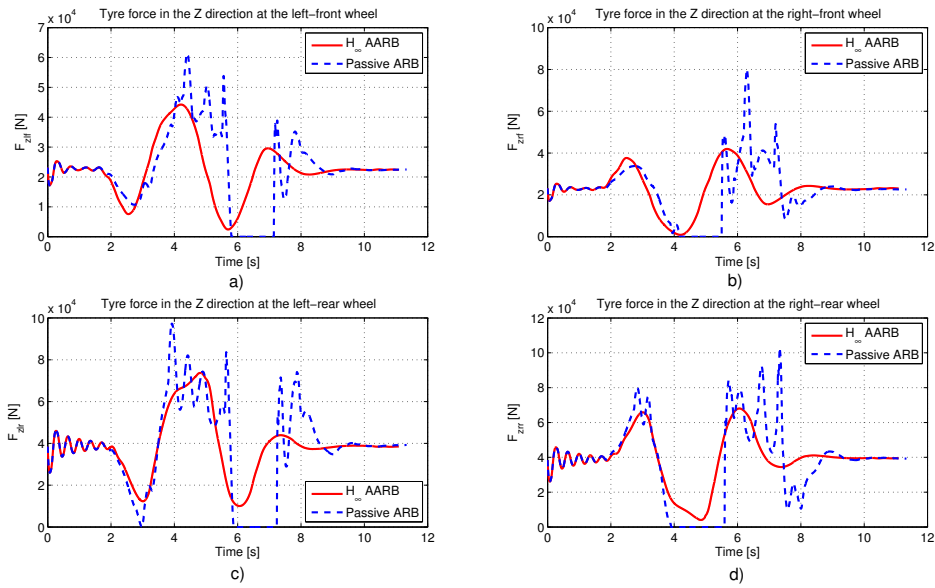
Optimisation de la commande H_∞ de la barre anti-roulis active à l'aide d'algorithmes génétiques.

• **Chapitre 6 :** *Validation de la commande H_∞ de la barre anti-roulis active en utilisant le logiciel TruckSim*

Le chapitre 6 présente la validation du contrôle de barres anti-roulis actif H_∞ en utilisant le logiciel TruckSim[®]. La simulation conjointe entre Matlab[®]/Simulink et TruckSim[®] permet la synthèse du contrôleur actif H_∞ de barres anti-roulis dans l'environnement Matlab[®]/Simulink. Dans TruckSim[®], nous pouvons également ajouter des éléments et des systèmes spécifiques du véhicule tels que des contrôles et les utiliser pour développer les algorithmes de commande. Grâce aux bons résultats de simulation obtenus en utilisant le modèle de véhicule non linéaire dans TruckSim[®], la validation du contrôle de barres anti-roulis actif H_∞ en temps réel sur un poids lourd réel sera intéressante dans le futur.



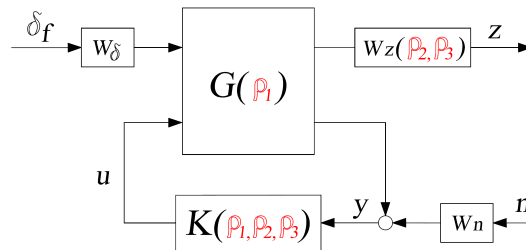
La simulation conjointe entre TruckSim[®] et Simulink[®]



Camion LCF entièrement chargé : réponse temporelle des forces du pneu dans la direction Z
 a) roue avant gauche, b) roue avant droite, c) roue arrière gauche et d) roue arrière droite.

La troisième partie se concentre sur l'approche LPV à base de grille pour le contrôle de barres anti-roulis actif. Ici, la synthèse du contrôleur utilise complètement la boîte à outils LPVToolsTM:

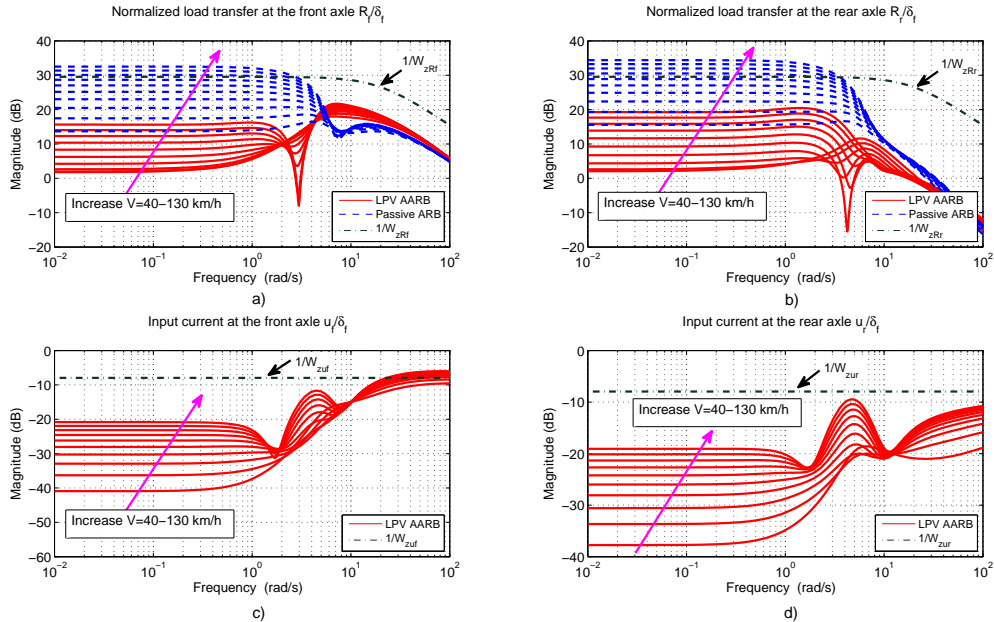
- **Chapitre 7 :** *Contrôle H_∞ /LPV multivariable pour les systèmes de barres anti-roulis actifs*



La structure d'interconnexion en boucle fermée de la commande LPV du système de barres anti-roulis actif.

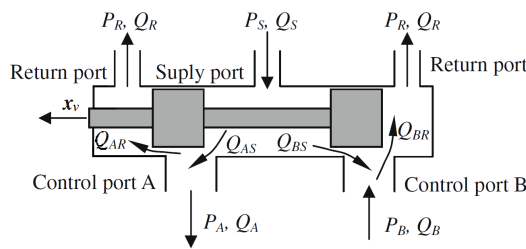
Le chapitre 7 envisage la vitesse longitudinale comme un paramètre variant de séquence. Le contrôleur actif H_∞ /LPV pour les barres anti-roulis est synthétisé en utilisant l'approche LPV à base de grille par l'intermédiaire de LPVToolsTM. Le schéma H_∞ /LPV est effectué en utilisant un paramètre dépendant de fonctions de pondération, ce qui permet l'adaptation de la performance en fonction du risque de renversement. Les résultats de simulation dans les domaines fréquentiel et temporel aussi bien que la vali-

dation en utilisant le logiciel TruckSim[®] montrent que le contrôleur actif H_∞/LPV de barres anti-roulis améliore drastiquement la stabilité vis-à-vis du roulis d'un poids lourd par rapport au système de barre anti-roulis passif.



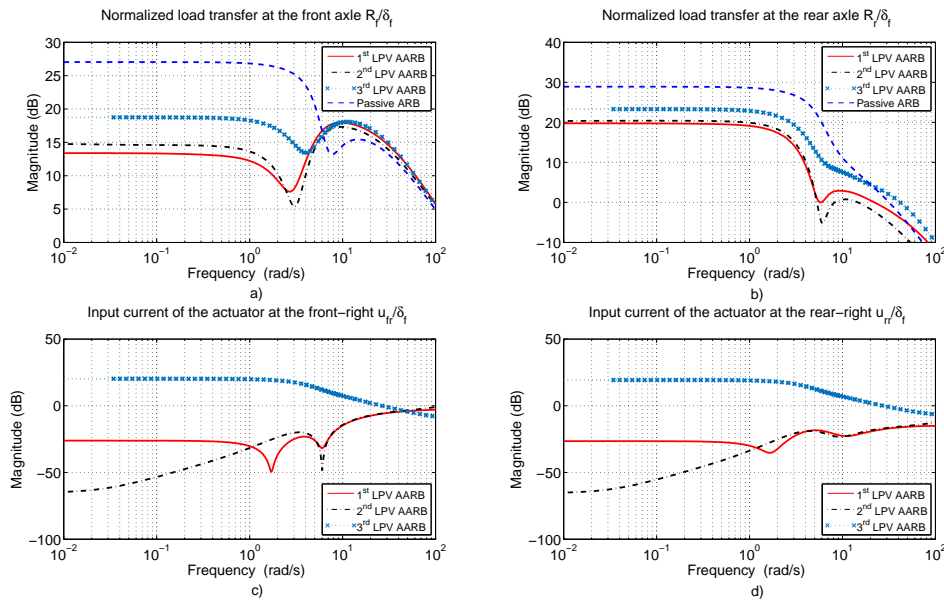
La grandeur de la fonction de transfert : (a, b) du transfert de charge normalisé $\frac{R_{f,r}}{\delta_f}$ et (c, d) des courants d'entrée $u_{f,r}$ aux deux essieux $\frac{u_{f,r}}{\delta_f}$.

• **Chapitre 8 :** *Effet d'une fuite d'huile à l'intérieur de la servo-valve sur les performances d'un système de barre anti-roulis actif*



Configuration de la servo-valve.

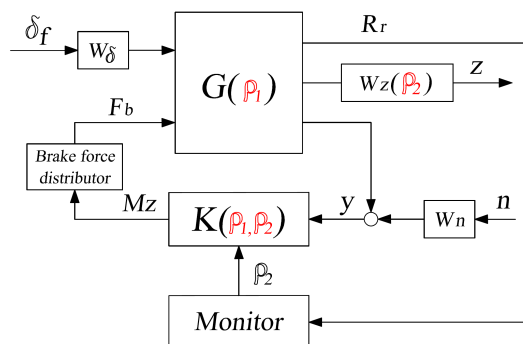
Le chapitre 8 analyse l'effet d'une fuite interne dans la servo-valve sur les systèmes en boucle ouverte ou fermée. Les résultats de l'analyse ont montré qu'avec le coefficient de pression du flux total $K_P = [5 \times 10^{-15}, 4 \times 10^{-10}] \frac{m^5}{Ns}$, les deux objectifs de renforcement de la stabilité vis-à-vis du roulis et de la saturation des actionneurs sont satisfaits simultanément. Ceci est une étape fondamentale pour la tolérance aux fautes du schéma de contrôle dans les futures recherches.



La grandeur de la fonction de transfert : (a, b) du transfert de charge normalisé $\frac{R_{f,r}}{\delta_f}$ sur les deux axes et (c, d) des courants d'entrée des actionneurs sur les essieux à l'avant droit $\frac{u_{fr}}{\delta_f}$ et à l'arrière droit $\frac{u_{rr}}{\delta_f}$.

La **partie finale** présente les conclusions générales de recherche de cette thèse, ainsi que quelques possibles directions futures utilisant le système de freinage actif de manière à prévenir le basculement du véhicule :

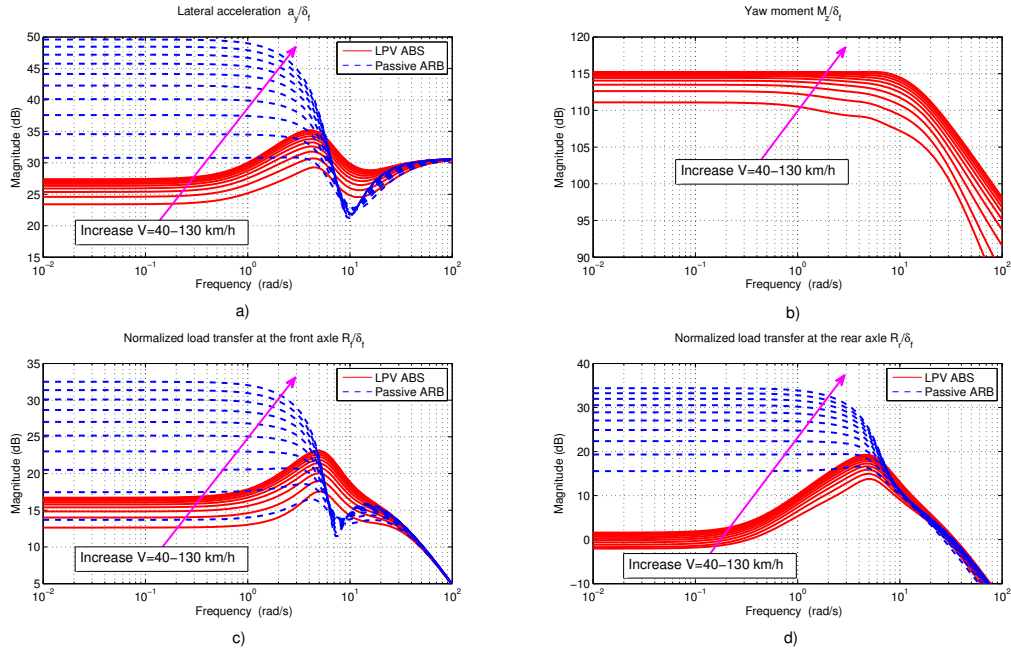
- **Chapitre 9 : Perspectives envisagées pour empêcher le renversement du véhicule en utilisant un système de freinage actif**



La structure d'interconnexion en boucle fermée du système de freinage actif.

Le chapitre 9 présente la combinaison du système de freinage actif avec le système de barre anti-roulis passif sur un poids lourd. Le contrôleur de freinage actif H_∞/LPV est

synthétisé pour empêcher le véhicule de basculer. Le système de freinage actif est seulement activé quand le véhicule se rapproche d'une situation dangereuse. Sont donnés les résultats initiaux de cette approche qui ouvre aussi quelques perspectives intéressantes de recherche pour le futur.



1^{er} cas : la grandeur de la fonction de transfert (a) de l'accélération latérale $\frac{a_y}{\delta_f}$, (b) du moment de lacet $\frac{M_z}{\delta_f}$, (c, d) des transferts de charge normalisés $\frac{R_{f,r}}{\delta_f}$ aux deux essieux.

- **Chapitre 10 : Conclusions générales et Perspectives**

Le chapitre 10 résume les résultats des trois années de la thèse. Des directions pour des recherches ultérieures sur le système de barres anti-roulis actif aussi bien que sur les systèmes actifs de contrôle d'instabilité en général sont aussi proposées.

Perspectives

Durant la thèse, de nombreux points intéressants méritaient d'être explorés. Parmi eux, les points suivants présentent un grand intérêt et devraient être poursuivis et développés dans le futur :

Perspectives à court terme :

- **Modèle de véhicule** : l'amélioration du modèle de véhicule avec un niveau supérieur non linéaire (comme le système de suspension non linéaire, le modèle à cadre flexible,

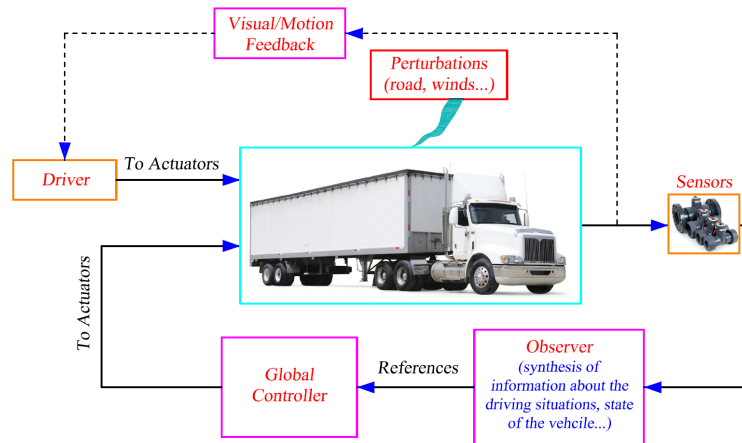
etc.) pour construire des contrôleurs réactifs aux situations cruciales aléatoires qui affectent le contrôle des performances. Il serait aussi intéressant de prendre en compte l'effet du système de barres anti-roulis actif sur le déplacement vertical du véhicule.

- **Modèle d'actionneur** : Il y a beaucoup de types d'actionneurs qui peuvent être utilisés pour le système de barres anti-roulis actif, mais la plupart d'entre eux ont des caractéristiques non linéaires (y compris l'actionneur ESVH utilisé dans cette thèse). Cependant, l'évaluation de l'efficacité des méthodes de contrôle sur le modèle d'actionneur non linéaire découlera de résultats plus précis.
- **Logiciel TruckSim[®]** : Bien que tous les paramètres du véhicule puissent facilement être déterminés à partir de la configuration du véhicule dans le logiciel TruckSim[®] software (donné dans le chapitre 6), les résultats de simulation montrent qu'il est nécessaire de résoudre le problème d'identification paramétrique. Ceci devrait rendre le modèle plus précis et totalement adaptable au modèle lacet-roulis.
- **Contrôle tolérant aux fautes** : Comme mentionné au chapitre 8, les fuites d'huile internes sont une caractéristique permanente de tous les actionneurs ESVH, même s'ils sont absolument neufs. Ces fuites ont un effet significatif sur la performance du système de barre anti-roulis actif ; par conséquent, la tolérance aux fautes devrait faire l'objet de recherches pour ce type de système [Choux 2011].

Perspectives à long terme :

- **Système de freinage actif** : Pour qu'un conducteur ait une maîtrise maximale d'un véhicule, il est très important que le système de freinage soit dans un état de marche correct. Les systèmes de freinage antiblocage (ABS), les systèmes de freinage électroniques (EBS) et les Programmes Électroniques de Stabilité (ESP) aident tous à prévenir le basculement du véhicule car ils ajustent automatiquement le mode de freinage pour chaque roue, apportant ainsi au conducteur une plus grande maîtrise. Les effets combinés de l'ABS, EBS, ESP et des capteurs de vitesse de lacet et d'angle de direction, se traduisent par une action correctrice qui permet au conducteur d'assurer le contrôle et ainsi de réduire le risque d'un basculement.
- **Véhicules à remorques** : Le nombre d'accidents mortels associés aux véhicules à remorques est plus élevé que celui d'autres véhicules. Avec une capacité de chargement accrue, une taille encombrante, l'amélioration de la stabilité vis-à-vis du roulis de ces véhicules à remorques devrait être une priorité. De nos jours, pour les longs véhicules à remorques, des compagnies comme Volvo utilisent souvent le système ESP pour prévenir les phénomènes de roulis. Cependant, le système de barres anti-roulis actif devrait être considéré comme une solution prometteuse.
- **Contrôle global du châssis** : Les systèmes de contrôle pour poids lourds sont progressivement développés, comme les systèmes actifs de freinage, les systèmes de conduite actifs, les systèmes de suspension actifs, les systèmes de barres anti-roulis actifs, etc. Cependant, ils ne peuvent agir de manière indépendante, ils ont toujours un impact

et une influence mutuels. En conséquence, le concept de "Contrôle global du châssis" devrait être également étudié plus en détail.



Contrôle global du châssis.

- **Application réelle :** Dans cette thèse, le système de barres anti-roulis actif a démontré son efficacité dans l'amélioration de la stabilité vis-à-vis du roulis des poids lourds. En conséquence, les évaluations et bilans, grâce à des tests sur des véhicules réels, seront d'un grand intérêt à l'avenir pour valider les études menées en simulation dans la plupart des travaux actuels.



(a)



(b)

Application réelle du système de barres anti-roulis actif.

List of Figures

1.1	Rollover of (a) a single unit heavy vehicle [<i>Carcruishing</i>], (b) a long combination vehicle [<i>Baogialai</i>].	10
1.2	Long combination vehicle in a Jack-knifing [<i>Jackknifing</i>].	12
1.3	A simplified roll model: a heavy vehicle in a steady state manoeuver.	14
1.4	Graphic presentation of the roll-equilibrium equation for a rigid vehicle.	16
1.5	Graphic presentation of the roll equation for a vehicle with compliant tyres.	17
1.6	Tyres and suspension roll motions occur at the different centers.	17
1.7	The effect of (a) the tyre and suspension stiffness, (b) the suspension roll axis on the vehicle rollover threshold.	18
1.8	Summary of previous studies on active anti-roll bar of a single unit heavy vehicle.	23
1.9	Summary of thesis contributions on the active anti-roll bar system.	25
2.1	An active anti-roll bar system applied on one axle of heavy vehicles [Miège 2000].	28
2.2	Structure of the general electronic servo-valve hydraulic system [Kalyoncu and Haydim 2009].	29
2.3	Diagram of the three-land-four-way spool valve [Merritt 1967].	30
2.4	Diagram of the flow directions of the three-land-four-way spool valve [Merritt 1967].	30
2.5	Diagram of the ESVH actuator [Miège 2000].	32
2.6	The Yaw-Roll model of a single unit heavy vehicle [Gaspar, Bokor, and Szaszi 2004].	34
2.7	Diagram of the passive anti-roll bars on vehicles.	37
2.8	Diagram of the fully integrated model using an active anti-roll bar system.	37
2.9	Diagram of a control-oriented integrated model using an active anti-roll bar system.	39
2.10	Geometrical description of the passive anti-roll bar system on heavy vehicles [Topac, Enginar, and Kuralay 2011].	42

2.11	Anti-roll bar geometry used in <i>SAE Spring Design Manual</i>	43
2.12	Transfer function magnitude of (a, b) normalized load transfers $\frac{R_{f,r}}{\delta_f}$ and (c, d) roll angles of suspension $\frac{\phi - \phi_{u_{f,r}}}{\delta_f}$ at the two axles of a single unit heavy vehicle.	44
2.13	Time response of the steering angle δ_f	46
2.14	Time response of (a, b) normalized load transfers $R_{f,r}$ and (c, d) suspension roll angles $\phi - \phi_{u_{f,r}}$ at the two axles.	46
3.1	Relation between the different classes of systems.	51
3.2	Standard problem: $P - K - \Delta$ structure.	56
3.3	(a) General control configuration with uncertainties, (b) $N\Delta$ structure.	57
3.4	H_∞ control problem scheme.	59
3.5	Generalized H_∞ control scheme.	61
3.6	Generalized LPV/H_∞ control problem.	63
3.7	LPV models defined on a rectangular grid.	67
3.8	Relation between MATLAB objects [Hjartarson, Seiler, and Packard 2015].	68
3.9	Example of a Pareto curve.	70
3.10	Genetic algorithm steps in developing generations of members.	71
3.11	Crossover and mutation operation.	72
4.1	First case, the transfer functions magnitude of (a, b) normalized load transfers ($\frac{R_{f,r}}{\delta_f}$) and (c, d) input currents ($\frac{u_{f,r}}{\delta_f}$) at the axles.	81
4.2	Second case, the transfer functions magnitude of (a, b) normalized load transfers ($\frac{R_{f,r}}{\delta_f}$) and (c, d) input currents ($\frac{u_{f,r}}{\delta_f}$) at the axles.	82
4.3	Time responses of steering angle δ_f [Gaspar, Bokor, and Szaszi 2004].	83
4.4	Time responses of (a, b) the normalized load transfers and (c, d) the input currents at the axles.	84
4.5	<i>RMS</i> of the signal's reduction: λ_1 (a), λ_2 (b)	85
4.6	Effect of the forward velocity on the maximum absolute value of (a,b) the normalized load transfers and of (c, d) the roll angle of suspensions at the front and rear axles.	87

4.7	Influence of the forward velocity on the maximum absolute value of the spool valve displacements.	88
4.8	Influence of the forward velocity on the maximum absolute value of the input currents.	89
4.9	Influence of the forward velocity on the maximum absolute value of the load flows.	90
4.10	Influence of the forward velocity on the maximum absolute value of the forces.	90
4.11	Phase-Plane $\beta - \dot{\beta}$ (a), Zoom in Phase-Plane $\beta - \dot{\beta}$ (b).	92
4.12	Stability index λ	92
5.1	The closed-loop structure of the H_∞ active anti-roll bar control.	97
5.2	Transfer function magnitude of the H_∞ controller: from lateral acceleration to (a) input current at front axle $\frac{u_f}{a_y}$, (b) input current at rear axle $\frac{u_r}{a_y}$; from roll rate to (c) input current at front axle $\frac{u_f}{\phi}$, (d) input current at rear axle $\frac{u_r}{\phi}$	98
5.3	Transfer functions magnitude of (a, b) the normalized load transfers ($\frac{R_{f,r}}{\delta_f}$) and (c, d) the roll angle of the unsprung masses ($\frac{\phi - \phi_{u_{f,r}}}{\delta_f}$) at the two axles.	100
5.4	Transfer functions magnitude of (a) the actuator forces ($\frac{F_{actf,r}}{\delta_f}$), (b) the load flow ($\frac{Q_{Lf,r}}{\delta_f}$), (c) the spool valve displacements ($\frac{X_{vf,r}}{\delta_f}$) and (d) the input currents ($\frac{u_{f,r}}{\delta_f}$) at the two axles.	100
5.5	Time responses of the steering angle δ_f [Gaspar, Bokor, and Szaszi 2004].	101
5.6	Time responses of (a, b) the normalized load transfers and (c, d) the suspensions roll angles.	101
5.7	Time responses of (a) the actuator force ($F_{actf,r}$), (b) the load flows ($Q_{Lf,r}$), (c) the spool valve displacements ($X_{vf,r}$) and (d) the input currents ($u_{f,r}$) at the two axles.	102
5.8	Controller optimization for the H_∞ active anti-roll bar using Genetic Algorithms.	104
5.9	The Pareto frontier for the active anti-roll bar on heavy vehicles using ESVH actuators.	108
5.10	Transfer function magnitude of the normalized load transfers (a) at the front axle $\frac{R_f}{\delta_f}$ and (b) at the rear axle $\frac{R_r}{\delta_f}$	109
5.11	Reduction of the transfer function magnitude of the normalized load transfers at the two axles compared to the passive anti-roll bar (in equation (5.9)).	110

5.12	Transfer function magnitude of the input currents (a) at the front axle $\frac{u_f}{\delta_f}$ and (b) at the rear axle $\frac{u_r}{\delta_f}$	110
5.13	Effect of the forward velocity on the normalized load transfers: (a) front axle R_f , (b) rear axle R_r	111
5.14	Effect of the forward velocity on the suspension roll angles: (a) front axle $\phi - \phi_{uf}$, (b) rear axle $\phi - \phi_{ur}$	111
5.15	Upper and Lower bounds for (a) RS , (b) RP	113
5.16	Performance analysis for the uncertain forward velocity at 10%, 40%, 70%, 94%.	114
5.17	Performance analysis for the uncertain sprung mass at 10%, 30%, 50%, 55%.	115
5.18	Transfer functions magnitude of (a, b) the normalized load transfers and (c, d) the suspension roll angles at the two axles.	116
5.19	Transfer functions magnitude of (a) the actuator forces (F_{actf}), (b) the load flows (Q_{Lf}), (c) the spool valve displacements (X_{vf}) and (d) the input currents (u_f): front axle.	116
5.20	Transfer functions magnitude of (a) the actuator forces (F_{actr}), (b) the load flows (Q_{Lr}), (c) the spool valve displacements (X_{vr}) and (d) the input currents (u_r): rear axle.	117
5.21	Influence of the forward velocity on the maximum absolute value of (a, b) the normalized load transfers and (c, d) the suspension roll angles at the two axles.	118
5.22	Influence of the forward velocity on the maximum absolute value of (a) the actuator forces ($F_{actf,r}$), (b) the load flows ($Q_{Lf,r}$), (c) the spool valve displacements ($X_{vf,r}$) and (d) the input currents ($u_{f,r}$) at the two axles.	119
5.23	Transfer functions magnitude of (a, b) the normalized load transfers ($\frac{R_{f,r}}{\delta_f}$) and (c, d) the roll angle of the suspension ($\frac{\phi - \phi_{uf,r}}{\delta_f}$) at the two axles.	120
5.24	Transfer functions magnitude of (a, b) the force of the actuators ($\frac{F_{actf,r}}{\delta_f}$) and (c, d) the input currents ($\frac{u_{f,r}}{\delta_f}$) at the two axles.	121
6.1	TruckSim [®] Intuitive Visualization [<i>Mechanical Simulation Corporation</i>].	124
6.2	TruckSim [®] Vehicle Coordinate System.	125
6.3	Diagram of TruckSim [®] -Simulink [®] Co-Simulation.	125
6.4	Tyre force in the Z direction.	127

6.5	Tour bus 2 axles (4×2) [<i>Tour-bus</i>].	128
6.6	Payload (left passengers).	129
6.7	Payload (right passengers).	130
6.8	Trajectory of the tour bus in the circular road test.	130
6.9	Unloaded tour bus: time response of (a) steering angle, (b) roll angle of sprung mass, (c,d) roll angle of unsprung masses at the front/rear axles.	131
6.10	Unloaded tour bus: time response of the tyre forces in the Z direction of (a) left-front wheel, (b) right-front wheel, (c) left-rear wheel, and (d) right-rear wheel.	132
6.11	Unloaded tour bus: time response of the characteristic of the ESVH actuators.	132
6.12	Trajectory of the tour bus in the cornering manoeuver.	133
6.13	Fully loaded tour bus: time response of (a) steering angle, (b) roll angle of sprung mass, (c,d) roll angle of unsprung masses at the front/rear axles.	134
6.14	Fully loaded tour bus: time response of the tyre forces in the Z direction of (a) left-front wheel, (b) right-front wheel, (c) left-rear wheel, and (d) right-rear wheel.	135
6.15	Fully loaded tour bus: time response of the characteristic of the ESVH actuators.	135
6.16	LCF truck 2 axles (4×2) [<i>LCF-Truck</i>].	136
6.17	Payload of LCF truck.	137
6.18	Trajectory of the LCF truck in the sine wave steering manoeuver.	138
6.19	Unloaded LCF truck: time response of (a) steering angle, (b) roll angle of sprung mass, (c,d) roll angle of unsprung masses at the front/rear axles.	139
6.20	Unloaded LCF truck: time response of the tyre forces in the Z direction of (a) left-front wheel, (b) right-front wheel, (c) left-rear wheel, and (d) right-rear wheel.	139
6.21	Unloaded LCF truck: time response of the characteristic of the ESVH actuators.	140
6.22	Trajectory of the LCF truck in the double lane change manoeuver.	141
6.23	Fully loaded LCF truck: time response of (a) steering angle, (b) roll angle of sprung mass, (c,d) roll angle of the unsprung masses at the front/rear axles.	141
6.24	Fully loaded LCF truck: time response of the tyre forces in the Z direction of (a) left-front wheel, (b) right-front wheel, (c) left-rear wheel, and (d) right-rear wheel.	142

6.25	Fully loaded LCF truck: time response of the characteristic of the ESVH actuators.	143
7.1	Diagram of the closed-loop system of the control-oriented integrated model. . .	149
7.2	The closed-loop interconnection structure of the LPV active anti-roll bar control.	150
7.3	Transfer function magnitude of controller: from lateral acceleration to (a) input current at front axle $\frac{u_f}{a_y}$, (b) input current at rear axle $\frac{u_r}{a_y}$; from roll rate to (c) input current at front axle $\frac{u_f}{\phi}$, (d) input current at rear axle $\frac{u_r}{\phi}$	153
7.4	Transfer function magnitude of (a, b) the normalized load transfers $\frac{R_{f,r}}{\delta_f}$, (c, d) the input currents $\frac{u_{f,r}}{\delta_f}$ at the two axles.	154
7.5	Transfer function magnitude of the normalized load transfers at the two axles $\frac{R_{f,r}}{\delta_f}$	155
7.6	Time responses of a heavy vehicle in a double lane change manoeuvre to avoid an obstacle.	156
7.7	Trajectory of the tour bus in the double lane change manoeuvre.	158
7.8	Time responses of the tour bus in the double lane change manoeuvre.	159
7.9	Trajectory of the truck in the sine wave manoeuvre.	160
7.10	Time responses of the truck in the sine wave steering manoeuvre.	161
8.1	Servo-valve configuration [Erylmaz and Wilson 2000].	165
8.2	Typical servo-valve leakage flow rate curve [Kalyoncu and Haydim 2009].	167
8.3	Diagram of the closed-loop system of the fully integrated model.	167
8.4	The three-land-four-way spool valve [Merritt 1967].	169
8.5	The transfer function magnitude of the normalized load transfer ($\frac{R_f}{\delta_f}$) at the front axle.	170
8.6	Transfer function magnitude of normalized load transfer ($\frac{R_r}{\delta_f}$) at the rear axle. .	171
8.7	Trajectory of the vehicle.	172
8.8	Time responses of the heavy vehicle and the actuators in the case of the steady state manoeuvre.	173
8.9	The closed-loop interconnection structure of the fully integrated model.	175

8.10	Transfer function magnitude of controller: from lateral acceleration to (a) input current at front-left $\frac{u_{fl}}{a_y}$, (b) input current at front-right $\frac{u_{fr}}{a_y}$, (c) input current at rear-left $\frac{u_{rl}}{a_y}$, (d) input current at rear-right $\frac{u_{rr}}{a_y}$	177
8.11	Transfer function magnitude of controller: from roll rate to (a) input current at front-left $\frac{u_{fl}}{\phi}$, (b) input current at front-right $\frac{u_{fr}}{\phi}$, (c) input current at rear-left $\frac{u_{rl}}{\phi}$, (d) input current at rear-right $\frac{u_{rr}}{\phi}$	177
8.12	Transfer function magnitude of (a, b) the normalized load transfers at the two axles $\frac{R_{f,r}}{\delta_f}$, (c, d) the input currents of the ESVH actuators at the front-right $\frac{u_{fr}}{\delta_f}$ and at the rear-right $\frac{u_{rr}}{\delta_f}$	178
8.13	The normalized load transfers and roll angle of the suspensions in the steady state manoeuver.	179
8.14	The characteristics of the ESVH actuators at the front axle.	179
8.15	The characteristics of the ESVH actuators at the rear axle.	180
8.16	The load flow of the four ESVH actuators in the steady state manoeuver.	180
8.17	The transfer function magnitude of (a, b) the normalized load transfers at the two axles $\frac{R_{f,r}}{\delta_f}$, (c, d) the input currents of the actuators at the front-right $\frac{u_{fr}}{\delta_f}$ and at the rear-right $\frac{u_{rr}}{\delta_f}$	182
8.18	Time responses of a single unit heavy vehicle in a double lane change manoeuver to overtake.	184
9.1	The evolution of braking systems [Savaresi and Tanelli 2010].	190
9.2	Yaw-Roll model of a single unit heavy vehicle [Gaspar, Bokor, and Szaszi 2004].	192
9.3	The closed-loop interconnection structure of the active braking system.	193
9.4	1 st case: transfer function magnitude of (a) the lateral acceleration $\frac{a_y}{\delta_f}$, (b) the yaw moment $\frac{M_z}{\delta_f}$, (c, d) the normalized load transfers $\frac{R_{f,r}}{\delta_f}$ at the two axles.	195
9.5	2 nd case: transfer function magnitude of (a) the lateral acceleration $\frac{a_y}{\delta_f}$, (b) the yaw moment $\frac{M_z}{\delta_f}$, (c, d) the normalized load transfers $\frac{R_{f,r}}{\delta_f}$ at the two axles.	196
9.6	Varying parameter $\rho_2 = f(R_r)$	198
9.7	Time responses of (a) the steering angle δ_f , (b) forward velocity v , (c) roll angle of the sprung mass ϕ and (d) lateral acceleration a_y	199
9.8	Time responses of the (a, b) normalized load transfers $R_{f,r}$ and (c, d) roll angle of the suspensions $\phi - \phi_{uf,r}$ at the two axles.	201

9.9	Time responses of the (a) brake force at the rear-left wheel F_{brl} , (b) braking force at the rear-right wheel F_{brr} , (c) phase - plane: $\beta - \dot{\beta}$ and (d) stability index λ	202
10.1	Global chassis control.	206
10.2	Real example of the application of the active anti-roll bar system on heavy vehicles [<i>Cambridge Vehicle Dynamics Consortium</i>].	206
B.1	Closed-loop system using a <i>LQR</i> active anti-roll bar controller.	209
B.2	Frequency responses of the characteristics of the ESVH actuators at the front axle.	210
B.3	Frequency responses of the characteristics of the ESVH actuators at the rear axle.	210
B.4	Time responses of the characteristics of the ESVH actuators at the front axle. .	211
B.5	Time responses of the characteristics of the ESVH actuators at the rear axle. .	211

List of Tables

2.1	Symbols and parameters of the ESVH actuator [Miège and Cebon 2002], [Rafa, Yahya, and Rawand 2009].	33
2.2	Symbols and parameters of the yaw-roll model [Gaspar, Bokor, and Szaszi 2005]. [Vu et al. 2016].	35
2.3	Reduction of the magnitude of transfer functions compared to the without anti-roll bar.	45
4.1	First case, the reduction of the magnitude of transfer functions (gain reduction) compared to the passive case.	81
4.2	Second case, the reduction of the magnitude of the transfer functions (gain reduction) compared to the passive anti-roll bar.	82
4.3	Reduction of the peak of the normalized load transfers compared to the passive case (100%).	85
4.4	Signals considered in the frequency and time domains.	86
5.1	Lower and upper bounds of the weighting functions.	105
5.2	Binding conditions.	106
5.3	Initial weighting functions parameters for the H_∞ active anti-roll bar.	106
5.4	The optimization results for the weighting functions of the H_∞ active anti-roll bar.	107
5.5	The comparison between the LQR control and the H_∞ control.	120
6.1	Validation cases of the H_∞ active anti-roll bar control by using co-simulation.	128
6.2	Parameters of the unloaded tour bus.	129
6.3	Time response comparison between the H_∞ active anti-roll bar and the passive anti-roll bar.	134
6.4	Parameters of the unloaded LCF truck.	137
6.5	Reduction of the signal magnitude compared to the passive anti-roll bar.	138

7.1	Reduction of the magnitude of transfer functions compared with the passive anti-roll bar at 40 <i>km/h</i> and 130 <i>km/h</i>	154
7.2	Validation cases of the H_∞/LPV active anti-roll bar control by using co-simulation.	158
7.3	Reduction of the signal magnitude compared with the passive case.	162
8.1	Synthesis of the time response in the steady state manoeuver.	174
8.2	The weighting functions of the H_∞/LPV synthesis for the fully integrated model.	175
8.3	Maximum absolute value of the signals in the double lane change manoeuver to overtake.	185
9.1	Reduction of the magnitude of the transfer functions compared to the passive anti-roll bar system.	197
9.2	The maximum absolute value of the signals.	200

Table of Acronyms

AARB	Active Anti-Roll Bar
ABS	Active Braking System
AEB	Autonomous Emergency Braking
CG	Center of Gravity
CVDC	Cambridge Vehicle Dynamics Consortium
DOF	Degree Of Freedom
EBS	Electronic Brake System
ESVH	Electronic Servo-Valve Hydraulic
FDI	Fault Detection and Identification
GAs	Genetic Algorithms
GCC	Global Chassis Control
LCF	Low Cab Forward
LFT	Linear Fractional Transformations
LMI	Linear Matrix Inequality
LPV	Linear Parameter Varying
LQG	Linear Quadratic Gaussian
LQR	Linear Quadratic Regulator
LTI	Linear Time Invariant
LTR	Loop Transfer Recovery
MCO	Multi Criteria Optimization
MIMO	Multi Inputs Multi Outputs
NHTSA	Federal National Highway Traffic Safety Administration
RP	Robust Performance
RS	Robust Stability
SISO	Single Input Single Output
TTR	Time To Rollover

\mathbb{R}	Real values set
\mathbb{C}	Complex values set
A^*	Conjugate of $A \in \mathbb{C}$
A^T	Transpose of $A \in \mathbb{R}$
$A \prec (\preceq) 0$	Matrix A is symmetric and negative (semi)definite
$A \succ (\succeq) 0$	Matrix A is symmetric and positive (semi)definite
$Co(X)$	Convex hull of set X
$A = A^T$	Matrix A is real symmetric
$He(A) = A^T + A$	

Thesis framework and Publications

Contents

0.1	Thesis framework	1
0.2	General introduction and problem statement of the thesis	2
0.3	Structure of the thesis	2
0.3.1	Part I: Thesis background and preliminary results	3
0.3.2	Part II: Active anti-roll bar control: LTI approach	3
0.3.3	Part III: Active anti-roll bar control: LPV approach	4
0.3.4	Part IV: Future direction and general conclusions	4
0.4	Publication list	6

0.1 Thesis framework

This dissertation presents the results of my three years PhD work (from January 2015 to October 2017), performed in the SLR (Systèmes Linéaires et Robustesse) team from the Control Systems Department of GIPSA-Lab. This thesis has been completed under the direction of **Olivier SENAME** (Professor Grenoble INP) and **Luc DUGARD** (Research Director CNRS). This work has been supported by the project 911 from the Ministry of Education and Training of Vietnam.

This thesis presents a continuation and further developments from the studies of Professor Peter Gaspar and his colleagues at the Hungarian Academy of Sciences [Gaspar, Bokor, and Szaszi 2004], [Gaspar, Szabo, and Bokor 2005b]. In these studies, the authors synthesized an LPV controller for the active anti-roll bar system and the active braking system, based on the yaw-roll model of a single unit heavy vehicle. The active anti-roll bar system operates continuously, while the active braking system is only activated when the vehicle reaches a critical rollover situation. This thesis concentrates mainly on the active anti-roll system in order to improve the roll stability of heavy vehicles. This is the first study on the rollover phenomenon of heavy vehicles within the SLR team. However, some contents of the control theory and the genetic algorithms mentioned in this thesis are based on former PhD studies in the same SLR team, such as [Poussot-Vassal 2008], [Aubouet 2010], [Do 2011], [Nwesaty 2015], [Nguyen 2016].

During the three years of research, the collaboration with Professor Peter Gaspar has always been maintained. In November 2016, I completed a very efficient and effective work visit at the Budapest University of Economics and Technology and the Hungarian Academy of Sciences. Here I have been introduced to the use of the TruckSim[®] software to evaluate the proposed control methods for the active anti-roll bar system. This work visit is the basis for the results

presented in Chapters 6, 7, 8. It is the important to notice that this work has led to common publications with Professor Peter Gaspar.

0.2 General introduction and problem statement of the thesis

Automotive vehicles are nowadays equipped with many modern technologies, intelligent sub-systems in different engineering fields such as mechanics, electronics, communications, and automatic control. This fact allows the automotive industry to respond to the requirements from customers concerning safe and comfortable vehicles together with lower fuel consumption. However, the latest technologies in automobiles are generally researched and applied to cars, not really many technologies are then applied to heavy vehicles. While the number of heavy vehicles account for a significant portion of the total number of vehicles involved in transport, and their role in economic development is extremely important.

Heavy vehicles are responsible of a large proportion of the total road accidents, and whose rollover accidents are the most dangerous and also the most serious. Therefore, it is important to study the systems which can assist the driver in reducing the rollover phenomenon. The active roll control systems have been studied for about two decades, including active braking system, active suspension system, active steering system and active anti-roll bar system. Among these solutions, the active anti-roll bar system has proven to be the most effective solution. By changing the moment between the sprung and unsprung masses, the vehicle's roll stability is improved in response to different behaviors.

The main body of work of this thesis concentrates on the topic of the active anti-roll bar on heavy vehicles. The contributions are mainly focussed in three directions:

- Electronic Servo-Valve Hydraulic (ESVH) actuators, the integrated model includes these actuators with the yaw-roll model of a single unit heavy vehicle;
- Some advanced control methods are used for this system, such as: LQR, H_∞ robust control, and LPV. For all of these control methods, the multi-objective problem is always considered to satisfy simultaneously two conflicting objectives: roll stability and energy consumption. The Genetic Algorithms approach is used to find the optimal selection of the weight functions of the H_∞ control synthesis;
- Confirmation of the effectiveness of control system by using TruckSim[®] software.

0.3 Structure of the thesis

In this thesis, the main contributions will be presented in the following organisation:

0.3.1 Part I: Thesis background and preliminary results

The first part gives some general introductions, vehicle modelling and control theory which allow to facilitate the reading of the thesis. This part is composed of the following chapters:

- Chapter 1 provides a general introduction to the vehicle rollover phenomenon. The mechanics of vehicle rollover and a review of previous research on active anti-roll bar systems are also presented. Finally the control objectives considered throughout the thesis are introduced.
- Chapter 2 aims to model the ESVH actuator, with the control signal being the input current and the output signal being the actuator force. An integrated model is proposed by combining the yaw-roll model of a single unit heavy vehicle with these actuators. Depending on the completeness of the model, there are two forms as: the fully integrated and the control-oriented integrated models. When compared to previous studies, the model developed in this chapter is a major improvement in the study of the active anti-roll bar system on heavy vehicles. A passive anti-roll bar system is also designed by using the SAE spring design manual.
- Chapter 3 presents some background on control theory and the necessary elements used in this thesis for the development of control design for vehicle dynamics. For this purpose, some well-known definitions, lemmas and theorems are recalled, concerning LTI, LPV systems, and the LQR, H_∞ and H_∞/LPV approaches for the state feedback and dynamic output feedback synthesis. Here the H_∞/LPV control design uses a grid-based LPV approach. The multi-objective optimization by using genetic algorithms is also mentioned as a highlight of this thesis. It is worth noting that, some contents to capture the essence of this study will also be presented when needed.

0.3.2 Part II: Active anti-roll bar control: LTI approach

The second part is devoted to one of the major contributions of the thesis which deals with the LTI approach for the active anti-roll bar control:

- Chapter 4 presents the initial results in evaluating the proposed integrated model, which was introduced in Chapter 2. An active anti-roll bar control was developed within the *LQR* approach, taking into account the normalized load transfer and input current limitations. The results obtained in the frequency and time domains show the efficiency of the *LQR* active anti-roll bar control approach to improve roll stability, so preventing the rollover phenomenon of heavy vehicles. The maximal admissible forward velocity of the heavy vehicle obtained (138 km/h) ensures that the ESVH actuator operates within its admissible operational limit (forces, load flows, spool valve displacements and input currents). It can be concluded that the ESVH actuator, controlled by the current, is completely justified for an active anti-roll bar control system on heavy vehicles.

- Chapter 5 concentrates on the active anti-roll bar control problem using the H_∞ approach. The robustness analysis in the frequency domain is done by using the μ analysis tool, with the forward velocity and the sprung mass considered as the two uncertain parameters. A weighting function optimization procedure using genetic algorithms for the H_∞ control has also been proposed. The conflicting objectives between the normalized load transfers and input currents are handled by using only one high level parameter, which is of great advantage to solve the multi-objective control problem.
- Chapter 6 presents the validation of the H_∞ active anti-roll bar control by using the TruckSim[®] software. The co-simulation between Matlab[®]/Simulink and TruckSim[®] allows the synthesis of the H_∞ active anti-roll bar controller in the Matlab[®]/Simulink environment, and in TruckSim[®] we can add specific vehicle elements and systems such as controls to the vehicle and use them to develop control algorithms. Thanks to good simulation results obtained by using the nonlinear vehicle model in TruckSim[®], the validation of the H_∞ active anti-roll bar control in real-time on the actual heavy vehicle will be of interest in the future.

0.3.3 Part III: Active anti-roll bar control: LPV approach

This part concentrates on the grid-based LPV approach for the active anti-roll bar control:

- Chapter 7 considers the forward velocity as a scheduling parameter. The H_∞/LPV active anti-roll bar controller is synthesized by using the grid-based LPV approach through the LPVTools[™] toolbox. The H_∞/LPV design is performed using parameter dependant weighting functions, which allows vehicle performance adaptation to the risk of rollover. The simulation results in the frequency and time domains as well as the validation by using the TruckSim[®] software show that the H_∞/LPV active anti-roll bar controller drastically improves the roll stability of the single unit heavy vehicle, when compared to the passive anti-roll bar.
- Chapter 8 analyzes the effect of the internal leakage inside the electronic servo-valve on the open-loop and closed-loop systems in view of road safety. The survey results have shown that with the total flow pressure coefficient $K_P = [5 \times 10^{-15}, 4 \times 10^{-10}] \frac{m^5}{Ns}$, the two objectives of enhancing roll stability and the saturation of the actuators are simultaneously satisfied. This represents the fundamental study for the fault tolerant control design in further research.

0.3.4 Part IV: Future direction and general conclusions

The final part presents possible future research directions using the active braking system in order to prevent vehicle rollover and the general conclusions of this thesis:

- Chapter 9 presents the combination between the active braking system and the passive anti-roll bar system of a single unit heavy vehicle. The H_∞/LPV active braking

controller is synthesized to best adapt to vehicle rollover. The active braking system is only activated when the vehicle comes close to a dangerous situation. This is the initial results of this approach and it also opens up some interesting future research initiatives.

- Chapter 10 summarizes the results of the thesis obtained during the last three years. Further possible research directions on active anti-roll bar as well as active roll control systems in general are also proposed.

0.4 Publication list

International journal paper

- J1** *Enhancing roll stability of heavy vehicle by LQR active anti-roll bar control using electronic servo-valve hydraulic actuators*, (V.T. Vu, O. Sename, L. Dugard, P. Gáspár),
In **Vehicle System Dynamics**, Vol 55(9), pp 1405-1429, April, 2017.

International conference papers with proceedings

- C1** *Multi objective H_∞ active anti-roll bar control for heavy vehicles*, (V.T. Vu, O. Sename, L. Dugard, P. Gáspár),
In Proceedings of the 20th **IFAC World Congress (WC)**, Toulouse, France, July, 2017.
- C2** *Active anti-roll bar control using electronic servo-valve hydraulic damper on single unit heavy vehicle*, (V.T. Vu, O. Sename, L. Dugard, P. Gáspár),
In Proceedings of the 8th **IFAC Symposium on Advances in Automotive Control (AAC)**, Norrköping, Sweden, June, 2016.
- C3** *H_∞ active anti-roll bar control to prevent rollover of heavy vehicles: a robustness analysis*, (V.T. Vu, O. Sename, L. Dugard, P. Gáspár),
In Proceedings of the 6th **IFAC Symposium on System Structure and Control (SSSC)**, Istanbul, Turkey, June, 2016.
- C4** *Optimal selection of weighting functions by genetic algorithms to design H_∞ anti-roll bar controllers for heavy vehicles*, (V.T. Vu, O. Sename, L. Dugard, P. Gáspár),
In Proceedings of the 15th **Vehicle System Dynamics, Identification and Anomalies (VSDIA)**, Budapest, Hungary, November, 2016.

Submitted journal and conference papers

- J2** *LPV control design by using LPVToolsTM for an active anti-roll bar system of heavy vehicles*, (V.T. Vu, O. Sename, L. Dugard, P. Gáspár),
Submitted to **Control Engineering Practice** (under review).
- C5** *H_∞ /LPV control for an active anti-roll bar system to improve the roll stability of heavy vehicles*, (V.T. Vu, O. Sename, L. Dugard, V.P. Dinh, T.P. Pham),
Submitted to the 10th **National conference on mechanics**, Hanoi, Vietnam, December, 2017.

Part I
Thesis background and preliminary
results

This part contains the first three chapters, with the main contents consisting of the vehicle rollover phenomenon, vehicle modelling, and a summary of the control theories used in this thesis. They are summarized as follows:

Chapter 1: Introduction

- A general introduction to the phenomenon of vehicle rollover and its related mechanics is presented. Here, we concentrate on the behavior of heavy vehicles with the characteristics of having a large load and a high center of gravity.
- We summarize previous research on active anti-roll bar systems, with two main parts including vehicle modelling and control methods.
- Finally, we introduce the control objectives which are considered throughout the thesis.

Chapter 2: Vehicle modelling

- A full model of the ESVH actuator is developed, with the control signal being the input current and the output signal being the actuator force.
- An integrated model is proposed by combining the yaw-roll model of a single unit heavy vehicle with the ESVH actuators. Depending on the completeness of the model, there are two forms: the fully integrated and the control-oriented integrated models. When compared to previous studies, the model developed in this chapter is a major improvement in the studies of heavy vehicles with active anti roll bar systems.
- A passive anti-roll bar system is designed by using the SAE spring design manual.

Chapter 3: Background on control theory and optimization

This chapter presents some background information on control theory and some necessary elements used in this thesis for the development of the control design in vehicle dynamics:

- Dynamical systems, signal and system norms, and robustness analysis of dynamical systems.
- Control methodologies: LQR, H_∞ and H_∞/LPV .
- Multi-objective optimization by using genetic algorithms.

Introduction

Contents

1.1 Rollover of heavy vehicles	9
1.1.1 Different categories of vehicle rollover accidents	10
1.1.2 Primary reasons for vehicle rollover	11
1.2 The mechanics of vehicle rollover	13
1.2.1 Vehicle rollover threshold	13
1.2.2 The simplified roll model	14
1.2.3 Rollover of the rigid vehicle	15
1.2.4 The vehicle with compliant tyres	16
1.2.5 The vehicle with roll-compliant suspension	17
1.3 Review of previous research	20
1.3.1 Different models of heavy vehicles	20
1.3.2 Control methods for the active anti-roll bar system on heavy vehicles	21
1.4 Control objectives	24
1.5 Perspectives	24
1.5.1 Some open research topics and potential extensions:	24
1.5.2 Perspectives "explored" in this thesis:	25

1.1 Rollover of heavy vehicles

Heavy vehicles are defined as goods vehicles having a maximum permissible gross weight (vehicle and load of over 3.5 tons), and includes trucks and buses [Evgenikos et al. 2016]. The use of heavy vehicles as a means of transport is of economic importance in most areas of the world. In the United States, for example, the commercial trucking sector employs nearly 10 million people and has annual revenues of more than US\$500 billion. Trucks transport over 11 billion tons of goods annually, about 60% of the total domestic tonnage shipped [Schwartz and Fleming 2007]. Additionally, North American intercity and charter buses carry an estimated 860 million passengers annually, which is more than those transported by commercial air carriers or rail [Knipling 2007].

We have to acknowledge the role of heavy vehicles in economic development. However due to

their high mass, there can be severe consequences for other road users when they are involved in accidents. The accidents related to heavy vehicles are also a complex issue not just in developing countries but also in developed countries like the USA and Europe. The rollover phenomenon is the most dangerous type of accident for heavy vehicles, although rollovers are relatively rare events, they can be deadly accidents when they occur. Loss of roll stability is the main cause of rollover accidents involving heavy vehicles. According to the Federal National Highway Traffic Safety Administration (NHTSA), in the United States, there were 333,000 heavy vehicles involved in traffic crashes during 2012. There were 3,921 people killed in rollover crashes and 104,000 people injured (an increase of 18% from 2011) [NHTSA]. In 2013, more than 4,500 persons were killed in road traffic accidents involving heavy vehicles in the EU, constituting almost 18% of all road accident fatalities for that year [Evgenikos et al. 2016]. While heavy vehicles account for just a small proportion of the vehicle fleet or the total vehicle kms travelled in the EU, they are more often involved in severe road accidents, creating a significant need to better understand the physical and mechanical characteristics specific to this vehicle group. Figure 1.1 illustrates two examples of the heavy vehicle rollover phenomenon.



Figure 1.1: Rollover of (a) a single unit heavy vehicle [Carcrushing], (b) a long combination vehicle [Baogialai].

1.1.1 Different categories of vehicle rollover accidents

The rollover of heavy vehicles is a very serious safety issue, which can result in large financial and environmental consequences. Rollover accidents are classified into four categories [Miège and Cebon 2002]:

- **Preventable:** the driver would have been able to avoid the accident if a warning device had been installed on the vehicle. This is closely linked to the "Time-To-Rollover (TTR)" concept [Chen and Peng 2001], [Yu, Guvenc, and Ozguner 2008]. The survey results indicated that this category accounts for about 3.3% of total rollover accidents.

- **Potentially preventable:** the accident might have been avoided, depending on the driver skills and on the performance of the warning device. It accounts about 38.4% of total rollover accidents.
- **Non-preventable:** regardless of the driver skills or the performance of the warning device, vehicle rollover will always happen. This group accounts about 49.7% of total rollover accidents.
- **Preventable unknown:** this category accounts for about 8.6% of total rollover accidents.

It is usually difficult for the driver to feel the rollover behaviour of a heavy vehicle. Investigations have shown that only a minority of rollover accidents could have been avoided with a warning device, potentially more with a skilled driver, but half of the rollover accidents were not preventable by driver action alone. The main cause of rollover accidents in which heavy vehicles are involved is the loss of roll stability when the tyre-road contact force on one of the side wheels becomes zero. Roll stability refers to the ability of a vehicle to overcome overturning moments generated during cornering and lane changing. It is well known that heavy vehicles do have relatively high centres of mass and narrow track widths and can lose roll stability at moderate levels of lateral acceleration [Boada et al. 2007].

1.1.2 Primary reasons for vehicle rollover

There are a lot of reasons why vehicle rollover occurs; they include objective as well as subjective factors including driver skills and the technical quality of the vehicle. We can mention here the main reasons for vehicle rollover as follows [Edwards 2011]:

- **Adverse weather conditions:** side wind gusts is one of the most obvious weather condition related to vehicle rollover. Studies have shown that, for a vehicle with a high centre of gravity, the probability of vehicle rollover is increased. As well as side wind gusts, other adverse weather conditions can also affect the road surface such as snow, rain, ice, etc. All these can contribute to vehicle rollover, because the contact between the tyres and road surface is reduced. Of course these adverse weather conditions are the objective factors related to vehicle rollover.
- **Sudden braking manoeuvres:** every driver would always want to have maximum control over its vehicle, therefore it is very important that the braking system is in correct working order. However, with conventional mechanical braking systems, they often have different braking forces between the wheels. So sometimes in an emergency, the braking system, especially in heavy vehicles could induce vehicle rollover. To overcome the drawback of the passive brake system, Anti-lock Braking Systems, Electronic Braking Systems and Electronic Stability Programs are used to help prevent vehicle rollover, because they can automatically adjust the braking force for each wheel, possibly giving the driver greater control in vehicles of poorer standards of quality and difficult driving conditions.

- **Avoidance of an obstacle:** when a driver attempts to avoid an obstacle in its path, the more natural human response is to make the turn too abruptly, resulting in a possible vehicle rollover situation. The turnover situation is usually caused through the over correction of the initial avoidance manoeuvre, resulting in a cumulative pendulum action, which may increase or decrease as the vehicle continues in a straight line. With vehicles that have a high centre of gravity, such as double deck trailer units, car transporters, liquid or powder tankers, etc., this pendulum action is often repeated, amplified and increases the rollover risk.
- **Driver error:** it is responsible for over three-quarters of all vehicle rollovers. Over 90 percent of the time, the rollover is not the "first" event - in other words, some other dangerous event occurs before the creation of the rollover event. It might be the lack of attention, drowsiness, distraction or simply not assessing the path ahead, all of these can result in a sudden awareness of danger, and therefore creating an acute reaction to avoid danger. This can cause the driver to turn sharply, and therefore can also contribute to vehicle rollover. Attentive driving can prevent most rollovers.
- **Excess speed:** the speed of the vehicle is always one of the most important factors related to the rollover phenomenon. The steering wheel velocity, magnitude of the steering angle and vehicle speed are the three factors that greatly affect the vehicle's roll stability. The compliance with the maximum allowable limiting speed is always a top priority and also compulsory for all drivers.



Figure 1.2: Long combination vehicle in a Jack-knifing [*Jackknifing*].

- **Jack-knifing:** it is a common trucking accident term that refers to a dangerous situation when a semi-trailer skids, causing the trailer to swing out to one side forming an angle that resembles the angle that the blade of a jackknife forms with its protective handle, as shown in Figure 1.2. The primary reason for jack-knifing to occur is equipment failure, wheels locking due to sudden hard braking and poor grip from adverse driving conditions. Depending on the speed that the vehicle is travelling, jack-knifing can result in vehicle rollover [Fossum and Lewis 1981].
- **Load:** the majority of vehicle rollover accidents occur due to factors associated with the load. This can be because the load is inadequately secured or loaded incorrectly.

The effect of the load is evident in the fact that it has twice the effect on rollover of other vehicle crashes. The load variation will lead to a change in the height of the centre of gravity, which directly affects the vehicle's centre of gravity, therefore altering the rollover threshold.

- **Road design:** The road design can also contribute significantly to vehicle rollover. Roundabouts, adverse cambers, slip roads, dual carriageway contra-flow lane changes and double bends can all play a role. Therefore, the design standards for roads and vehicles must focus on maximum safety.
- **Suspension systems:** there are many types of suspension systems on vehicles. It is extremely important to have the appropriate suspension settings aligned to different situations. Incorrectly set ride height, poor condition and wrong pressures for air suspension units, and failure to reset the ride height control valve after loading/unloading can all increase the likelihood of vehicle rollover. The controlled suspension has been researched for the purpose of improving roll stability of the vehicle. For heavy vehicles, this approach is limited by too much energy consumption. Meanwhile, for cars, it has proven to be quite effective.

In addition to the main causes listed above, there are many others that can lead to vehicle rollover. Determining the causes and offering alternate solutions to reduce the vehicle rollover phenomenon are an extremely important task, but it also has many difficulties. It depends on the type of vehicle and its' specific operating conditions and so far, there is no such thing as a perfect solution.

1.2 The mechanics of vehicle rollover

There are limits to achievable roll stability that are inherent in any vehicle. By understanding these limits, it is possible to formulate a set of objectives for the control system design and to measure the performance of a potential controller against the best performance theoretically possible. The final objective is to design an active anti-roll bar system that can improve roll stability of heavy vehicles. Therefore it is necessary to first study the mechanics of the vehicle rollover process and then, it is possible to identify the different and important mechanisms of the active anti-roll bar system.

1.2.1 Vehicle rollover threshold

The vehicle rollover threshold is often used to quantify roll stability. The most important input that can cause vehicle rollover is the lateral acceleration at the CG during a cornering manoeuvre. The effects of side wind gusts, excessive road camber and irregularities in the road surface are of secondary importance and are not considered here. The vehicle rollover threshold concept is defined as follows [Sampson 2000]:

Definition 1.2.1 (Vehicle rollover threshold). *The vehicle rollover threshold is the limit of the steady state lateral acceleration that a vehicle can sustain without losing roll stability.*

It is clear that both static and dynamic problems have an influence on the vehicle roll stability, however a steady state analysis of the vehicle roll stability is sufficient to give an insight into the major elements governing the roll response of the vehicle [Sampson 2000].

1.2.2 The simplified roll model

There is a very strong relationship between the static roll stability of heavy vehicles and the actual occurrence of rollover accidents. However, as previously mentioned, it has already been proven that a steady state analysis of roll stability is sufficient to give an insight into the major elements governing the roll response of the vehicle [Sampson 2000]. Accordingly, this section will discuss the mechanics of the vehicle rollover phenomenon in a steady state manoeuvre in order to explain how this fundamental performance property derives from the mechanical behavior of the various components of the vehicle.

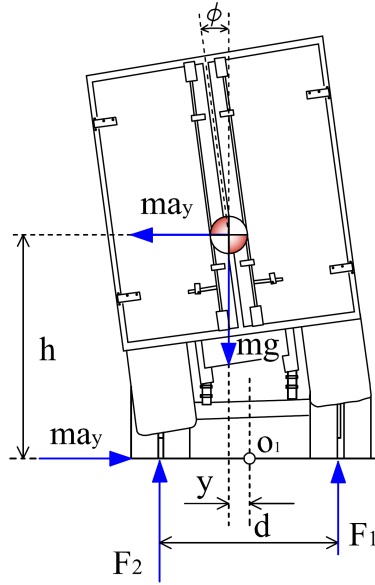


Figure 1.3: A simplified roll model: a heavy vehicle in a steady state manoeuvre.

Figure 1.3 presents a simplified heavy vehicle model in a steady state manoeuvre, its tyres, and suspension system have been aggregated into a single roll model, where F_i are the vertical tyre loads ($i = 1, 2$), a_y the lateral acceleration, h the height of the CG, d the track width, m the weight of the vehicle, y the lateral motion of the CG relative to the track. The equilibrium equation for the roll moment about a point on the ground at the center of the track (point O_1) is as follows:

$$m a_y h = (F_2 - F_1) \frac{d}{2} - m g y \quad (1.1)$$

There are three different moments acting on the vehicle as follows:

- $M_1 = ma_y h$: the primary overturning moment arises from the lateral acceleration. It is a destabilizing moment.
- $M_2 = (F_2 - F_1)\frac{d}{2}$: the restoring moment arises by the lateral load transfer from the inside tyres to the outside tyres. It is a stabilizing moment.
- $M_3 = mgy$: the lateral displacement moment arises from the roll motion which displaces the centre of mass laterally from the nominal centre line of the vehicle. It is a destabilizing moment.

In equation (1.1) the left part is from the external imposition of the lateral acceleration while the right part is from the internal compliant reaction of the vehicle. The two destabilizing moments (M_1, M_3) are opposed by one stabilizing moment (M_2). The maximum possible value of the stabilizing moment is $mg\frac{d}{2}$ which occurs when all the load is transferred to one side of the vehicle, i.e., when $F_2 = mg$ and $F_1 = 0$. According to the value of the lateral motion of the CG relative to the track y (as see in Figure 1.6), there are three cases of interest as follows:

- **The first case, $y = y_0$:** the vehicle is a rigid-body, the role of the suspension and tyres is ignored, so the lateral motion of the CG $y_0 = 0$. This case is called the rigid vehicle.
- **The second case, $y = y_1$:** the role of the suspension is ignored. Due to the effect of the tyre deflection, the lateral motion of the CG is y_1 . This case is called the vehicle with compliant tyres.
- **The third case, $y = y_1 + y_2$:** the role of the suspension and the tyres are considered. The lateral motion of the CG y_2 is made by the effect of the suspension deflection. This case is called the vehicle with a roll-compliant suspension.

Today, almost all modern vehicles are equipped with the passive suspension system, so the role of the suspension and tyres would not be ignored. To better understand the vehicle rollover phenomenon, the three cases that are mentioned above will be detailed and compared in the next sections.

1.2.3 Rollover of the rigid vehicle

A graphic representation of equation (1.1) for a completely rigid vehicle is shown in Figure 1.4. The left side of the equation (1.1) is presented on the left side of the graph in a plot of the roll moment versus the lateral acceleration. The right side of equation (1.1) is presented on the right side of the graph in a plot of the roll moment versus the roll angle.

Due to the rigidity of this vehicle, any roll of the vehicle results immediately in complete transfer of the whole vertical load onto the tyres at one side of the vehicle. The unloaded

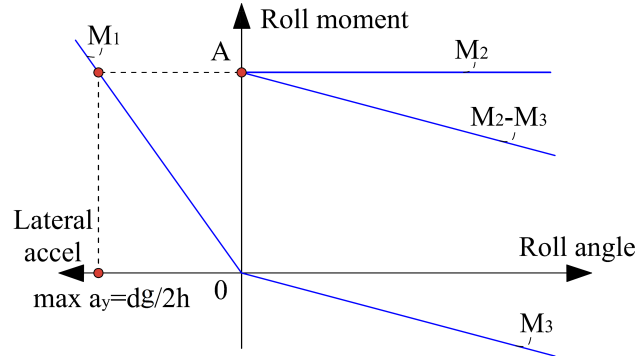


Figure 1.4: Graphic presentation of the roll-equilibrium equation for a rigid vehicle.

tyres would immediately lift from the ground. This is reflected in the plot of the restoring moment shown as an horizontal line at the maximum value of $M_{2max} = mg\frac{d}{2}$ (point A). However, the lateral displacement moment grows proportionately (and negatively) with the roll angle. This behavior is shown in the downward sloping plot of the lateral displacement moment (M_3). The sum of the restoring moment and the (negative) lateral displacement moment ($M_2 - M_3$) constitutes the total vehicle reaction as expressed by the right side of equation (1.1). The graph shows that this combined function achieves its maximum value at zero roll angle. The negative slope of this plot at all roll angles, indicates that the vehicle becomes immediately unstable as its tyres lift from the ground. By projecting the maximum value of this right side total onto the plot of the left side of equation (1.1), it can be seen that the maximum lateral acceleration that can be sustained by this rigid vehicle in an equilibrium condition is as follows:

$$a_{ymax} = \frac{dg}{2h} \quad (1.2)$$

It is well known that the rigid vehicle stability factor of $\frac{d}{2h}$, is the most fundamental vehicle property which influences basic roll stability [Christopher and Robert 1999], [Sampson 2000].

1.2.4 The vehicle with compliant tyres

The tyres are represented by linear vertical springs. The vehicle rolls about a point located on the ground plane at the center of the track (point O_1), as shown in Figure 1.3. The left tyre compresses, while the right tyre extends. The lateral motion of the CG relative to the track y is approximated as follows:

$$y_1 = h\phi \quad (1.3)$$

A graphic representation of equation (1.1) for a vehicle with compliant tyres is shown in Figure 1.5. The restoring moment M_2 is shown to develop progressively with the roll angle. The maximum restoring moment is achieved when the right tyre lifts off from the ground, with the roll angle being ϕ_L . At ϕ_L , the lateral displacement moment M_3 has grown to a negative value of $mgh\phi_L$. The maximum value of the total vehicle reaction moment ($M_2 - M_3$) is achieved just as the right tyre lifts from the ground at the roll angle of ϕ_L (point B). The

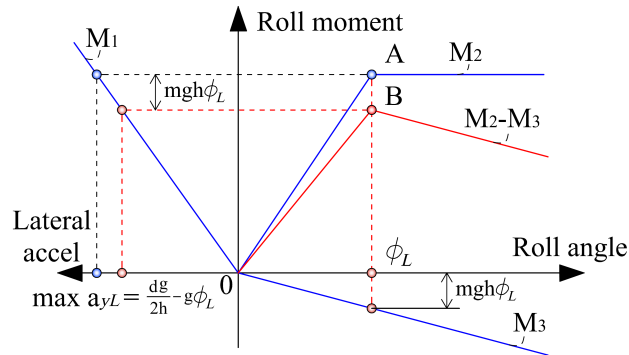


Figure 1.5: Graphic presentation of the roll equation for a vehicle with compliant tyres.

maximum value of the lateral acceleration a_{yL} is determined in equation (1.4) [Segel and Dorgham 1987].

$$a_{yLmax} = \frac{dg}{2h} - g\phi_L \quad (1.4)$$

From Figure 1.5, we can see that the maximum value of the total vehicle reaction moment ($M_2 - M_3$) is in this case less than that of the rigid vehicle. So the compliant tyres will reduce roll stability of the vehicle, compared to the rigid vehicle. When the roll angle is greater than ϕ_L , the lateral displacement moment M_3 continues to increase but the restoring moment M_2 is saturated. The resulting downward slope of the total vehicle reaction again indicates an unstable system.

1.2.5 The vehicle with roll-compliant suspension

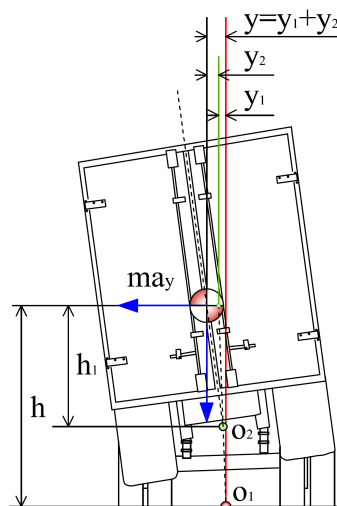


Figure 1.6: Tyres and suspension roll motions occur at the different centers.

There are two axes of roll motion when considering the role of both the suspension and the tyres. They are the roll axis for the tyres only (point O_1) and the roll axis of the sprung mass above the unsprung mass (point O_2), as shown in Figure 1.6. The effect of roll compliance of the suspension is very similar to the effect of tyre compliance, however the suspension roll motion takes place about a roll axis which is typically well above the ground (point O_2). The lateral motion of the CG is y_1 due to the effect of the tyre deflection, while y_2 is due to the effect of the suspension deflection. The total lateral motion of the CG is defined as: $y = y_1 + y_2$. From Figure 1.6, it is clear that the height of the suspension roll axis has two influences: (a) for a given roll angle condition, the lateral motion of CG is less if the suspension roll axis is higher (h_1 small). (b) for a given CG height, the roll moment acting on the suspension is less if the suspension roll axis is higher. This leads to a reduction of the roll angle of the vehicle [Christopher et al. 2000].

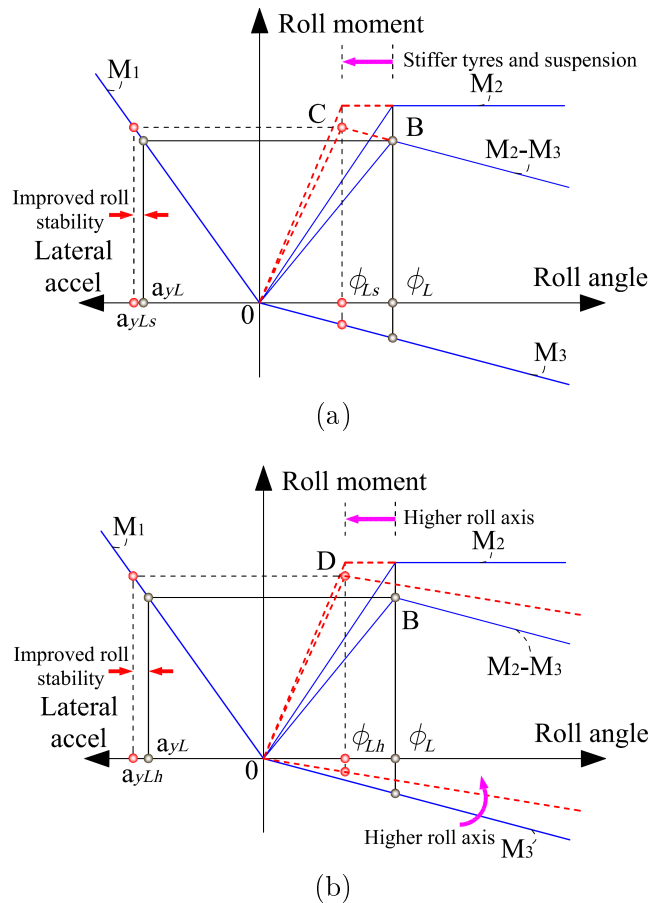


Figure 1.7: The effect of (a) the tyre and suspension stiffness, (b) the suspension roll axis on the vehicle rollover threshold.

In the following section, we will examine the effect of the tyres and suspension stiffness, and the height of the suspension roll axis O_2 on the vehicle rollover threshold. It is worth noting that in Figure 1.7, the initial vehicle behaviour is plotted by the continuous line. When the right

tyre starts to lift off from the ground, the roll angle and lateral acceleration are respectively ϕ_L , a_{yL} , as defined in equation (1.4). In the two cases of the stiffer tyres and suspension along with the higher suspension roll axis, the vehicle behaviours are plotted by the dash line.

- **The effect of the tyre and suspension stiffness:** if the roll stiffness (tyre and suspension stiffness) increases, then the vehicle roll angle reduces. Consequently, at the point when the right tyre lifts off from the ground with the vehicle roll angle ϕ_{Ls} , the lateral displacement moment M_3 is smaller. As shown in Figure 1.7a, the maximum value of the lateral acceleration a_{yLs} is higher than a_{yL} . It means that the roll stability of the vehicle is improved with the stiffer tyres and suspension.
- **The effect of the height of the suspension roll axis:** as mentioned above, due to increasing the height of the suspension roll axis, the vehicle roll angle and the lateral displacement moment M_3 will be reduced. At the time when the right tyre starts to lift off from the ground, the vehicle roll angle ϕ_{Lh} is smaller than ϕ_L , as shown in Figure 1.7b. Due to the maximum value of the lateral acceleration a_{yLh} being higher than a_{yL} , so the roll stability of the vehicle is also improved with the higher suspension roll axis.

As mentioned above, heavy vehicles often use a passive suspension system, so the role of the suspension and tyres always exists. However, the stiffness of the tyres and the suspension, as well as the suspension roll axis only have little change. Therefore most heavy vehicles are equipped with the passive anti-roll bar system on all axles in order to improve roll stability. The passive anti-roll bar force is applied at each side of the vehicle so that the left force has the same magnitude as the right one, but in the opposite direction. The passive anti-roll bar has the advantage to reduce the body roll acceleration and roll angle during single wheel lifting and cornering manoeuvres. By reducing the body roll motion, vehicle safety and roll stability are highly improved. However, passive anti-roll bars do have drawbacks. During cornering manoeuvres, the anti-roll bar will transfer the vertical forces of one side of the suspension to the other one, creating therefore a yaw moment [Zulkarnain et al. 2012].

In order to overcome such drawbacks, several schemes concerned with the possible active intervention on vehicle dynamics have been proposed as follows:

- Active steering system [Imine, Fridman, and Madani 2012], [Lee 2013], [Imine and Djemaï 2016];
- Active braking system [Odenthal, Bunte, and Ackermann 1999], [Lee 2013];
- Active suspension system [Cole 2001], [Ieluzzi, Turco, and Montiglio 2006], [Imine 2014], [Amin 2015];
- Active anti-roll bars system [Sampson 2000], [Yu, Guvenc, and Ozguner 2008], [Yu et al. 2010], [Babesse and Ameddah 2014].

Among them, the most common method used to improve the vehicle roll stability is the active anti-roll bar system. In the next section, a detailed survey will be conducted to synthesize

previous studies of active systems and how they have been used to improve roll stability of heavy vehicles, specifically the author focuses on the active anti-roll bar system.

1.3 Review of previous research

It is necessary to emphasize that during the last twenty years, the interest and efficiency of active anti-roll bars for heavy vehicles have been studied and demonstrated in numerous pieces of literature. Several models and control methods have indeed been used for the two main types of heavy vehicles:

- **Long combination heavy vehicles:** exemplary studies of the active anti-roll bar system on long combination heavy vehicles include those from the University of Cambridge in UK, led by Professor David Cebon. They succeeded in studying theoretical simulations [Sampson and Cebon 1998] and the Cambridge Vehicle Dynamics Consortium (CVDC) sponsored the construction of the experimental vehicle [Miège and Cebon 2005a]. The experimental results clearly demonstrated the effectiveness of the active anti-roll bar system for improving roll stability of a articulated vehicle [Miège and Cebon 2005b]. This approach has also recently been of interest to other authors, as in the study [Hsun-Hsuan, Rama, and Dennis 2012]. However, long combination heavy vehicles are beyond the scope of this study.
- **Single unit heavy vehicle:** The basic study of the active anti-roll bar system on a single unit heavy vehicle also came from the University of Cambridge, when Dorling and Sampson conducted their doctoral dissertations under the supervision of Professor David Cebon [Dorling 1996], [Sampson 2000]. However, the direction of this research has been further developed, and we must mention the studies of Professor Peter Gaspar and his colleagues at the Hungarian Academy of Sciences [Gaspar, Bokor, and Szaszi 2004], [Gaspar, Bokor, and Szaszi 2005]. In this thesis, the single unit heavy vehicle will also be used in combination with specific actuators.

In the following sections, the author will summarize the main previous studies of the active anti-roll bar system of a single unit heavy vehicle, with different vehicle models and control methods. Therefore, it will highlight the developmental directions of this thesis.

1.3.1 Different models of heavy vehicles

Two main models are used to study the active anti-roll bar system of single unit heavy vehicles: the Roll model and the Yaw-Roll model (see Chapter 2 for details). In both of these models, the role of the vertical motion is not taken into consideration. This is perfectly acceptable because the purpose of the active anti-roll bar system is to improve the roll stability of heavy vehicles.

1.3.1.1 The Roll model

We can mention the following typical studies: [Cole 2001], [Miège and Cebon 2002], [Yu, Guvenc, and Ozguner 2008]. In this model, the disturbance input is the lateral acceleration at the CG, two suspension systems at the two axles are merged to be one, the control signal is the torque generated by the active anti-roll bar system. In [Miège and Cebon 2002], the roll model of heavy vehicles is considered with a servo-valve hydraulic actuator and the input control signal is the spool valve displacement of the servo-valve. Besides the use of this model for a single unit heavy vehicle, it is also used for the articulated vehicle [Miège 2000]. This model has the advantage of being simple to synthesize the controller, however such a model cannot be used to assess the entire behavior of the single unit heavy vehicle.

1.3.1.2 The Yaw-Roll model

Most studies on active anti-roll bar systems use the yaw-roll model with the force (or torque) as the input control signal [Sampson 2000], [Gaspar, Bokor, and Szaszi 2004], [Boada et al. 2007]. In this model, the role of the two suspension systems is completely independent, the input signal is the steering angle. This model has been proven to be stable and consistent with the behavior of the single unit heavy vehicle. Nevertheless, it still lacks accuracy since no actuator model is included.

Thus, the yaw-roll model taking into account the presence of the actuators is a very important requirement for further research on the active anti-roll bar system of heavy vehicles. However, the type of actuator and its operability are also a prerequisite to the quality of the real system when applied in practice. This problem will be discussed and a solution proposed in Chapter 2.

1.3.2 Control methods for the active anti-roll bar system on heavy vehicles

Some of the control methods applied for the active anti-roll bar control of heavy vehicles are the optimal control (LQR, LQG), the neural network control and the robust control. It can be seen in general that the control methods used for this system are not as diverse as in other studies of vehicle control systems, such as active or semi-active suspension systems. They are briefly presented below.

1.3.2.1 Optimal control

Sampson *et al* [Sampson and Cebon 1998], [Sampson and Cebon 2003a] and Miego *et al* [Miège and Cebon 2005b] proposed a state feedback controller which was designed by finding an optimal controller based on a linear quadratic regulator (LQR) for both single unit and articulated heavy vehicles. They used the control torques acting between the axle groups and the sprung mass as the input control signal. This led to reducing the steady state and

peak transient load transfer significantly when compared to a passive vehicle. The influence of frame flexibility on the controller design was also investigated. However their LQR designs required that all the internal states of the system are available for feedback. Typically this is not practical because it may be difficult or prohibitively expensive to measure certain states, for example, side-slip angle. Furthermore the sensor output signals will be corrupted to some extent by noise, so to accurately deduce all the different states even from a complete set of measured outputs is not straightforward. In [Sampson 2000], the author used LQG control by combining the LQR controller and the Kalman filter. The loop transfer recovery (LTR) method was also developed; it is a technique for indirectly shaping the singular values of the LQG loop transfer function with the aim of recovering the guaranteed favourable stability margins of the LQR control. The two step LQG-LTR control design procedure consists of a loopshaping step and a recovery step. Simulations show that the active anti-roll bar control can increase the rollover threshold of a torsionally rigid single unit vehicle by 23%. The improvements in roll stability in severe transient manoeuvres can be even greater. The author guessed a possible reduction in the frequency of rollover accidents of up to 50%. However, the effectiveness of the active anti-roll bar control is only assessed when the vehicle speed is constant at 60 *km/h*. In other velocity regions, there are no surveys.

H. Yu *et al* [Yu, Guvenc, and Ozguner 2008] proposed a rollover threat warning system that uses the real-time dynamic model-based time-to-rollover metric as a basis for online rollover detections. The simulations performed using TruckSim[®] indicated that a rollover threat detection system was further enhanced in combination with an active roll control system. This was done by designing an optimal control strategy (LQR), which was able to improve the dynamic roll stability in vehicle turning and emergency driving situations.

1.3.2.2 Neural network control

The main advantages of the implemented neural network control are its good performance to control non-linear systems; it is a free-model control and it learns on-line, so that the system can adapt to changes produced in the environment. In [Boada et al. 2007], the authors proposed a reinforcement learning algorithm using neural networks to improve roll stability for a single unit heavy vehicle. The input control signals are the torques at the axles. In this case, it is only necessary to measure a unique variable (the sprung mass roll angle) to control the vehicle, so both the number of sensors and cost are reduced. Simulation results show the effectiveness of the proposed control system during different manoeuvres such as J-turn and double change lane. Even if the neural network control has some advantages as mentioned above, it is however not suitable for embedded control.

1.3.2.3 Robust control (LPV)

The most representative studies that applied the robust control or Linear Parameter Varying (LPV) on the active anti-roll bar system of a single unit heavy vehicle came from a team led by Professor Peter Gaspar at the Hungarian Academy of Sciences [Gaspar, Bokor, and Szaszi 2004], [Gaspar, Bokor, and Szaszi 2005]. They applied the LPV approach for the active

anti-roll bar system combined with the active brake control system. The goal is to design the controller that uses the active anti-roll bar system continuously to prevent rollover. The controlled braking system is only activated when the vehicle comes close to the rollover situation. In a normal driving situation the brake part of the control should not be activated. However, if the normalized load transfer reaches a critical value, the brake system has to minimize the lateral acceleration to prevent rollover. The critical value of the normalized load transfer is determined when the load transfer of one of the inner curve wheels tends to zero. The authors also used a Fault Detection and Identification (FDI) filter. The purpose of the FDI filter is to identify the different actuator failures together with the time of their occurrence and their values. The FDI filter design is based on the LPV model of the vehicle, in which the scheduling parameter is the forward velocity of the vehicle. In the case of a detected failure, the operation of the control mechanism must be modified. For this purpose, the normalized fault parameter is also applied as a scheduling parameter. Using fault information, this reconfigurable feature leads to an enhanced roll stability when a fault occurs in the hydraulic actuator.

The simulation results have proven the effectiveness of the control design based on LPV modelling, in which the forward velocity and the normalized lateral load transfer at the rear are chosen as scheduling parameters. However, the adaptation weighting function is only considered for the lateral acceleration. They did not take into account directly the varying weighting functions for the normalized load transfers at the two axles. Although they considered the possibility of hydraulic actuator failures, the vehicle model does not include the actuator, so the evaluation of this fault is only qualitative.

In the above sections, the author gives an overview of the previous studies on the active anti-roll bar system with single unit heavy vehicles. For a better view, the synthesis of vehicle models and control methods is shown in Figure 1.8, with the symbol "+", indicating that the research was done. We can see that there is a poor study of the active anti-roll bar system on heavy vehicles, so further research is needed on this system.

		Vehicle model	
		(Single unit heavy vehicle)	
		Roll model	Yaw-Roll model
Control methods	LQR, LQG	+	+
	Neural networks		+
	LPV		+

Figure 1.8: Summary of previous studies on active anti-roll bar of a single unit heavy vehicle.

1.4 Control objectives

As mentioned previously, due to the potential that heavy vehicles often have a large weight and a high CG, rollover is an important road safety problem world-wide. The active anti-roll bar system is designed to meet simultaneously the three following objectives:

- **Roll stability:** the main objective of the active anti-roll bar system is to use roll moments from actuators to maximise roll stability of the vehicle. The general notion of roll stability must be translated into a specific set of plant outputs to be regulated. Roll stability is achieved by limiting the normalized load transfers at all axles in the range $[-1, 1]$, in the frequency range to over 4 rad/s [Sampson 2000].
- **Saturation of the actuators:** apart from the main objective of improving roll stability, the saturation of the actuators is extremely important. For example, in the electronic servo-valve hydraulic actuator that will be used in this thesis, the saturation is expressed by the maximum absolute value of the spool valve displacement less than $4.85 \times 10^{-4} \text{ m}$ [Rafa, Yahya, and Rawand 2009], input currents of less than 20 mA [Rafa, Yahya, and Rawand 2009], load flows of less than $2.2 \times 10^{-3} \text{ m}^3/\text{s}$ [Sampson 2000], and forces of less than 120 kN [Sampson 2000].
- **Limits of the suspension travel:** expressed by the roll angles between the sprung and unsprung masses ($\phi - \phi_{u,f,r}$) being less than 7 to 8 deg [Gaspar, Bokor, and Szaszi 2004].

These objectives may be considered to form a preliminary design specification for an active anti-roll bar system. The following chapters consider the fundamental limitations to how well this preliminary specification can be met.

1.5 Perspectives

As emphasized in this chapter, the rollover of heavy vehicles and the role of an active anti-roll bar system seem to be a very interesting problem for further theoretical investigations, but also for practical applications where many problems are still not solved. In this framework, one of the new challenges lies with both actuators and the active anti-roll bar control where control methods are not widely explored yet.

1.5.1 Some open research topics and potential extensions:

A - Potential topics that should be explored in the next years (vehicle and actuator modelling):

- The yaw-roll model does not include the vertical motion, so one full vehicle model of a single unit heavy vehicle using an active anti-roll bar system would be necessary.

- There are many types of actuators that can be used for the active anti-roll bar system, but most of them have nonlinear characteristics. Therefore, the evaluation of the effectiveness of the control methods considering nonlinear actuator models will result in more accurate results.

B - Moreover, concerning vehicle control (and estimation), potential issues are related with:

- The synthesis of fault tolerant controllers that handle an actuator failure, so that it is possible to manage the vehicle dynamical problem by using another actuator. This problem is related to fault detection problems, reconfiguration, etc. which are close to observation, switch, and LPV theories.
- The developments of new active anti-roll bar strategies that can improve roll stability and reduce energy consumption of the actuators.
- The collaboration between the different active roll control systems, such as active anti-roll bar, active braking, active steering and active suspension systems. That will come close to the concept of "Global Chassis Control".

1.5.2 Perspectives "explored" in this thesis:

In this thesis, firstly based on the yaw-roll model presented in [Gaspar, Bokor, and Szaszi 2004], an integrated model is proposed with four Electronic Servo-Valve Hydraulic (ESVH) actuator models in a single unit heavy vehicle yaw-roll model. Secondly, some advance control methods are used for the active anti-roll bar system, such as: LQR, H_∞ , LPV. Then the effectiveness of the active anti-roll bar system is confirmed by the use of TruckSim[®] software. The main contributions of this thesis are summarized in Figure 1.9. In Chapter 9, the author also mentions the initial research on the active brake system, with the control aim to allow the active brake system to keep working when vehicles reach their rollover limit.

		Vehicle model (Single unit heavy vehicle)			
		Roll model	Yaw-roll model	Integrated model <i>(ESVH actuators + Yaw-roll)</i>	TruckSim [®] <i>(ESVH actuators + TruckSim)</i>
Control methods	LQR			+	
	H_∞			+	+
	LPV			+	+

Figure 1.9: Summary of thesis contributions on the active anti-roll bar system.

Vehicle Modeling

Contents

2.1	Introduction	27
2.2	An electronic servo-valve hydraulic actuator model	29
2.2.1	The electronic servo-valve model	29
2.2.2	The hydraulic cylinder model	32
2.3	The Yaw-Roll model of a single unit heavy vehicle	34
2.4	The integrated model of a single unit heavy vehicle	37
2.4.1	The fully integrated model	37
2.4.2	The control-oriented integrated model	39
2.4.3	The variables of interest	41
2.5	The design of a passive anti-roll bar system	42
2.5.1	The design of the passive anti-roll bar by using the <i>SAE</i> spring design manual	42
2.5.2	The effectiveness of the passive anti-roll bar on vehicle roll stability	44
2.6	Conclusion	46

2.1 Introduction

Active roll control systems for heavy vehicles have been studied for more than two decades, and it has been proven that roll stability can be improved and rollover can be prevented in an emergency situation. Among active roll control systems, the most common methods used to improve roll stability are active anti-roll bar systems which are usually made with a pair of hydraulic actuators. Indeed lateral acceleration makes vehicles with a conventional passive suspension tilt out in corners. The center of the sprung mass shifts outward of the vehicle centerline, which then, on the other hand, creates a destabilizing moment that degrades roll stability. The lateral load response is reduced by an active anti-roll bar system that generates a stabilizing moment to counterbalance the overturning moment in such a way that the control torque leans the vehicle into the corners. Figure 2.1 describes the ideal structure of an active anti-roll bar system applied on one axle of a heavy vehicle.

There are two main models used to study an active anti-roll bar system on a single unit heavy vehicle:

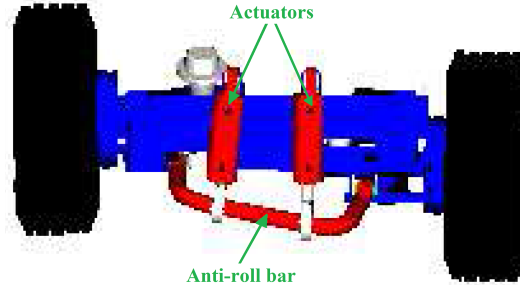


Figure 2.1: An active anti-roll bar system applied on one axle of heavy vehicles [Miège 2000].

- The *Roll model* [Miège and Cebon 2002], [Yu, Guvenc, and Ozguner 2008], [Cole 2001];
- The *Yaw-Roll model* [Sampson 2000], [Gaspar, Bokor, and Szaszi 2005].

In Miegé *et al* [Miège and Cebon 2002], the roll model for heavy vehicles (2 DOF) is considered with a servo-valve hydraulic actuator and the input control signal is the spool valve displacement of the servo-valve. However such a model cannot be used to assess the entire behavior of the heavy vehicle.

Most studies on the active anti-roll bar system use the yaw-roll model with the force (or torque) as the input control signal [Boada et al. 2007], [Gaspar, Bokor, and Szaszi 2004]. This model has been proven to be stable and consistent with the behavior of a single unit heavy vehicle. Nevertheless, it still lacks accuracy since no actuator model is included.

Based on the yaw-roll model presented in [Gaspar, Bokor, and Szaszi 2004], this chapter proposes an integrated model with four Electronic Servo-Valve Hydraulic (ESVH) actuators in a single unit heavy vehicle yaw-roll model. The spool valve displacements are controlled to distribute high pressure oil into the two chambers of the hydraulic cylinders. The input currents of the ESVH actuators are controlled to generate the force in various manoeuvring situations. The use of four ESVH actuators in a yaw-roll model of a single unit heavy vehicle is an evolution, compared to previous studies.

Here, we consider two types of integrated models for the active anti-roll bar system in a single unit heavy vehicle:

- A fully integrated model, with the four ESVH actuators being independently controlled.
- A control-oriented integrated model, using one ESVH actuator on the right at the front axle and one ESVH actuator on the right at the rear axle. This model has been presented in “*Enhancing roll stability of heavy vehicle by LQR active anti-roll bar control using electronic servo-valve hydraulic actuators, Vehicle System Dynamics, Vol 55(9), pp 1405-1429, 2017*” and “*Active anti-roll bar control using electronic servo-valve hydraulic damper on single unit heavy vehicle, 8th IFAC Symposium on Advances in Automotive Control, Sweden, 2016*”.

In the next section, the model of the considered controlled hydraulic actuator will be proposed and presented. The control signal is the electrical current u opening the electronic servo-valve, the output is the force F_{act} generated by the hydraulic actuator.

2.2 An electronic servo-valve hydraulic actuator model

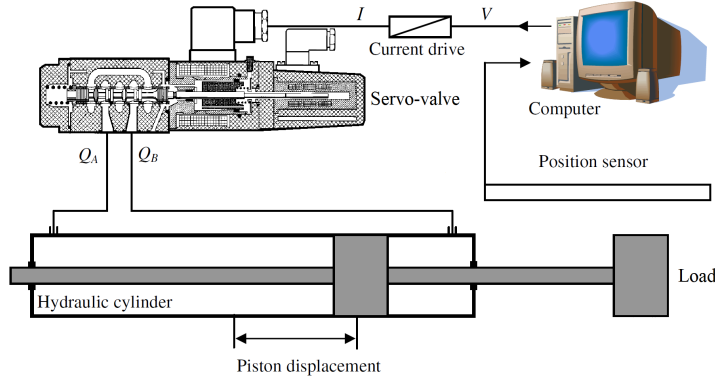


Figure 2.2: Structure of the general electronic servo-valve hydraulic system [Kalyoncu and Haydim 2009].

An Electronic Servo-Valve Hydraulic (ESVH) system is one of the most important drive systems in the industrial sector and most engineering practices due to its high power to weight ratio, stiffness response, good performance, and smooth fast action. The range of applications for ESVH systems are diverse, and includes: manufacturing systems, material test machines, active systems on vehicles, mining machinery, fatigue testing, flight simulation, marine engineering, robotics, etc [Has et al. 2014].

The ESVH actuator includes the main elements such as: (1) a servo regulator (controller), (2) a servo-valve, (3) an hydraulic cylinder, (4) a feedback position transducer and (5) a power supply. Figure 2.2 illustrates the diagram of the general ESVH system. The two elements of the ESVH actuator (the electronic servo-valve, the hydraulic cylinder) will be modelled in the sequel.

2.2.1 The electronic servo-valve model

The three-land-four-way spool valve is used in the ESVH actuator with the diagram shown in Figure 2.3. The displacement of the spool valve X_v is controlled by the electrical current u . The effects of hysteresis and flow forces on the servo-valve are neglected here, then the dynamical behavior of the electronic servo-valve can be approximated by a first-order model [Rafa, Yahya, and Rawand 2009], [Renn and Wu 2007], as:

$$\frac{dX_v}{dt} + \frac{1}{\tau}X_v - \frac{K_v}{\tau}u = 0 \quad (2.1)$$

where τ is the time constant and K_v the gain of the servo-valve model.

The diagram of the flows direction of the three-land-four-way spool valve is shown in Figure 2.4. The four orifices are completely analogous to the four arms of a wheatstone bridge. Arrows at the ports indicate the assumed direction of the different flows, and the numbers at the ports

refer to the subscripts of the flow and the area at the ports. Because the compressibility flows are zero therefore the continuity equations for the two valve chambers are:

$$Q_L = Q_1 - Q_4 = Q_3 - Q_2 \quad (2.2)$$

where Q_L is the load flow through the actuator, and $Q_{i(i=1,4)}$ the load flow through the orifices, respectively.

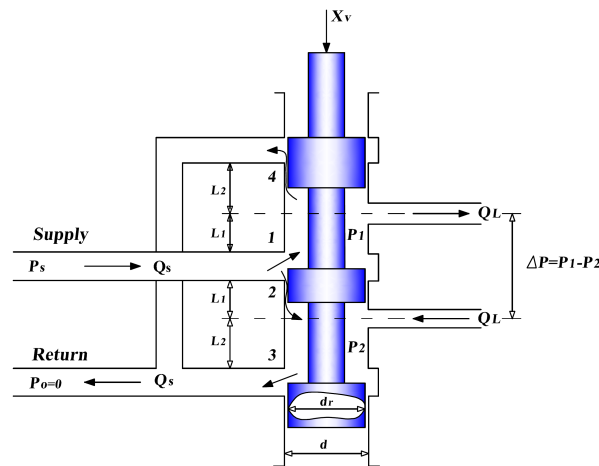


Figure 2.3: Diagram of the three-land-four-way spool valve [Merritt 1967].

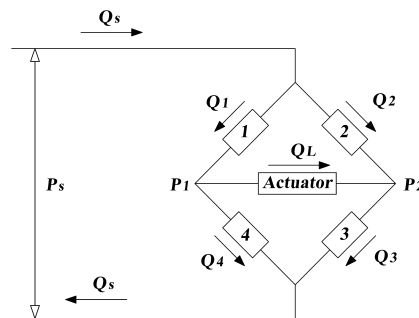


Figure 2.4: Diagram of the flow directions of the three-land-four-way spool valve [Merritt 1967].

The differential pressure inside the hydraulic cylinder is defined as:

$$\Delta P = P_1 - P_2 \quad (2.3)$$

The different flows through the valve orifices are described as follows [Merritt 1967]:

$$\begin{cases} Q_1 = C_d A_1 \sqrt{\frac{2}{\rho}(P_s - P_1)} \\ Q_2 = C_d A_2 \sqrt{\frac{2}{\rho}(P_s - P_2)} \\ Q_3 = C_d A_3 \sqrt{\frac{2}{\rho}P_2} \\ Q_4 = C_d A_4 \sqrt{\frac{2}{\rho}P_1} \end{cases} \quad (2.4)$$

where ρ is the fluid mass density, A_i the orifice areas, and C_d the discharge coefficient. The orifice areas (A_1, A_2, A_3, A_4) depend on the valve geometry and they are function of the spool valve displacement X_v as follows:

$$\begin{cases} A_1 = A_1(X_v) \\ A_2 = A_2(-X_v) \\ A_3 = A_3(X_v) \\ A_4 = A_4(-X_v) \end{cases} \quad (2.5)$$

Remark 2.1: *The valve orifices are usually matched and symmetrical. The requirement for the matched orifices are: $A_1 = A_3, A_2 = A_4$; and for the symmetrical orifices are: $A_1(X_v) = A_2(-X_v), A_3(X_v) = A_4(-X_v)$.*

Due to the orifices being symmetrically matched, the different flows in the diagonally opposite arms of the bridge in Figure 2.3 are:

$$\begin{cases} Q_1 = Q_3 \\ Q_2 = Q_4 \end{cases} \quad (2.6)$$

From equations (2.4) and (2.6), the oil supply high pressure is:

$$P_s = P_1 + P_2 \quad (2.7)$$

The pressures inside the two chambers of the hydraulic cylinder are determined from equations (2.3) and (2.7) as follows:

$$\begin{cases} P_1 = \frac{P_s + \Delta P}{2} \\ P_2 = \frac{P_s - \Delta P}{2} \end{cases} \quad (2.8)$$

From equations (2.2), (2.4), (2.6) and (2.8), for a matched and symmetrical servo-valve, the load flow through the hydraulic cylinder (Q_L) is defined as:

$$Q_L = C_d A_1 \sqrt{\frac{1}{\rho}(P_s - \Delta P)} - C_d A_2 \sqrt{\frac{1}{\rho}(P_s + \Delta P)} \quad (2.9)$$

The nonlinear algebraic equation (2.9) can be written as follows [Merritt 1967], [Rydberg 2016]:

$$Q_L = K_x X_v - K_P \Delta P \quad (2.10)$$

where the valve flow gain K_x and the total flow pressure coefficient K_P are defined as:

$$K_x = \frac{\delta Q_L}{\delta X_v}, \quad K_P = \frac{\delta Q_L}{\delta \Delta P} \quad (2.11)$$

In equation (2.10), the load flow of the ESVH actuator includes two parts: the first part ($Q_{L1} = K_x X_v$) is the orifice load flow through the servo-valve and is adjusted by the movement of the spool valve displacement X_v . The second part ($Q_{L2} = K_P \Delta P$) is the internal leakage load flow through the contact surface between the spool valve and the body of the servo-valve. The effect of the internal leakage inside the electronic servo-valve on the performance of the active anti-roll bar system will be considered in Chapter 8.

2.2.2 The hydraulic cylinder model

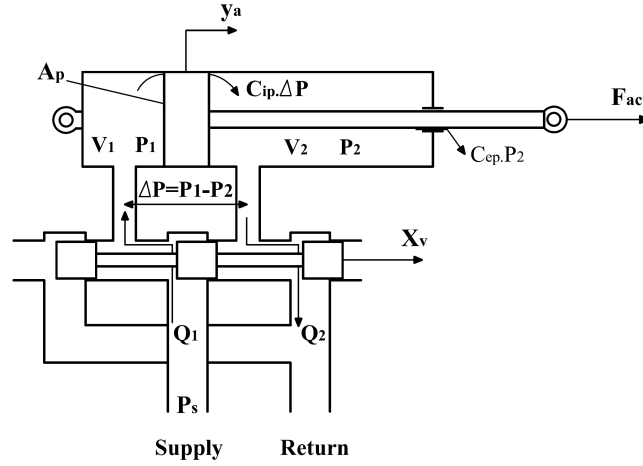


Figure 2.5: Diagram of the ESVH actuator [Miège 2000].

Figure 2.5 illustrates the diagram of an hydraulic cylinder in combination with an electronic servo-valve. The spool valve of the electronic servo-valve is controlled by a current which generates a displacement X_v . The high pressure oil supply P_s is always stored outside the electronic servo-valve and the moving spool valve distributes the high pressure oil into two chambers of the hydraulic cylinder. The difference of pressure $\Delta P = P_1 - P_2$ between the two chambers produces the output force F_{act} given by:

$$F_{act} = A_P \Delta P \quad (2.12)$$

where A_P is the area of the piston.

The equations for each chamber of the hydraulic cylinder can be written as:

$$\begin{cases} \frac{dV_1}{dt} + \frac{V_1}{\beta_e} \frac{dP_1}{dt} = Q_1 - C_{ip}(P_1 - P_2) - C_{ep}P_1 \\ \frac{dV_2}{dt} + \frac{V_2}{\beta_e} \frac{dP_2}{dt} = C_{ip}(P_1 - P_2) - C_{ep}P_2 - Q_2 \end{cases} \quad (2.13)$$

where β_e is the effective bulk modulus of the oil, C_{ep} and C_{ip} are the external and internal leakage coefficients of the hydraulic cylinder.

The volume in each chamber varies with the piston displacement y_a as:

$$\begin{cases} V_1 = V_{01} + A_p y_a \\ V_2 = V_{02} - A_p y_a \end{cases} \quad (2.14)$$

Table 2.1: Symbols and parameters of the ESVH actuator [Miège and Cebon 2002], [Rafa, Yahya, and Rawand 2009].

Symbols	Description	Value	Unit
A_P	Area of the piston	0.0123	m^2
K_x	Valve flow gain coefficient	2.5	m^2/s
K_P	Total flow pressure coefficient	4.2×10^{-11}	$m^5/(Ns)$
C_{tp}	Total leakage coefficient of the actuator	0	-
V_t	Total volume of trapped oil	0.0014	m^3
β_e	Effective bulk modulus of the oil	6.89×10^6	N/m^2
τ	Time constant of the servo-valve	0.01	s
K_v	Servo-valve gain	0.0239	m/A

where V_{01} and V_{02} are the initial volumes in each chamber. Assuming that $V_{01} = V_{02} = V_0$, the total volume of trapped oil is given by:

$$V_t = V_1 + V_2 = V_{01} + V_{02} = 2V_0 \quad (2.15)$$

Therefore, the equations in each chamber become:

$$\begin{cases} A_p \frac{dy_a}{dt} + \frac{V_0 + A_p y_a}{\beta_e} \frac{dP_1}{dt} = Q_1 - C_{ip}(P_1 - P_2) - C_{ep}P_1 \\ -A_p \frac{dy_a}{dt} + \frac{V_0 - A_p y_a}{\beta_e} \frac{dP_2}{dt} = C_{ip}(P_1 - P_2) - C_{ep}P_2 - Q_2 \end{cases} \quad (2.16)$$

Subtracting the second equation from the first one leads to:

$$2Q_L = Q_1 + Q_2 = 2C_{tp}\Delta P + 2A_p \frac{dy_a}{dt} + \frac{V_0}{\beta_e} \frac{d\Delta P}{dt} \quad (2.17)$$

where $C_{tp} = 2C_{ip} + C_{ep}$ is the total leakage coefficient of the hydraulic cylinder.

From equations (2.10) and (2.17), the dynamic equation of the servo-valve hydraulic cylinder is obtained as follows:

$$\frac{V_t}{4\beta_e} \frac{d\Delta P}{dt} + (K_P + C_{tp})\Delta P - K_x X_v + A_P \frac{dy_a}{dt} = 0 \quad (2.18)$$

where y_a is the displacement of the piston inside the hydraulic cylinder.

From the equations (2.1), (2.12), (2.18) the dynamical equations of the ESVH actuator are summarized in equation (2.19). Here the input signal is the current u and the output is the force F_{act} . The symbols and parameters of the model are shown in Table 2.1.

$$\begin{cases} F_{act} = A_P \Delta P \\ \frac{V_t}{4\beta_e} \frac{d\Delta P}{dt} + (K_P + C_{tp})\Delta P - K_x X_v + A_P \frac{dy_a}{dt} = 0 \\ \frac{dX_v}{dt} + \frac{1}{\tau} X_v - \frac{K_v}{\tau} u = 0 \end{cases} \quad (2.19)$$

Remark 2.2: As presented later, according to the given actuator model, the torque generated by the active anti roll bar system at each axle is given by: $T = -l_{act}F_{actl} + l_{act}F_{actr}$. Here l_{act} is half the distance between the two actuators, $F_{actl,r}$ the actuator forces on the left and on the right.

2.3 The Yaw-Roll model of a single unit heavy vehicle

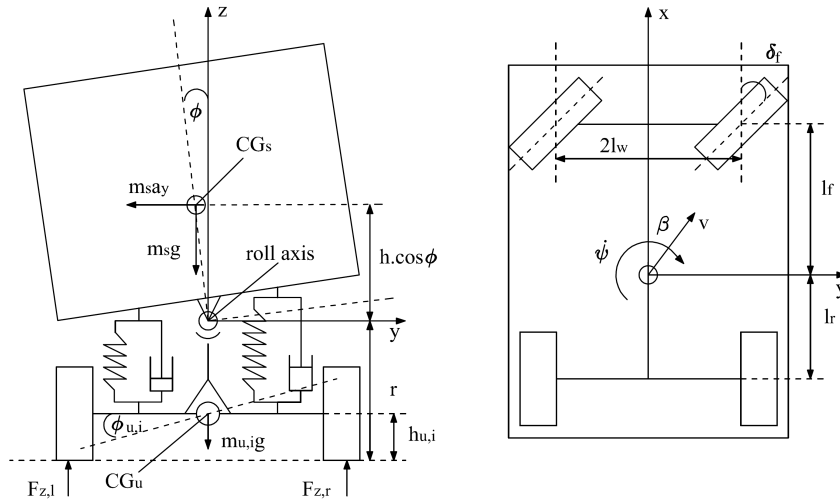


Figure 2.6: The Yaw-Roll model of a single unit heavy vehicle [Gaspar, Bokor, and Szaszi 2004].

Fig 2.6 illustrates the combined yaw-roll dynamics of the vehicle modeled by a three-body system, in which m_s is the sprung mass, m_{uf} the unsprung mass at the front including the front wheels and axle, and m_{ur} the unsprung mass at the rear for the rear wheels and axle. The vehicle as a whole can translate longitudinally and laterally, and can yaw. The sprung mass can rotate about a horizontal axis (the roll axis). The location of the roll axis depends on the kinematic properties of the front and rear suspensions. The unsprung masses can also rotate in roll, enabling the effect of the vertical compliance of the tyres on the roll performance to be included in the model. The effects of the aerodynamic inputs (wind disturbances) and road inputs (cross-gradients, dips and bumps) are neglected.

The suspension springs, dampers and anti-roll bars generate moments between the sprung and unsprung masses in response to roll motions. The active anti-roll bar control system at each axle consists of a pair of actuators and a series of mechanical linkages, which are in parallel with the existing passive springs and dampers, and these active anti-roll bar systems generate additional (controlled) roll moments between the sprung and unsprung masses. The roll stiffness and damping of the vehicle suspension systems are assumed to be constant for the range of roll motions considered. The symbols of the yaw-roll model are found in Table 2.2.

Table 2.2: Symbols and parameters of the yaw-roll model [Gaspar, Bokor, and Szaszi 2005]. [Vu et al. 2016].

Symbols	Description	Value	Unit
m_s	Sprung mass	12487	kg
$m_{u,f}$	Unsprung mass on the front axle	706	kg
$m_{u,r}$	Unsprung mass on the rear axle	1000	kg
m	The total vehicle mass	14193	kg
v	Forward velocity	-	$\frac{Km}{h}$
v_{wi}	Components of the forward velocity	-	$\frac{h}{Km}$
h	Height of sprung mass from the roll axis	1.15	m
$h_{u,i}$	Height of unsprung mass from the ground	0.53	m
r	Height of roll axis from the ground	0.83	m
a_y	Lateral acceleration	-	$\frac{m}{s^2}$
β	Side-slip angle at the center of mass	-	rad
ψ	Heading angle	-	rad
$\dot{\psi}$	Yaw rate	-	$\frac{rad}{s}$
α	Side slip angle	-	rad
ϕ	Sprung mass roll angle	-	rad
$\phi_{u,i}$	Unsprung mass roll angle	-	rad
δ_f	Steering angle	-	rad
u_i	Control current	-	A
C_f	Tyre cornering stiffness on the front axle	582	$\frac{kN}{rad}$
C_r	Tyre cornering stiffness on the rear axle	783	$\frac{kN}{rad}$
k_f	Suspension roll stiffness on the front axle	380	$\frac{kNm}{rad}$
k_r	Suspension roll stiffness on the rear axle	684	$\frac{kNm}{rad}$
b_f	Suspension roll damping on the front axle	100	$\frac{kN}{rad}$
b_r	Suspension roll damping on the rear axle	100	$\frac{kN}{rad}$
k_{tf}	Tyre roll stiffness on the front axle	2060	$\frac{kNm}{rad}$
k_{tr}	Tyre roll stiffness on the rear axle	3337	$\frac{kNm}{rad}$
I_{xx}	Roll moment of inertia of sprung mass	24201	kgm^2
I_{xz}	Yaw-roll inertial of sprung mass	4200	kgm^2
I_{zz}	Yaw moment of inertia of sprung mass	34917	kgm^2
l_f	Length of the front axle from the CG	1.95	m
l_r	Length of the rear axle from the CG	1.54	m
l_w	Half of the vehicle width	0.93	m
μ	Road adhesion coefficient	1	-
D_f	Outer diameter of the front anti-roll bar	32	mm
D_r	Outer diameter of the rear anti-roll bar	34	mm
E	Young's modulus of material	206000	MPa

In the vehicle modelling, the differential equations of motion of the yaw-roll dynamics of the single unit vehicle, i.e. the lateral dynamics, the yaw moment, the roll moment of the sprung mass, the roll moment of the front and the rear unsprung masses, are formalized in the following equations (2.20):

$$\left\{ \begin{array}{l} mv(\dot{\beta} + \dot{\psi}) - m_s h \ddot{\phi} = F_{yf} + F_{yr} \\ -I_{xz} \ddot{\phi} + I_{zz} \ddot{\psi} = F_{yf} l_f - F_{yr} l_r \\ (I_{xx} + m_s h^2) \ddot{\phi} - I_{xz} \ddot{\psi} = m_s g h \phi + m_s v h (\dot{\beta} + \dot{\psi}) - k_f (\phi - \phi_{uf}) \\ \quad - b_f (\dot{\phi} - \dot{\phi}_{uf}) + M_{ARf} + T_f - k_r (\phi - \phi_{ur}) - b_r (\dot{\phi} - \dot{\phi}_{ur}) + M_{ARr} + T_r \\ -r F_{yf} = m_{uf} v (r - h_{uf}) (\dot{\beta} + \dot{\psi}) + m_{uf} g h_{uf} \phi_{uf} - k_{tf} \phi_{uf} \\ \quad + k_f (\phi - \phi_{uf}) + b_f (\dot{\phi} - \dot{\phi}_{uf}) + M_{ARf} + T_f \\ -r F_{yr} = m_{ur} v (r - h_{ur}) (\dot{\beta} + \dot{\psi}) - m_{ur} g h_{ur} \phi_{ur} - k_{tr} \phi_{ur} \\ \quad + k_r (\phi - \phi_{ur}) + b_r (\dot{\phi} - \dot{\phi}_{ur}) + M_{ARr} + T_r \end{array} \right. \quad (2.20)$$

where T_f, T_r are the torques generated by the active anti-roll bar system at the each axle. The lateral tyre forces $F_{y,i}$ in the direction of the velocity at the wheel ground contact points are modelled by using linear stiffness coefficients as:

$$\left\{ \begin{array}{l} F_{yf} = \mu C_f \alpha_f \\ F_{yr} = \mu C_r \alpha_r \end{array} \right. \quad (2.21)$$

with the tyre side slip angles:

$$\left\{ \begin{array}{l} \alpha_f = -\beta + \delta_f - \frac{l_f \dot{\psi}}{v} \\ \alpha_r = -\beta + \frac{l_r \dot{\psi}}{v} \end{array} \right. \quad (2.22)$$

Let us now detail how the moments M_{ARf} and M_{ARr} in (2.20) are computed. When the vertical displacements of the left and the right wheels differ, the passive anti-roll bar with the rotational stiffness k_{AO} creates an anti-roll moment, resulting in the anti-roll forces F_{AU} , see Figure 2.7, which are acting on the unsprung mass as follows:

$$F_{AUl} = -F_{AUr} = k_{AU} (\Delta Z_{Ar} - \Delta Z_{Al}) \quad (2.23)$$

and the anti-roll forces F_{AS} acting on the sprung mass are:

$$F_{ASl} = -F_{ASr} = F_{AUl} \frac{t_A}{t_B} = k_{AS} (\Delta Z_{Ar} - \Delta Z_{Al}) \quad (2.24)$$

where $\Delta Z_{Ar,l}$ are the displacements of the connection point between the anti-roll bars and the wheels, t_A is half the distance between the two suspensions, t_B is half the distance of the chassis, c is the length of the anti-roll bars' arm, k_{AU} and k_{AS} are the modified rotational stiffness corresponding to the unsprung and sprung mass, respectively:

$$k_{AU} = k_{AO} \frac{1}{c^2} \quad \text{and} \quad k_{AS} = k_{AO} \frac{t_A}{t_{BC}^2} \quad (2.25)$$

The moment of the passive anti-roll bar impacts the unsprung and sprung masses at the front axle as follows:

$$M_{ARf} = 4k_{AO} f \frac{t_A t_B}{c^2} \phi - 4k_{AO} f \frac{t_A^2}{c^2} \phi_{uf} \quad (2.26)$$

The moment of the passive anti-roll bar impacts the unsprung and sprung masses at the rear axle as follows:

$$M_{ARr} = 4k_{AO_r} \frac{t_A t_B}{c^2} \phi - 4k_{AO_r} \frac{t_A^2}{c^2} \phi_{ur} \quad (2.27)$$

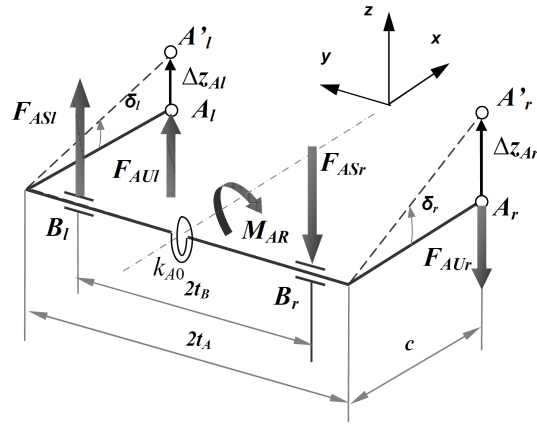


Figure 2.7: Diagram of the passive anti-roll bars on vehicles.

2.4 The integrated model of a single unit heavy vehicle

2.4.1 The fully integrated model

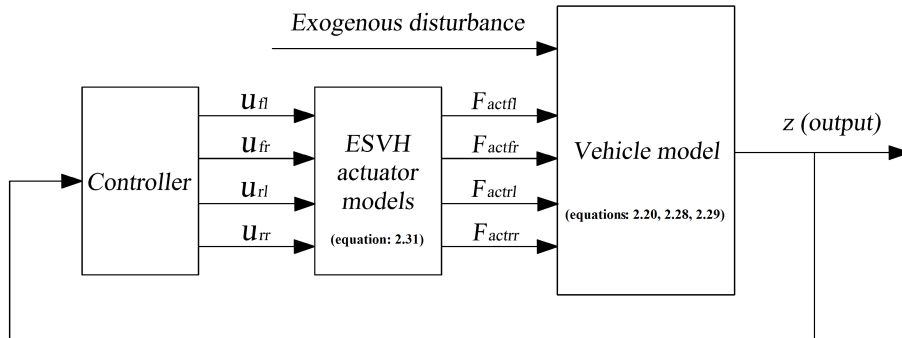


Figure 2.8: Diagram of the fully integrated model using an active anti-roll bar system.

Figure 2.8 shows the fully integrated model using an active anti-roll bar system. This model includes a linear single unit heavy vehicle yaw-roll model with the differential equations of motion given in equation (2.20) and the four Electronic Servo-Valve Hydraulic (ESVH) actuators (two at the front axle and two at the rear axle) with the differential equations of motion given in equations (2.1), (2.12), (2.18). The controller receives the information from the output

(z) and computes the input currents $(u_{fl}, u_{fr}, u_{rl}, u_{rr})$, where u_{fl} and u_{fr} are respectively the input currents of the electronic servo-valves on the left and right at the front axle, u_{rl} and u_{rr} at the rear axle. The forces $(F_{actfl}, F_{actfr}, F_{actrl}, F_{actrr})$ of the hydraulic actuators are applied to the vehicle model, where F_{actfl} and F_{actfr} are respectively the forces of the hydraulic actuators on the left and on the right at the front axle, F_{actrl} and F_{actrr} at the rear axle. Therefore the torque generated by the active anti-roll bar system at the front axle is determined by:

$$T_f = -l_{act}F_{actfl} + l_{act}F_{actfr} = -l_{act}A_p\Delta_{Pfl} + l_{act}A_p\Delta_{Pfr} \quad (2.28)$$

and the torque generated by the active anti-roll bar system at the rear axle is:

$$T_r = -l_{act}F_{actrl} + l_{act}F_{actrr} = -l_{act}A_p\Delta_{Prl} + l_{act}A_p\Delta_{Prr} \quad (2.29)$$

where l_{act} is half the distance between the two actuators, Δ_{Pfl} and Δ_{Pfr} are respectively the difference of pressure inside the hydraulic cylinders on the left and right at the front axle, Δ_{Prl} and Δ_{Prr} are respectively the difference of pressure inside the hydraulic cylinders on the left and right at the rear axle. They are given by the state equation (2.31).

The displacements of the piston inside the hydraulic cylinders on the left and right at the front axle (y_{afl}, y_{afr}) and at the rear axle (y_{arl}, y_{arr}) are approximately calculated as follows [Miège and Cebon 2002]:

$$\begin{cases} y_{afl} = -l_{act}(\phi - \phi_{uf}) \\ y_{afr} = l_{act}(\phi - \phi_{uf}) \\ y_{arl} = -l_{act}(\phi - \phi_{ur}) \\ y_{arr} = l_{act}(\phi - \phi_{ur}) \end{cases} \quad (2.30)$$

From equations (2.19) and (2.30), the dynamical equations of these ESVH actuators are shown as:

$$\begin{cases} \frac{V_t}{4\beta_e}\dot{\Delta}_{Pfl} + (K_P + C_{tp})\Delta_{Pfl} - K_x X_{vfl} - A_p l_{act} \dot{\phi} + A_p l_{act} \dot{\phi}_{uf} = 0 \\ \dot{X}_{vfl} + \frac{1}{\tau} X_{vfl} - \frac{K_v}{\tau} u_{fl} = 0 \\ \frac{V_t}{4\beta_e}\dot{\Delta}_{Pfr} + (K_P + C_{tp})\Delta_{Pfr} - K_x X_{vfr} + A_p l_{act} \dot{\phi} - A_p l_{act} \dot{\phi}_{uf} = 0 \\ \dot{X}_{vfr} + \frac{1}{\tau} X_{vfr} - \frac{K_v}{\tau} u_{fr} = 0 \\ \frac{V_t}{4\beta_e}\dot{\Delta}_{Prl} + (K_P + C_{tp})\Delta_{Prl} - K_x X_{vrl} - A_p l_{act} \dot{\phi} + A_p l_{act} \dot{\phi}_{ur} = 0 \\ \dot{X}_{vrl} + \frac{1}{\tau} X_{vrl} - \frac{K_v}{\tau} u_{rl} = 0 \\ \frac{V_t}{4\beta_e}\dot{\Delta}_{Prr} + (K_P + C_{tp})\Delta_{Prr} - K_x X_{vrr} + A_p l_{act} \dot{\phi} - A_p l_{act} \dot{\phi}_{ur} = 0 \\ \dot{X}_{vrr} + \frac{1}{\tau} X_{vrr} - \frac{K_v}{\tau} u_{rr} = 0 \end{cases} \quad (2.31)$$

The combination of equations from (2.20) to (2.31) are the motion differential equations of the fully integrated model.

The fully integrated model is written in the *LTI* state-space representation form:

$$\dot{x} = A^f .x + B_1^f .w + B_2^f .u \quad (2.32)$$

where the state vector is given by:

$$x = [\beta \quad \dot{\psi} \quad \phi \quad \dot{\phi} \quad \phi_{uf} \quad \phi_{ur} \quad \Delta_{Pfl} \quad X_{vfl} \quad \Delta_{Pfr} \quad X_{vfr} \quad \Delta_{Prl} \quad X_{vrl} \quad \Delta_{Prr} \quad X_{vrr}]^T$$

The exogenous disturbance (steering angle) is:

$$w = [\delta_f]^T$$

and the control inputs (input currents):

$$u = [u_{fl} \ u_{fr} \ u_{rl} \ u_{rr}]^T$$

Here, the matrices A^f , B_1^f and B_2^f are matrices of appropriate dimensions.

Remark 2.3:

- The matrices A^f , B_1^f and B_2^f are given in Appendix A,
- The fully integrated model of a single unit heavy vehicle will be used in Chapter 8.

Remark 2.4: In Appendix B we will show, according to the simulation results obtained in the frequency and time domains for the fully integrated model, that if at each axle, the right and left ESVH actuators are identical and symmetrically mounted, then the forces of the two electronic servo-valve hydraulic actuators do have the same magnitude and the opposite direction, therefore the active anti-roll bar system does not have an influence on the vertical motion of the heavy vehicle.

2.4.2 The control-oriented integrated model

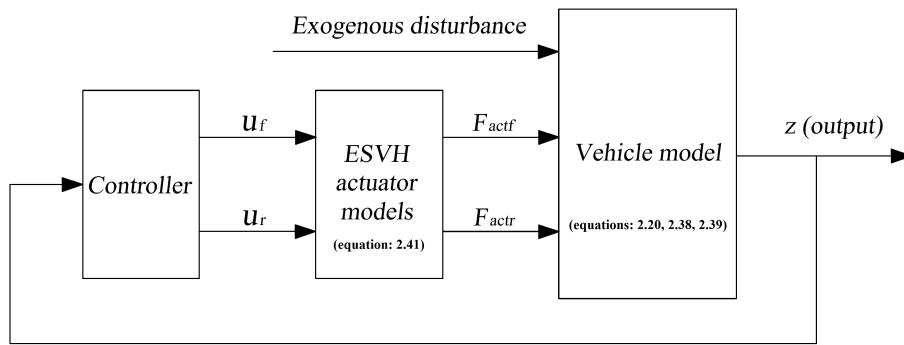


Figure 2.9: Diagram of a control-oriented integrated model using an active anti-roll bar system.

It is assumed that, at each axle, the right and left ESVH actuators are identical and symmetrically mounted. Therefore, at each axle, the characteristics of the two electronic servo-valve hydraulic actuators do have the same magnitude and the opposite direction (see Remark 2.4) as follows:

- Forces:

$$F_{actfl} = -F_{actfr} \quad \text{and} \quad F_{actrl} = -F_{actrr} \quad (2.33)$$

- Load flows:

$$Q_{Lfl} = -Q_{Lfr} \quad \text{and} \quad Q_{Lrl} = -Q_{Lrr} \quad (2.34)$$

- Spool valve displacements:

$$X_{vfl} = -X_{vfr} \quad \text{and} \quad X_{vrl} = -X_{vrr} \quad (2.35)$$

- Input currents:

$$u_{fl} = -u_{fr} \quad \text{and} \quad u_{rl} = -u_{rr} \quad (2.36)$$

where Q_{Lfl} and Q_{Lfr} are respectively the different load flows of the electronic servo-valves on the left and on the right at the front axle; Q_{Lrl} and Q_{Lrr} at the rear axle. X_{vfl} and X_{vfr} are respectively the spool valve displacements of the electronic servo-valves on the left and on the right at the front axle; X_{vrl} and X_{vrr} at the rear axle.

The torques generated by the active anti-roll bar system at the two axles are determined in equations (2.28)-(2.29); furthermore the forces, as well as other characteristics of the ESVH actuators at each axle, do have the same magnitude and the opposite direction, therefore we can consider that the torque generated by the active anti-roll bar system at each axle is twice the torque generated by one ESVH actuator. Using the hypothesis concerning the model symmetry given above, a model reduction is detailed in the sequel.

Figure 2.9 shows the diagram of a control-oriented integrated model using an active anti-roll bar, where u_f , u_r and F_{actf} , F_{actr} are respectively the input currents and the forces of one of the two ESVH actuators at the front and rear axles. In this study, the characteristics of the ESVH actuators on the right at the front axle, and on the right at the rear axle will be used. From Figure 2.8 and Figure 2.9, the mathematical relationships between the forces as well as the input currents at each axle are given as:

$$\left\{ \begin{array}{l} F_{actfl} = -F_{actfr} \\ F_{actrl} = -F_{actrr} \\ F_{actf} = F_{actfr} \\ F_{actr} = F_{actrr} \\ u_f = u_{fr} \\ u_r = u_{rr} \end{array} \right. \quad (2.37)$$

From equations (2.28), (2.29) and (2.37), the torque generated by the active anti-roll bar system at the front axle is now determined by:

$$T_f = 2l_{act}F_{actf} = 2l_{act}A_p\Delta P_f \quad (2.38)$$

and the torque generated by the active anti-roll bar system at the rear axle is:

$$T_r = 2l_{act}F_{actr} = 2l_{act}A_p\Delta P_r \quad (2.39)$$

where ΔP_f and ΔP_r are respectively the difference of pressure of the hydraulic actuator at the front and rear axles. They are given by the state equation (2.41).

The displacements ($y_{af,r}$) of the piston of the hydraulic actuators at each axle are approximately calculated as follows [Miège and Cebon 2002]:

$$y_{af,r} = l_{act}(\phi - \phi_{uf,r}) \quad (2.40)$$

From equations (2.1), (2.12), (2.18) and (2.40), the equations of these electronic servo-valve actuators are given by:

$$\begin{cases} \frac{V_t}{4\beta_e} \dot{\Delta}_{Pf} + (K_P + C_{tp})\Delta_{Pf} - K_x X_{vf} + A_p l_{act} \dot{\phi} - A_p l_{act} \dot{\phi}_{uf} = 0 \\ \dot{X}_{vf} + \frac{1}{\tau} X_{vf} - \frac{K_v}{\tau} u_f = 0 \\ \frac{V_t}{4\beta_e} \dot{\Delta}_{Pr} + (K_P + C_{tp})\Delta_{Pr} - K_x X_{vr} + A_p l_{act} \dot{\phi} - A_p l_{act} \dot{\phi}_{ur} = 0 \\ \dot{X}_{vr} + \frac{1}{\tau} X_{vr} - \frac{K_v}{\tau} u_r = 0 \end{cases} \quad (2.41)$$

Defining the state vector of the reduced model:

$$x = [\beta \quad \dot{\psi} \quad \phi \quad \dot{\phi} \quad \phi_{uf} \quad \phi_{ur} \quad \Delta_{Pf} \quad X_{vf} \quad \Delta_{Pr} \quad X_{vr}]^T$$

where X_{vf} and X_{vr} are the spool valve displacements at the front and rear axles, respectively, the motion differential equations (2.20)-(2.41) can be rewritten in the *LTI* state-space representation as:

$$\dot{x} = A^c .x + B_1^c .w + B_2^c .u \quad (2.42)$$

where A^c , B_1^c , B_2^c are model matrices of appropriate dimensions. The exogenous disturbance is:

$$w = [\delta_f]^T$$

and the control inputs:

$$u = [u_f \quad u_r]^T$$

Remark 2.5:

- The matrices A^c , B_1^c and B_2^c are shown in Appendix C,
- The state vectors x in equations 2.32 and 2.42 are different,
- The control-oriented integrated model will be used in Chapters 4, 5, 6 and 7.

2.4.3 The variables of interest

For the integrated model of a single unit heavy vehicle, the variables of interest include:

1. The characteristics of the single unit heavy vehicle: $\beta, \dot{\psi}, \phi, \dot{\phi}, \phi_{uf}, \phi_{ur}, \phi - \phi_{uf}, \phi - \phi_{ur}$
2. The characteristics of the actuators:
 - Fully integrated model: $Q_{Lfl}, Q_{Lfr}, Q_{Lrl}, Q_{Lrr}, F_{actfl}, F_{actfr}, F_{actrl}, F_{actrr}, X_{vfl}, X_{vfr}, X_{vrl}, X_{vrr}, u_{fl}, u_{fr}, u_{rl}, u_{rr}$

- Control-oriented integrated model: $Q_{Lf}, Q_{Lr}, F_{actf}, F_{actr}, X_{vf}, X_{vr}, u_f, u_r$
3. The roll stability includes: R_f, R_r

where R_f and R_r are respectively the normalized load transfer at the front and rear axles, defined as follows [Gaspar, Bokor, and Szaszi 2004], [Hsun-Hsuan, Rama, and Dennis 2012]:

$$R_f = \frac{\Delta F_{zf}}{F_{zf}}, \quad R_r = \frac{\Delta F_{zr}}{F_{zr}} \quad (2.43)$$

where F_{zf} is the total axle load at the front axle and F_{zr} at the rear axle. ΔF_{zf} and ΔF_{zr} are respectively the lateral load transfers at the front and rear axles, which can be given by:

$$\Delta F_{zf} = \frac{k_{uf}\phi_{uf}}{l_w}, \quad \Delta F_{zr} = \frac{k_{ur}\phi_{ur}}{l_w} \quad (2.44)$$

where k_{uf} and k_{ur} are the stiffness of the tyres, ϕ_{uf} and ϕ_{ur} are the roll angles of the unsprung masses at the front and rear axles, and l_w is equal to half of the vehicle's width.

2.5 The design of a passive anti-roll bar system

2.5.1 The design of the passive anti-roll bar by using the *SAE* spring design manual

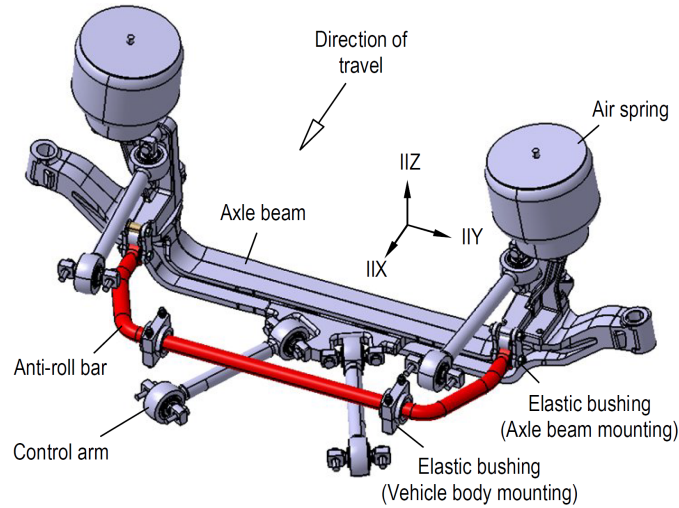


Figure 2.10: Geometrical description of the passive anti-roll bar system on heavy vehicles [Topac, Enginar, and Kuralay 2011].

The passive anti-roll bar is a rod or tube that connects the right and left suspension members, as illustrated in Figure 2.10. It can be used in the front suspension, the rear suspension or in both suspensions, no matter if the suspensions are a solid axle type or an independent type. The ends of the passive anti-roll bar are connected to the suspension links while the center of

the bar is connected to the vehicle frame, such that it is free to rotate. The ends of the arms are attached to the suspension as close to the wheels as possible. If both ends of the bar move equally, the bar rotates in its bushing and provides no torsional resistance.

The design of an anti-roll bar actually means obtaining the required anti-roll stiffness that improves the vehicle stability and handling performances without exceeding the mechanical limitations of the bar material (for general information about torsion bars and their manufacturing processing, see *Spring Design Manual* [SAE 1996], [Bharane et al. 2014]). Anti-roll bars are special cases of torsion bars. Some useful formulae to calculate the torsional stiffness of anti-roll bars and deflection at the end point of the bar under a given loading, are provided in this manual. However, the formulations can only be applied to the bars with standard shapes (simple, torsion bar shaped anti-roll bars), whose geometry is shown in Figure 2.11.

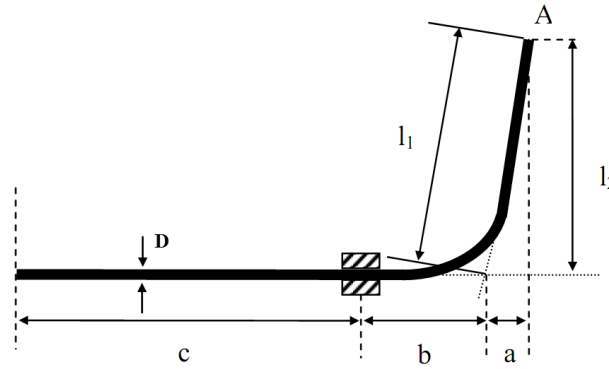


Figure 2.11: Anti-roll bar geometry used in *SAE Spring Design Manual*.

The loading \mathcal{F} is applied at point A, inward to or outward from the plane of the page. The roll stiffness of such a bar can be calculated as:

$$k_{AO} = \frac{\mathcal{F}L^2}{2f_A} \quad (2.45)$$

where:

f_A - Deflection of point A:

$$f_A = \frac{\mathcal{F}}{3EI} [l_1^3 - a^3 + \frac{L}{2}(a+b)^2 + 4l_2^2(b+c)] \quad (2.46)$$

L - Half track length of anti-roll bar:

$$L = a + b + c \quad (2.47)$$

I - Moment of inertia of anti-roll bar:

$$I = \pi \frac{D^4}{64} \quad (2.48)$$

with, D - Outer diameter, E - Young's modulus of material.

The material of the anti-roll bar is issued from *AISI 1065*, $E = 206000MPa$ [Bharane et al.

2014]. The outer diameter of the anti-roll bar on the front axle $D_f = 32mm$ [Topac, Enginar, and Kuralay 2011], then the torsional stiffness of the anti-roll bar at the front axle is:

$$k_{AO_f} = 10730 \left(\frac{Nm}{rad} \right)$$

The outer diameter of the anti-roll bar on the rear axle $D_r = 34mm$ [Topac, Enginar, and Kuralay 2011], then the torsional stiffness of the anti-roll bar at the rear axle is:

$$k_{AO_r} = 15480 \left(\frac{Nm}{rad} \right)$$

2.5.2 The effectiveness of the passive anti-roll bar on vehicle roll stability

In this section, the effectiveness of the passive anti-roll bar on the roll stability of a single unit heavy vehicle is illustrated in both the frequency and time domains, when they are compared to the "without anti-roll bar". The control-oriented integrated model proposed in section 2.4.2 is used with the values of the vehicle parameters found in Table 2.2. The forward velocity is considered at $70 km/h$. The performance criteria used to evaluate the effectiveness of the passive anti-roll bar include: the normalized load transfers $R_{f,r}$ and the roll angles of the suspension $\phi - \phi_{u_{f,r}}$ at the two axles.

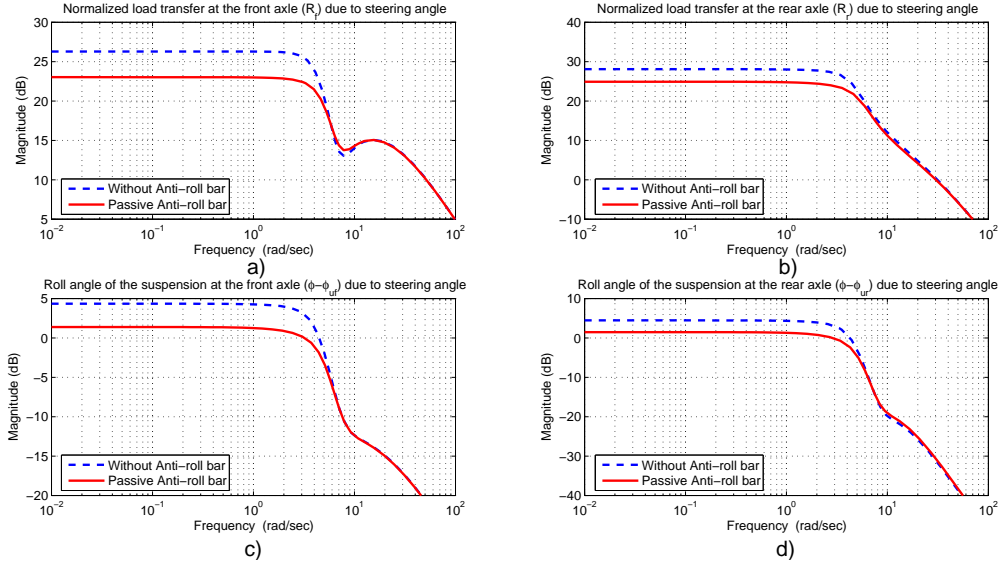


Figure 2.12: Transfer function magnitude of (a, b) normalized load transfers $\frac{R_{f,r}}{\delta_f}$ and (c, d) roll angles of suspension $\frac{\phi - \phi_{u_{f,r}}}{\delta_f}$ at the two axles of a single unit heavy vehicle.

2.5.2.1 The effectiveness of the passive anti-roll bar in the frequency domain

It is necessary to evaluate the effectiveness of the passive anti-roll bar in the frequency range to over 4 rad/s . Indeed this limitation characterizes the limited bandwidth of the driver [Sampson and Cebon 2003b], [Gaspar, Bokor, and Szaszi 2004].

Figures 2.12*a,b* show the transfer function magnitude of the normalized load transfers $\frac{R_{f,r}}{\delta_f}$ at the front and rear axles. The passive anti-roll bar reduces the transfer function magnitude of the normalized load transfer at the front axle $\frac{R_f}{\delta_f}$ by about 4dB in the frequency range up to 5 rad/s . Meanwhile, the transfer function magnitude of the normalized load transfer at the rear axle $\frac{R_r}{\delta_f}$ is reduced by about 2.5dB in the frequency range up to 4.5 rad/s , when compared to the "without anti-roll bar". Figure 2.12*a* and Figure 2.12*b* also indicate that the normalised load transfers build up more quickly at the rear axle than at the front axle in the cases of the "without anti-roll bar" and the passive anti-roll bar. This is consistent with previous results [Sampson 2000], because it is affected by the suspension stiffness to load ratio, which is greater at the rear axle than at the front one.

Figures 2.12*c,d* show that the transfer function magnitude of the roll angle of the suspension at the front axle ($\phi - \phi_{uf}$) and rear axle ($\phi - \phi_{ur}$) are drastically reduced in the desired frequency range when compared to the "without anti-roll bar".

The reduction of the magnitude of transfer functions is summarized in Table 2.3, when the passive anti-roll bar is compared to the without anti-roll bar.

Table 2.3: Reduction of the magnitude of transfer functions compared to the without anti-roll bar.

Transfer functions	$\frac{R_f}{\delta_f}$	$\frac{R_r}{\delta_f}$	$\frac{\phi - \phi_{uf}}{\delta_f}$	$\frac{\phi - \phi_{ur}}{\delta_f}$
Reduction	4dB $[0, 5 \frac{\text{rad}}{\text{s}}]$	2.5dB $[0, 4.5 \frac{\text{rad}}{\text{s}}]$	4dB $[0, 5 \frac{\text{rad}}{\text{s}}]$	3dB $[0, 4.5 \frac{\text{rad}}{\text{s}}]$

2.5.2.2 The effectiveness of the passive anti-roll bar in the time domain

To evaluate the roll stability effectiveness of the passive anti-roll bar in the time domain, a double lane change manoeuver will be used as an example. This manoeuver characterizes the situation when the driver wishes to avoid an obstacle in an emergency. The time response of the steering angle is shown in Figure 2.13.

Figure 2.14 shows the roll stability effectiveness of the passive anti-roll bar in the time domain. The simulation results showed that the normalized load transfers in the case of the passive anti-roll bar reduce respectively by about 30% and 42% at the front and rear axles compared to the "without anti-roll bar". The roll angle of the suspension at the two axles is also reduced in the case of the passive anti-roll bar.

From the analysis in the frequency and time domains, it indicates that the passive anti-roll bar improves the roll stability of a single unit heavy vehicle. This explains why nowadays

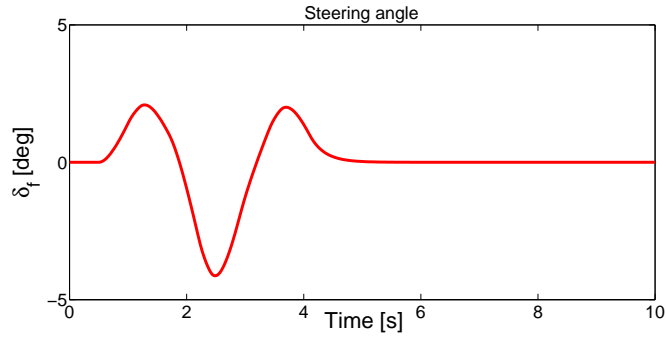


Figure 2.13: Time response of the steering angle δ_f .

almost all heavy vehicles are equipped with the passive anti-roll bar on all axles.

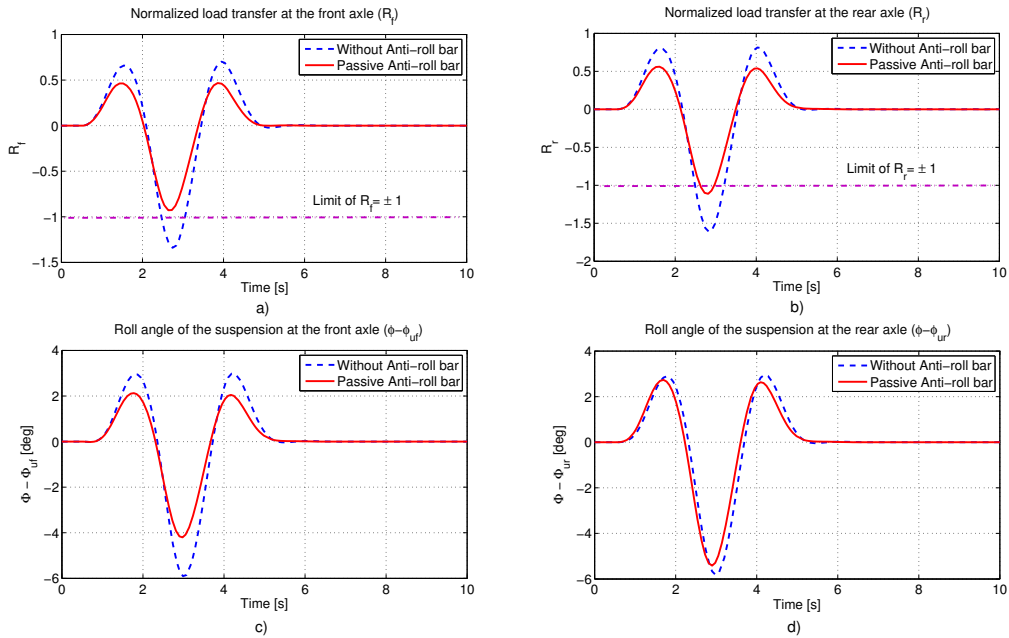


Figure 2.14: Time response of (a, b) normalized load transfers $R_{f,r}$ and (c, d) suspension roll angles $\phi - \phi_{u,f,r}$ at the two axles.

2.6 Conclusion

This chapter proposed two types of integrated models (fully integrated model and control-oriented integrated model) including four Electronic Servo-Valve Hydraulic (ESVH) actuators (two at the front and two at the rear axles) and a linear single unit heavy vehicle yaw-roll

model. In the fully integrated model, the four ESVH actuators are independently controlled. While, the control-oriented integrated model uses one ESVH actuator on the right at the front axle and one ESVH actuator on the right at the rear axle. The fully integrated model will be used in Chapter 8 to evaluate the effect of the oil leakage inside the electronic servo-valve on the performance of the system. The control-oriented integrated model will be used to synthesize the LQR, H_∞ and H_∞/LPV active anti-roll bar controllers in Chapters 4, 5, 6, 7. The passive anti-roll bar can be designed by using the *SAE* spring design manual. Although the passive anti-roll bar system reduces the normalized load transfers at two axles, so improving roll stability in both the frequency and time domains, they suffer from inherent drawbacks: the torsional stiffness of the anti-roll bars are constant and cannot change during the various vehicle manoeuvres. Therefore, for cornering manoeuvres, the passive anti-roll bar will transfer the vertical forces of one side of the suspension to the other one, creating a yaw moment [Zulkarnain et al. 2012], which could lead to stability problems. Therefore, this highlights the need for an active anti-roll bar system, which will be illustrated in the next chapters.

Background on control theory and optimization

Contents

3.1	Introduction	49
3.2	Dynamical systems	50
3.2.1	Nonlinear dynamical systems	50
3.2.2	LTI dynamical systems	51
3.2.3	LPV dynamical systems	52
3.3	Signal and system norms	54
3.3.1	Signal norms	54
3.3.2	System norms	54
3.4	Robustness analysis of dynamical systems	55
3.5	Linear Quadratic Regulator control	58
3.6	LTI/H_∞ control problem and design	59
3.6.1	H_∞ optimal control problem	59
3.6.2	LTI/H_∞ control design	60
3.7	LPV/H_∞ control problem and design	62
3.7.1	General problem formulation	62
3.7.2	LPV/H_∞ control synthesis	64
3.7.3	Grid-based LPV approach	66
3.7.4	The LPVTools TM toolbox	67
3.8	Multi-objective optimization by using genetic algorithms	68
3.8.1	Multi-criteria optimization and Pareto-optimal solutions	69
3.8.2	Genetic algorithms	70
3.9	Conclusion	72

3.1 Introduction

This chapter presents some theoretical background on the control theory and optimization used in this thesis for advanced control design and analysis. This will help readers to better

understand the various developments presented in this study. First, a brief presentation of linear and non linear systems is introduced to the reader about physical systems modelling and state-space representations. Then, the Linear Quadratic Regulator (LQR) control, LTI/H_∞ control and LPV/H_∞ control are also introduced. Here the author focuses on the grid-based LPV approach for the LPV/H_∞ synthesis. Finally, multi-optimization by using genetic algorithms is presented briefly.

It is worth noting that the theoretical developments are not the core contribution of this thesis. It should be kept in mind that these theoretical backgrounds have been widely developed in the past by the following authors, just to mention a few, [Doyle, Francis, and Tannenbaum 1990], [Wu 1995], [Scherer, Gahinet, and Chilali 1997], [Apkarian and Gahinet 1995], [Apkarian and Adams 1998], [Hjartarson, Seiler, and Balas 2013], [Ehrgott 2005], [Holland 1975]. This chapter's vocation is to provide a summary of the tools involved in this thesis. The objective is to present the main ideas and concepts. As a matter of fact, the material provided in this chapter gives the fundamental mathematical elements. The interested reader could find more details in the given references above and in some textbooks in robust control.

3.2 Dynamical systems

In this section, the fundamental mathematical notations and definitions concerning dynamical systems are introduced. A dynamical system defines how a system of variables interacts and changes with time. In fact, most of the real practical systems are fundamentally nonlinear and very few physical dynamical systems are truly linear. In order to study the linear and nonlinear systems in the control theory, the dynamical systems are mostly modeled using a set of linear or nonlinear Ordinary Differential Equations (ODEs). The most generic models are nonlinear, obtained from the physical equations, but the most common method to design controllers is to start by linearizing these models around some operating conditions, which yields linear models, and then to use linear control techniques. In the control theory, the different types of systems are shown in Figure 3.1. They include the LTI, LPV<V, qLPV&TS and Nonlinear systems.

3.2.1 Nonlinear dynamical systems

The nonlinear dynamical modelling of real physical systems are derived thanks to the system knowledge and the physical equations, etc. We are interested in the nonlinear dynamical systems which can be described by the nonlinear ODEs.

Definition 3.2.1 (Nonlinear dynamical system). *For given functions $f : \mathbb{R}^n \times \mathbb{R}^q \mapsto \mathbb{R}^n$ and $g : \mathbb{R}^n \times \mathbb{R}^q \mapsto \mathbb{R}^r$, a nonlinear dynamical system $(\Sigma_{\mathcal{NL}})$ can be described as:*

$$\Sigma_{\mathcal{NL}} : \begin{cases} \dot{x}(t) = f(x(t), w(t)) \\ z(t) = g(x(t), w(t)) \end{cases} \quad (3.1)$$

where $x(t)$ is the state which takes values in a state space $X \in \mathbb{R}^n$, $w(t)$ is the input taking

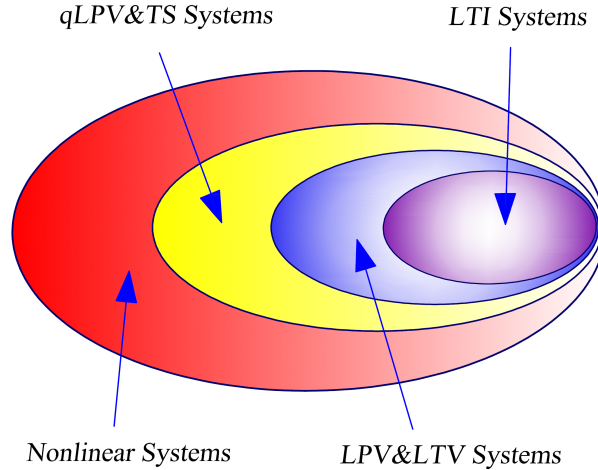


Figure 3.1: Relation between the different classes of systems.

values in the input space $W \in \mathbb{R}^q$ and $z(t)$ is the output that belongs to the output space $Z \in \mathbb{R}^r$.

The main advantage of nonlinear dynamical modelling is that it can fit most of the real system phenomena. However, the complexity of the nonlinear models introduces several difficulties while trying to study them, especially to find the adequate mathematical and methodological tools for identification, observation, control synthesis and analysis. In many physical systems studies, the nonlinear dynamical models are more suitable for the simulation and performance analysis but they are often difficult to use for the synthesis objectives.

3.2.2 LTI dynamical systems

The linear approach starts with the transformation of the nonlinear system into a linear one. Therefore, the LTI dynamical modelling is often adopted for control and observation purposes for both SISO and MIMO systems. The LTI dynamical modelling consists in describing the system through linear ODEs. According to the previous nonlinear dynamical system definition, the LTI modelling leads to a local description of the nonlinear behavior (e.g. it locally describes, around a linearizing point, the real system behavior).

Definition 3.2.2 (LTI dynamical system). *Given matrices $A \in \mathbb{R}^{n \times n}$, $B \in \mathbb{R}^{n \times q}$, $C \in \mathbb{R}^{r \times n}$ and $D \in \mathbb{R}^{r \times q}$, a Linear Time Invariant (LTI) dynamical system $(\Sigma_{\mathcal{LTI}})$ can be described as:*

$$\Sigma_{\mathcal{LTI}} : \begin{cases} \dot{x}(t) = Ax(t) + Bw(t) \\ z(t) = Cx(t) + Dw(t) \end{cases} \quad (3.2)$$

where $x(t)$ is the state which takes values in a state space $X \in \mathbb{R}^n$, $w(t)$ is the input taking values in the input space $W \in \mathbb{R}^q$ and $z(t)$ is the output that belongs to the output space $Z \in \mathbb{R}^r$.

As mentioned above, the main restriction is that LTI models are only valid around the linearization points and describe locally the real physical system behavior. When compared to the nonlinear models, they lack information and, as a consequence, are incomplete and may not provide global stabilization. To overcome this drawback, the LPV dynamical system can be considered. The LPV dynamical system can maintain the accuracy of nonlinear dynamical systems while they can also use some tools of linear dynamics.

3.2.3 LPV dynamical systems

3.2.3.1 LPV systems

Linear Parameter Varying (LPV) systems are an important system class, whose dynamics depend linearly on the state and input of the system, but also on some scheduling parameter. Hence an LPV system describes a family of linear systems. The LPV paradigm states that no a priori information about the scheduling parameter values is available, but that the parameter can be measured or estimated online [Rugh 1990], [Shamma and Athans 1990]. The interest in LPV systems is motivated by their use in gain-scheduling control techniques, and by the possibility to embed nonlinear systems into the LPV framework by covering nonlinearities within the scheduling parameter. Therefore the LPV framework enables, to some extent, the application of linear control methods to nonlinear systems, while providing rigorous statements on stability and performance of the closed-loop system [Besselmann, Lofberg, and Morari 2012]. Indeed, the gain-scheduling technique is only efficient for systems with slow varying parameters while in an LPV design, more information on scheduling parameters (i.e. the parameter bounds and rate bounds if any) can be taken into account [Apkarian and Adams 1998], [Wu 2001]. Moreover the resulting LPV controllers are automatically gain-scheduled and do not require any ad hoc methods of gain-scheduling as in the classical methodology. According to the previous nonlinear and LTI dynamical system definitions, a extension of the LTI dynamical system definition lies in the LPV dynamical system description which gives somehow a tradeoff between the nonlinear and LTI formulations. The LPV system can be represented as a linear system where the matrices A, B, C and D are functions of some vector of varying, measurable parameters. In the sequel, the focus will be on the state-space representation of LPV systems as follows:

Definition 3.2.3 (LPV dynamical system). *Given the linear matrix functions $A \in \mathbb{R}^{n \times n}$, $B \in \mathbb{R}^{n \times q}$, $C \in \mathbb{R}^{r \times n}$ and $D \in \mathbb{R}^{r \times q}$, a Linear Parameter Varying (LPV) dynamical system ($\Sigma_{\mathcal{L}PV}$) can be described as:*

$$\Sigma_{\mathcal{L}PV} : \begin{cases} \dot{x}(t) = A(\rho(\cdot))x(t) + B(\rho(\cdot))w(t) \\ z(t) = C(\rho(\cdot))x(t) + D(\rho(\cdot))w(t) \end{cases} \quad (3.3)$$

where $x(t)$ is the state which takes values in a state space $X \in \mathbb{R}^n$, $w(t)$ is the input taking values in the input space $W \in \mathbb{R}^q$ and $z(t)$ is the output that belongs to the output space $Z \in \mathbb{R}^r$.

In equation (3.3), $\rho(\cdot)$ is a varying parameter vector that takes values in the parameter space

\mathcal{P}_ρ such that,

$$\mathcal{P}_\rho := \{\rho(\cdot) := [\rho_1(\cdot) \ \dots \ \rho_p(\cdot)]^T \in \mathbb{R}^p \text{ and } \rho_i \in [\underline{\rho}_i \ \bar{\rho}_i] \forall i = 1, \dots, p\} \quad (3.4)$$

where p is the number of varying parameters.

According to the varying parameter $\rho(\cdot)$, there are four classes systems of (3.3) as follows:

- $\rho(\cdot) = \rho$, a constant value, (3.3) is a Linear Time Invariant (LTI) system.
- $\rho(\cdot) = \rho(t)$, a parameter vector whose time dependence is a priori known, (3.3) is a Linear Time Varying (LTV) system.
- $\rho(\cdot) = \rho(t)$ is an external parameter vector, (3.3) is an LPV system.
- $\rho(\cdot) = \rho(x(t))$, (3.3) is a quasi-Linear Parameter Varying (qLPV) system.

An LPV system ensures a good approximation of a nonlinear model by using a state-space varying parameter representation that is close to the real dynamical behaviour of the nonlinear model (a nonlinear system linearized along the varying parameters trajectories, characterized by $\rho \in \mathcal{P}_\rho$). The advantage of the LPV system is that it keeps a linear structure which allows the use of several synthesis and analysis mathematical tools for linear systems with some modifications.

3.2.3.2 Stability of the LPV systems

Definition 3.2.4 (Quadratic stability [Wu 1995]). *System (3.3) is said to be quadratically stable if there exists a quadratic Lyapunov function $V(x(t)) = x(t)^T P x(t) > 0$ for every $x \neq 0$ and $V(0) = 0$ such that*

$$\dot{V}(t) = x(t)^T (A(\rho)^T P + P A(\rho)) x(t) < 0 \quad (3.5)$$

for every $x \neq 0$ and $V(0) = 0$, for all $\rho \in \mathcal{P}_\rho$.

Definition 3.2.5 (Robust stability [Wu 1995]). *System (3.3) is said to be robustly stable if there exists a parameter-dependent Lyapunov function $V(x(t)) = x(t)^T P(\rho) x(t) > 0$ for every $x \neq 0$ and $V(0) = 0$ such that*

$$\dot{V}(t) = x(t)^T (A(\rho)^T P(\rho) + P(\rho) A(\rho) + \dot{\rho} \frac{\partial P}{\partial \rho}) x(t) < 0 \quad (3.6)$$

for every $x \neq 0$ and $V(0) = 0$, for all $\rho \in \mathcal{P}_\rho$.

It should be noticed that equations (3.5) and (3.6) are infinite dimensional problems since ρ can take any value in \mathcal{P}_ρ .

3.3 Signal and system norms

One way to describe the performance of a control system is in terms of the size of certain signals of interest. For example, the performance of a tracking system could be measured by the size of the error signal. In order to introduce the mathematical background on systems, the norm and control synthesis and the basic notions are recalled here to provide the reader all the elements to understand the notations and concepts that are used in some definitions. Readers are also invited to refer to the books [Doyle, Francis, and Tannenbaum 1990], [Zhou, Doyle, and Glover 1996], where all the following definitions and additional information are given.

3.3.1 Signal norms

In the following definitions, the assumption used is that $x(t)$ is a function in the complex space where $x(t) \in \mathbb{C}$, then the conjugate of $x(t)$ is denoted as $x^*(t)$. When signals are real (i.e. $x(t) \in \mathbb{R}$), $x^*(t) = x^T(t)$. The signal norms are defined as follows:

Definition 3.3.1 (\mathcal{L}_1 , \mathcal{L}_2 , \mathcal{L}_∞ norms).

- **1-Norm:** the 1-Norm of a function $x(t)$ is given by,

$$\|x(t)\|_1 = \int_0^{+\infty} |x(t)| dt \quad (3.7)$$

- **2-Norm:** the 2-Norm (that introduces the energy norm) is given by,

$$\begin{aligned} \|x(t)\|_2 &= \sqrt{\int_0^{+\infty} x^*(t)x(t) dt} \\ &= \sqrt{\frac{1}{2\pi} \int_{-\infty}^{+\infty} X^*(j\omega)X(\omega) d\omega} \end{aligned} \quad (3.8)$$

- **∞ -Norm:** the ∞ -Norm is given by,

$$\|x(t)\|_\infty = \sup_t |x(t)| \quad (3.9)$$

$$\|X\|_\infty = \sup_{\text{Re}(s) \geq 0} \|X(s)\| = \sup_\omega \|X(j\omega)\| \quad (3.10)$$

if the signals that admit the Laplace transform, are analytic in $\text{Re}(s) \geq 0$ (i.e. $\in \mathcal{H}_\infty$).

3.3.2 System norms

We consider the systems that are LTI, causal, and finite-dimensional. The two norms for the transfer are introduced as follows:

Definition 3.3.2 (H_2 norm). *The H_2 norm of a strictly proper LTI system, defined as on (3.2.2) from input $w(t)$ to output $z(t)$, is the energy (\mathcal{L}_2 norm) of the impulse response $g(t)$ defined as,*

$$\begin{aligned}\|G(j\omega)\|_2 &= \sqrt{\int_{-\infty}^{+\infty} g^*(t)g(t)dt} \\ &= \sqrt{\frac{1}{2\pi} \int_{-\infty}^{+\infty} \text{Tr}[G^*(j\omega)G(j\omega)]d\omega} \\ &= \sup_{w(s) \in H_2} \frac{\|z(s)\|_\infty}{\|w(s)\|_2}\end{aligned}\quad (3.11)$$

The norm H_2 is finite if and only if $G(s)$ is strictly proper.

Remark 3.1: *For the MIMO systems, the H_2 norm is the impulse-to-energy gain of $z(t)$ in response to a white noise input $w(t)$. While in the case of the SISO systems, the H_2 norm represents the area located below the Bode diagram. The H_2 norm can be computed analytically (by using the controllability and observability Grammians) or numerically (by using LMIs).*

Definition 3.3.3 (H_∞ norm). *The H_∞ norm of a proper LTI system defined as on (3.2.2) from input $w(t)$ to output $z(t)$, is the induced energy-to-energy gain (\mathcal{L}_2 to \mathcal{L}_2 norm) defined as,*

$$\begin{aligned}\|G(j\omega)\|_\infty &= \sup_{\omega \in \mathbb{R}} \bar{\sigma}(G(j\omega)) \\ &= \sup_{w(s) \in H_2} \frac{\|z(s)\|_2}{\|w(s)\|_2} \\ &= \max_{w(t) \in \mathcal{L}_2} \frac{\|z\|_2}{\|w\|_2}\end{aligned}\quad (3.12)$$

Remark 3.2: *The H_∞ norm represents the maximal gain of the frequency response of the system. It is also called the worst case attenuation level in the sense that it measures the maximum amplification that the system can deliver over the whole frequency set. Unlike the H_2 norm, the H_∞ norm can be only obtained from numerical solutions such as LMI resolution. For the SISO (resp. MIMO) systems, it represents the maximal peak value on the Bode magnitude (resp. singular value).*

For LPV systems (as for nonlinear systems) the H_∞ performance is defined as the \mathcal{L}_2 - induced gain of the input-output relationship.

3.4 Robustness analysis of dynamical systems

As mentioned above, there is no mathematical model that is entirely equivalent to the real system. Linear or even nonlinear models are not able to capture all the physical phenomena involved in the dynamics of the considered system. This could be the result of non-exact measurements or the complexity of the system. Therefore, a choice has to be made between considering a complex model, or using a simplified one that takes into account some errors referred to as modelling uncertainties. This key concept is introduced as describing the mismatch between the mathematical model and the real physical system.

The concept of robustness is very large and involves many different areas. For control systems, this concept is often referred to in studies of the H_∞ control design. The main goal

of robust control techniques is to take these uncertainties into account when analyzing or designing a controller for the considered system. Let us recall that uncertainties may have several mathematical representations:

- Parametric uncertainties (ex: sensors errors, measurements errors,..etc).
- Dynamic uncertainties (ex: unmodeled dynamics).

For analysis they are classified in two categories:

- Unstructured uncertainties: we ignore the structure of Δ , considered as a full complex perturbation matrix, such that $\|\Delta\|_\infty \leq 1$.
- Structured uncertainties: we take into account the structure of Δ , (always such that $\|\Delta\|_\infty \leq 1$).

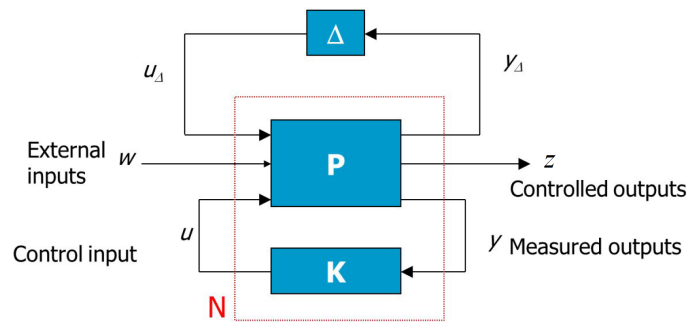


Figure 3.2: Standard problem: $P - K - \Delta$ structure.

The control scheme shown in Figure 3.2 is often used for the robustness analysis (and even design), it defines a linear fractional transformation, where:

- P is the system model, that can be either LTI, LPV, switched... Usually P includes both actuators and sensors models.
- K is the controller (it could be LTI, LPV, nonlinear...).
- Δ represents the considered modelling uncertainties.
- w represents the exogenous system inputs (reference, disturbances, noise, etc.).
- z is the controlled output.
- y is the output (or measured) signal provided by set of sensors on the system, it is sent to the controller.
- u is the control signal provided by the controller K that feeds the system P .

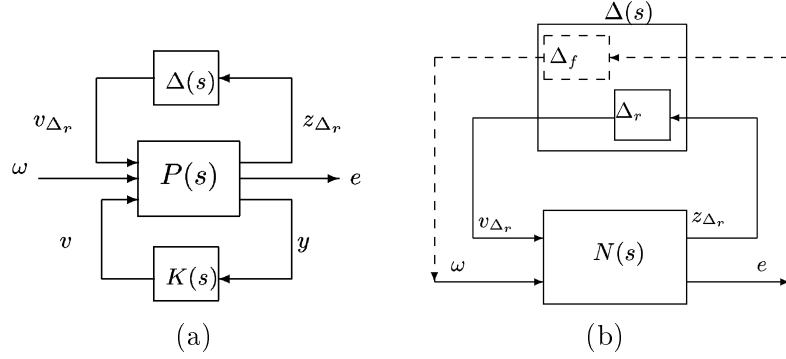


Figure 3.3: (a) General control configuration with uncertainties, (b) $N\Delta$ structure.

The starting point of the robustness analysis is the block-diagonal representation of the uncertainties set:

$$\underline{\Delta} = \{\text{diag}\{\Delta_1, \dots, \Delta_q, \delta_1 I_{r_1}, \dots, \delta_r I_{r_r}, \epsilon_1 I_{c_1}, \dots, \epsilon_c I_{c_c}\} \in \mathbb{C}^{k \times k}, \Delta_i \in \mathbb{C}^{k_i \times k_i}, \delta_i \in \mathbb{R}, \epsilon_i \in \mathbb{C}\}.$$

where $\Delta_i(s), i = 1, \dots, q$, represent the full block of complex uncertainties, $\delta_i(s), i = 1, \dots, r$, the real parametric uncertainties, and $\epsilon_i(s), i = 1, \dots, c$, the complex parametric uncertainties. Taking into account these uncertainties leads to the General Control Configuration given in Figure 3.3a, where $\Delta \in \underline{\Delta}$. Here, only the real parametric uncertainties (Δ_r) are considered for RS analysis. RP analysis also needs a fictive full block complex uncertainty, as shown in Figure 3.3b.

where $N(s) = \begin{bmatrix} N_{11}(s) & N_{12}(s) \\ N_{21}(s) & N_{22}(s) \end{bmatrix}$, and the closed-loop transfer matrix is:

$$T_{ew}(s) = N_{22}(s) + N_{21}(s)\Delta(s)(I - N_{11}(s))^{-1}N_{12}(s) \quad (3.13)$$

Note that in equation (3.13), $N_{22}(s) = N_{ew}$ is the nominal closed-loop transfer matrix. If it is stable, the instability in equation (3.13) may only come from $(I - N_{11}(s))^{-1}$.

As we consider structured uncertainties, a μ -analysis is used for the RS and RP analysis. First the structured singular value is defined as:

$$\mu_{\underline{\Delta}}(M)^{-1} := \min\{\bar{\sigma}(\Delta) : \Delta \in \underline{\Delta}, \det(I - \Delta M) \neq 0\} \quad (3.14)$$

For RS , we determine how large Δ (in the sense of H_{∞}) can be without destabilizing the feedback system. From equation (3.13), the feedback system becomes unstable if $\det(I - N_{11}(s)) = 0$ for some $s \in \mathbb{C}, \Re(s) \geq 0$. The following theorem is used.

Theorem 3.4.1. [Skogestad and Postlethwaite 2001] *Assume that the nominal system N_{ew} and the perturbations Δ are stable. Then the feedback system is stable for all allowed perturbations Δ such that $\|\Delta(s)\|_{\infty} < 1/\beta$ if and only if $\forall \omega \in \mathbb{R}, \mu_{\underline{\Delta}}(N_{11}(j\omega)) \leq \beta$.*

Assuming nominal stability, the RS and RP analysis for structured uncertainties are therefore

such that:

$$\text{RS} \Leftrightarrow \mu_{\Delta_r}(N_{11}) < 1, \forall \omega \quad (3.15)$$

$$\text{RP} \Leftrightarrow \mu_{\Delta}(N) < 1, \forall \omega, \Delta = \begin{bmatrix} \Delta_f & 0 \\ 0 & \Delta_r \end{bmatrix} \quad (3.16)$$

Finally, let us remark that the structured singular value cannot be explicitly determined. The method consists then in calculating an upper bound and a lower bound, as close as possible to μ .

Remark 3.3: *In chapter 5, the robustness analysis for the H_{∞} active anti-roll bar control system on heavy vehicles is done in the frequency domain by using the μ analysis tool. The forward velocity and the sprung mass are considered as the uncertainties parameters.*

3.5 Linear Quadratic Regulator control

The linear time-invariant (*LTI*) model is described by equation (3.2). For controller design, it is assumed that all the states are available from measurements or can be estimated. Then, let us consider the state feedback control law:

$$u = -Kx \quad (3.17)$$

where K is the state feedback gain matrix. The optimization procedure consists in determining the control input u which minimizes some performance index J . This index includes the performance characteristic requirement as well as the controller input limitations, usually expressed by:

$$J = \int_0^{\infty} (x^T Q x + u^T R u) dt \quad (3.18)$$

where Q and R are positive definite weighting matrices. To obtain a solution for the optimal controller (3.17), the *LTI* system must be stabilizable, which is true for the system (3.2).

From the linear optimal control theory [Zhou, Doyle, and Glover 1996], the gain K minimizing (3.18) has the following form:

$$K = R^{-1} B^T P \quad (3.19)$$

where the matrix P is the solution of the *Algebraic Riccati Equation (ARE)*:

$$A P + A^T P - P B R^{-1} B^T P + Q = 0 \quad (3.20)$$

The optimal closed-loop system is obtained from equations (3.2), (3.17) and (3.19) as follows:

$$\dot{x} = (A - B_2 K)x + B_1 w \quad (3.21)$$

Remark 3.4: *In chapter 4, the linear quadratic regulator control method will be used for the active anti-roll bar system, in order to emphasize how it can cope with multi-objective requirements in terms of roll stability and actuator constraints.*

3.6 LTI/ H_∞ control problem and design

In the last decades, the H_∞ robust control theory for physical systems has seen remarkable growth in its usage. Both industrial and academical communities have been interested in the use of the analysis and the synthesis tools that this control theory provides. Indeed, the H_∞ methods are used in control theory to synthesize controllers achieving stabilization with guaranteed performance [Zhou, Doyle, and Glover 1996], [Skogestad and Postlethwaite 2001]. The H_∞ control design is expressed as a mathematical optimization problem and it has the advantage of being applicable to the problems involving multivariable systems with cross-coupling between channels.

Figure 3.4 presents a standard H_∞ control problem scheme. The plant $\Sigma(s)$ has two input vectors, the exogenous input w , that includes reference signal and disturbances, and the manipulated variables u . There are two output vectors, the controlled outputs z that we want to minimize, and the measured variables y that are used as the inputs of the controller $K(s)$ to calculate the control signal u . The effect of w on z after closing the loop is measured in terms of the energy and the worst disturbance w .

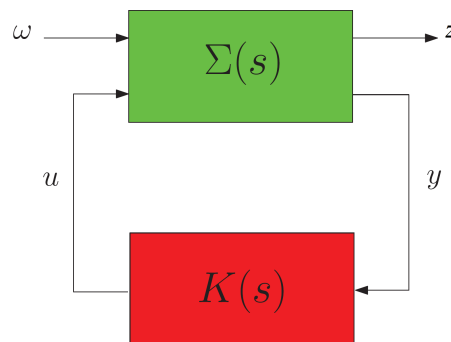


Figure 3.4: H_∞ control problem scheme.

3.6.1 H_∞ optimal control problem

The objective is to find a controller $K(s)$ using the information of the output y that generates a control signal u which ensures the internal stability of the closed-loop system and counteracts the influence of the disturbances w on the controlled outputs z , thereby minimizing the closed-loop norm from w to z . Let's bear in mind that, while trying to regulate the performance, the internal stability has to be maintained. The effect of w on z after closing the loop is measured in terms of the energy and the worst disturbance w . This can be described by the H_∞ norm which is the supremum over all disturbances different from zero and of the quotient of the energy flowing out of the system and the energy flowing into the system. Note that, the scheme in Figure 3.4, has no robust property included. Therefore, this generalized LTI

system can be described mathematically as follows:

$$\begin{bmatrix} \dot{x} \\ z \\ y \end{bmatrix} = \begin{bmatrix} A & B_1 & B_2 \\ C_1 & D_{11} & D_{12} \\ C_2 & D_{21} & D_{22} \end{bmatrix} \begin{bmatrix} x \\ w \\ u \end{bmatrix} \quad (3.22)$$

where $x \in \mathbb{R}^n$, $z \in \mathbb{R}^r$, $y \in \mathbb{R}^p$, $w \in \mathbb{R}^q$ and $u \in \mathbb{R}^m$. This formulation will be used to solve the optimization problem in the control theory framework for LTI Σ .

The objective of the synthesis is to find a controller K of the form (3.24) such that the closed-loop system is quadratically stable and that, for a given positive real γ_∞ , the induced- \mathcal{L}_2 norm of the operator mapping w into z is bounded by γ_∞ i.e.

$$\sup_{w \neq 0, w \in L_2} \frac{\|z\|_2}{\|w\|_2} \leq \gamma_\infty \quad (3.23)$$

According to this general formulation, the controller K is defined as:

$$\begin{bmatrix} \dot{x}_c \\ u \end{bmatrix} = \begin{bmatrix} A_c & B_c \\ C_c & D_c \end{bmatrix} \begin{bmatrix} x_c \\ y \end{bmatrix} \quad (3.24)$$

where $x_c \in \mathbb{R}^n$, $u \in \mathbb{R}^m$, $y \in \mathbb{R}^p$. The closed-loop system can be derived from the generalized plant $P(s)$ and the controller $K(s)$ as follows:

$$\begin{bmatrix} \dot{\xi} \\ z \end{bmatrix} = \begin{bmatrix} \mathcal{A} & \mathcal{B} \\ \mathcal{C} & \mathcal{D} \end{bmatrix} \begin{bmatrix} \xi \\ w \end{bmatrix} \quad (3.25)$$

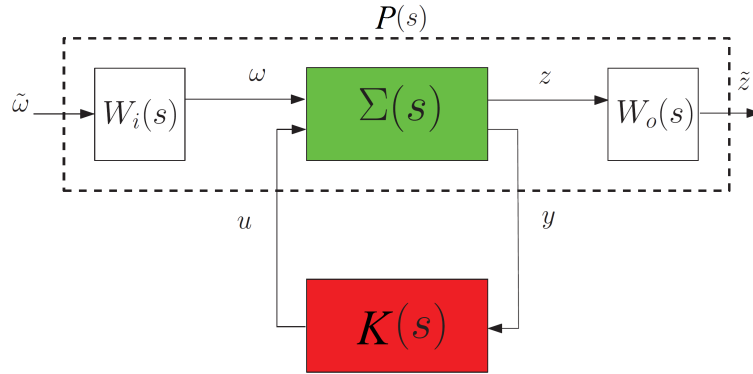
where $\xi = [x^T \ x_c^T]^T \in \mathbb{R}^{2n}$, $z \in \mathbb{R}^r$, $w \in \mathbb{R}^q$. To simplify, we will consider here only strictly proper systems i.e it is assumed that $D_{22} = 0$. The matrices of the closed-loop system are then given as follows:

$$\begin{cases} \mathcal{A} = \begin{bmatrix} A + B_2 D_c C_2 & B_2 C_c \\ B_c C_2 & A_c \end{bmatrix} \\ \mathcal{B} = \begin{bmatrix} B_1 + B_2 D_c D_{21} \\ B_c D_{21} \end{bmatrix} \\ \mathcal{C} = [C_1 + D_{12} D_c C_2 \quad D_{12} C_c] \\ \mathcal{D} = D_{11} + D_{12} D_c D_{21} \end{cases} \quad (3.26)$$

The main objective of the H_∞ controller is to make \mathcal{A} Hurwitz (i.e. that the closed loop system is stable) and to achieve some performance specification. Therefore, it consists of finding a stabilizing controller that stabilizes the closed loop system and minimizes the impact of the input disturbances w to controlled outputs z . It is worth noting that all control problems can be viewed as a stabilization problem (with or without constraint, like H_2 , H_∞ , etc.).

3.6.2 LTI/ H_∞ control design

In the H_∞ framework, to satisfy performance specifications, some weighting functions $W_i(s)$ and $W_o(s)$ are added onto the input disturbances and the controlled outputs respectively as

Figure 3.5: Generalized H_∞ control scheme.

illustrated in Figure 3.5. These weighting functions allow the shaping of some specific controlled output in the frequency domain. The interconnection between the weighting functions and the system $\Sigma(s)$ provides the generalized system $P(s)$. The generalized LTI system $P(s)$ can be described as in equation (3.22). The main idea of the H_∞ control synthesis is to minimize the impact of the input disturbances $\tilde{w}(t)$ on the controlled output $\tilde{z}(t)$. The solution of the H_∞ control problem using a dynamic output-feedback for the LTI system is given in the following:

Proposition 3.6.1 (LTI/ H_∞ solution [Scherer, Gahinet, and Chilali 1997]). *Consider the system (3.22), a dynamical output feedback controller $K(s)$ as in (3.24) that solves the H_∞ control problem, is obtained by solving the following LMIs in $(\mathbf{X}, \mathbf{Y}, \tilde{\mathbf{A}}, \tilde{\mathbf{B}}, \tilde{\mathbf{C}}$ and $\tilde{\mathbf{D}})$, while minimizing γ_∞ ,*

$$\begin{bmatrix} M_{11} & (*)^T & (*)^T & (*)^T \\ M_{21} & M_{22} & (*)^T & (*)^T \\ M_{31} & M_{32} & M_{33} & (*)^T \\ M_{41} & M_{42} & M_{43} & M_{44} \end{bmatrix} \prec 0 \quad (3.27)$$

$$\begin{bmatrix} \mathbf{X} & I_n \\ I_n & \mathbf{Y} \end{bmatrix} \succ 0$$

where,

$$\begin{aligned} M_{11} &= \mathbf{A}\mathbf{X} + \mathbf{X}\mathbf{A}^T + B_2\tilde{\mathbf{C}} + \tilde{\mathbf{C}}^T B_2^T \\ M_{21} &= \tilde{\mathbf{A}} + \mathbf{A}^T + C_2^T \tilde{\mathbf{D}}^T B_2^T \\ M_{22} &= \mathbf{Y}\mathbf{A} + \mathbf{A}^T \mathbf{Y} + \tilde{\mathbf{B}}C_2 + C_2^T \tilde{\mathbf{B}}^T \\ M_{31} &= B_1^T + D_{21}^T \tilde{\mathbf{D}}^T B_2^T \\ M_{32} &= B_1^T \mathbf{Y} + D_{21}^T \tilde{\mathbf{B}}^T \\ M_{33} &= -\gamma_\infty I_m \\ M_{41} &= C_1 \mathbf{X} + D_{12} \tilde{\mathbf{C}} \\ M_{42} &= C_1 + D_{12} \tilde{\mathbf{D}} C_2 \\ M_{43} &= D_{11} + D_{12} \tilde{\mathbf{D}} D_{21} \\ M_{44} &= -\gamma_\infty I_p \end{aligned} \quad (3.28)$$

Then, the reconstruction of the controller K is obtained by the following equivalent transfor-

mation,

$$\begin{cases} D_c &= \tilde{\mathbf{D}} \\ C_c &= (\tilde{\mathbf{C}} - D_c C_2 \mathbf{X}) M^{-T} \\ B_c &= N^{-1}(\tilde{\mathbf{B}} - Y B_2 D_c) \\ A_c &= N^{-1}(\tilde{\mathbf{A}} - Y A X - Y B_2 D_c C_2 \mathbf{X} - N B_c C_2 \mathbf{X} - Y B_2 C_c M^T) M^{-T} \end{cases} \quad (3.29)$$

where M and N are defined such that $MN^T = I_n - XY$ which can be solved through a singular value decomposition plus a Cholesky factorization.

Remark 3.5: For the numerical issues, the set of LMIs is solved step by step as follows:

- The first step: the LMI (3.27) is solved to find γ_∞^* , the optimal bound solution. Then, we will often solve the LMIs with a fixed higher attenuation level $\gamma_\infty = \gamma_\infty^*(1 + \nu)$, (ν being a percentage) [Scherer, Gahinet, and Chilali 1997].
- The second step: the second statement of (3.27) is replaced by,

$$\begin{bmatrix} X & \alpha I_n \\ \alpha I_n & Y \end{bmatrix} > 0 \quad (3.30)$$

where $\alpha > 0$, and the optimization to be done consists in maximizing α . This procedure maximizes the minimal eigenvalue of XY , and hence pushes it away from I_n , and therefore avoids bad conditioning when inverting M and N in the controller reconstruction step (3.29).

3.7 LPV/ H_∞ control problem and design

In this section, the extension of the results presented in the previous section is done with the LPV system. More particularly we will focus on the Grid-based LPV approach.

3.7.1 General problem formulation

The LPV system under consideration is described as in Definition (3.2.3) i.e.:

$$\Sigma_{\mathcal{L}PV} : \begin{cases} \dot{x}(t) = A(\rho)x(t) + B(\rho)w(t) \\ z(t) = C(\rho)x(t) + D(\rho)w(t) \end{cases} \quad (3.31)$$

The generalized LPV system is rewritten into a more general form as follows:

$$\Sigma(\rho) : \begin{bmatrix} \dot{x} \\ z \\ y \end{bmatrix} = \left[\begin{array}{c|cc} A(\rho) & B_1(\rho) & B_2(\rho) \\ \hline C_1(\rho) & D_{11}(\rho) & D_{12}(\rho) \\ C_2(\rho) & D_{21}(\rho) & D_{22}(\rho) \end{array} \right] \begin{bmatrix} x \\ w \\ u \end{bmatrix} \quad (3.32)$$

Let assume that $x \in \mathbb{R}^n$, $z \in \mathbb{R}^r$, $y \in \mathbb{R}^p$, $w \in \mathbb{R}^q$ and $u \in \mathbb{R}^m$, where x is the state vector of the system plus the state vector of the weighting functions, z the controlled output vector, y the measured output vector, w the disturbance vector, and u the control input vector. $\rho = (\rho_1(t), \rho_2(t), \dots, \rho_p(t)) \in \mathcal{P}_\rho$, is a vector of time-varying parameters and is assumed to be known (measurable or estimable).

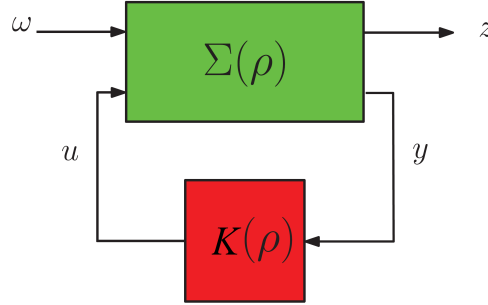


Figure 3.6: Generalized LPV/ H_∞ control problem.

The LPV controller $K(\rho)$ with the scheme as shown in Figure 3.6 is defined as:

$$\begin{bmatrix} \dot{x}_c \\ u \end{bmatrix} = \begin{bmatrix} A_c(\rho) & B_c(\rho) \\ C_c(\rho) & D_c(\rho) \end{bmatrix} \begin{bmatrix} x_c \\ y \end{bmatrix} \quad (3.33)$$

where $x_c \in \mathbb{R}^n$, $u \in \mathbb{R}^m$, $y \in \mathbb{R}^p$.

Let assume that the matrix $D_{22}(\rho) = 0$, so the closed-loop system $\Sigma_{CL}(\rho) = LFT(\Sigma(\rho), K(\rho))$ can be derived from the generalized plant $\Sigma(\rho)$ (3.32) and the controller $K(\rho)$ (3.33) as follows:

$$\begin{bmatrix} \dot{\xi} \\ z \end{bmatrix} = \begin{bmatrix} \mathcal{A}(\rho) & \mathcal{B}(\rho) \\ \mathcal{C}(\rho) & \mathcal{D}(\rho) \end{bmatrix} \begin{bmatrix} \xi \\ w \end{bmatrix} \quad (3.34)$$

where

$$\begin{cases} \mathcal{A} = \begin{bmatrix} A(\rho) + B_2(\rho)D_c(\rho)C_2(\rho) & B_2(\rho)C_c(\rho) \\ B_c(\rho)C_2(\rho) & A_c(\rho) \end{bmatrix} \\ \mathcal{B} = \begin{bmatrix} B_1(\rho) + B_2(\rho)D_c(\rho)D_{21}(\rho) \\ B_c(\rho)D_{21}(\rho) \end{bmatrix} \\ \mathcal{C} = [C_1(\rho) + D_{12}(\rho)D_c(\rho)C_2(\rho) \quad D_{12}(\rho)C_c(\rho)] \\ \mathcal{D} = D_{11}(\rho) + D_{12}(\rho)D_c(\rho)D_{21}(\rho) \end{cases} \quad (3.35)$$

with $\xi = [x^T \ x_c^T]^T \in \mathbb{R}^{2n}$, $z \in \mathbb{R}^r$, $w \in \mathbb{R}^q$.

The control goal is to find an LPV controller $K(\rho)$ expressed in equation (3.33). The matrix $A_c(\rho)$, $B_c(\rho)$, $C_c(\rho)$, $D_c(\rho)$ are continuous bounded matrix functions. The LPV controller $K(\rho)$ minimizes the induced \mathcal{L}_2 norm of the closed-loop LPV system $\Sigma_{CL}(\rho) = LFT(\Sigma(\rho), K(\rho))$, with zero initial conditions, i.e.:

$$\| \Sigma_{CL}(\rho) \|_{2 \rightarrow 2} = \sup_{\substack{\rho \in \mathcal{P} \\ \bar{\nu} \leq \dot{\rho} \leq \underline{\nu}}} \sup_{\substack{w \in \mathcal{L}_2 \\ \|w\|_2 \neq 0}} \frac{\|z\|_2}{\|w\|_2} \quad (3.36)$$

The existence of a controller that solves the parameter dependent LPV γ -performance problem can be expressed as the feasibility of a set of linear matrix inequalities (LMIs), which can be solved numerically [Gaspar, Bokor, and Szaszi 2004], [Gaspar, Szabo, and Bokor 2005a], [Gaspar, Szabo, and Bokor 2005b].

It is worth noting that:

- The above problem can be solved considering the parameter dependent stability of LPV systems, which is the generalization of the quadratic stability concept. Applying the parameter dependent stability concept, it is assumed that the derivative of parameters can also be measured in real time. This concept is less conservative than the quadratic stability [Wu 1995], [Wu 2001], [Wu et al. 1996].
- The possible controller dependence on $\dot{\rho}$ will be stated by the adopted solution in terms of the parameter-dependence, or not, of the Lyapunov matrix.

3.7.2 LPV/ H_∞ control synthesis

The H_∞ control synthesis solution for LPV systems is extended from the LTI ones as follows.

Proposition 3.7.1 (LMI-based LPV/ H_∞ solution). *Consider the system (3.32). A dynamical output feedback controller $K(s)$ (3.33) that solves the H_∞ control problem, is obtained by solving the LMIs (3.37) in $(\mathbf{X}(\rho), \mathbf{Y}(\rho), \tilde{\mathbf{A}}(\rho), \tilde{\mathbf{B}}(\rho), \tilde{\mathbf{C}}(\rho)$ and $\tilde{\mathbf{D}}(\rho))$ while minimizing γ_∞ , $\forall \rho \in \mathcal{P}_\rho$*

$$\begin{bmatrix} M_{11} & (*)^T & (*)^T & (*)^T \\ M_{21} & M_{22} & (*)^T & (*)^T \\ M_{31} & M_{32} & M_{33} & (*)^T \\ M_{41} & M_{42} & M_{43} & M_{44} \end{bmatrix} \prec 0 \quad (3.37)$$

$$\begin{bmatrix} \mathbf{X}(\rho) & I_n \\ I_n & \mathbf{Y}(\rho) \end{bmatrix} \succ 0$$

where,

$$\begin{aligned} M_{11} &= A(\rho)\mathbf{X}(\rho) + \mathbf{X}(\rho)A(\rho)^T + \frac{\partial \mathbf{X}(\rho)}{\partial \rho} \dot{\rho} + B_2 \tilde{\mathbf{C}}(\rho) + \tilde{\mathbf{C}}(\rho)^T B_2^T \\ M_{21} &= \tilde{\mathbf{A}}(\rho) + A(\rho)^T + C_2^T \tilde{\mathbf{D}}(\rho)^T B_2^T \\ M_{22} &= \mathbf{Y}(\rho)A(\rho) + A(\rho)^T \mathbf{Y}(\rho) + \frac{\partial \mathbf{Y}(\rho)}{\partial \rho} \dot{\rho} + \tilde{\mathbf{B}}(\rho)C_2 + C_2^T \tilde{\mathbf{B}}(\rho)^T \\ M_{31} &= B_1(\rho)^T + D_{21}(\rho)^T \tilde{\mathbf{D}}(\rho)^T B_2^T \\ M_{32} &= B_1(\rho)^T \mathbf{Y}(\rho) + D_{21}(\rho)^T \tilde{\mathbf{B}}(\rho)^T \\ M_{33} &= -\gamma_\infty I_m \\ M_{41} &= C_1(\rho)\mathbf{X}(\rho) + D_{12}(\rho)\tilde{\mathbf{C}}(\rho) \\ M_{42} &= C_1(\rho) + D_{12}(\rho)\tilde{\mathbf{D}}(\rho)C_2 \\ M_{43} &= D_{11}(\rho) + D_{12}(\rho)\tilde{\mathbf{D}}(\rho)D_{21}(\rho) \\ M_{44} &= -\gamma_\infty I_p \end{aligned} \quad (3.38)$$

Then, the reconstruction of the controller K is obtained by the following equivalent transformation (for $\frac{\partial X(\rho)}{\partial \rho} \dot{\rho} = 0$)

$$\begin{cases} D_c(\rho) &= \tilde{D}(\rho) \\ C_c(\rho) &= (\tilde{C}(\rho) - D_c(\rho)C_2(\rho)\mathbf{X}(\rho))M(\rho)^{-T} \\ B_c(\rho) &= N(\rho)^{-1}(\tilde{B}(\rho) - \mathbf{Y}(\rho)B_2(\rho)D_c(\rho)) \\ A_c(\rho) &= N(\rho)^{-1}(\tilde{A}(\rho) - \mathbf{Y}(\rho)A(\rho)\mathbf{X}(\rho) - \mathbf{Y}(\rho)B_2(\rho)D_c(\rho)C_2(\rho)\mathbf{X}(\rho) \\ &\quad - N(\rho)B_c(\rho)C_2(\rho)\mathbf{X}(\rho) - \mathbf{Y}(\rho)B_2(\rho)C_c(\rho)M(\rho)^T)M(\rho)^{-T} \end{cases} \quad (3.39)$$

where $M(\rho)$ and $N(\rho)$ are defined such that $M(\rho)N(\rho)^T = I_n - X(\rho)Y(\rho)$ which can be solved through a singular value decomposition plus a Cholesky factorization.

We can see that due to the infinite number of possible values of the scheduling parameters, in order to design the LPV controller, we need to solve many parameter-dependent sets of matrix inequalities, which results in an infinite dimensional problem. Then to relax it into a finite dimension problem, three different kinds of approaches are commonly found in the literature [Hoffmann and Werner 2014]:

- **Linear Fractional Transformations (LFT)** [Packard 1994], [Apkarian and Gahinet 1995]: The LFT models have state matrices that are rational functions of the parameter. Hence, their dependence on the parameter vector is modeled explicitly.
- **Polytopic solution:** The polytopic system is a convex combination of the systems defined at each vertex of a polytope given by the bounds of the scheduling parameters [Scherer, Gahinet, and Chilali 1997]. The synthesis of such a controller can be made in the framework of LPV/ H_∞ based on the LMI solution for polytopic systems (the framework of quadratic stabilization). This can be applied to LPV systems with an affine dependence on the parameters only.
- **Linearizations on a gridded domain (grid-based LPV)** [Wu 1995], [Becker 1993], which are obtained through Jacobian linearization at each grid point. Each linearization approximates the system's dynamics in the vicinity of a particular grid point, and the grid of linearizations captures the system's parameter dependence implicitly.

Since the linearization based LPV models do not require any special dependence on the parameter vector, in this thesis, the author is interested in the grid-based LPV approach for the active anti-roll bar system of heavy vehicles using the LPVToolsTM toolbox [Hjartarson, Seiler, and Balas 2013]. Indeed such an approach is interesting when the number of parameters increases since the polytopic approach may lead to very conservative results (due to the augmented size of the parameter set and the single Lyapunov function). It has been used successfully in several studies [Hjartarson, Seiler, and Balas 2013], [Wang et al. 2016], [Marcos and Balas 2004] and is now available in the LPVToolsTM toolbox [Hjartarson, Seiler, and Packard 2015].

Some brief reminders on the synthesis of dynamic and feedback controllers for LPV are presented here. More details can be found in the studies [Wu 1995], [Wu 2001], [Wu et al. 1996].

The following theorem describes the LPV analysis problem when it is formulated in terms of the induced \mathcal{L}_2 norm of $G(\rho)$ and the rate-bounds $(\bar{\nu}, \underline{\nu})$ of the parameter are taken into account [Gaspar, Bokor, and Szaszi 2004].

Theorem 3.7.1: *Given a compact set $\mathcal{P} \subset \mathcal{R}^S$, the performance level γ and the LPV system (3.32), with restriction $D_{11}(\rho) = 0$, the parameter-dependent γ -performance problem is solvable if there exist a continuously differentiable function $X: \mathcal{R}^S \rightarrow \mathcal{R}^{n \times n}$, and $Y: \mathcal{R}^S \rightarrow \mathcal{R}^{n \times n}$, such that for all $\rho \in \mathcal{P}$, $X(\rho) = X^T(\rho) > 0$, $Y(\rho) = Y^T(\rho) > 0$ and*

$$\begin{bmatrix} \hat{A}(\rho)X(\rho) + X(\rho)\hat{A}^T(\rho) - \sum_{i=1}^s (\nu_i \frac{\partial X}{\partial \rho_i}) - B_2(\rho)B_2^T(\rho) & X(\rho)C_1^T(\rho) & \gamma^{-1}B_1(\rho) \\ C_1(\rho)X(\rho) & -I_{ne} & 0 \\ \gamma^{-1}B_1^T(\rho) & 0 & -I_{nd} \end{bmatrix} < 0, \quad (3.40)$$

$$\begin{bmatrix} \tilde{A}^T(\rho)Y(\rho) + Y(\rho)\tilde{A}(\rho) + \sum_{i=1}^s (\nu_i \frac{\partial Y}{\partial \rho_i}) - C_2^T(\rho)C_2(\rho) & Y(\rho)B_1(\rho) & \gamma^{-1}C_1^T(\rho) \\ B_1^T(\rho)Y(\rho) & -I_{nd} & 0 \\ \gamma^{-1}C_1(\rho) & 0 & -I_{ne} \end{bmatrix} < 0, \quad (3.41)$$

$$\begin{bmatrix} X(\rho) & \gamma^{-1}I_n \\ \gamma^{-1}I_n & Y(\rho) \end{bmatrix} \geq 0 \quad (3.42)$$

where $\hat{A}(\rho) = A(\rho) - B_2(\rho)C_1(\rho)$, $\tilde{A}(\rho) = A(\rho) - B_1(\rho)C_2(\rho)$. If the conditions are satisfied, there exists a controller (3.33) to solve that problem. The Theorem (3.7.1) and its proof are found in [Wu 1995], [Wu 2001], [Wu et al. 1996].

The constraints set by the LMIs in Theorem (3.7.1) are infinite dimensional, as is the solution space. The variables are $X, Y: \mathcal{R}^S \rightarrow \mathcal{R}^{n \times n}$, which restricts the search to the span of a collection of known scalar basis functions. By selecting scalar continuous differentiable basis functions $\{g_i: \mathcal{R}^S \rightarrow \mathcal{R}\}_{i=1}^{N_x}$, $\{f_i: \mathcal{R}^S \rightarrow \mathcal{R}\}_{i=1}^{N_y}$, then the variables in Theorem (3.7.1) can be parametrized as:

$$X(\rho) = \sum_{i=1}^{N_x} g_i(\rho)X_i, \quad Y(\rho) = \sum_{i=1}^{N_y} f_i(\rho)Y_j \quad (3.43)$$

Currently, there is no analytical method to select the basis functions, namely g_i and f_i . An intuitive rule for the basis function selection is to use those present in the open-loop state-space data.

3.7.3 Grid-based LPV approach

The LPV system in the equation (3.32) is conceptually represented by a state-space system $S(\rho)$ that depends on a time varying parameter vector $\rho \in \mathcal{P}_\rho$. A grid-based LPV model of this system is a collection of linearizations on a gridded domain of parameter values [Hjartarson, Seiler, and Packard 2015]. For general LPV systems, this conceptual representation requires storing the state-space system at an infinite number of points in the domain of ρ . For each grid point $\hat{\rho}_k$, there is a corresponding LTI system $(A(\hat{\rho}_k), B(\hat{\rho}_k), C(\hat{\rho}_k), D(\hat{\rho}_k))$ which describes

the dynamics of $S(\hat{\rho}_k)$ when $\hat{\rho}_k$ is held constant. It is worth noting that $\hat{\rho}_k$ represents a constant vector corresponding to the k^{th} grid point, while ρ_i is later used to denote the i^{th} element of the vector ρ . All the linearized systems on the grid have identical inputs u , outputs y and state vectors x . Together they form a LPV system approximation of $S(\rho)$ [Marcos and Balas 2004], [Hecker 2014].

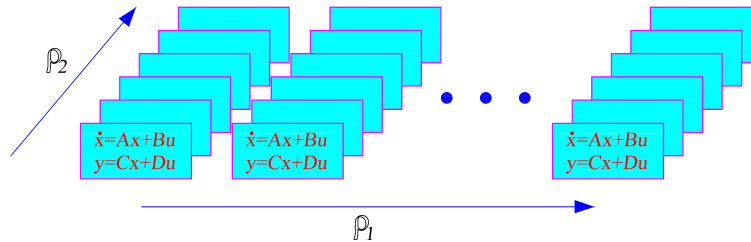


Figure 3.7: LPV models defined on a rectangular grid.

The grid-based approach is pictorially represented in Figure 3.7, here is an example of such a system that depends on two parameters (ρ_1, ρ_2) . The grid based LPV approach approximates this conceptual representation by storing the LPV system as a state-space array defined on a finite, gridded domain. In this thesis such a grid-based approach will be used to find the LPV controller (3.33).

3.7.4 The LPVToolsTM toolbox

LPVToolsTM was developed by MUSYN, Inc. (G. Balas and the authors) but has been made freely available to the community. The toolbox is available for download at:

www.aem.umn.edu/SeilerControl/software.shtml

LPVToolsTM is a MATLAB toolbox for modeling and design of Linear Parameter-Varying (LPV) systems. The toolbox contains data structures to represent LPV systems in both the LFT and gridded (Jacobian-linearization) framework. The core of the toolbox is a collection of functions for model reduction, analysis, synthesis and simulation of LPV systems. The toolbox introduces several class-based data structures for modeling LPV systems. These data structures extend the functionality associated with standard MATLAB data structures from the Control Systems Toolbox and the Robust Control Toolbox into the LPV framework. This is shown in Figure 3.8. The core LPVToolsTM data structures are direct extensions of existing data structures, and provide a parameter dependent interpretation of the original object. Note that LPV systems are time varying, and as such do not have a valid frequency response interpretation. Hence, the parameter dependent frequency response objects are simply a convenience to hold frequency response data at fixed parameter values, and do not imply a time-varying frequency response.

Each LPVToolsTM object implements the capabilities of its corresponding standard object,

wherever applicable. The motivation for this approach is to provide a seamless and intuitive interface between existing MATLAB data structures and the new LPVToolsTM data structures. The standard MATLAB data structures become a special case of the LPV data structures, such that if the parameter dependence in a LPV data structure is eliminated, it reverts back to a standard Linear Time-Invariant (LTI) MATLAB data structure.

Readers are also invited to refer to the publications [Hjartarson, Seiler, and Balas 2013], [Hjartarson, Seiler, and Packard 2015], where all the LPVToolsTM implementation and capabilities are given.

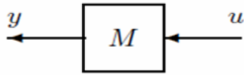
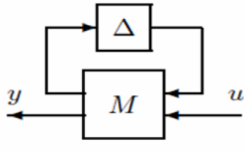
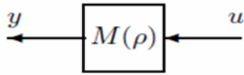
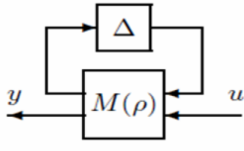
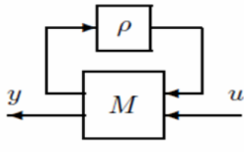
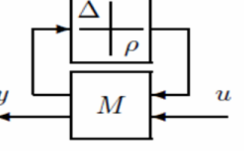
Object Type	Block	Matrix	System	Frequency Response
Nominal		<code>double</code>	<code>ss</code>	<code>frd</code>
Uncertain		<code>umat</code>	<code>uss</code>	<code>ufrd</code>
Nominal Gridded LPV		<code>pmat</code>	<code>pss</code>	<code>pfrd</code>
Uncertain Gridded LPV		<code>upmat</code>	<code>upss</code>	<code>upfrd</code>
Nominal LFT LPV		<code>pmatlft</code>	<code>psslft</code>	
Uncertain LFT LPV		<code>pmatlft</code>	<code>psslft</code>	

Figure 3.8: Relation between MATLAB objects [Hjartarson, Seiler, and Packard 2015].

3.8 Multi-objective optimization by using genetic algorithms

In this thesis, the active anti-roll bar control problem will be linked to different objectives such as roll stability and input current entering the ESVH actuators. Hence the multi-objective framework is an important issue.

3.8.1 Multi-criteria optimization and Pareto-optimal solutions

A Multi-Criteria Optimization (MCO) problem can be described in mathematical terms as follows [Ehrgott 2005]:

$$\min_{x \in S} F(x) = [f_1(x), f_2(x), \dots, f_n(x)] \quad (3.44)$$

where x is called the decision vector, $F(x)$ the objective vector, $n > 1$ and S the set of constraints defined above. The space in which the objective vector belongs is called the objective space, and the image of the feasible set under F is called the attained set. In the following, such a set will be denoted by $C = \{y \in R^n : y = f(x), x \in S\}$. The scalar concept of “optimality” does not apply directly in the multi-criteria setting. Here the notion of Pareto optimality is introduced. Essentially, a vector $x^* \in S$ is said to be Pareto optimal for a multi-criteria problem if all the other vectors $x \in S$ do not have a higher value for at least one of the objective functions f_i , with $i = 1, \dots, n$, or have the same value for all the objective functions. The concept of Pareto optimal is defined as follows.

Definition 3.8.1 (Pareto-Ranking). *Consider two decision vectors $a, b \in S$. Vector a dominates b if and only if:*

$$\begin{cases} \forall i \in \{1, 2, \dots, n_{obj}\} : f_i(a) \leq f_i(b) \\ \exists j \in \{1, 2, \dots, n_{obj}\} : f_j(a) < f_j(b) \end{cases} \quad (3.45)$$

All decision vectors which are not dominated by any other decision vector are called non-dominated or Pareto optimal. The family of non-dominated vectors is denoted as Pareto-front. In the Pareto-front, one cannot improve any objective without degrading at least one other objective.

There are many formulations to solve the problem (3.44) such as weighted min-max method, weighted global criterion method, goal programming methods... [Marler and Arora 2004] and references therein. Here, one uses a particular case of the weighted sum method, where the multi-criteria functions vector F is replaced by the convex combination of objectives:

$$\min_{x \in S} J = \sum_{i=1}^n \alpha_i f_i(x), \quad \sum_{i=1}^n \alpha_i = 1, \quad s.t., \quad x \in S \quad (3.46)$$

The vector $\alpha = (\alpha_1, \alpha_2, \dots, \alpha_n)$ represents the gradient of function J . By using various sets of α , one can generate several points in the Pareto set. However, the function J shown in equation (3.46) has the following drawbacks:

- The single objective optimization procedure has to be repeated many times with different values of α .
- Although there are many methods to solve the problem (3.44), however none of them is absolutely perfect [Do 2011].
- If the Pareto curve is not convex, there does not exist any α to obtain points which lie in the nonconvex part. Even if the Pareto curve is convex, an even spread of weights does not produce an even distribution of points on the Pareto curve [Das and Dennis 1997], [Marler and Arora 2004].

- The choice of the functions $f_i(x)$, will greatly affect the form of the Pareto curve, as well as the result of the optimization problem.

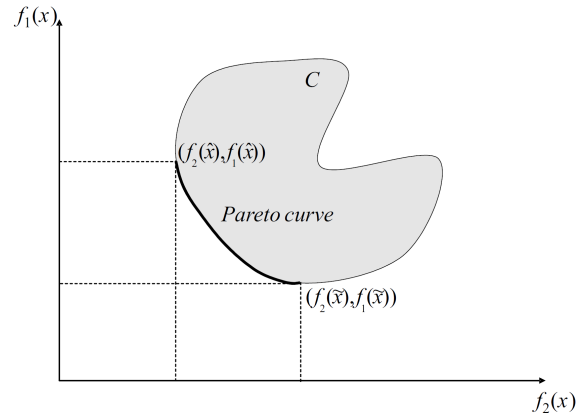


Figure 3.9: Example of a Pareto curve.

The shape of the Pareto surface indicates the nature of the trade-off between the different objective functions. An example of a Pareto curve is reported in Figure 3.9, where all the points between $(f_2(\hat{x}), f_1(\hat{x}))$ and $(f_2(\tilde{x}), f_1(\tilde{x}))$ define the Pareto front. These points are called non-inferior points.

3.8.2 Genetic algorithms

A Genetic Algorithm (GA), as presented by J.H. Holland [Holland 1975] is a model of machine learning, which derives its behavior from a metaphor of the process of evolution in nature. These algorithms have been proven to be very effective in optimization with many real life applications such as in finance and investment strategies, robotics, engineering design, telecommunications, etc. GAs are executed iteratively on a set of coded chromosomes, called a population, with three basic genetic operations: selection, crossover and mutation [Marler and Arora 2004]. Each member of the population, called a chromosome (or individual) is represented by a string. GAs use only the objective function information and probabilistic transition rules for genetic operations. The primary operation of GAs is the crossover. The crossover happens with a probability of 0.9 and the mutation happens with a small probability 0.095 [Goldberg 1989], [Davis 1991]. Some genetic idioms are widely used in the description of the different parts of GAs, and are listed as follows:

- Member or individual: it refers to any possible solution in decision space where any acceptable combination of the parameters can form an individual.
- Generation or population: it relates to a group of individuals.
- Chromosome: it refers to one parameter among the individual parameters.
- Genome: it refers to the chromosome in the individual.

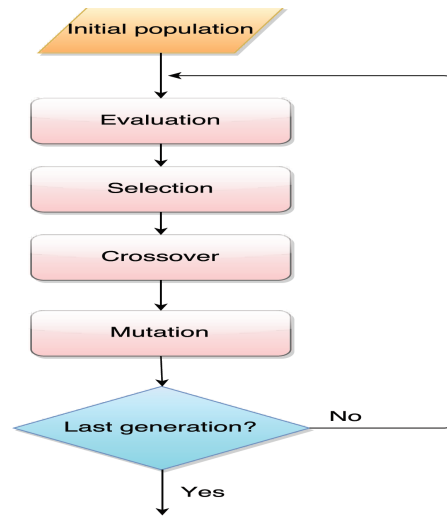


Figure 3.10: Genetic algorithm steps in developing generations of members.

Figure 3.10 shows the principle of GAs. At the beginning, GAs initialize with a random population. Through the genetic operation: selection, crossover and mutation, new populations will be obtained. By using a selection process, the fittest individuals based on their fitness values will be chosen; crossover and mutation will be then applied to create the new population. The process is terminated when the desired number of generation is achieved. The main four steps are described in detail as follows:

- **Fitness function:** the fitness of an individual is useful for choosing between good and bad individuals. An individual with a high fitness value will have a great chance to be selected.
- **Selection:** this is used to sort and copy individuals by order of satisfaction of the fitness function. If the higher the value of the fitness (associated to an individual), then the greater the individual's chances to be selected to participate in the next generation.
- **Crossover:** this is the main operation acting on the population of parents. It consists of an exchange of chain parts between two selected individuals (parents) to form two new individuals (children). This exchange may be due either to a single point or to multiple points. An example for a binary coding crossover is shown in Figure 3.11.
- **Mutation:** this operates on a single individual by changing randomly a part of it. In the case of binary coding, this is done by reversing one or more sections in a chromosome as shown in Figure 3.11.

The method of GAs is used in this thesis for the multi-criteria optimization of the active anti-roll bar control. The pursued objective is to select the weighting functions of the H_∞ controller synthesis, where there exists a large set of parameters (9 parameters) to be determined for the combination between roll stability and energy consumption of the system. Specifically, it will be described later in section 5.3.1.

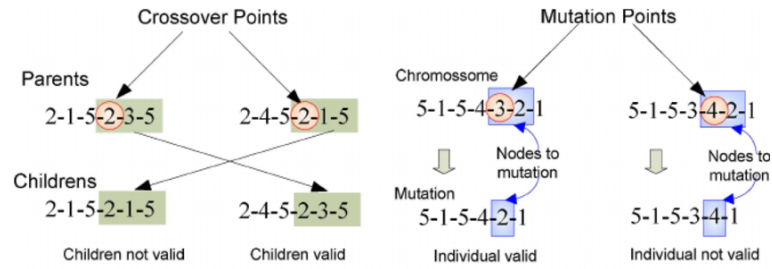


Figure 3.11: Crossover and mutation operation.

3.9 Conclusion

In this chapter, the author has introduced the dynamical systems, LQR control, LTI/H_∞ control and LPV/H_∞ control, as well as multi-optimization by using genetic algorithms involved in this thesis. The author stresses that there is no particular unique contribution in this chapter. The aim is simply to introduce the tools used in this thesis for vehicle controller synthesis.

In these three first chapters, a general introduction, the ESVH actuators involved in the vehicle modelling and mathematical background were given. In the following chapters, the control methods will be applied to the active anti-roll bar system of a single unit heavy vehicle.

Part II
Active anti-roll bar control: LTI
approach

The aim of rollover prevention is to provide a vehicle with the ability to resist overturning moments which can be generated during difficult vehicle manoeuvres. Roll stability is determined by the height of the center of mass, the track width and the kinematic properties of the suspension. The primary overturning moment arises from the lateral acceleration acting on the center of gravity of the vehicle. More destabilizing moment can arise during cornering manoeuvres when the center of gravity of the vehicle shifts laterally. Roll stability of the vehicle can be guaranteed, if the sum of the destabilizing moment is compensated during a lateral manoeuvre.

In this part, we focus on the control methodologies of the LTI approach for the active anti-roll bar system. Specifically, they are the Linear Quadratic Regulator (LQR) and H_∞ control methods. It is worth noting that the control-oriented integrated model proposed in Chapter 2 is used throughout this part. The content of this part consists of three chapters as follows:

Chapter 4: Enhancing the roll stability of heavy vehicles by using LQR active anti-roll bar control

- An optimal *LQR* is developed for the active anti-roll bar system. The *LQR* controller is provided in order to emphasize how it can cope with multi-objective requirements in terms of roll stability and actuator constraints.
- The simulation results obtained in the frequency and time domains show that the *LQR* active anti-roll bar control system improves the roll stability, so preventing the rollover phenomenon of heavy vehicles.
- The handling performance of the vehicle is assessed by using the stability index (λ) as well as the phase-plane ($\beta - \dot{\beta}$).

Chapter 5: H_∞ robust control for active anti-roll bar system to prevent vehicle rollover

- The H_∞ control method is applied to the active anti-roll bar system with the aim of improving the roll stability of heavy vehicles. Here we consider the Multi-Criteria Optimization (MCO) problem including the normalized load transfers and the limitation of the input currents at all axles.
- The genetic algorithms method is used to find the optimal weighting functions for the H_∞ active anti-roll bar control system.
- The robust stability analysis of the H_∞ controller is performed by using the μ -analysis method. The two uncertain parameters considered are the forward velocity and the sprung mass.

Chapter 6: Validation of the H_∞ active anti-roll bar control by using TruckSim[®] software

- The proposed H_∞ active anti-roll bar control is validated by using the co-simulation between Matlab[®]/Simulink and TruckSim[®].
- We consider two different kinds of vehicle: a tour bus and a LCF truck. They are validated in different simulation scenarios and at different forward velocities.
- The simulation results clearly confirm the effectiveness of the H_∞ active anti-roll bar control system in improving the roll stability of heavy vehicles.

Control objective, problem statement

The main objective of the active anti-roll bar control system is to maximize roll stability of heavy vehicles, so preventing a rollover phenomenon in an emergency situation. However, we have to pay attention to the physical limits of the suspension, as well as the saturation of the actuators. Therefore when designing an active anti-roll bar system for heavy vehicles, the following three main objectives must be met simultaneously:

- **The roll stability** expressed by the limits of the normalized load transfers at all axles (equation (2.43)) in the range of $[-1, 1]$, and in the frequency range to over 4 rad/s [Sampson 2000], [Gaspar, Bokor, and Szaszi 2004]. The normalized load transfers $R_{f,r} = \pm 1$ value corresponds to the largest possible load transfers. Roll stability is achieved by limiting the normalized load transfers within the levels corresponding to wheel lift-off.
- **The saturation of the actuators** expressed by the maximum absolute value of the spool valve displacement less than $4.85 \times 10^{-4} \text{ m}$ [Rafa, Yahya, and Rawand 2009], of the input current less than 20 mA [Rafa, Yahya, and Rawand 2009], of the load flow less than $2.2 \times 10^{-3} \text{ m}^3/\text{s}$ [Sampson 2000], and of the actuator forces less than 120 kN [Sampson 2000].
- **The limits of the suspension travel** expressed by the roll angles between the sprung and unsprung masses ($\phi - \phi_{u_{f,r}}$), which allow the maximum stabilizing moment of the active anti-roll bar system to be increased. They should stay within the limits of the suspension travel from 7 to 8 deg [Gaspar, Bokor, and Szaszi 2004], [Sampson 2000].

In the following chapters, the chosen control objective is to minimize the effect of the steering angle δ_f on the normalized load transfers $R_{f,r}$ at the two axles. Besides that, the limitation of the input currents $u_{f,r}$ entering the Electronic Servo-Valve Hydraulic (ESVH) actuators is crucial for practical implementation.

Enhancing the roll stability of heavy vehicles by using LQR active anti-roll bar control

Contents

4.1	Introduction	77
4.2	The active anti-roll bar <i>LQR</i> control	79
4.3	Simulation results analysis	80
4.3.1	Analysis in the frequency domain	80
4.3.2	Analysis in the time domain	83
4.4	Analysis of the effect of the forward velocity on the closed-loop system	86
4.4.1	The effect of the forward velocity on vehicle roll stability	86
4.4.2	The effect of the forward velocity on the physical constraints of the ESVH actuator	88
4.5	Analysis of the handling performance	91
4.5.1	Selecting the criteria to evaluate the handling performance	91
4.5.2	The handling performance analysis	91
4.6	Conclusion	93

4.1 Introduction

The H_2 or linear quadratic optimisation is the fundamental technique in optimal control theory. The linear quadratic optimisation controller design method is a signal-based approach that enables an explicit trade-off between performance and the level of control activity for MIMO systems [Lin 1994a]. An active anti-roll bar control system design can be cast as a problem of the load transfer regulation in the presence of steering disturbances.

The suitability of using several variations of the basic linear quadratic optimal control problem for the active anti-roll bar controller design on a single unit heavy vehicle will be explored in this chapter. An important variation of the basic problem, the Linear Quadratic Regulator (*LQR*) problem, has been used to design the active anti-roll bar control system to improve the

roll stability of single unit heavy vehicles [Lin 1994b], [Lin, Cebon, and Cole 1996], [Sampson and Cebon 1998], [Sampson and Cebon 2003a], [Miège and Cebon 2005b], [Yu, Guvenc, and Ozguner 2008]. In the previous studies, the authors only considered how to improve the roll stability to prevent vehicle rollover. They often used the control torques acting between the axle groups and the sprung mass as the input control signal. This led to reducing the steady state and peak transient load transfer significantly when compared with the use of a passive anti-roll bar. However they still had not taken into account the characteristics of the actuators.

This chapter will use the control-oriented integrated model presented in Chapter 2, with four Electronic Servo-Valve Hydraulic (ESVH) actuator models in a single unit heavy vehicle yaw-roll model. Then the *LQR* control method is applied to the active anti-roll bar system and focuses on showing how it can provide a wide set of solutions to solve the multi-objective problem for the improvement of roll stability, while still taking into account the characteristics of the ESVH actuators. Hence, the contributions of this chapter are the following:

- An optimal *LQR* is developed, where the optimal criterion is formulated from vehicle dynamics specifications in terms of roll stability. A generic definition of the control objectives is proposed to cope with most of the industrial performance requirements for heavy vehicle dynamics control.
- A detailed comparison of several tuning options of the *LQR* controllers is provided in order to emphasize how they can cope with multi-objective requirements in terms of roll stability (normalized load transfers) and actuator constraints (input current limitations).
- The simulation results show that the *LQR* active anti-roll bar control using four ESVH actuators drastically improves the vehicle roll stability throughout the main frequency range compared to the passive anti-roll bar. It also allows the assessment of the effects of the induced normalized load transfer, of the input current limitations, as well as of the operation of the ESVH actuators.
- The handling performance of the single unit heavy vehicle is also assessed by using the phase-plane ($\beta - \dot{\beta}$) and the stability index (λ). It indicates that besides improving roll stability to prevent vehicle rollover, the use of the *LQR* active anti-roll bar controllers also enhances vehicle handling performance.

The application of the LQR control method to the control-oriented integrated model has been presented in the two following publications:

- *Enhancing roll stability of heavy vehicle by LQR active anti-roll bar control using electronic servo-valve hydraulic actuators*, *Vehicle System Dynamics*, Vol 55(9), pp 1405-1429, 2017;
- *Active anti-roll bar control using electronic servo-valve hydraulic damper on single unit heavy vehicle*, 8th IFAC Symposium on Advances in Automotive Control, Sweden, 2016.

4.2 The active anti-roll bar *LQR* control

The main objective here is to maximize vehicle roll stability. The sprung mass roll angle (ϕ), the roll angle of the suspensions ($\phi - \phi_{uf,r}$) and the normalized load transfers ($R_{f,r}$) are variables directly affecting roll stability of the vehicle, so they are to be minimized. Besides, it is important to handle the input current limitations (u_f , u_r) of the electronic servo-valve hydraulic actuators. For these reasons, the performance index J in equation (3.18) is selected as follows:

$$J = \int_0^{\infty} (\rho_1 \phi^2 + \rho_2 R_f^2 + \rho_3 R_r^2 + \rho_4 (\phi - \phi_{uf})^2 + \rho_5 (\phi - \phi_{ur})^2 + R_{uf} u_f^2 + R_{ur} u_r^2) dt \quad (4.1)$$

where ρ_1 , ρ_2 , ρ_3 , ρ_4 , ρ_5 , R_{uf} and R_{ur} are the weighting parameters of J .

According to the choice of these parameters, equation (4.1) permits the handling of a larger set of different criteria focusing on anti-roll bar performances and/or on the limitation of the consumption of the actuator.

In this chapter, to assess the quality of the active anti-roll bar control system, three controllers have been designed and compared, using three different sets of weighting parameters:

- **First control design (*LQR*₁ - Nominal):** Roll stability and controller input current limitations are considered. The weighting parameters values are chosen as:

$$\rho_1 = \rho_2 = \rho_3 = \rho_4 = \rho_5 = 1; \quad R_{uf} = R_{ur} = 1$$

With this controller, the role of the input current limitations and roll stability is considered as balanced.

- **Second control design (*LQR*₂ - Normalized load transfer oriented):** Roll stability is taken into account and the normalized load transfers (R_f , R_r) are the most important objectives, while keeping the controller input current limitations. The weighting parameter values are chosen as:

$$\rho_1 = \rho_4 = \rho_5 = R_{uf} = R_{ur} = 1; \quad \rho_2 = \rho_3 = 10, 50, 100, 200, 500, 1000, 10000$$

where the weighting parameter values ρ_2 , ρ_3 are changed from 10 to 10000; this selection is used to consider the roll stability, the behavior of the heavy vehicle as well as of the electronic servo-valve hydraulic actuators when the normalized load transfers are more and more penalized.

- **Third control design (*LQR*₃ - Input limitation oriented):** Controller input current limitations (u_f , u_r) are taken more into account, while keeping the roll stability objective. The weighting parameters values are chosen as:

$$\rho_1 = \rho_2 = \rho_3 = \rho_4 = \rho_5 = 1; \quad R_{uf} = R_{ur} = 10, 50, 100, 200, 500, 1000, 10000$$

In this case, the weighting parameter values R_{uf} , R_{ur} are changed from 10 to 10000, the objective is to consider the roll stability, the behavior of the heavy vehicle as well as the electronic servo-valve hydraulic actuator with harder input current limitations.

Remark 4.1:

- *Of course, other controllers could be designed using (4.1) with other choices of the weighting parameters, according to different specifications;*
- *The relationship between the matrices \mathcal{Q} , \mathcal{R} in equation (3.18) and the weighting parameters $\rho_1, \rho_2, \rho_3, \rho_4, \rho_5, R_{uf}, R_{ur}$ in equation (4.1) is given in Appendix D.*

4.3 Simulation results analysis

In this section, the simulation results using the control-oriented integrated model (see section 2.4.2) with a full-state feedback controller are shown in both the frequency and time domains. The parameter values of the ESVH actuators and of the yaw-roll model are those given in Tables 2.1 and 2.2. The forward velocity is considered constant at 70 km/h.

4.3.1 Analysis in the frequency domain

Various closed loop transfer functions of the control-oriented integrated model are shown in this section. To assess the effect of the weighting parameters ρ_2 and ρ_3 of the LQR_2 design and the weighting parameters R_{uf} and R_{ur} of the LQR_3 design, two cases are considered and detailed:

1. First case: the transfer functions are shown for the **passive** anti-roll bar, the LQR_1 **design** (nominal) and the LQR_2 **design** (normalized load transfer),
2. Second case: the transfer functions are shown for the **passive** anti-roll bar, the LQR_1 **design** (nominal) and the LQR_3 **design** (input limitation).

They are detailed in the sequel.

4.3.1.1 First case: the effect of ρ_2 and ρ_3 on the transfer functions $\frac{R_{f,r}}{\delta_f}$ and $\frac{u_{f,r}}{\delta_f}$

The main objective of the active anti-roll bar system is to reduce the normalized load transfer at each axle. Figures 4.1a, b show the transfer function of the normalized load transfers at the front axle ($\frac{R_f}{\delta_f}$) and at the rear axle ($\frac{R_r}{\delta_f}$), respectively. As shown in Table 4.1, both LQR_1 and LQR_2 designs allow the reduction of the normalized load transfers (at the two axles) when compared with the passive anti-roll bar. When ρ_2 and ρ_3 increase, the transfer function magnitudes of the normalized load transfers decrease in the case of the LQR_2 design.

The reduction of normalized load transfers at the axles is due to the active anti-roll bar system. Indeed, when the vehicle rolls into the corner, unlike in the case of the passive anti-roll bar, the active one generates a stabilizing lateral displacement moment, which balances

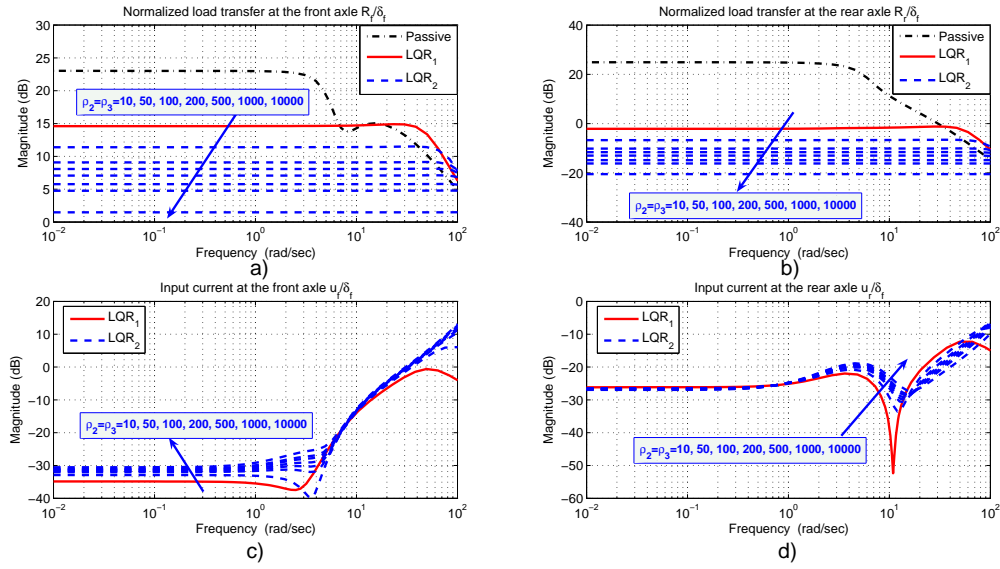


Figure 4.1: First case, the transfer functions magnitude of (a, b) normalized load transfers ($\frac{R_{f,r}}{\delta_f}$) and (c, d) input currents ($\frac{u_{f,r}}{\delta_f}$) at the axles.

the destabilizing overturning moment caused by the lateral acceleration [Gaspar, Bokor, and Szaszi 2004], [Sampson and Cebon 2003b].

Table 4.1: First case, the reduction of the magnitude of transfer functions (gain reduction) compared to the passive case.

Transfer functions	using LQR_1	using LQR_2
$\frac{R_f}{\delta_f}$	8 dB [0, 6 rad/s]	11 dB ($\rho_2 = \rho_3 = 10$), 21 dB ($\rho_2 = \rho_3 = 10000$) [0, 40 rad/s]
$\frac{R_r}{\delta_f}$	27 dB [0, 30 rad/s]	30 dB ($\rho_2 = \rho_3 = 10$), 43 dB ($\rho_2 = \rho_3 = 10000$) [0, 50 rad/s]

Figures 4.1c, d show the transfer functions gains of the input currents at the front ($\frac{u_f}{\delta_f}$) and rear axles ($\frac{u_r}{\delta_f}$), respectively. When ρ_2 and ρ_3 increase, the controller input currents ($u_{f,r}$) increase. This indicates that when the weighting parameters ρ_2 , ρ_3 increase, the LQR_2 design requires more input current (i.e. energy) than does the LQR_1 design. This emphasises the usual trade-off between performance and control limitation.

The simulation results in the frequency domain have shown that the LQR_2 design improves roll stability when ρ_2 and ρ_3 increase. However, it also increases the controller input current. This consistently fulfils the objective of the designed controllers. But as the current is limited to 20 mA [Rafa, Yahya, and Rawand 2009], ρ_2 and ρ_3 should not be increased too much to ensure all operations are within the current constraints.

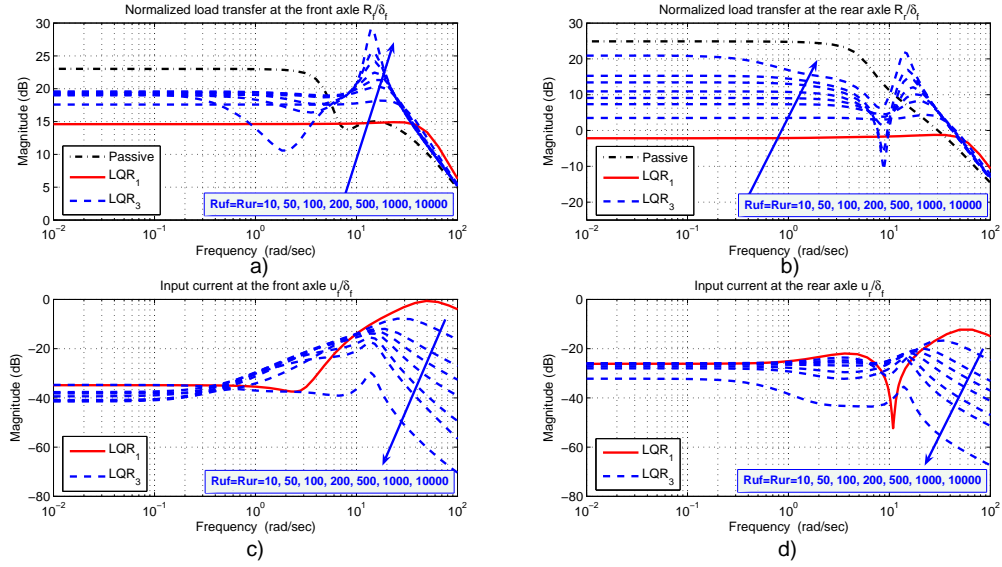


Figure 4.2: Second case, the transfer functions magnitude of (a, b) normalized load transfers ($\frac{R_{f,r}}{\delta_f}$) and (c, d) input currents ($\frac{u_{f,r}}{\delta_f}$) at the axles.

4.3.1.2 Second case: the effect of R_{uf} and R_{ur} on the transfer functions $\frac{R_{f,r}}{\delta_f}$ and $\frac{u_{f,r}}{\delta_f}$

The LQR_1 design is configured to enhance roll stability while considering also the controller input current limitations ($u_{f,r}$). Conversely, the LQR_3 design considers mainly the controller input current limitations and pays less attention to the roll stability. Figures 4.2a, b show the transfer functions gains of the normalized load transfer at the front axle ($\frac{R_f}{\delta_f}$) and rear axle ($\frac{R_r}{\delta_f}$), respectively. In Table 4.2, the reduction of the normalized load transfers (at the two axles) are shown for the LQR_1 and LQR_3 designs when compared with the passive anti-roll bar. They show that, compared to LQR_1 , the LQR_3 design does not improve so much roll stability, when R_{uf} and R_{ur} increase from 10 to 10000. This is coherent w.r.t. its synthesis objectives.

Table 4.2: Second case, the reduction of the magnitude of the transfer functions (gain reduction) compared to the passive anti-roll bar.

Transfer functions	using LQR_1	using LQR_3
$\frac{R_f}{\delta_f}$	8 dB [0, 6 rad/s]	5.5 dB ($R_{uf} = R_{ur} = 10$), 3.5 dB ($R_{uf} = R_{ur} = 10000$) [0, 5 rad/s]
$\frac{R_r}{\delta_f}$	27 dB [0, 30 rad/s]	21 dB ($R_{uf} = R_{ur} = 10$), 4 dB ($R_{uf} = R_{ur} = 10000$) [0, 10 rad/s]

Figures 4.2c, d show the transfer functions gains of the input currents at the front ($\frac{u_f}{\delta_f}$) and rear axles ($\frac{u_r}{\delta_f}$), respectively. When R_{uf} and R_{ur} increase, the controller input currents ($u_{f,r}$) decrease. This indicates that when R_{uf} and R_{ur} increase, the LQR_3 design requires less energy than the LQR_1 design.

From Figure 4.2, we can see that the LQR_3 design does not improve the roll stability when R_{uf} and R_{ur} increase. As the main objective of the active anti-roll bar system is to enhance the roll stability, R_{uf} and R_{ur} cannot be increased too much.

The results above indicate that the roll stability and the energy consumption are conflicting objectives. The objective of the active anti-roll bar on heavy vehicles is to maximize roll stability to prevent rollover in dangerous situations. However, such a performance objective must be balanced with the energy consumption of the anti-roll bar system, which is not a trivial task.

The selection of the performance index J , as well as the weighting parameters ($\rho_1, \rho_2, \rho_3, \rho_4, \rho_5, R_{uf}$ and R_{ur}) in the equation (4.1) depend on the design objectives, which are the vehicle roll stability (the normalized load transfers, the limits of the suspension travel) and the saturation of the actuators (the spool valve displacement, the input current, the load flow, and the actuator force).

4.3.2 Analysis in the time domain

In this section, some results in the time domain are shown for four different situations: the passive anti-roll bar, the LQR_1 controller (Nominal), the LQR_2 controller ($\rho_2 = \rho_3 = 100$, Normalized load transfer oriented) and the LQR_3 controller ($R_{uf} = R_{ur} = 100$, Input limitation oriented). The vehicle manoeuvre is a double lane change which is often used to avoid an obstacle in an emergency. The manoeuvre has a 2.5 m path deviation over 100 m. The steering angle δ_f is shown in Figure 4.3.

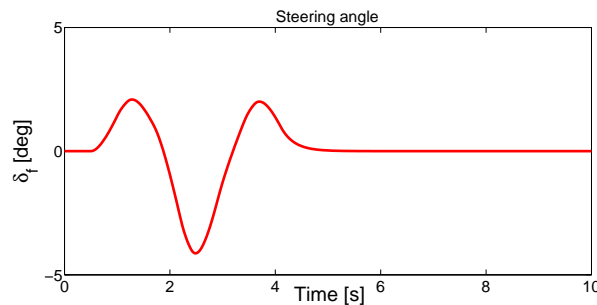


Figure 4.3: Time responses of steering angle δ_f [Gaspar, Bokor, and Szaszi 2004].

4.3.2.1 Performance criteria

To evaluate the efficiency of the controllers, two criteria are considered:

- The maximum absolute value of the signals. This indicator is very important for the normalized load transfers $R_{f,r}$, because if $R_{f,r}$ takes on the value ± 1 , then the inner wheel in the bend lifts off the ground.
- The *Root Mean Square (RMS)* of the signals defined as:

$$RMS(y) = \sqrt{\frac{1}{T} \int_0^T y^2(t) dt} \tag{4.2}$$

4.3.2.2 Analysis of the roll stability and the ESVH actuator

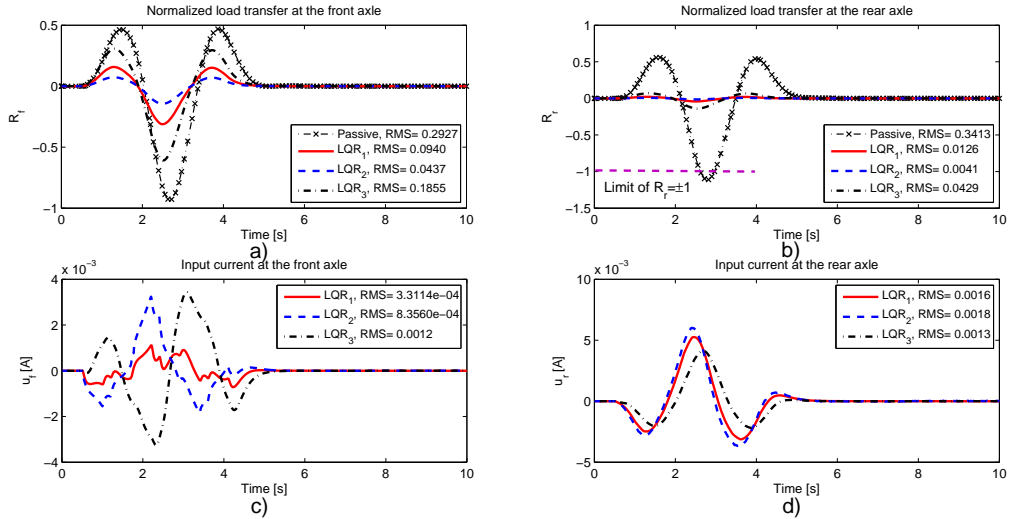


Figure 4.4: Time responses of (a, b) the normalized load transfers and (c, d) the input currents at the axles.

In Figure 4.4, the time responses for the LQR_1 controller (continuous line), the LQR_2 controller (dashed line), the LQR_3 controller (dashed-dot line) and the passive anti-roll bar (dashed-dot asterisk line) are shown.

Figures 4.4a, b show the normalized load transfers at the front and rear axles, respectively. Notice that, in the case of the passive anti-roll bar, the value of the normalized load transfer at the rear axle (R_r) at 2.8 seconds exceeds -1 so that the inner wheels lift off the ground (but not at the front axle). For the three LQR active anti-roll bar controllers, the roll stability is achieved because the limits of the normalized load transfers always stay within ± 1 . In Table 4.3, the reduction of the peak of the normalized load transfers (at the two axles) are shown for the three LQR controllers compared to the passive anti-roll bar case. This confirms the simulation results in the frequency domain which are shown in Figures 4.1a, b and 4.2a, b.

Table 4.3: Reduction of the peak of the normalized load transfers compared to the passive case (100%).

Normalized load transfers	LQR_1	LQR_2	LQR_3
R_f	70%	83%	37%
R_r	96%	98%	89%

To assess the roll stability and the energy consumption of the actuators using the three active anti-roll bar controllers, the simulation results are summarized in Figure 4.5.

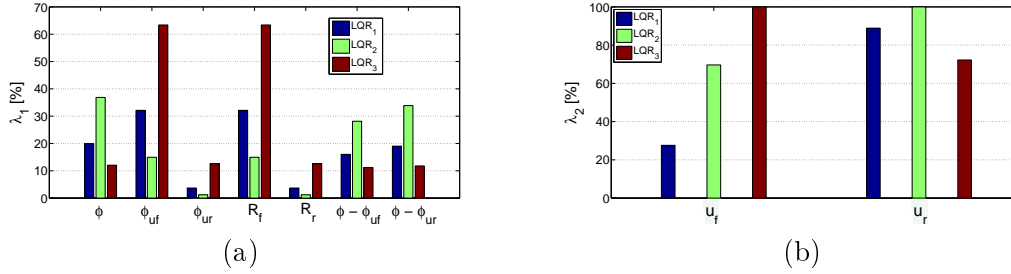


Figure 4.5: *RMS* of the signal's reduction: λ_1 (a), λ_2 (b)

For the roll stability, we consider the percentage of *Root Mean Square (RMS)* compared to that of the passive anti-roll bar case (100%) as:

$$\lambda_1(.) = \frac{RMS(active)}{RMS(passive)} 100\% \quad (4.3)$$

For the energy consumption of the actuators, the percentage of *RMS* compares with the maximum *RMS* of input currents with respect to each axle as:

$$\lambda_2(.) = \frac{RMS(u_{f,r})}{RMS(u_{f,rmax})} 100\% \quad (4.4)$$

Figure 4.5a shows that for the three *LQR* active anti-roll bar controllers, the *RMS* of the signals have dropped from 63% to 88% for the roll angle of sprung mass (ϕ), from 37% to 85% for the roll angle of the unsprung mass at the front axle (ϕ_{uf}), from 87% to 98% for the roll angle of the unsprung mass at the rear axle (ϕ_{ur}), from 37% to 85% for the normalized load transfer at the front axle (R_f), from 87% to 98% for the normalized load transfer at the rear axle (R_r), from 72% to 89% for the roll angle of the suspension at the front axle ($\phi - \phi_{uf}$) and from 66% to 88% for the roll angle of suspension at the rear axle ($\phi - \phi_{ur}$).

Figure 4.5b indicates that the input currents in case of the LQR_2 controller are always higher than those of the LQR_1 controller, this consistently fulfils the objective of the designed controllers. Nevertheless in the case of the LQR_3 controller, the input current at the front axle is higher than that of the LQR_1 and LQR_2 controllers, which confirms the simulation

Table 4.4: Signals considered in the frequency and time domains.

Signal	Frequency domain	Time domain
Normalized load transfers at the front/rear axles ($R_{f,r}$)	X	X
Input currents at the front/rear axles ($u_{f,r}$)	X	X
Roll angle of the sprung mass (ϕ)		X
Roll angle of the unsprung masses at the front/rear axles ($\phi_{u,f,r}$)		X
Roll angle of the suspensions at the front/rear axles ($\phi - \phi_{u,f,r}$)		X
Side-slip angle (β) - Side-slip angle velocity ($\dot{\beta}$)		X
Stability index (λ)		X

results in the frequency domain, shown in Figures 4.1c and 4.2c, since in the time domain, the steering angle is considered at 4 rad/s in an emergency.

So we can claim that the three LQR active anti-roll bar controllers significantly enhance roll stability when compared to the passive anti-roll bar case. As explained for the choice of the coefficients for the performance index J , the simulation results consistently fulfil the objective of the described controllers. This provides the control engineering a generic design method for designing LQR controllers according to the required performance criteria (through the choice of the parameters ρ_i).

Remark 4.2: *To evaluate the effect of the three LQR active anti-roll bar controllers on the roll stability and the electronic servo-valve hydraulic actuator of the integrated model in the frequency and time domains, the signals considered are listed in detail in Table 4.4.*

4.4 Analysis of the effect of the forward velocity on the closed-loop system

The forward velocity of heavy vehicles continuously varies during operation, especially in the case of an emergency, vehicle rollover often occurs for forward velocities from 60 to 110 km/h. In this section, one considers the forward velocity of the single unit heavy vehicle up to 160 km/h in order to evaluate the roll stability. Even if it may seem extremely high, we wish to determine the critical velocity at which the ESVH actuators reach their physical limits. In what follows, the disturbance is the steering angle (δ_f) which corresponds to a double lane change manoeuvre, shown in Figure 4.3 [Gaspar, Bokor, and Szaszi 2004].

4.4.1 The effect of the forward velocity on vehicle roll stability

Figures 4.6a, b show the effect of the forward velocity on the maximum absolute value of the normalized load transfers at the front and rear axles, respectively.

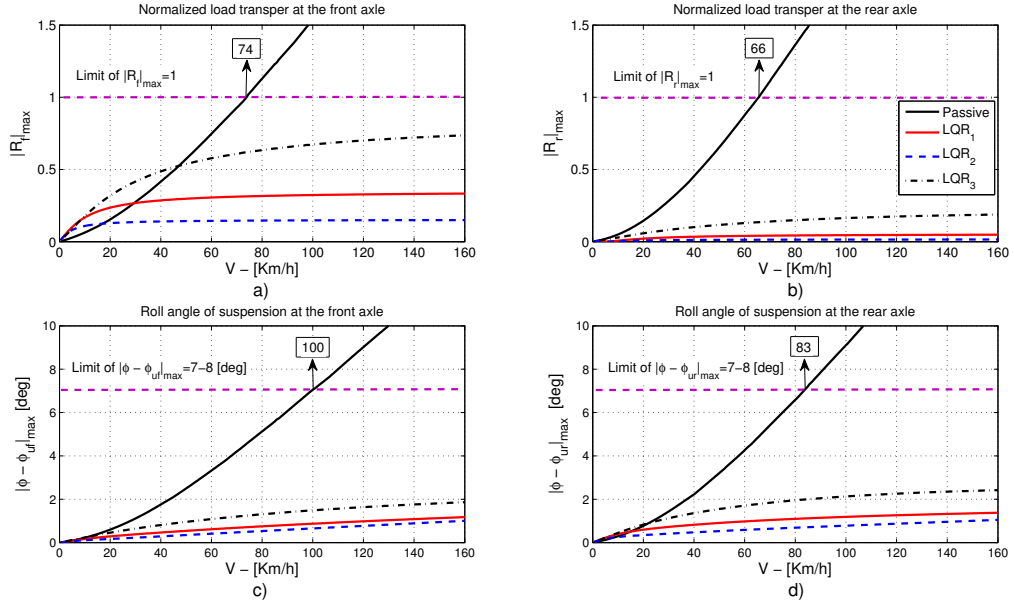


Figure 4.6: Effect of the forward velocity on the maximum absolute value of (a,b) the normalized load transfers and of (c, d) the roll angle of suspensions at the front and rear axles.

In the case of the passive anti-roll bar, the maximum absolute values of the normalized load transfers ($R_{f,r}$) at the front and rear axles reach their limitations when the forward velocities are 74 and 66 km/h , respectively. Meanwhile, in the case of the three LQR active anti-roll bar controllers, these indices are always within their limitations. The maximum absolute values of the signals in the case of the LQR_2 controller are always less than for the LQR_1 and LQR_3 controllers. It means that the LQR_2 controller provides a better improvement in roll stability than the two other controllers. This fulfils consistently the objective of the described controllers.

Note that, for the passive anti-roll bar system, vehicle rollover will occur at the rear axle (66 km/h) before the front axle (74 km/h). This is a characteristic of the rollover of a single unit heavy vehicle (conventional truck), because the rollover of the vehicle is affected by the suspension stiffness to load ratio, which is greater at the rear axle than at the front one [Sampson 2000], [Gaspar, Bokor, and Szaszi 2005]. So in the following studies, the author will consider the rollover at the rear axle for designing the other controllers.

Figures 4.6c, d show the effect of the forward velocity on the maximum absolute value of the roll angles of the suspension at the two axles ($\phi - \phi_{ur}$). The results indicate that with all of the three LQR active anti-roll bar controllers, the roll angles of the suspension are always less than the limitations of 7 to 8 deg . However for the passive anti-roll bar case, the roll angles of the suspension reach the limitations when the forward velocities are 100 km/h and 83 km/h , respectively. Figures 4.6 also indicates that the vehicle reaches the limitations of the normalized load transfers ($R_{f,r} = \pm 1$) before that of the roll angles of the suspension. For this reason, in the following studies the author only considers the normalized load transfers at the two axles for evaluating vehicle rollover.

4.4.2 The effect of the forward velocity on the physical constraints of the ESVH actuator

The physical constraints of the ESVH actuator are important to assess its applicability to the active anti-roll bar system. We consider the influence of the forward velocity on the ESVH actuators to determine their operational limits for the electronic servo-valve and the hydraulic actuator. The maximum absolute value of the spool valve displacements, the input currents, the load flows and the forces of the ESVH actuators will be use in the sequel.

Remark 4.3: *Although the control-oriented integrated model is used in this chapter, however the physical constraint of the ESVH actuator is still an important indication. Let us mention that the value of such a physical constraint may be slightly different in practice due to uncertainties.*

4.4.2.1 The electronic servo-valve: spool valve displacement and input current limitations

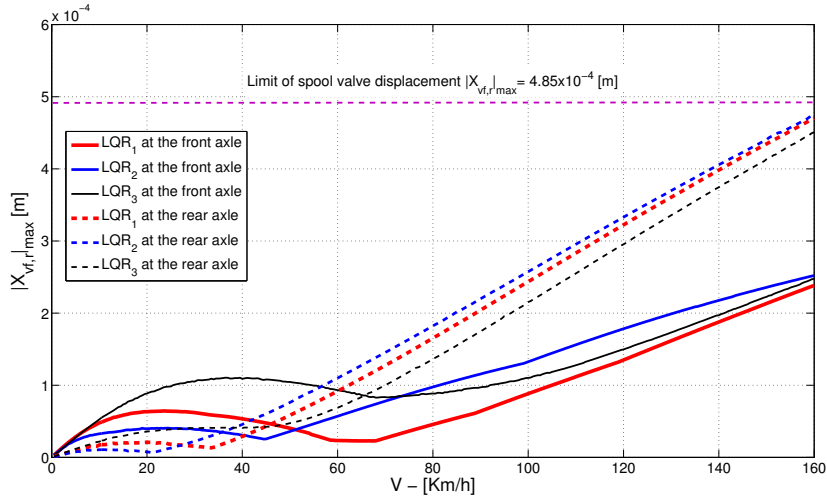


Figure 4.7: Influence of the forward velocity on the maximum absolute value of the spool valve displacements.

Figure 4.7 shows the effect of the forward velocity on the maximum absolute value of the spool valve displacements at the two axles ($X_{v_f,r}$). The maximum of the spool valve displacement recommended is 4.85×10^{-4} m [Rafa, Yahya, and Rawand 2009]. For the forward velocity of the heavy vehicle up to 160 km/h, the maximum absolute value of the spool valve displacements stays within the limit.

Figure 4.8 shows the effect of the forward velocity on the maximum absolute value of the input currents at the two axles ($u_{f,r}$). As the maximum of the input current recommended is 20 mA [Rafa, Yahya, and Rawand 2009], there is no problem because the input currents always

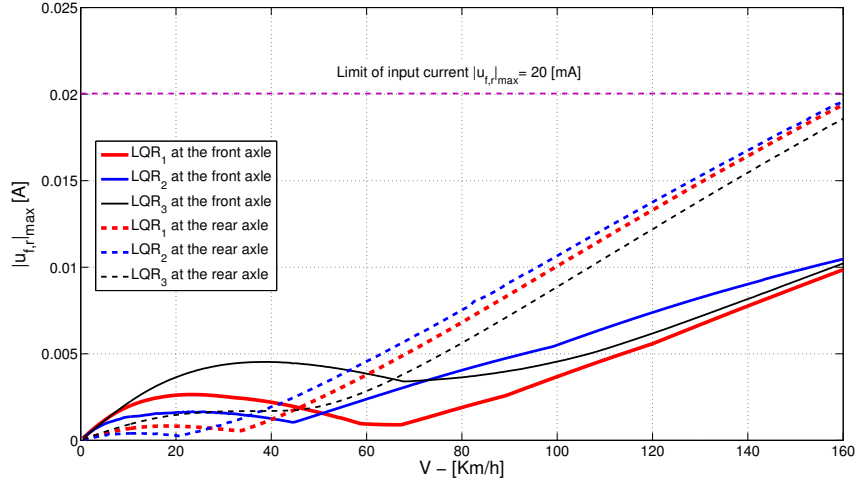


Figure 4.8: Influence of the forward velocity on the maximum absolute value of the input currents.

stay within the limit for the forward velocities of less than 160 km/h .

4.4.2.2 The hydraulic actuator: load flow and force limitations

As well, the maximum recommended load flow of oil into the hydraulic actuator is $2.2 \times 10^{-3} m^3/s$, see McKevitt [Sampson 2000]. Figure 4.9 shows that the load flows stay within the limit for the forward velocity up to 160 km/h .

Figure 4.10 shows that the maximal admissible limit for the forward velocity of the heavy vehicle is 138 km/h , in order to ensure that the forces stay within the limit (120 kN) recommended by McKevitt [Sampson 2000].

From Figure 4.7 to Figure 4.10, we can see that the maximum absolute value of the spool valve displacements, the input currents, the load flows, as well as the forces of the ESVH actuators at the rear axle are always higher than those at the front axle. It means that the actuators at the rear axle need much more energy than the actuators at the front axle.

As shown in the effect of the forward velocity on the roll stability and on the physical constraints of the ESVH actuator, the maximal admissible forward velocity of the vehicle obtained (138 km/h) ensures that the ESVH actuator operates within its admissible operational limit (forces, load flows, spool valve displacements and input currents), meanwhile the roll stability is improved significantly (shown in Figure 4.6). It can therefore be concluded that the ESVH actuator is completely justified for use with the active anti-roll bar control system on heavy vehicles.

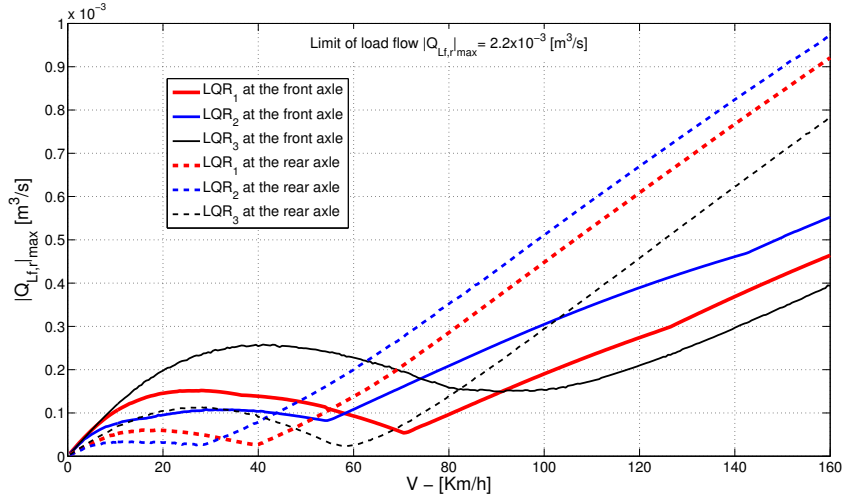


Figure 4.9: Influence of the forward velocity on the maximum absolute value of the load flows.

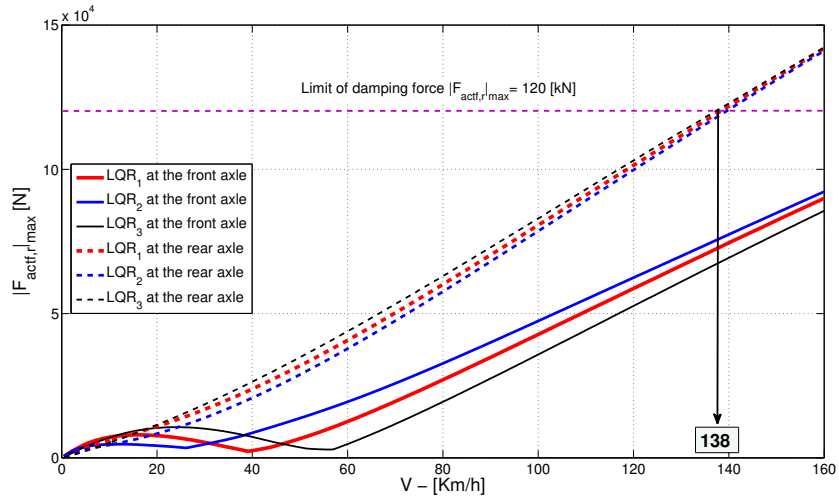


Figure 4.10: Influence of the forward velocity on the maximum absolute value of the forces.

4.5 Analysis of the handling performance

Besides improving roll stability to prevent vehicle rollover, it is important to evaluate the effect of the *LQR* active anti-roll bar system on vehicle handling performance using the ESVH actuators. Here, to evaluate the handling performance, the author will use the phase-plane ($\beta - \dot{\beta}$) [Junjie 2005], [Henk 2000], which can be assessed through the stability index (λ) [Junjie and Crolla 2006].

4.5.1 Selecting the criteria to evaluate the handling performance

The phase-plane method is a graphical method for finding the transient response of second-order systems to initial conditions or simple constant inputs and is particularly powerful for the stability analysis. Vehicle stability is naturally related to the side-slip motion of the vehicle. Therefore, the phase-plane ($\beta - \dot{\beta}$) is chosen for the states in examining vehicle stability. The vehicle is stable when its phase-plane ($\beta - \dot{\beta}$) is inside the stability region boundaries, which are chosen as follows [Junjie 2005]:

$$|\dot{\beta} + k_{\beta\dot{\beta}}\beta| < b \quad (4.5)$$

where $b = 24$ and the slope of the reference region boundaries $k_{\beta\dot{\beta}} = 4$. Therefore, $b/k_{\beta\dot{\beta}}$ is the half width of the region boundaries. In practice, the choice of parameters in equation (4.5) means that for the steady state conditions ($\dot{\beta} = 0$) the absolute value of the side-slip angle is always less than 6 *deg*.

In [Junjie and Crolla 2006], the authors proposed the use of the stability index (λ). Therefore, the vehicle stability region is derived from the phase-plane ($\beta - \dot{\beta}$) which can be assessed through the stability index (λ) in equation (4.6):

$$\lambda = |2.39\dot{\beta} + 9.55\beta| \quad (4.6)$$

The vehicle is in the stability region when $\lambda < 1$ [Junjie and Crolla 2006], [Sename, Gaspar, and Bokor 2013], [Fergani et al. 2016].

In fact, these two criteria are often used to evaluate the handling performance of cars; however, since the vehicle model in this study is a single unit with the two axes, therefore they are quite acceptable for this model. In the sequel, the author will evaluate the effect of the *LQR* active anti-roll bar control on the handling performance in both the phase-plane ($\beta - \dot{\beta}$) and the stability index (λ).

4.5.2 The handling performance analysis

The double lane change is also used as the vehicle manoeuvre, with the steering angle as shown in Figure 4.3. The forward velocity is considered constant at 70 *km/h*.

Figure 4.11a shows that the phase-plane $\beta - \dot{\beta}$ of the single unit heavy vehicle for all of the three *LQR* active anti-roll bar controllers, as well as the passive case, are inside the stability

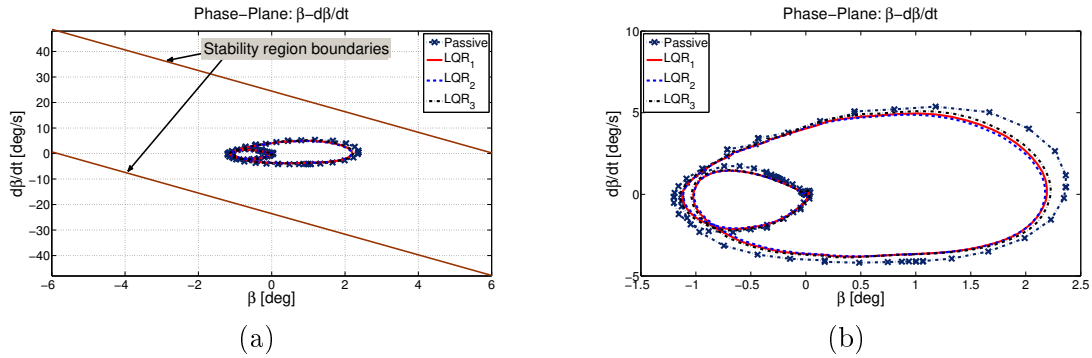


Figure 4.11: Phase-Plane $\beta - \dot{\beta}$ (a), Zoom in Phase-Plane $\beta - \dot{\beta}$ (b).

region boundaries. In Figure 4.11b, the phase-plane $\beta - \dot{\beta}$ of the vehicle in the cases of the three *LQR* active anti-roll bar controllers are always inside the phase-plane $\beta - \dot{\beta}$ of the passive anti-roll bar. Figure 4.12 also indicates that in the case of the three *LQR* active anti-roll bar controllers, the stability index λ is always less than that of the passive anti-roll bar. The reduction is about 12% for the three active anti-roll bar controllers, when compared to the passive anti-roll bar. Therefore, the *LQR* active anti-roll bar controllers also improve the handling performance of heavy vehicles, in addition to enhancing roll stability to prevent vehicle rollover. This is very important as it allows drivers to feel the real behavior of the vehicle.

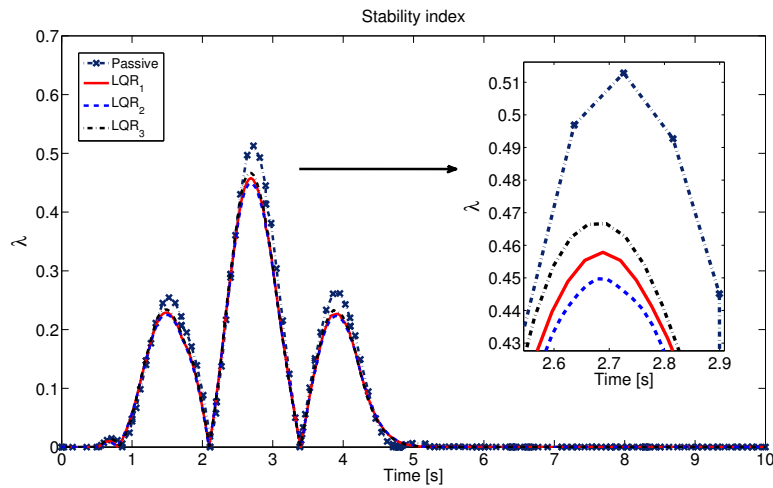


Figure 4.12: Stability index λ .

We can conclude that although the *LQR* active anti-roll bar controllers focus on the normalized load transfers and input currents, they also slightly improve the vehicle handling performance. Of course, the *LQR* active anti-roll bar controller can improve the handling performance much

more if the performance index J in equation (4.1) takes into account the side-slip angle at the center of mass (β) and its velocity ($\dot{\beta}$), which is related directly to the stability of the vehicle.

4.6 Conclusion

Based on the control-oriented integrated model including four ESVH actuators (two at the front and two at the rear axles) and a linear single unit heavy vehicle yaw-roll model, an active anti-roll bar control was developed within the *LQR* approach, taking into account the normalized load transfer and input current limitations. As shown in the simulation section, the maximal admissible forward velocity of the vehicle obtained (138 km/h) ensures that the ESVH actuator operates within its admissible operational limit (forces, load flows, spool valve displacements and input currents). It can then be concluded that the ESVH actuator, controlled by the current, is completely justified for use in an active anti-roll bar control system on heavy vehicles.

The results obtained in the frequency and time domains show the efficiency of the *LQR* active anti-roll bar control approach to improving roll stability and preventing the rollover phenomenon of heavy vehicles. The simulations also show the drastic improvements with respect to the passive anti-roll bar case. The author would like to stress that the given methodology provides a means to solve a multi-objective problem through the definition of an optimal criterion function of several tuning parameters ρ_i . This tuning facility allows an interesting degree of freedom to handle different industrial performance requirements.

Finally, it is worth saying that, for implementation, the LQR state-feedback control will need a state observer that could be designed in future works.

H_∞ robust control for active anti-roll bar system to prevent vehicle rollover

Contents

5.1	Introduction	95
5.2	H_∞ robust control synthesis to prevent vehicle rollover	97
5.2.1	H_∞ control synthesis for an active anti-roll bar system	97
5.2.2	Simulation results analysis with the nominal value	99
5.3	Optimal selection of the weighting functions for the H_∞ active anti-roll bar control	102
5.3.1	Multi-criteria optimization (MCO) of the active anti-roll bar control	103
5.3.2	Using genetic algorithms for the MCO problem in the H_∞ active anti-roll bar control	105
5.3.3	Evaluation of the optimization results	108
5.4	Robustness analysis in the frequency domain using the μ-tool	112
5.4.1	Robustness analysis configuration	112
5.4.2	Effect of the forward velocity uncertainties on the closed-loop system	115
5.5	Comparison between the LQR control and the H_∞ control for the active anti-roll bar system	119
5.6	Conclusion	121

5.1 Introduction

Modern control techniques allow engineers to optimize the control systems for their cost and performance. However, optimal control algorithms are not always tolerant to changes in the control system or the environment. Robust control is an approach to controller design that explicitly deals with uncertainty. Robust control methods are designed to function properly provided that uncertain parameters or disturbances are found within some (typically compact) set. This method aims to achieve robust performance and/or stability in the presence of bounded modelling errors.

As mentioned in Chapter 1, the Linear Parameter Varying (LPV) approach was applied to the

active anti-roll bar system of a single unit heavy vehicle by the team of Professor Peter Gaspar [Gaspar, Bokor, and Szaszi 2004], [Gaspar, Bokor, and Szaszi 2005]. They used the LPV approach for the active anti-roll bar system combined with the active brake control system. However, they did not specifically mention the use of H_∞ control method for these systems. In addition, we did not find any study by other authors that used the H_∞ control method for the active anti-roll bar system. Therefore, the content of this chapter is the first detailed study for applying the H_∞ control method to this system of heavy vehicles.

Based on the control-oriented integrated model presented in Chapter 2, this chapter proposes an H_∞ control for the active anti-roll bar system, and the robustness analysis in the frequency domain is done by using the μ tool. The GAs method is used to solve the Multi-Criteria Optimization (MCO) problem for the H_∞ synthesis through an optimal selection of the weighting functions. The latter work is hereby extended and provides three new main contributions:

- The synthesis of an H_∞ controller for the active anti-roll bar system is realized considering the integrated model of a single unit heavy vehicle. The aim is to improve the roll stability of heavy vehicles. The normalized load transfers and the limitation of the input currents generated by the controllers are considered in the MCO problem.
- The GAs method is applied to find the optimal weighting functions solving the MCO H_∞ control problem. Thanks to GAs, the conflicting objectives between the normalized load transfers and the input currents are handled by using only one single high level parameter.
- The performance analysis, made in the frequency and time domains, shows that the H_∞ active anti-roll bar control drastically reduces the normalized load transfer, compared to the passive anti-roll bar. It also shows that the H_∞ active anti-roll bar control is robust with respect to the forward velocity and the sprung mass variation. The robust stability analysis of the designed controller is performed by using the μ - analysis method.

In relation to this content, the author also published two conference papers:

- *H_∞ active anti-roll bar control to prevent rollover of heavy vehicles: a robustness analysis*, 6th IFAC Symposium on Symposium on System Structure and Control, Turkey, June, 2016;
- *Optimal selection of weighting functions by genetic algorithms to design H_∞ anti-roll bar controllers for heavy vehicles*, 15th Vehicle System Dynamics, Identification and Anomalies, Hungary, November, 2016.

In these studies, the author has presented a robust stability analysis by using the μ analysis method, and GAs have been used to select optimal weighting functions of the H_∞ control for the active anti-roll bar system in the **yaw-roll model** (see section 2.3). The normalized load transfers and the limitation of the torque generated by the actuators in various manoeuvre situations have been considered. However the content of these publications is not included in this chapter. The author emphasizes that in this chapter the **control-oriented integrated**

model (see section 2.4.2) of a single unit heavy vehicle is used with the normalized load transfers and the limitation of the input currents generated by the controllers, which are considered in the MCO problem.

5.2 H_∞ robust control synthesis to prevent vehicle rollover

As mentioned in the control objective and problem statement (section 1.4), the main objective when designing an active anti-roll bar system is to minimize the effect of the steering angle δ_f on the normalized load transfers $R_{f,r}$ at the two axles. Besides that, the limitation of the input currents $u_{f,r}$ entering the Electronic Servo-Valve Hydraulic (ESVH) actuators is crucial for practical implementation. This section follows the H_∞ approach presented in Chapter 3 (section 3.6) to synthesize the H_∞ controller for the active anti-roll bar system.

5.2.1 H_∞ control synthesis for an active anti-roll bar system

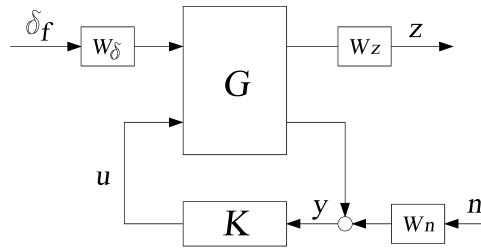


Figure 5.1: The closed-loop structure of the H_∞ active anti-roll bar control.

Figure 5.1 shows the closed-loop structure of the H_∞ control design for an active anti-roll bar system using the control-oriented integrated model. In the diagram, the feedback structure includes the nominal model G , the controller K to be synthesized, the performance output z , the control input u , the measured output y , the measurement noise n . δ_f is the steering angle considered as a disturbance signal and is set by the driver. The weighting functions W_δ, W_z, W_n are presented below.

According to Figure 5.1, the concatenation of the linear model (2.42) with performance weighting functions leads to the state-space representation of $P(s)$:

$$\begin{bmatrix} \dot{x} \\ z \\ y \end{bmatrix} = \begin{bmatrix} A & B_1 & B_2 \\ C_1 & D_{11} & D_{12} \\ C_2 & D_{21} & D_{22} \end{bmatrix} \begin{bmatrix} x \\ w \\ u \end{bmatrix} \quad (5.1)$$

with the exogenous input:

$$w = \begin{bmatrix} \delta_f & n \end{bmatrix}$$

the control input:

$$u = \begin{bmatrix} u_f & u_r \end{bmatrix}^T$$

where u_f and u_r are the input currents at the two axles, the performance output vector:

$$z = [u_f \quad u_r \quad R_f \quad R_r \quad a_y]^T$$

and the measured output vector:

$$y = [a_y \quad \dot{\phi}]^T$$

$A, B_1, B_2, C_1, D_{11}, D_{12}, C_2, D_{21}, D_{22}$ are model matrices of appropriate dimensions. The matrices A, B_1, B_2 are shown in Appendix B.

The input scaling weight W_δ normalizes the steering angle to the maximum expected command. It is selected as $W_\delta = \pi/180$, which corresponds to a 1° steering angle command. W_n is selected as a diagonal matrix, which accounts for sensor noise models in the control design. The noise weights are chosen as $0.01(m/s^2)$ for the lateral acceleration and $0.01(^\circ/sec)$ for the derivative of the roll angle $\dot{\phi}$ [Gaspar, Bokor, and Szaszi 2004]. Other low pass filters could also be selected.

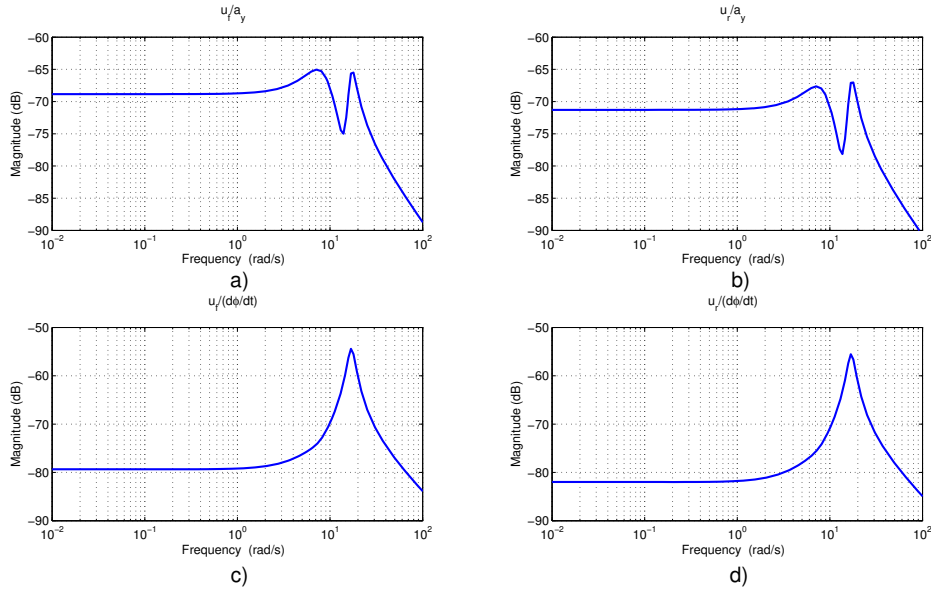


Figure 5.2: Transfer function magnitude of the H_∞ controller: from lateral acceleration to (a) input current at front axle $\frac{u_f}{a_y}$, (b) input current at rear axle $\frac{u_r}{a_y}$; from roll rate to (c) input current at front axle $\frac{u_f}{\dot{\phi}}$, (d) input current at rear axle $\frac{u_r}{\dot{\phi}}$.

The weighting function W_z represents the performance output and contains the components W_{zu}, W_{zR}, W_{za} . The purpose of the weighting functions is to keep as small as possible the control inputs (W_{zu}), normalized load transfers (W_{zR}) and the lateral acceleration (W_{za}) over the desired frequency range. The weighting functions chosen for the performance outputs can be considered as penalty functions, that is, weights that should be large in the frequency range where small signals are desired and small where larger performance outputs can be tolerated. The weighting function W_{za} is selected as:

$$W_{za} = \frac{(s/2000 + 109.25)}{(s/0.01 + 0.01)} \quad (5.2)$$

Here, the weighting function W_{za} corresponds to a design that avoids the rollover situation with the bandwidth of the driver in the frequency range to over 4 rad/s [Gaspar, Bokor, and Szaszi 2004], [Sampson 2000]. This weighting function will minimize directly the lateral acceleration when it reaches the critical value to avoid the rollover.

The weighting function W_{zu} is a diagonal matrix with diagonal entries $1/0.2$, which correspond to the front and rear input currents generated by the H_∞ controller. The weighting function W_{zR} is selected as $\text{diag}(0.1, 0.1)$ for the control design, which means that the maximal gain of the normalized load transfers can be “1” in the frequency domain for the front and rear axles. The MATLAB software environment yields a solution for a multi-variable full-order H_∞ controller with the optimal γ obtained at $\gamma_{opt} = 1.9332$. The transfer function magnitude of the H_∞ active anti-roll bar controller is shown in Figure 5.2. The controller includes two inputs (the lateral acceleration a_y , the roll rate $\dot{\phi}$) and two outputs (the input currents at the front axle u_f and at the rear u_r).

5.2.2 Simulation results analysis with the nominal value

The simulation results for a single unit heavy vehicle using the control-oriented integrated model (section 2.4.2) will be shown in both the frequency and time domains. The parameter values of the ESVH actuators and of the yaw-roll model are those given in Tables 2.1 and 2.2. The forward velocity is considered constant at 70 km/h .

5.2.2.1 Analysis in the frequency domain

Figure 5.3a shows that the H_∞ active anti-roll bar (H_∞ AARB) controller reduces the transfer function magnitude of the normalized load transfer at the front axle $\frac{R_f}{\delta_f}$ (about 23dB) in the frequency range up to 5.0rad/s , compared to the passive anti-roll bar. Figure 5.3b also shows that the H_∞ active anti-roll bar controller reduces the transfer function magnitude of the normalized load transfer at the rear axle $\frac{R_r}{\delta_f}$ (about 9.5dB) throughout the main frequency range of interest. The simulation results in Figures 5.3c, b indicate that the H_∞ active anti-roll bar controller also reduces the transfer functions magnitude of the suspension roll angles $\frac{\phi - \phi_{u_{f,r}}}{\delta_f}$ (about 10dB) throughout the main frequency range. As a consequence, the H_∞ active anti-roll bar can improve the roll stability of heavy vehicles in the desired frequency range, so preventing vehicle rollover.

Fig 5.4 shows the characteristics of the ESVH actuators at the two axles, which include the transfer functions magnitude of the actuator forces $\frac{F_{actf,r}}{\delta_f}$, the load flows $\frac{Q_{Lf,r}}{\delta_f}$, the spool valve displacements $\frac{X_{vf,r}}{\delta_f}$ and the input currents $\frac{u_{f,r}}{\delta_f}$.

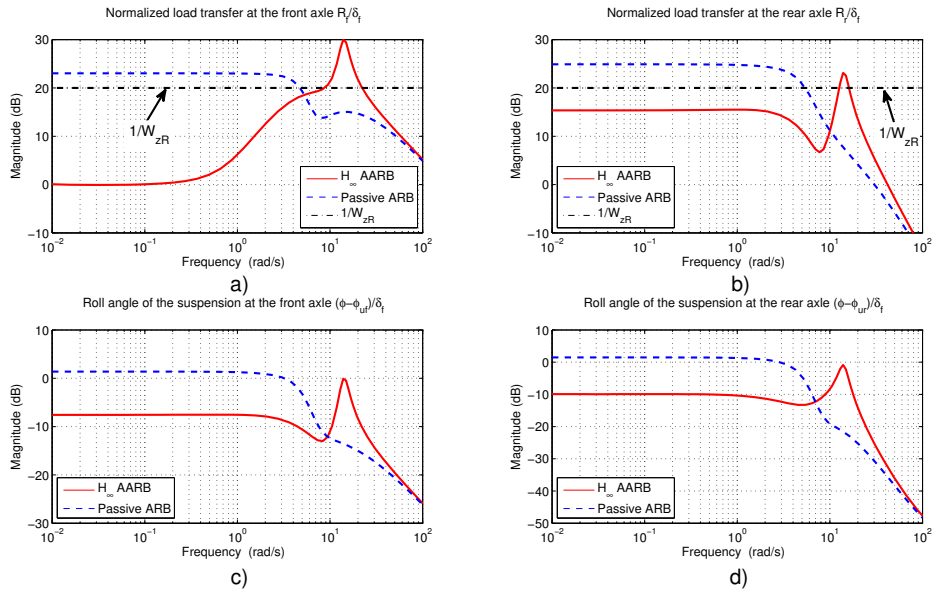


Figure 5.3: Transfer functions magnitude of (a, b) the normalized load transfers ($\frac{R_{f,r}}{\delta_f}$) and (c, d) the roll angle of the unsprung masses ($\frac{\phi - \phi_{u,f,r}}{\delta_f}$) at the two axes.

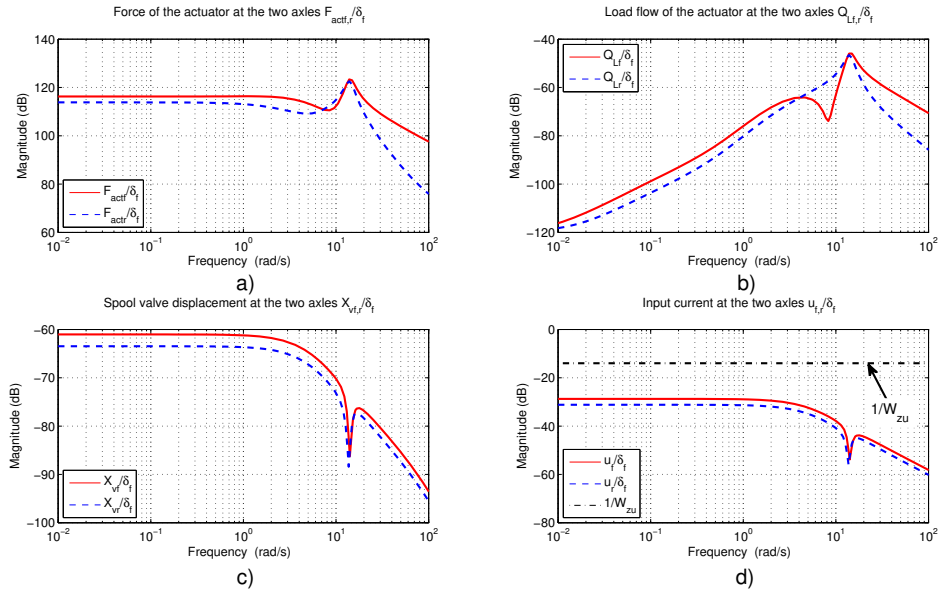


Figure 5.4: Transfer functions magnitude of (a) the actuator forces ($\frac{F_{act,f,r}}{\delta_f}$), (b) the load flow ($\frac{Q_{Lf,r}}{\delta_f}$), (c) the spool valve displacements ($\frac{X_{vf,r}}{\delta_f}$) and (d) the input currents ($\frac{u_{f,r}}{\delta_f}$) at the two axes.

5.2.2.2 Analysis in the time domain

In this section, the steering angle applied in the simulation is a step signal. Figure 5.5 shows the steering angle δ_f corresponding to a cornering manoeuvre.

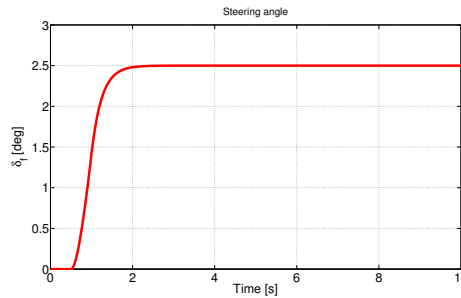


Figure 5.5: Time responses of the steering angle δ_f [Gaspar, Bokor, and Szaszi 2004].

Figure 5.6 shows the time responses of the normalized load transfers and the suspensions roll angles at the two axles. The H_∞ active anti-roll bar controller reduces significantly the normalized load transfers and the suspension roll angles at the two axles. So the H_∞ active anti-roll bar controller has improved the roll stability of the single unit heavy vehicle. Figure 5.7 shows the characteristics of the ESVH actuators at the two axles.

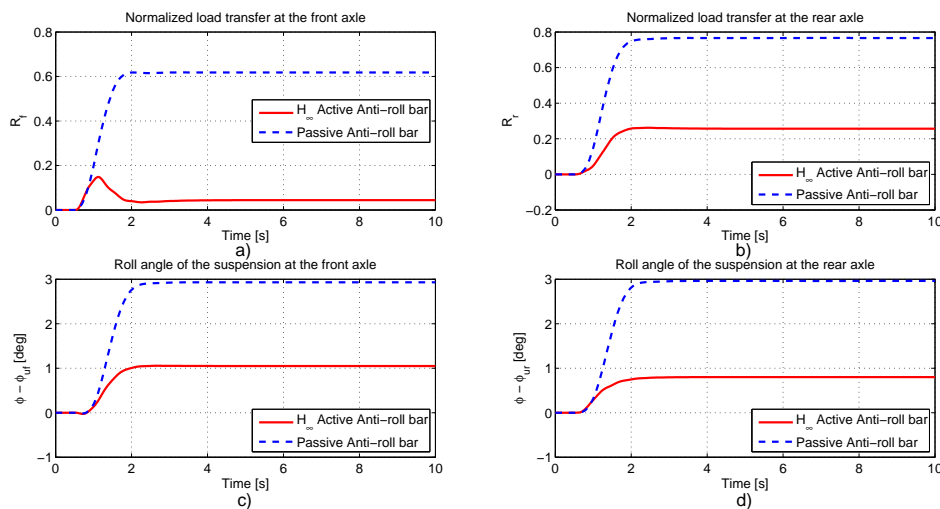


Figure 5.6: Time responses of (a, b) the normalized load transfers and (c, d) the suspensions roll angles.

The simulation results in the frequency and time domains indicated that the H_∞ active anti-roll bar controller significantly improves roll stability with the nominal value of a single unit

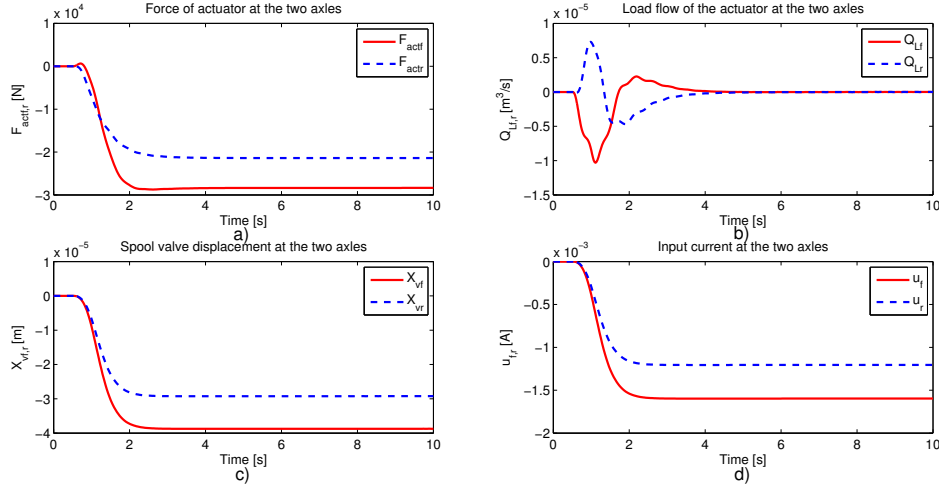


Figure 5.7: Time responses of (a) the actuator force ($F_{actf,r}$), (b) the load flows ($Q_{Lf,r}$), (c) the spool valve displacements ($X_{vf,r}$) and (d) the input currents ($u_{f,r}$) at the two axes.

heavy vehicle. However, there are two issues that need to be addressed:

- How to reasonably select the weighting functions for the H_∞ controller?
- It is a fact that in the process of using the vehicles, the sprung mass often changes when they are loaded, and the forward velocity continuously varies during the vehicle manoeuvre, therefore it is necessary to analyse the robustness of the closed-loop system.

The answers to both these issues above will be covered in the next sections.

5.3 Optimal selection of the weighting functions for the H_∞ active anti-roll bar control

The H_∞ control design approach is an efficient tool for improving the performance of a closed-loop system in pre-defined frequency ranges. The key step of the H_∞ control design is the selection of weighting functions which depend on the skill and experience of the engineers [Skogestad and Postlethwaite 2001]. In many real world applications, the difficulty in choosing the weighting functions increases significantly because the performance specification is not accurately defined i.e., it is simple to achieve the best possible performance (optimal design) or to achieve an optimally joint improvement of more than one objective (multi-objectives design). So the optimization of weighting functions to satisfy all the desired performances is still an interesting and challenging problem. In [Hu, Bohn, and Wu 2000] it is proposed to consider each system, no matter how complex it is, as a combination of sub-systems of the first and second order, for which it is easy to find good weighting functions to be used in

the H_∞ control methodology. However, there is no explicit method to find these functions in the general case. The usual way is to proceed by trial-and-error. Recently, the idea to use an optimization tool was proposed in [Alfaro-Cid, McGookin, and Murray-Smith 2008]. The choice of Genetic Algorithms (GAs) seems natural because their formulation is well suited for this type of problems [Do et al. 2011].

In a previous section, the H_∞ active anti-roll bar control system is proposed with the aim of improving roll stability of a single unit heavy vehicle. The simulation results indicated that in the active anti-roll bar control on a single unit heavy vehicle using the four ESVH actuators, roll stability and energy consumption of the ESVH actuators are two essential but conflicting performance objectives.

This section aims to solve a Multi-Criteria Optimization (MCO) problem formulated as an H_∞ control problem where the weighting functions are optimally selected through the use of Genetic Algorithms (GAs). Thanks to GAs, roll stability and energy consumption are handled by using a single high level parameter and illustrated via the Pareto optimality. Simulation results emphasize the simplicity and efficiency of using the GAs method for a MCO problem in the H_∞ active anti-roll bar control on heavy vehicles. It is worth noting that this is a new approach in the use of GAs to determine the optimal weight functions of the H_∞ controller, which is completely independent of that of former PhD studies in the same SLR team, such as [Do 2011], [Nwesaty 2015].

5.3.1 Multi-criteria optimization (MCO) of the active anti-roll bar control

5.3.1.1 The MCO for the H_∞ active anti-roll bar control

As mentioned above, the objective of the active anti-roll bar control system is to improve roll stability of heavy vehicles. However, such a performance objective must be balanced with energy consumption of the anti-roll bar system due to the input current entering the electronic servo-valve of the actuators. Therefore, the objective function is selected as follows:

$$f = \alpha f_{Normalized-load-transfer} + (1 - \alpha) f_{Control-cost} \quad (5.3)$$

The vector $\alpha = [0 \div 1]$ is the gradient of function f . When α moves to 0, the optimal problem focusses on minimizing input currents. And conversely, when α moves to 1, the optimal problem focusses on minimizing the normalized load transfers.

In the objective function (5.3), $f_{Normalized-load-transfer}$ and $f_{Control-cost}$ are performance indices corresponding to the normalized load transfers and input currents at the two axles, which are defined as follows:

$$\begin{cases} f_{Normalized-load-transfer} = \frac{1}{2} \left(\sqrt{\frac{1}{T} \int_0^T R_f^2(t) dt} + \sqrt{\frac{1}{T} \int_0^T R_r^2(t) dt} \right) \\ f_{Control-cost} = \frac{1}{2} \left(\sqrt{\frac{1}{T} \int_0^T u_f^2(t) dt} + \sqrt{\frac{1}{T} \int_0^T u_r^2(t) dt} \right) \end{cases} \quad (5.4)$$

Since the function for the normalized load transfers ($f_{Normalized-load-transfer}$) is a quantity without unit, whereas the unit of the function for the input currents ($f_{Control-cost}$) is ampe.

Therefore, in order for the optimal problem to be effective, a conversion factor between these two functions must be determined. Here this value is found to be 546.45 for $f_{Control-cost}$. The MCO problem represented by the equation (5.3) can not be resolved directly in the synthesis of the H_∞ controller. Thus, we can summarise the implementation phase completed in this section as described in Figure 5.8. The generalized plant includes the integrated model and the weighting functions. The controller is synthesised by using the H_∞ method. The conflicting objective between roll stability and energy consumption is the computation of the closed-loop performance. Depending on the purpose of the MCO problem, the weighting functions are appropriately selected by GAs. The optimal parameters obtained from GAs are sent to the weighting functions to calculate the controller.

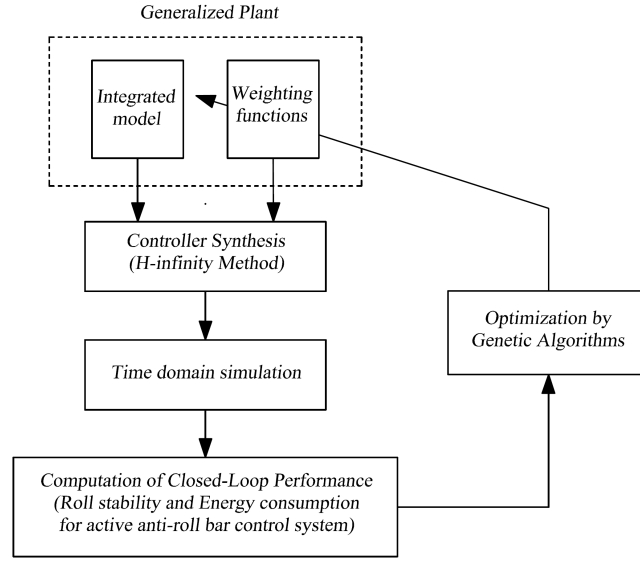


Figure 5.8: Controller optimization for the H_∞ active anti-roll bar using Genetic Algorithms.

5.3.1.2 Form of the weighting functions for the H_∞ control synthesis

In the active anti-roll bar control system, roll stability and energy consumption of the ESVH actuators are two essential but conflicting performance objectives. Therefore, the weighting functions represented for the performance output should be considered in the MCO problem. From the closed-loop structure of the H_∞ active anti-roll bar control shown in Figure 5.1, the elements of the weighting function W_z are redefined as:

The weighting function $W_{zu} = \text{diag}[W_{zuf}, W_{zur}]$, corresponds to the input currents at the front and rear axles, and is chosen as:

$$W_{zuf} = \frac{1}{Z_1}; \quad W_{zur} = \frac{1}{Z_2} \quad (5.5)$$

The weighting function $W_{zR} = \text{diag}[W_{zRf}, W_{zRr}]$, corresponds to the normalized load transfers at the front and rear axles, and is selected as:

$$W_{zRf} = \frac{1}{Z_3}; \quad W_{zRr} = \frac{1}{Z_4} \quad (5.6)$$

The weighting function W_{za} is selected as (in the similar form as equation (5.2)):

$$W_{za} = Z_{51} \frac{Z_{52}s + Z_{53}}{Z_{54}s + Z_{55}} \quad (5.7)$$

From equations (5.5) - (5.7), Z_i and $Z_{5,j}$ are the constant parameters. By using these weighting functions, the H_∞ active anti-roll bar controller will directly minimize the lateral acceleration when it reaches the critical value, so avoiding vehicle rollover.

As mentioned before, the key step of the H_∞ control design is how to select the weighting functions. The following variables are to be selected: $Z_1, Z_2, Z_3, Z_4, Z_{51}, Z_{52}, Z_{53}, Z_{54}, Z_{55}$. In the next section, the GAs method will be used to find these variables, which are suited for the MCO problem.

Remark 5.1: *The H_∞ active anti-roll bar controller presented in section 5.2.1 is a particular case given in Table 5.3.*

5.3.2 Using genetic algorithms for the MCO problem in the H_∞ active anti-roll bar control

This section introduces the MCO problem for the H_∞ active anti-roll bar control on heavy vehicles, which is solved by using the GAs method.

5.3.2.1 Solving multi-criteria optimization by genetic algorithms

In this section, the procedure will use the GAs method presented in Chapter 3 (section 3.8.2). From the objective function in (5.3), the MCO problem for the H_∞ active anti-roll bar control can be defined as:

$$\begin{aligned} \min_{p \in P} F(p) \quad s.t. \quad F(p) &:= [f_{Normalized-load-transfer} \quad , \quad f_{Control-cost}]^T \\ P &:= \left\{ p = [Z_1, Z_2, Z_3, Z_4, Z_{51}, Z_{52}, Z_{53}, Z_{54}, Z_{55}]^T \in R \mid p^l \leq p \leq p^u \right\} \end{aligned} \quad (5.8)$$

where $F(p)$ is the vector of the objectives, p denotes the vector of the weighting function parameters, p^l and p^u represent the lower and upper bounds of the parameters, as given in Table 5.1.

Table 5.1: Lower and upper bounds of the weighting functions.

Bounds	W_{zuf}	W_{zur}	W_{zRf}	W_{zRr}	W_{za}				
	Z_1	Z_2	Z_3	Z_4	Z_{51}	Z_{52}	Z_{53}	Z_{54}	Z_{55}
Lower bound	0.001	0.001	0.1	0.1	0.5	$\frac{1}{3000}$	1	10	0.001
Upper bound	10	10	100	100	100	10	900	1000	20

Besides the minimization of the objective function from equations (5.3) and (5.8), we also have to account for the limitations of the normalized load transfers, suspension roll angles, as well

Table 5.2: Binding conditions.

No	Note	Maximum value	Unit
1	$ \phi - \phi_{uf} $	< 7	<i>deg</i>
2	$ \phi - \phi_{ur} $	< 7	<i>deg</i>
3	$ R_f $	< 1	-
4	$ R_r $	< 1	-
5	$ u_f $	< 20	<i>mA</i>
6	$ u_r $	< 20	<i>mA</i>

as the input currents at each axle. These limitations are considered as the optimal conditions (binding conditions) shown in Table 5.2.

The proposed weighting function optimization procedure for the H_∞ active anti-roll bar control synthesis is as follows:

- **Step 1:** Initialize the weighting functions parameters (it depends on the engineer skill and experience), at $p = p_0$.
Here, the initial value of the weighting functions is chosen as in Section 5.2.1. They are shown in Table 5.3. This value will greatly affect the convergence rate of the optimal problem.

Table 5.3: Initial weighting functions parameters for the H_∞ active anti-roll bar.

Controller	W_{zuf}	W_{zur}	W_{zRf}	W_{zRr}	W_{za}				
	Z_1	Z_2	Z_3	Z_4	Z_{51}	Z_{52}	Z_{53}	Z_{54}	Z_{55}
Original (p_0)	0.2	0.2	10	10	1	$\frac{1}{2000}$	109.25	100	0.01

- **Step 2:** Select the lower bound, upper bound, the scaling factor, the offset and the start point.
 1. **Lower and upper bounds (bounding condition):** they are chosen as in Table 5.1. These values are selected according to the author's survey results, and there is currently no specific method to choose the lower and upper bounds.
 2. **The scaling factor, offset and starting point:** The following commands are done in Matlab for the scaling factor, offset and start point:
 - $p_0 = (p_{lb} + p_{ub})/2$; (*Parameter lower and parameter upper bounds in Table 5.1*)
 - $p_{skal} = 1./(p_{ub} - p_{lb})$; (*Scaling factor*)
 - $p_{off} = p_{lb}$; (*Offset*)
 - $x_{lb} = p_{skal} \cdot (p_{lb} - p_{off})$; (*Lower bound for each step*)
 - $x_{ub} = p_{skal} \cdot (p_{ub} - p_{off})$; (*Upper bound for each step*)
 - $x_0 = p_{skal} \cdot (p_0 - p_{off})$; (*Starting point*)

- **Step 3:** Select the objective function (5.3) with the variation of the gradient from 0 to 1 and then solve the minimization problem.
- **Step 4:** Select the individuals, apply crossover and mutation to generate a new generation: $p = p_{new}$. The following commands are made in Matlab:
 $OPTIONS = gaoptimset('ga');$
 $OPTIONS = gaoptimset(OPTIONS, 'PopulationSize', 50, 'TolFun', 1e-3,$
 $'TolCon', 1e-3);$
 $[p, f, exitflag, output] = ga(@ActiveAntirollbarObject, 9, [], [], [], [], plb, pub)$
 $Z_1 = p(1); Z_2 = p(2); Z_3 = p(3); Z_4 = p(4);$
 $Z_{51} = p(5); Z_{52} = p(6); Z_{53} = p(7); Z_{54} = p(8); Z_{55} = p(9);$
- **Step 5:** Synthesize the new H_∞ controller with the new generation.
- **Step 6:** Run the closed-loop system with the new controller in the time domain.
- **Step 7:** Evaluate the new generation by comparing with the binding conditions. If the criteria of interest are not satisfied, go to step 3 with $p = p_{new}$; otherwise, stop and save the best individual value: $p_{opt} = p_{new}$.

5.3.2.2 Optimization results

Table 5.4: The optimization results for the weighting functions of the H_∞ active anti-roll bar.

Controllers	W_{zuf}	W_{zur}	W_{zRf}	W_{zRr}	W_{za}				
	Z_1	Z_2	Z_3	Z_4	Z_{51}	Z_{52}	Z_{53}	Z_{54}	Z_{55}
$\alpha = 0$	0.060	0.020	0.100	0.965	0.673	0.948	1.063	972.212	0.855
$\alpha = 0.25$	0.057	0.052	0.51	0.863	0.863	0.664	155.627	651.707	0.573
$\alpha = 0.5$	0.099	0.0773	1.403	0.217	0.812	0.813	88.666	407.658	1.001
$\alpha = 0.7$	0.057	0.066	0.412	0.221	0.832	0.514	139.609	357.401	1.901
$\alpha = 0.9$	0.066	0.072	0.616	0.482	0.724	0.492	202.316	455.747	0.544
$\alpha = 1$	0.07	0.090	0.655	0.305	0.545	0.245	444.397	839.299	0.163

Thanks to the GAs method, Table 5.4 gives a synthesis of the values of the variables Z_i, Z_{5j} in six cases for $\alpha = [0; 0.25; 0.5; 0.7; 0.9; 1]$, as explained in equation (5.3). When $\alpha = 0$, $f = f_{Control-cost}$, the optimal problem focusses only on the input currents and when $\alpha = 1$, $f = f_{Normalized-load-transfer}$, the optimal problem focusses only on the normalized load transfers.

Figure 5.9 shows the conflicting relationship between the normalized load transfers and the control costs at the six Pareto-optimal points ($\alpha = [0; 0.25; 0.5; 0.7; 0.9; 1]$) computed for the H_∞ active anti-roll bar on heavy vehicles. The original value corresponds to the controller described in section 5.2.1.

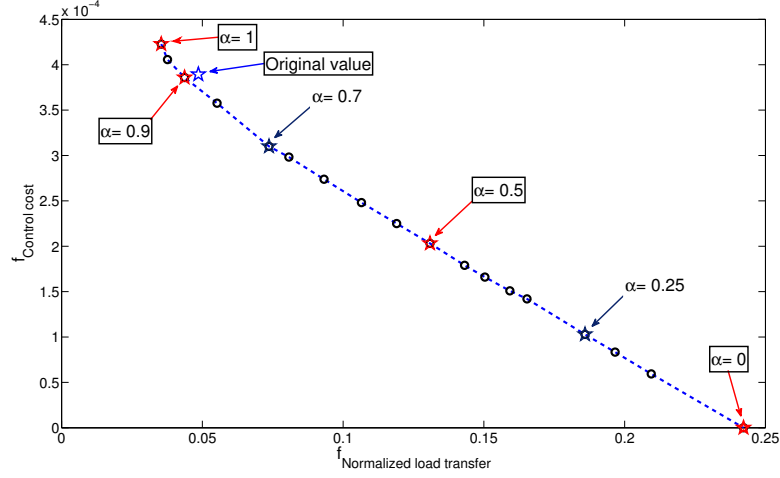


Figure 5.9: The Pareto frontier for the active anti-roll bar on heavy vehicles using ESVH actuators.

5.3.3 Evaluation of the optimization results

To evaluate the optimization procedure, in the next section, the simulations in the frequency and time domains are made and compared for five cases: passive ARB (anti-roll bar) and H_∞ AARB (active anti-roll bar) with $\alpha = [0; 0.5; 0.9; 1]$.

5.3.3.1 Evaluation of optimization results in the frequency domain

The frequency response is shown in the nominal parameters case of a single unit heavy vehicle in Tables 2.1, 2.2. The forward velocity V is considered constant at 70 km/h and the road adhesion coefficient $\mu = 1$. Figure 5.10 shows the transfer function magnitude of the normalized load transfers at the two axles $\frac{R_{f,r}}{\delta_f}$.

To assess the roll stability of the vehicle using the four H_∞ active anti-roll bar controllers, the reduction of the transfer function magnitudes compared to that of the passive anti-roll bar is considered at 10^{-2} rad/s and at 2 rad/s as:

$$\lambda_{(X)} = \frac{X_{active}}{\delta_f} - \frac{X_{passive}}{\delta_f} \quad (5.9)$$

where the variables of interest X are the normalized load transfers $R_{f,r}$.

Figure 5.11 shows the reduction of the transfer function magnitude of the normalized load transfers, when compared to the passive anti-roll bar at 10^{-2} rad/s and at 2 rad/s . We can see that at 10^{-2} rad/s the controller with $\alpha = 0$ decreases roll stability, meanwhile, when α increases, roll stability of the vehicle improves. However, as seen in Figure 5.10, the transfer functions are close to each other starting from 2 rad/s . This is mainly due to the effect of the internal oil leakage inside the electronic servo-valve on the performance of the active anti-roll

bar system. This problem will be investigated in Chapter 8.

Figure 5.12 shows the transfer function magnitude of the input currents at the two axles $\frac{u_{f,r}}{\delta_f}$: when α increases (the MCO problem focusses on minimizing the normalized load transfers), the total input currents also increase. It is proven that the normalized load transfer and the input current are two conflicting performance objectives.

Thus the MCO problem allows to get the weighting functions to enhance roll stability of the heavy vehicle in the low frequency range as well as in the high frequency range to over $4rad/s$, which is the limited bandwidth of the driver [Gaspar, Bokor, and Szaszi 2004], [Sampson 2000].

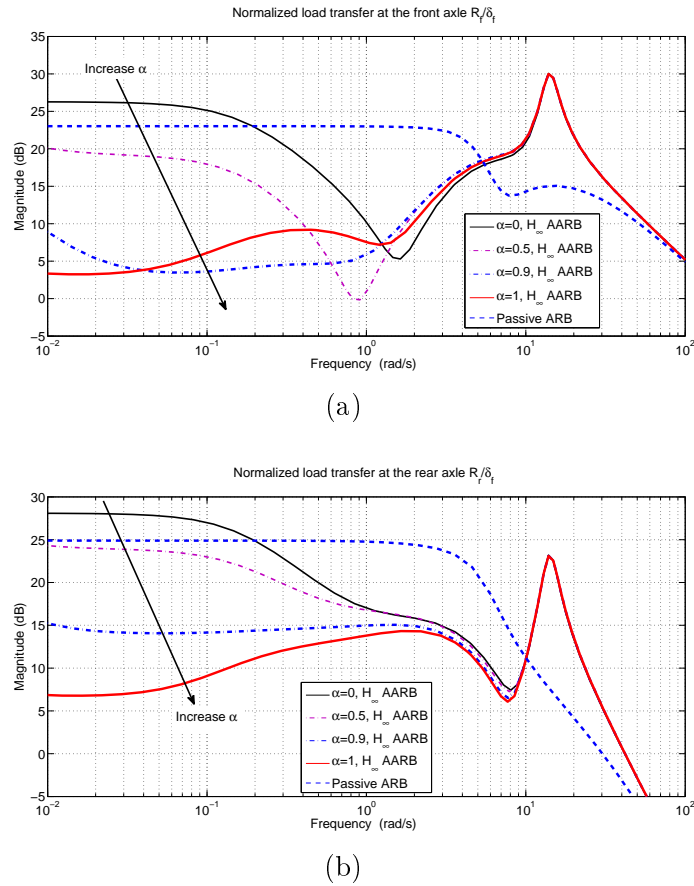


Figure 5.10: Transfer function magnitude of the normalized load transfers (a) at the front axle $\frac{R_f}{\delta_f}$ and (b) at the rear axle $\frac{R_r}{\delta_f}$.

5.3.3.2 Evaluation of the optimization results in the time domain

In this section, the cornering responses of a single unit heavy vehicle can be seen. The steering angle applied in the simulation is a step signal as in Figure 5.5. In Figures 5.13, 5.14 we consider the forward velocity of the vehicle up to $160 km/h$ in order to evaluate roll stability

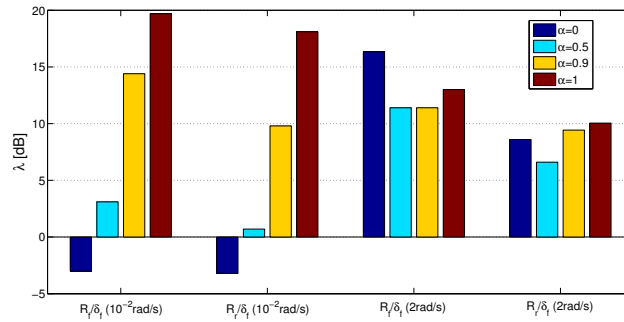
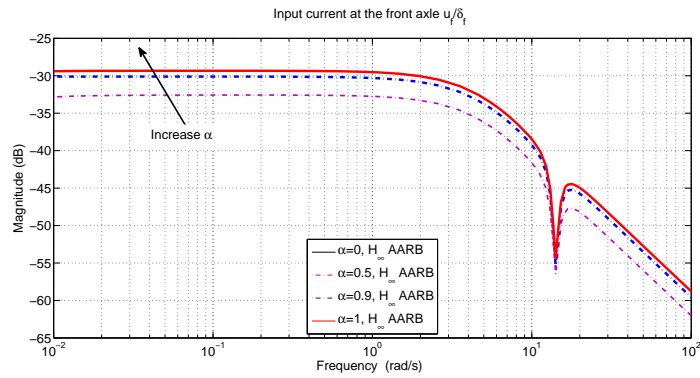
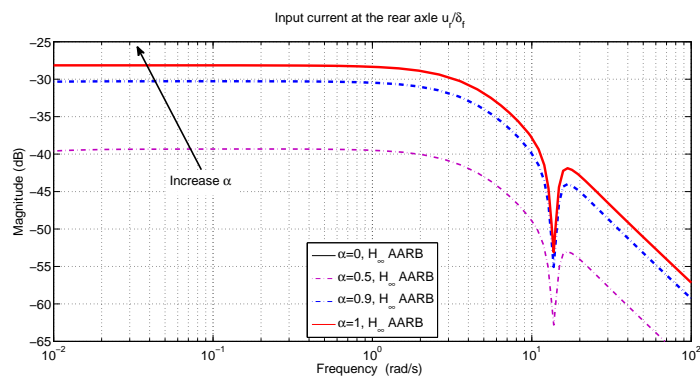


Figure 5.11: Reduction of the transfer function magnitude of the normalized load transfers at the two axes compared to the passive anti-roll bar (in equation (5.9)).



(a)



(b)

Figure 5.12: Transfer function magnitude of the input currents (a) at the front axle $\frac{u_f}{\delta_f}$ and (b) at the rear axle $\frac{u_r}{\delta_f}$.

when the normalized load transfers and the suspension roll angles reach their limitations. From Figure 5.13a, we can see that the maximum absolute value of normalized load transfers at the front axle reaches the limit “1”, for $\alpha = [0; 0.5; 0.9; 1]$, when the forward velocities are respectively 74, 110, 139, 144 km/h. Note that in the case of the passive anti-roll bar, we get 90 km/h for the forward velocity.

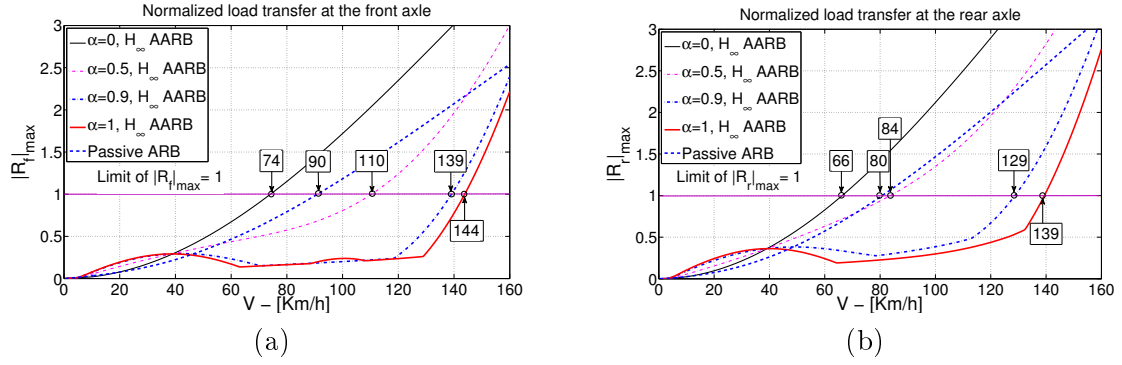


Figure 5.13: Effect of the forward velocity on the normalized load transfers: (a) front axle R_f , (b) rear axle R_r .

Considering Figure 5.13b, the maximum absolute value of the normalized load transfers at the rear axle reaches the limit of “1”, for $\alpha = [0; 0.5; 0.9; 1]$, when the forward velocities are respectively 66, 84, 129, 139 km/h. Note that in the case of the passive anti-roll bar, we get 80 km/h for the forward velocity.

From Figure 5.13, we can see that the forward velocity of the vehicle, at which the normalized load transfers at the rear axle reach their limit is smaller than the forward velocity, at which the normalized load transfers at the front axle reach their limit. So the risk of rollover at the rear axle is higher than at the front axle. The reason is the suspension stiffness, which is greater at the rear axle than at the front one.

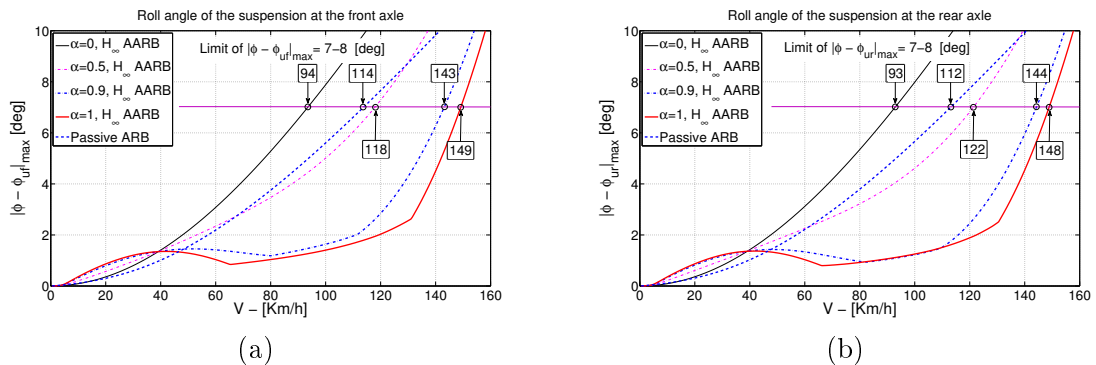


Figure 5.14: Effect of the forward velocity on the suspension roll angles: (a) front axle $\phi - \phi_{uf}$, (b) rear axle $\phi - \phi_{uf}$.

Figure 5.14 shows the maximum absolute value of the suspension roll angles, when the forward velocity is considered up to 160 km/h . From Figures 5.13 and 5.14, we can see that the normalized load transfers reach their limit before the values of the suspension roll angle. Therefore, for the H_∞ active anti-roll bar controller, the limit of the suspension travel is maintained if roll stability is satisfied.

5.4 Robustness analysis in the frequency domain using the μ -tool

Robustness analysis in the presence of modelled parametric uncertainties is carried out using μ -analysis. These techniques are detailed in [Skogestad and Postlethwaite 2005] and applied to practical problems in [Kahrobaeian and Mohamed 2013], [Sename and Dugard 2003], [Lam, Bratcu, and Riu 2016] for example. In this section, we also use this tool to evaluate the robustness of the H_∞ active anti-roll bar control system by considering two uncertain parameters: the forward velocity and the sprung mass.

5.4.1 Robustness analysis configuration

A control system is robust if it is insensitive to differences between the actual real system and the model used to design the controller. Let us recall that, in addition to nominal stability and performance, the objectives of any control system include:

- **Robust Stability (RS):** The system remains stable for all perturbed plants around the nominal model, up to the worst-case model uncertainty.
- **Robust Performance (RP):** The system satisfies the performance specifications for all perturbed plants around the nominal model, up to the worst-case model uncertainty.

The current application is concerned by parametric uncertainties. In particular, the forward velocity and the sprung mass are assumed to be largely unknown. In the considered control-oriented integrated model in equation (2.42), the forward velocity is the most varying parameter. The other parameter variations come from industrial manufacturing only. We wish to evaluate the robustness w.r.t. the forward velocity in the range from 30 to 110 km/h , with the nominal value of 70 km/h . The uncertainties are therefore represented as:

$$\begin{aligned}\bar{V} &= V(1 + p_V \delta_V), & p_V &= 57.14\%, & \delta_V &\in [-1; 1] \\ \bar{m}_s &= m_s(1 + p_{m_s} \delta_{m_s}), & p_{m_s} &= 30\%, & \delta_{m_s} &\in [-1; 1]\end{aligned}$$

Using an ad hoc *LFT* representation of the parametric uncertainties, we can pull out the perturbations in a diagonal block as: $\Delta_r = \text{diag}\{\delta_V I_V, \delta_{m_s} I_{m_s}\}$.

In this section we will apply the method presented in Chapter 3 (section 3.4) in order to quantify the maximum allowed uncertainties, so preserving the stability (and performance)

of the H_∞ active anti-roll bar control, considering with the forward velocity and the sprung mass as uncertain parameters.

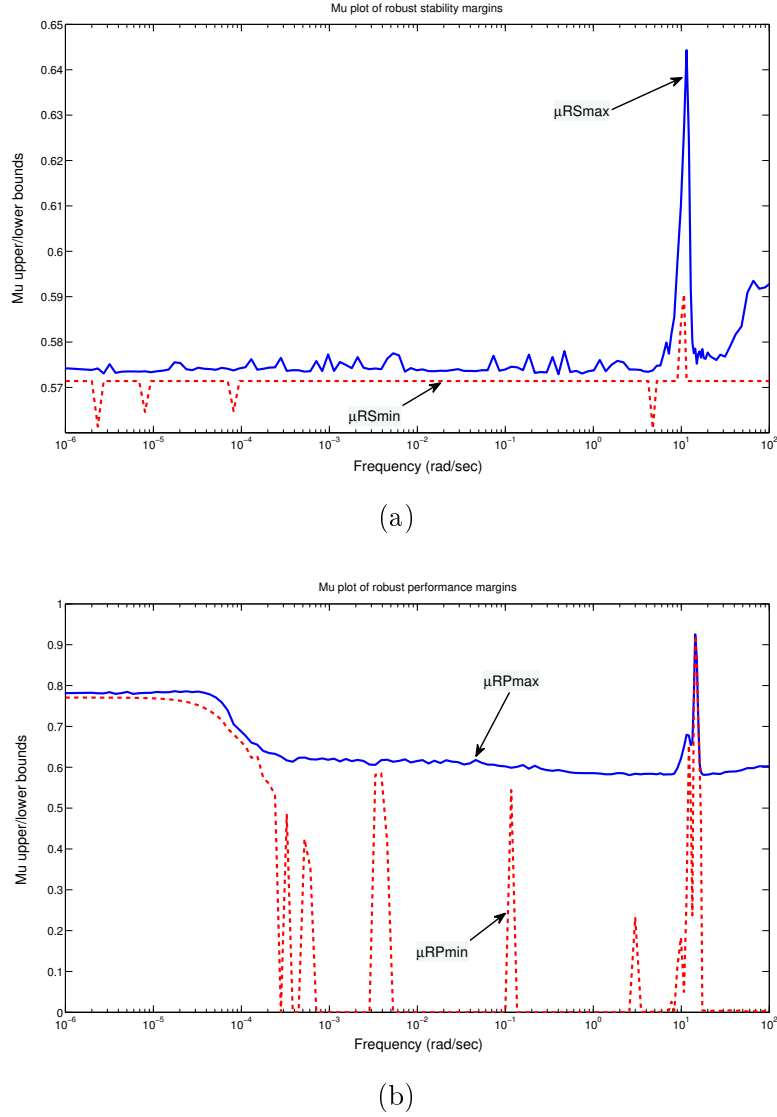


Figure 5.15: Upper and Lower bounds for (a) RS , (b) RP .

Applying the Theorem 3.4.1, an upper bound of μ for RS and RP is given in Figure 5.15. From Figure 5.15a we can see that the maximum value of the $\mu_{\Delta_r}(N_{11})$ is 0.645 ($\mu_{\Delta_r}(N_{11}) \leq 0.645$), so the Robust Stability is satisfied. Hence the H_∞ controller ensures stability for the considered uncertainties. Moreover, this means that the closed-loop system remains stable for larger uncertainties, i.e.:

$$V = 70 \text{ km/h} \pm (57.14/0.645)\% = 70 \text{ km/h} \pm 88.6\%$$

$$m_s = 12487 \text{ kg} \pm (30/0.645)\% = 12487 \text{ kg} \pm 46.5\%$$

On the other hand, as $\mu_\Delta(N) < 1$ (see Figure 5.15b), we can conclude that the Robust

Performance is satisfied in this uncertainty case.

These results have shown that the closed-loop system is completely robust w.r.t. the uncertain parameters considered above. However, it is necessary to define the limits of each uncertain parameter with which the robustness of the system is satisfied. In the next section we will independently evaluate the robust performance (RP) of the H_∞ controller for both the forward velocity and the sprung mass.

5.4.1.1 Robust performance analysis according to the forward velocity

Here we consider the forward velocity as the only uncertain parameter, while the sprung mass is held constant at the nominal value of 12487 kg . Figure 5.16 shows the RP μ -bounds plot for the uncertainty levels of 10%, 40%, 70%, 94%. It can be observed that the closed-loop system remains robust in performance up to a 94% uncertainty around its design value of 70 km/h , which corresponds to $\mu_{\Delta_{max}}(N) = 1$. This means that the closed-loop system is robust when the forward velocity is in the range of $[4.2 \div 135.8]\text{ km/h}$. These velocities ensure the operating range of most heavy vehicles in the world.

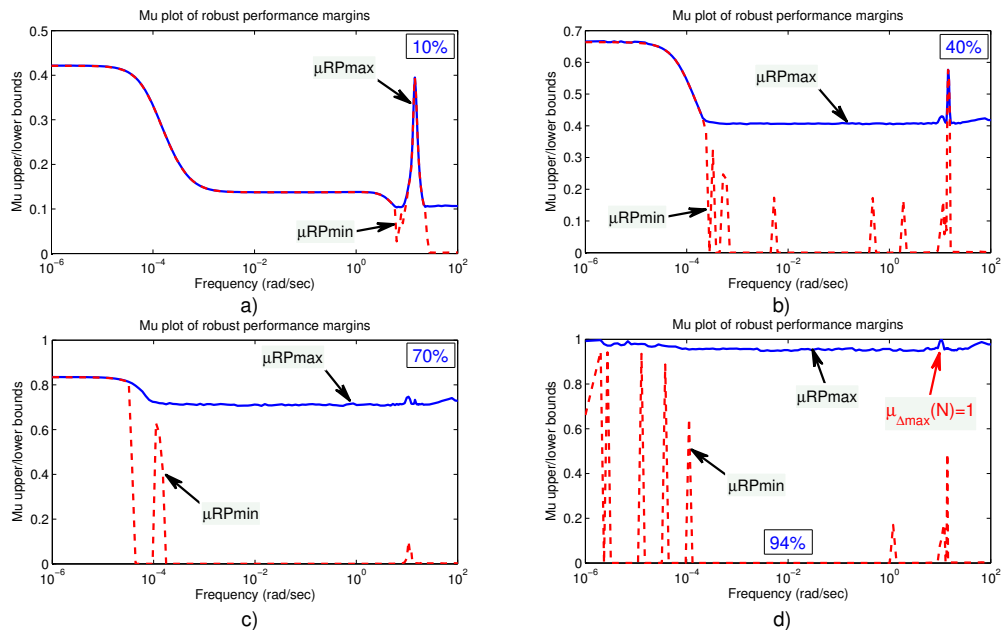


Figure 5.16: Performance analysis for the uncertain forward velocity at 10%, 40%, 70%, 94%.

5.4.1.2 Robust performance analysis according to the sprung mass

The sprung mass of vehicles consist of two main components: one is the vehicle weight, the other is the load (total load for trucks, passenger weight for buses). However, the sprung mass

often changes before the vehicle departs, nowadays in many modern vehicles this value can be measured directly.

In this case, the forward velocity is constant at 70 km/h , meanwhile the sprung mass is considered as the uncertain parameter. Figure 5.17 shows the RP μ -bounds plot for the uncertainty levels of 10%, 30%, 50%, 55%. We can see that $\mu_{\Delta_{max}}(N) = 1$ has an uncertainty of 55%. By considering the nominal value of the sprung mass at 12487 kg , the closed-loop system is robust when this uncertainty is in the range of $[5619.15 \div 19354.85] \text{ kg}$.

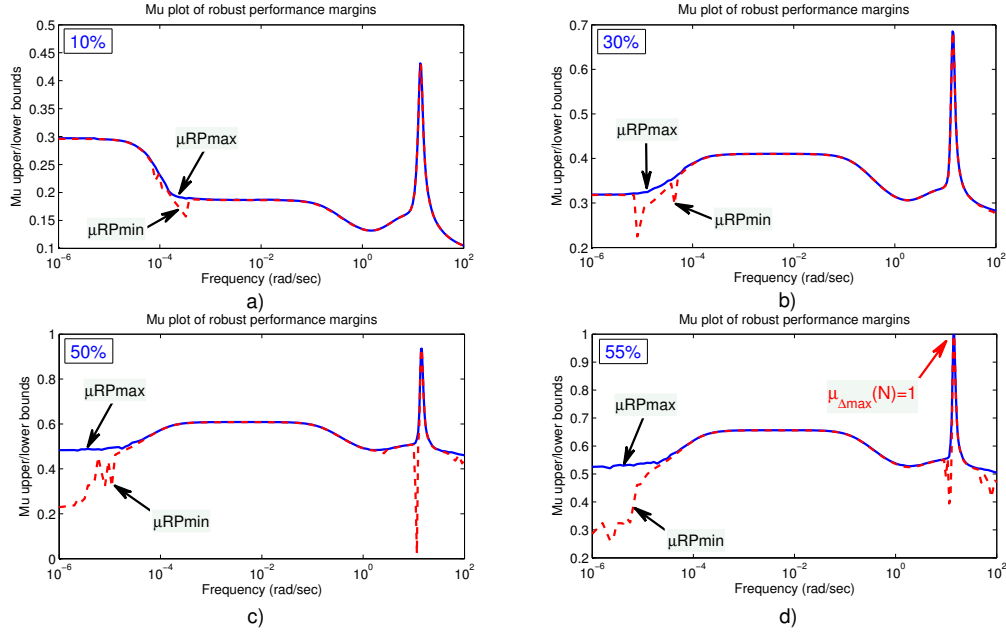


Figure 5.17: Performance analysis for the uncertain sprung mass at 10%, 30%, 50%, 55%.

5.4.2 Effect of the forward velocity uncertainties on the closed-loop system

The forward velocity continuously varies during the vehicle operation, especially in the case of an emergency. Rollover often occurs when the forward velocity is within 60 to 110 km/h . Therefore, the assessment of the effectiveness of the H_{∞} controller in a wide range of the forward velocity is absolutely necessary.

5.4.2.1 Effect of the forward velocity uncertainties in the frequency domain

In this section, the robustness of the active anti-roll bar control is evaluated by changing the forward velocity from 50 km/h to 110 km/h .

Figures 5.18a, b show the transfer function magnitude of the normalized load transfers at the front axle $\frac{R_f}{\delta_f}$ and at the rear axle $\frac{R_r}{\delta_f}$ with a forward velocity variation from 50 km/h to

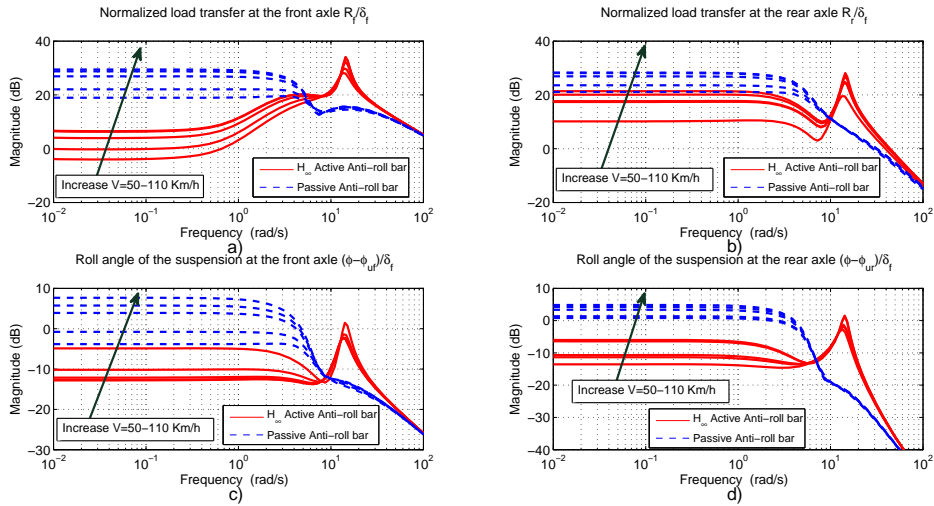


Figure 5.18: Transfer functions magnitude of (a, b) the normalized load transfers and (c, d) the suspension roll angles at the two axles.

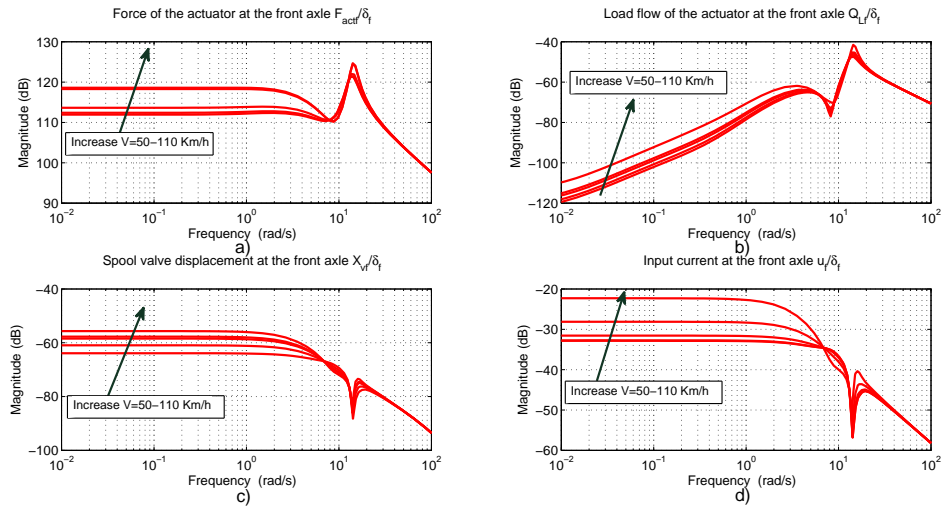


Figure 5.19: Transfer functions magnitude of (a) the actuator forces (F_{actf}), (b) the load flows (Q_{Lf}), (c) the spool valve displacements (X_{vf}) and (d) the input currents (u_f): front axle.

110 km/h. When compared to the passive anti-roll bar, one sees that the normalized load transfers at the front axle R_f , in the case of the H_∞ active anti-roll bar control, have been reduced in the frequency range up to 5 rad/s. Meanwhile the normalized load transfers at the rear axle R_r have been reduced in the frequency range up to 10 rad/s. Figures 5.18c, d show the transfer function magnitude of the roll angle of the suspension at the front axle $\frac{\phi - \phi_{ur}}{\delta_f}$ and at the rear axle $\frac{\phi - \phi_{ur}}{\delta_f}$. We can see that in the case of the H_∞ active anti-roll bar control the suspension roll angles have been reduced throughout the main frequency range of interest, when compared to the passive anti-roll bar case.

With the reduction of the normalized load transfers and the suspension roll angles at the two axles in the desired frequency range, the H_∞ active anti-roll bar controller then improves roll stability to prevent vehicle rollover.

Figures 5.19 and 5.20 show the transfer functions magnitude of the characteristics of the ESVH actuators at the two axles, which include the actuator forces $F_{actf,r}$, the load flows $Q_{Lf,r}$, the spool valve displacements $X_{vf,r}$ and the input currents $u_{f,r}$. We can see that when the forward velocity increases, all of the physical characteristics of the ESVH actuators also increase, this means that the controller requires more energy.

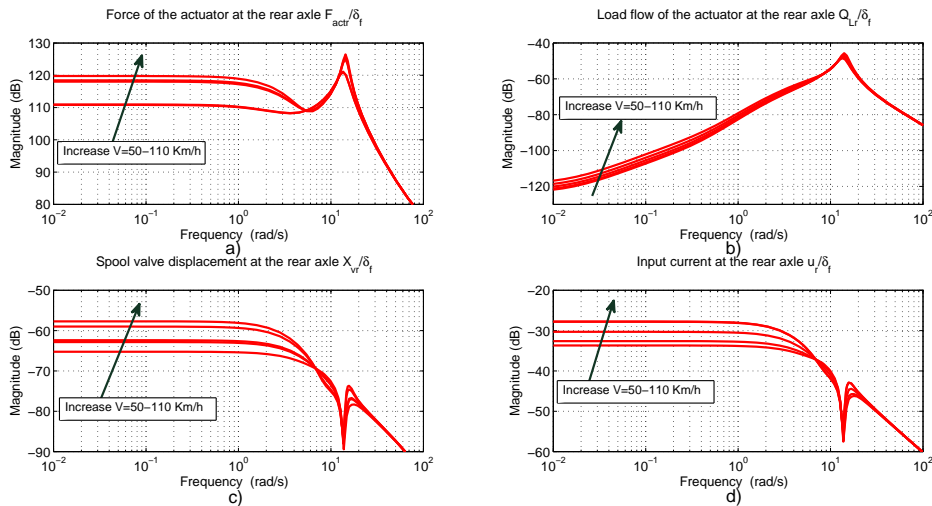


Figure 5.20: Transfer functions magnitude of (a) the actuator forces (F_{actr}), (b) the load flows (Q_{Lr}), (c) the spool valve displacements (X_{vr}) and (d) the input currents (u_r): rear axle.

5.4.2.2 Effect of the forward velocity uncertainties in the time domain

In this section, one considers the forward velocity up to 160 km/h in order to evaluate roll stability, as well as to determine the critical forward velocity at which the actuators reach their physical limits. In the next step, the disturbance is the steering angle (δ_f) corresponding to a cornering maneuver, shown in Figure 5.5.

Figure 5.21 shows the effect of the forward velocity on the maximum absolute value of the

normalized load transfers and the suspension roll angles at the front and rear axles. In the case of the passive anti-roll bar, the maximum absolute values of the normalized load transfers $R_{f,r}$ at the front and rear axles reach their limitations when the forward velocities are 90 and 80 km/h, respectively. Meanwhile, in the case of the H_∞ active anti-roll bar controller, these indices reach their limitations when the forward velocities are 145 and 132 km/h. The suspension roll angle recommendations are that they should stay within the limits of the suspension travel from 7 to 8 deg [Gaspar, Bokor, and Szaszi 2004]). From Figure 5.21, we can see that the suspension roll angles are always satisfied if the normalized load transfers at the two axles stay within their limitations.

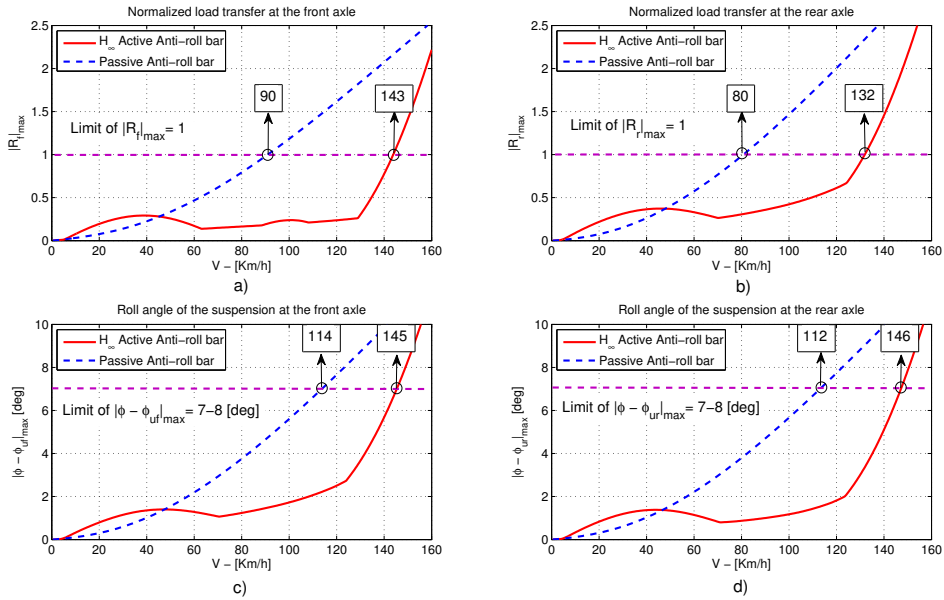


Figure 5.21: Influence of the forward velocity on the maximum absolute value of (a, b) the normalized load transfers and (c, d) the suspension roll angles at the two axles.

Figure 5.22 shows the characteristics of the ESVH actuators at the two axles. The maximum absolute value of the spool valve displacements ($X_{v,f,r}$) recommended is $4.85 \times 10^{-4} m$ [Rafa, Yahya, and Rawand 2009], the maximum absolute value recommended load flows ($Q_{L,f,r}$) of the oil into the hydraulic actuator is $2.2 \times 10^{-3} m^3/s$, the maximum absolute value of the input currents ($u_{f,r}$) recommended is 20 mA [Rafa, Yahya, and Rawand 2009] and the actuator forces ($F_{act,f,r}$) stay within the limit of 120 kN as recommended by McKevitt [Sampson 2000]. Thus with reference to the above limits, the physical constraints of the ESVH actuators always ensure that the parameters stay within their limits when the forward velocity up to 160 km/h is considered.

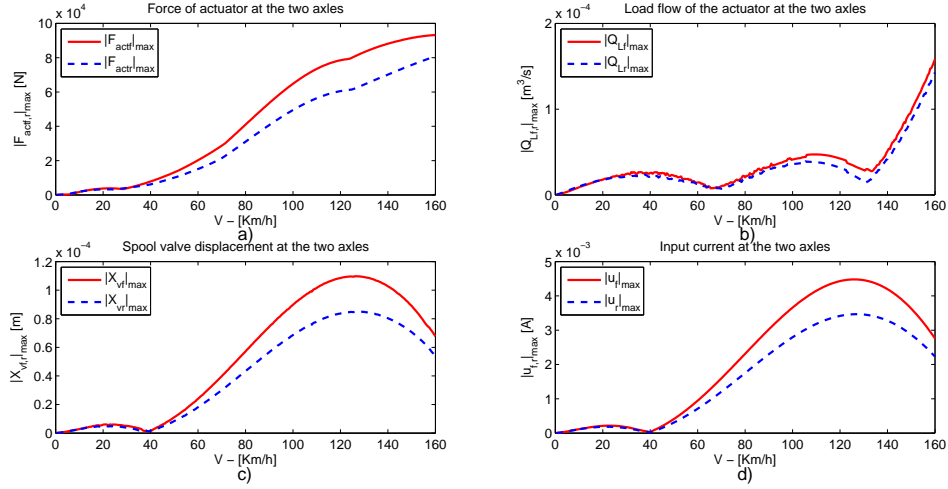


Figure 5.22: Influence of the forward velocity on the maximum absolute value of (a) the actuator forces ($F_{actf,r}$), (b) the load flows ($Q_{Lf,r}$), (c) the spool valve displacements ($X_{vf,r}$) and (d) the input currents ($u_{f,r}$) at the two axes.

5.5 Comparison between the LQR control and the H_∞ control for the active anti-roll bar system

This section aims to compare the two control methodologies used for the active anti-roll bar system: the LQR control (in Chapter 4) and the H_∞ control (in this chapter). The LQR controller needs measurement (or estimation) of the system state variables which includes 10 variables: $\beta, \dot{\psi}, \phi, \dot{\phi}, \phi_{uf}, \phi_{ur}, \Delta Pf, X_{vf}, \Delta Pr, X_{vr}$. Meanwhile the H_∞ controller needs only 2 measurements, which are the lateral acceleration a_y , and the roll rate $\dot{\phi}$. Hence the H_∞ controller will use less sensors than the LQR controller; this is very important in practice because it will significantly reduce the cost of the control system. According to the previous simulation results, the effectiveness of the LQR control depends entirely on the value of the weighting parameters, whereas it is the value of the weighting functions for the H_∞ control, so the comparison of these two control methodologies is only relative. In the following simulation results, we compare the two controllers when the forward velocity is considered constant at 70 km/h:

- **LQR controller:** we use the first LQR control design with the weighting parameter values as chosen in Section 4.2 ($\rho_i = R_{uf,r} = 1$, nominal design);
- **H_∞ controller:** we use the H_∞ control with the original weighting functions as chosen in Section 5.2.1 (see Table 5.3).

Figure 5.23 shows the transfer functions magnitude of the normalized load transfers and the suspension roll angles at both axles. The simulation results show that the H_∞ active anti-roll bar controller can focus on reducing the normalized load transfers and the suspension roll

angles in the desired frequency range up to 4 rad/s. Meanwhile, the LQR active anti-roll bar controller can reduce these signals up to 50 rad/s. However, the frequency range from 4 rad/s to 50 rad/s is beyond of the driver's bandwidth, so it is not necessary.

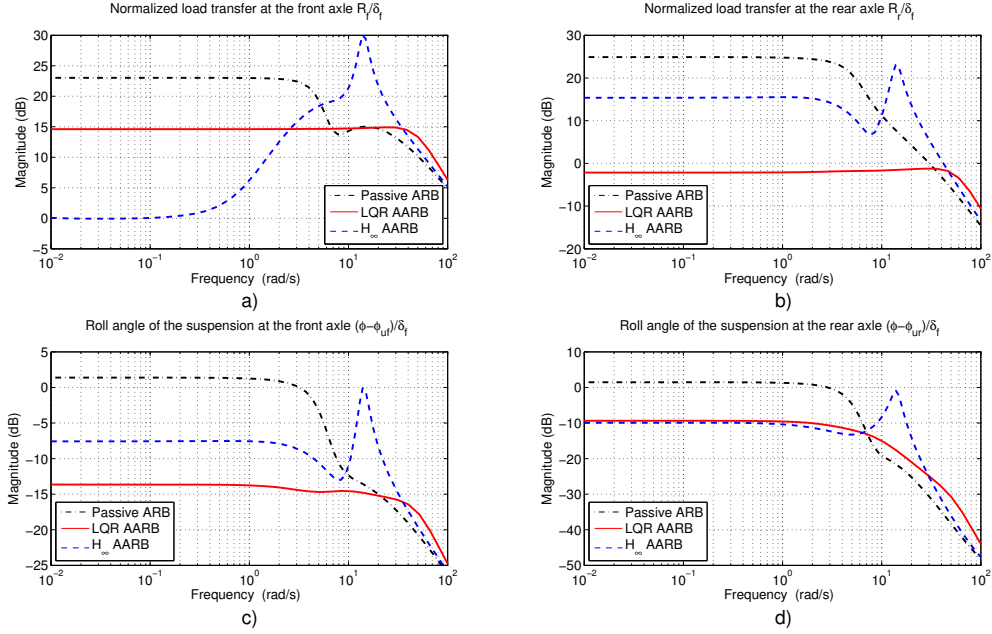


Figure 5.23: Transfer functions magnitude of (a, b) the normalized load transfers ($\frac{R_{f,r}}{\delta_f}$) and (c, d) the roll angle of the suspension ($\frac{\phi - \phi_{ur}}{\delta_f}$) at the two axles.

The transfer functions magnitude of the characteristics of the ESVH actuators are shown in Figure 5.24. We can see that the H_∞ controller needs fairly balanced input currents at both axles, and the forces generated by the actuators are fairly uniform within the frequency range from 0 to 4 rad/s.

The comparison between the LQR control and the H_∞ control for the active anti-roll bar system of heavy vehicles is listed in detail in Table 5.5.

Table 5.5: The comparison between the LQR control and the H_∞ control.

Evaluations	LQR control	H_∞ control
Number of the sensors (variables)	10 (full state)	2 (a_y, ϕ)
Improvement of roll stability	yes	yes
Focus on the desired frequency range	no (up to 50 rad/s)	yes (0 to 4 rad/s)
Considering the measurement noise	no	yes
Controller depends on	weighting parameters	weighting functions
Conflicting objectives	yes	yes

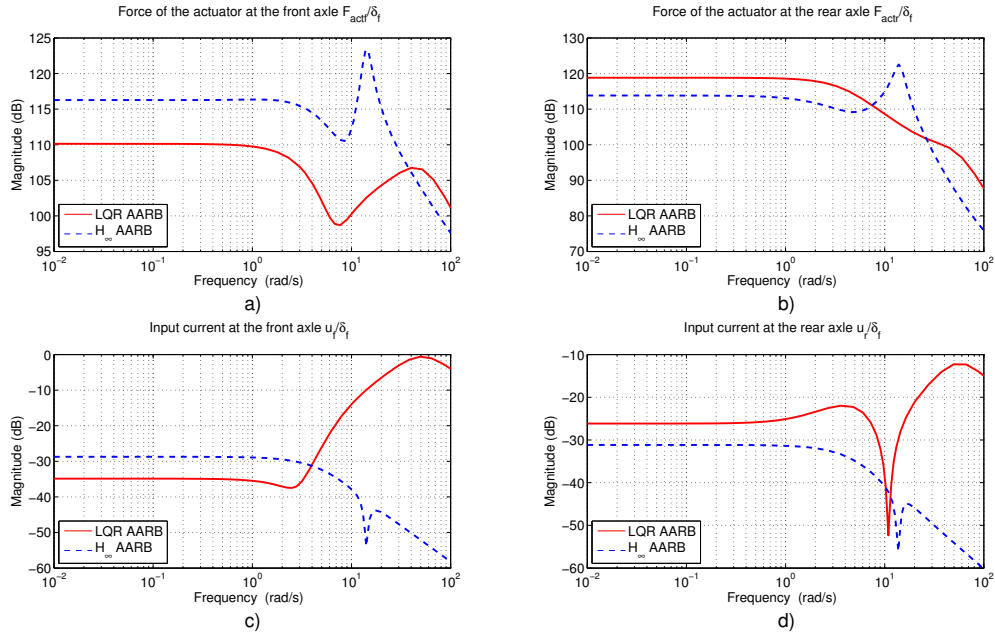


Figure 5.24: Transfer functions magnitude of (a, b) the force of the actuators ($\frac{F_{actf,r}}{\delta_f}$) and (c, d) the input currents ($\frac{u_{f,r}}{\delta_f}$) at the two axes.

5.6 Conclusion

In this chapter, the control-oriented integrated model of a single unit heavy vehicle including four ESVH actuators is used to develop a linear H_∞ control scheme which maximizes its roll stability in order to prevent vehicle rollover. The normalized load transfers and the limitations of the input currents are considered in the design.

Simulation results, both in the frequency and time domains, demonstrate that the H_∞ active anti-roll bar control completely reduces the normalized load transfers and the suspension roll angles compared to the passive anti-roll bar. A μ -analysis confirms that the closed-loop system remains stable for larger uncertainties, with the forward velocity $V = 70 \text{ km/h} \pm 88.6\%$ and the sprung mass $m_s = 12487 \text{ kg} \pm 46.5\%$.

A weighting function optimization procedure using GAs for the H_∞ active anti-roll bar control has also been proposed. The conflicting objectives between the normalized load transfers and input currents are handled by using only one high level parameter, which is a great advantage to solve the multi-objective control problem. The simulation results have shown the efficiency of the GAs to obtain a suitable controller to satisfy the MCO problem.

The above results have demonstrated the effectiveness of the H_∞ active anti-roll bar control for improving the roll stability of a single unit heavy vehicle to prevent rollover. In the next chapter the H_∞ active anti-roll bar control will be validated with a nonlinear high order freedom vehicle by using the TruckSim[®] software.

Validation of the H_∞ active anti-roll bar control by using TruckSim[®] software

Contents

6.1	Introduction	124
6.2	Performance criteria	126
6.3	Simulation scenario	127
6.4	Validation with the tour bus	128
6.4.1	Parameters of the tour bus (s-s, 4×2)	129
6.4.2	Simulation results in the case of the unloaded tour bus (Circular road test)	130
6.4.3	Simulation results in the case of the fully loaded tour bus (Cornering manoeuvre)	133
6.5	Validation with the LCF truck	136
6.5.1	Parameters of the LCF truck (s-s, 4×2)	136
6.5.2	Simulation results in the case of the unloaded LCF truck (Sine wave steering)	137
6.5.3	Simulation results in the case of the fully loaded LCF truck (Double lane change)	140
6.6	Conclusion	143

This chapter presents the validation of the H_∞ active anti-roll bar control proposed in Chapter 5 by using the TruckSim[®] software. The results of this chapter were partly obtained during my 2 weeks work at the Department of Control for Transportation and Vehicle Systems, Budapest University of Technology and Economics, Hungary. The TruckSim software used here is a copyrighted software from the Mechanical Simulation Corporation and purchased by the Budapest University of Technology and Economics. I would like to extend my thanks and gratitude to Professor Péter Gáspár, and Mr. András Mihály. The amount of time and help they gave me allowed me to carry out the theoretical and simulation ideas of this chapter and also moving through the implementation phase to the final application.



Figure 6.1: TruckSim[®] Intuitive Visualization [*Mechanical Simulation Corporation*].

6.1 Introduction

Since the 1960's, the Mechanical Simulation Corporation has developed a group of vehicle simulation software products under the title of VehicleSim(VS). VehicleSim includes three main products: CarSim[®], TruckSim[®], and BikeSim[®]. So in the following, let us summarise some advantages of TruckSim[®]. This software delivers the most accurate, detailed and efficient methods for simulating the performance of multi-axle commercial vehicles such as 4×2 tractors, 6×4 tractors as well as box trucks and buses. With TruckSim[®], we can build vehicle models by defining hundreds of vehicle parameters which affect the dynamical behaviour of the model. In addition to this, we can build trailers, add payloads and design various test manoeuvres to provide different models and scenarios. With manufacturers facing compressed product development cycles, TruckSim[®] provides an intuitive set of tools for engineers to quickly evaluate complete vehicles, truck sub-components, and active controllers in complex driving environments.

TruckSim[®] predicts the performance of vehicles in response to driver control inputs (steering, accelerators, brakes, clutch, and gear shifting) in a given environment (road geometry, coefficients of friction, wind). In terms of performance factors, we can consider the following: vehicle motions, forces, and moments involved in acceleration, handling and braking. Just about any test of a vehicle that would be conducted on a test track or road can be simulated. We can additionally study changes in vehicle behavior that result from modifying any of the hundreds of vehicle parameters, control inputs, or the driving environment. We can also add vehicle elements and systems such as controls (ABS, traction control, stability control) to the

vehicle and use them to develop control algorithms.

The main applications of TruckSim[®] can be listed as follows: Electronic Stability Control, ABS Braking, Off Tracking Analysis, Active Suspension, Autonomous Driving, Anti-roll Controls, Performance Based Standards, Anti-sway Controls, Alternate Powertrains, Driver Alertness Technologies, Roadway Engineering, Lane Departure Warnings, Fuel Economy Studies, Active Braking, Vehicle to Vehicle Communications. Here, we are interested in **Anti-roll Controls**.

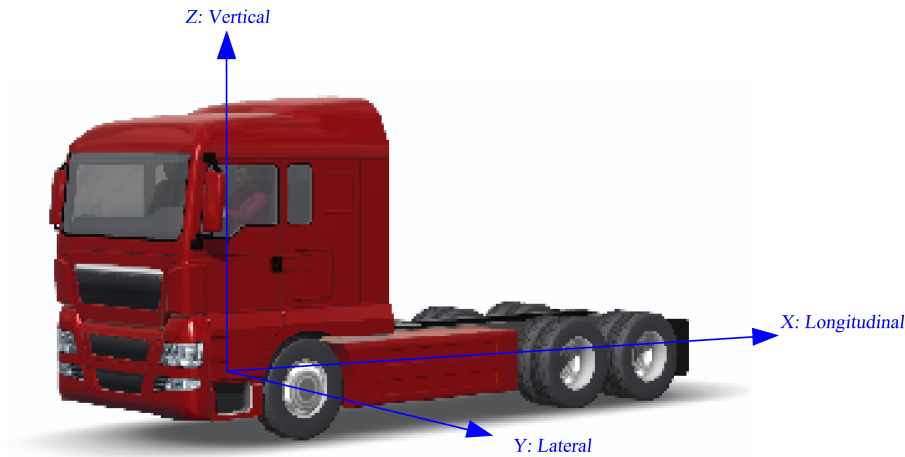


Figure 6.2: TruckSim[®] Vehicle Coordinate System.

In fact, TruckSim[®] was used extensively for developing the vehicle model and performing validation testing. When using this software, it is important to recognize that a unique vehicle coordinate system is used when defining certain parameters. An illustration of this coordinate system is given in Figure 6.2. As we can see, the origin of the coordinate system is at the front axle and at the middle of the track width. The vertical coordinate points upward (Z), the lateral coordinate points leftward (Y) and the longitudinal coordinate points rearward (X).

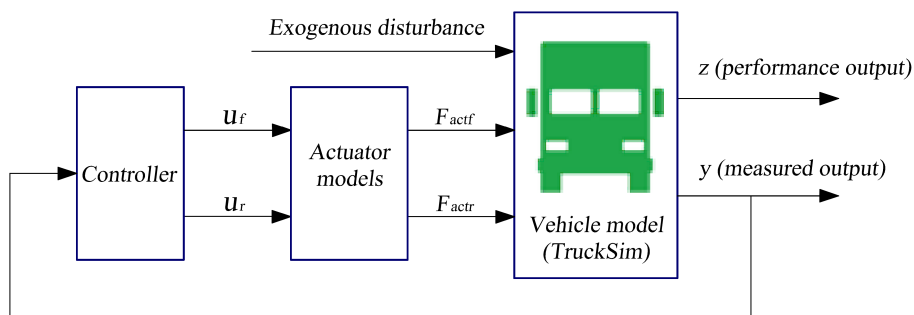


Figure 6.3: Diagram of TruckSim[®]-Simulink[®] Co-Simulation.

To survey the control systems for the nonlinear vehicle model in TruckSim[®], usually a co-simulation will be used. In this thesis, the author will use the co-simulation between Matlab[®]/Simulink and TruckSim[®]; the diagram of the co-simulation is shown in Figure 6.3. The nonlinear vehicle model is determined from TruckSim[®] software, based on using the block S-function of Simulink. Meanwhile, the controller and the actuators are built directly in the Matlab[®]/Simulink environment.

In Figure 6.3, the output of the block S-function represented for the nonlinear vehicle model includes the performance and measurement outputs. We consider the two measurement outputs which are the lateral acceleration and the roll rate of the sprung mass. The input of the block S-function includes the exogenous disturbance and the two auxiliary moments from the active anti-roll bar system at the two axles. The controllers are synthesized as in Chapter 5, with the H_∞ control method. The characteristics of the actuators are modelled in Chapter 2. In the co-simulation between Matlab[®]/Simulink and TruckSim[®], there are two following solutions for the steering angle. In this thesis, the second solution is used.

- First solution: the steering angle is defined in Simulink[®] and entered to TruckSim[®] through the S-function as shown in Figure 6.3. With this solution, the trajectories of the vehicle in the cases of the passive anti-roll bar and of the active anti-roll bar are often different, indicated by the effect of the wheels lift off from the road. This means that it affects the direction of the vehicle. Therefore, it is difficult to evaluate the effectiveness of the active anti-roll bar system, and so this solution is not considered in this thesis.
- Second solution: the steering angle is defined in TruckSim[®], according to two possible choices. In the 1st case, the closed-loop driver model is used and the steering angle is automatically changed to adapt to the vehicle trajectory. Here, the vehicle trajectories in the case of the passive anti-roll bar and of the active anti-roll bar will follow the target path which fits the driver's wishes. In the 2nd case, the open loop driver model is used and the steering angles are the same for both the active and passive anti-roll bar systems.

In the following validations, the author will test the H_∞ active anti-roll bar control with two different types of vehicle: a tour bus and a LCF (Low Cab Forward) truck, with two different load options: unloaded and fully loaded. The tour bus uses two solid suspension systems at both axles, with the engine mounted at the rear of the vehicle. The LCF truck also uses the two solid suspension systems at both axles, but the engine is mounted at the front of the vehicle. The parameters of the tour bus, as well as of the LCF truck are found in the vehicle configuration of TruckSim[®] and they will be shown in the following sections.

6.2 Performance criteria

In the previous chapters, to evaluate the rollover behavior of a vehicle, we used the normalized load transfers $R_{f,r}$ at the two axles, when the values of $R_{f,r}$ take on the limit of ± 1 , rollover will occur, which means that there will be wheel lift off from the road. In TruckSim[®] we can

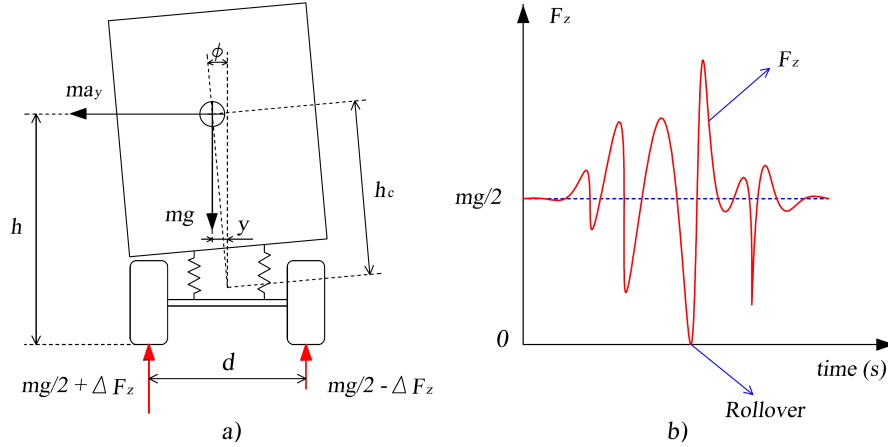


Figure 6.4: Tyre force in the Z direction.

calculate directly the tyre force in the Z direction at each wheel. In Figure 6.4a we can see the tyre force in the Z direction defined as:

$$F_z = \frac{mg}{2} \pm \Delta F_z \quad (6.1)$$

where ΔF_z is the load transfer and $\frac{mg}{2}$ the static load at each wheel. The value of the tyre force in the Z direction fluctuates around the static load. In Figure 6.4b, we can see that when the value $F_z = 0$, the wheel will start to lift off from the road and at that time we can consider that vehicle rollover has occurred. So in the following, we will use the tyre force in the Z direction (F_z) at each wheel to evaluate vehicle rollover behaviour.

6.3 Simulation scenario

In this chapter, we will use the four common simulation scenarios to evaluate the effect of active anti-roll bar systems on heavy vehicles, with the objective of improving roll stability and preventing the rollover phenomenon.

- **The 1st simulation scenario:** Double lane change to overtake, the vehicle running at 100 km/h,
- **The 2nd simulation scenario:** Handling test on a circular test circuit with a diameter of 1000ft and a road bank angle of 10%, the vehicle running at 100 km/h,
- **The 3rd simulation scenario:** A cornering manoeuvre with a 180 deg steering angle, the vehicle running at 50 km/h,
- **The 4th simulation scenario:** A sine wave (\sim) steering manoeuvre, the vehicle running at 100 km/h.

Table 6.1 shows the validation cases of the H_∞ active anti-roll bar control by using co-simulation between Matlab[®]/Simulink and TruckSim[®]. All of the simulation scenarios with respect to the tour bus and the LCF truck with unloaded and fully loaded options are surveyed. The simulation results show that by using the H_∞ active anti-roll bar control, roll stability is improved to prevent the risk of vehicle rollover. Only the four cases highlighted by the bold lettering (red color) will be shown in the following sections.

Table 6.1: Validation cases of the H_∞ active anti-roll bar control by using co-simulation.

Scenario	Unloaded bus	Loaded bus	Unloaded truck	Loaded truck
Circular road test	X 100 km/h	X	X	X
Cornering manoeuver	X	X 50 km/h	X	X
Sine wave steering	X	X	X 100 km/h	X
Double lane change	X	X	X	X 100 km/h

6.4 Validation with the tour bus

The commercial passenger buses are probably the most popular people carrying vehicles in the world. Typically they are vehicles with two axles (bus 2A) and a capacity of 45 passengers. The maximum forward velocity of these buses usually reaches 130 km/h in France or more than 130 km/h in some other countries. Therefore, bus rollover is an important problem in the case of an emergency. Here, we consider the tour bus with the solid suspension systems for both axles and the engine mounted at the rear of the vehicle. The single tyre is used for the front axle and the dual tyre for the rear axle. The two different cases of vehicle loading will be considered: unloaded and fully loaded.



Figure 6.5: Tour bus 2 axles (4×2) [*Tour-bus*].

6.4.1 Parameters of the tour bus (s-s, 4×2)

Figure 6.5 shows the tour bus (s-s, 4×2), in the unloaded state, all of the vehicle parameters can be easily determined from the vehicle configuration block in TruckSim[®]. They are summarized in Table 6.2, with a total weight of 7620 kg and 5 m length for the wheelbase.

Table 6.2: Parameters of the unloaded tour bus.

Parameter	Value	Parameter	Value	Parameter	Value
m_s	6360 kg	b_f	20.6 $\frac{kN}{rad}$	I_{xx}	7696 kgm^2
$m_{u,f}$	500 kg	b_r	86.8 $\frac{kN}{rad}$	I_{zz}	30782 kgm^2
$m_{u,r}$	760 kg	k_{tf}	2019 $\frac{kNm}{rad}$	r	0.51 m
m	7620 kg	k_{tr}	3401 $\frac{kNm}{rad}$	h	1.2 m
$h_{u,f}$	0.51 m	k_f	309 $\frac{kNm}{rad}$	l_f	3 m
$h_{u,r}$	0.528 m	k_r	1562 $\frac{kNm}{rad}$	l_r	2 m
C_f	401 $\frac{kN}{rad}$	C_r	573 $\frac{kN}{rad}$		

For the fully loaded state, we assume that all the passengers are sitting on the seats and they are evenly distributed, so the payload on each side is as a box, with a length of 7 m, height 1 m, width 1 m, with the center of gravity being $(-2.750m, \pm 0.75m, 1.75m)$ from the origin. Figures 6.6, 6.7 show the payloads for the right and left passengers, respectively. For this case, the parameters to be added in Table 6.2 are the mass of each payload $m_{sPayload}$ 1500 kg, roll inertia ($I_{xxPayload}$) 250 kgm^2 , pitch inertia ($I_{yyPayload}$) 6250 kgm^2 , yaw inertia ($I_{zzPayload}$) 6250 kgm^2 .

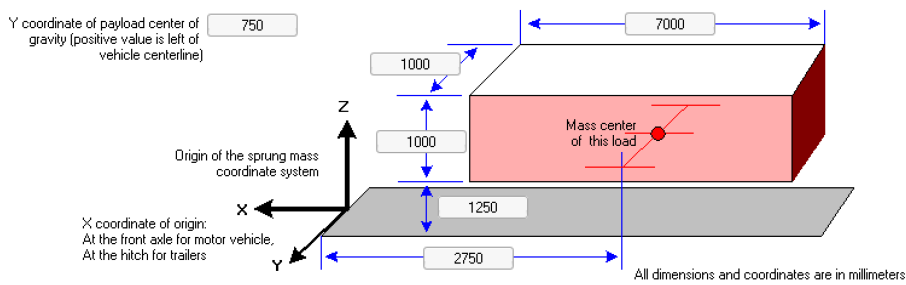


Figure 6.6: Payload (left passengers).

In the following, for unloaded and fully loaded conditions, we will test the effect of the H_∞ active anti-roll bar control of the tour bus on improving roll stability and preventing the rollover phenomenon. The simulation scenarios are the circular road test with a forward velocity of 100 km/h and the cornering manoeuvre when the forward velocity is 50 km/h.

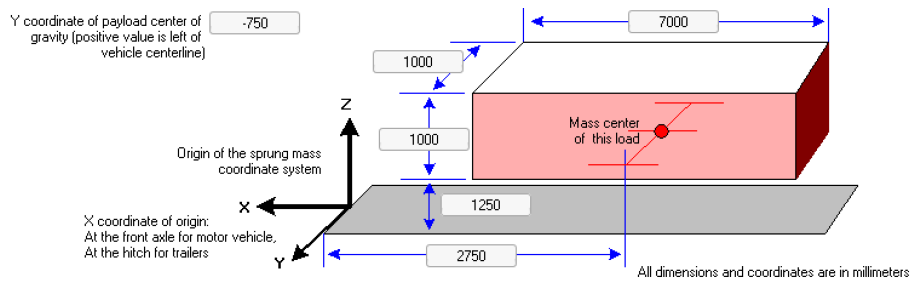


Figure 6.7: Payload (right passengers).

6.4.2 Simulation results in the case of the unloaded tour bus (Circular road test)

In this validation, the handling test on the circular road with a diameter of 1000ft and a road bank angle of 10% is used to evaluate the roll stability of the tour bus when it runs at 100 km/h . This is a typical form of the road surface in the proving ground, with the slope of the road (banking) toward the center of the circle.

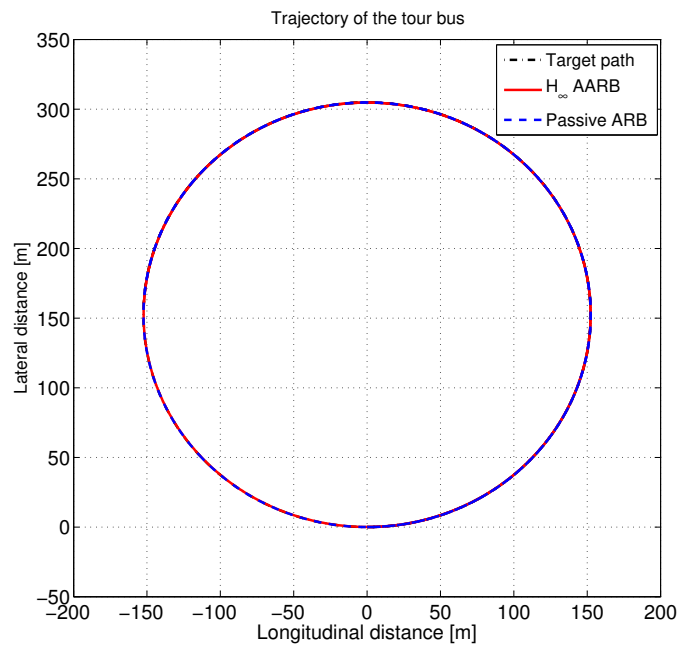


Figure 6.8: Trajectory of the tour bus in the circular road test.

Figure 6.8 shows the trajectory of the tour bus in the circular road test. Figure 6.9 shows the time response of (a) the steering angle, (b) the roll angle of sprung mass, and (c,d) the roll angle of the unsprung masses at the two axles, respectively. In order to ensure that the

vehicle moves in the same circle with a diameter of $1000ft$, the steering angle is kept constant at 50 deg in the case of the H_∞ active anti-roll bar control, and at 63 deg in the case of the passive anti-roll bar. This means that the trajectories of the vehicle in the H_∞ active anti-roll bar control case and the passive anti-roll bar case coincide with the desired trajectory.

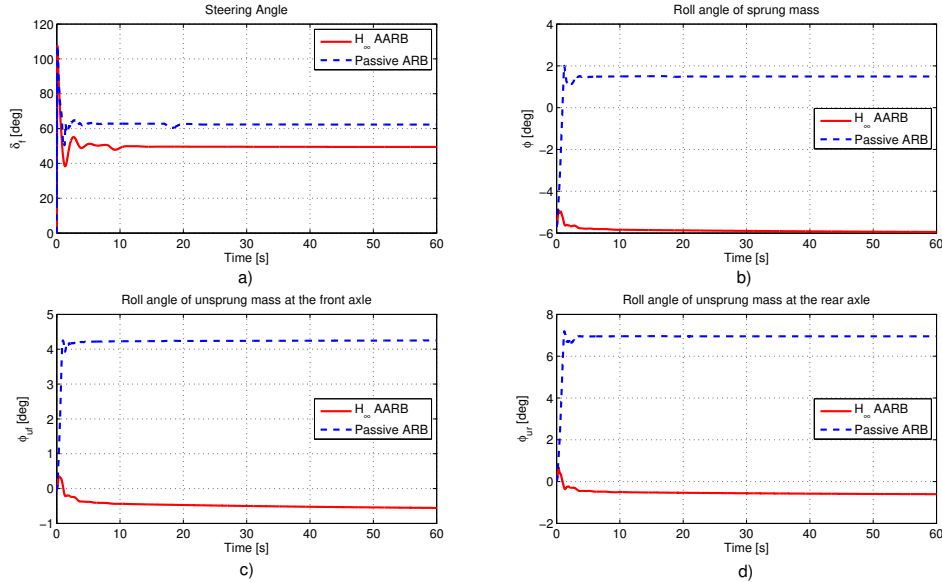


Figure 6.9: Unloaded tour bus: time response of (a) steering angle, (b) roll angle of sprung mass, (c,d) roll angle of unsprung masses at the front/rear axles.

From the Figures 6.9b,c,d, we can see that, in the case of the passive anti-roll bar, under the action of the inertial force, the tour bus rolls outwards of the corner, while it rolls into the corner in the case of the H_∞ active anti-roll bar control system. Thanks to this rolling response, the tour bus can improve its roll stability capacity. This is entirely consistent with the previous studies [Sampson and Cebon 2003a], [Gaspar, Bokor, and Szaszi 2004], [Sampson and Cebon 2003b], [Hsun-Hsuan, Rama, and Dennis 2012], [Miège and Cebon 2005b] and [Yu, Guvenc, and Ozguner 2008].

Figure 6.10 shows the time response of the tyre forces in the Z direction of all the wheels. We can see that in the case of the H_∞ active anti-roll bar controller, all the tyre forces are positive, which means that there is no wheel lift off the road. But in the case of the passive anti-roll bar, the tyre force in the Z direction of the left-front wheel is always zero (see Figure 6.10a). So it indicates that when the tour bus runs at 100 km/h , the left-front wheel lifts off the road, and at all times there are only three wheels on the ground. From these results, it shows that the H_∞ active anti-roll bar control improves the roll stability of the unloaded tour bus, when compared to the passive anti-roll bar.

Figure 6.11 shows the time response of the characteristics of the ESVH actuators at the two axles, they are (a) the actuator forces, (b) the load flows, (c) the spool valve displacements and (d) the input currents. The results indicate that the maximum absolute value of the above

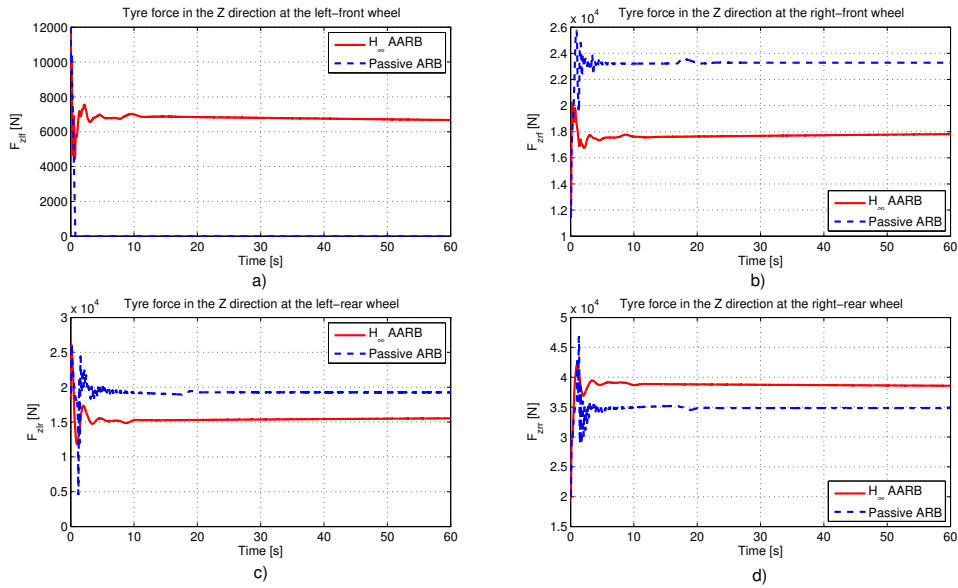


Figure 6.10: Unloaded tour bus: time response of the tyre forces in the Z direction of (a) left-front wheel, (b) right-front wheel, (c) left-rear wheel, and (d) right-rear wheel.

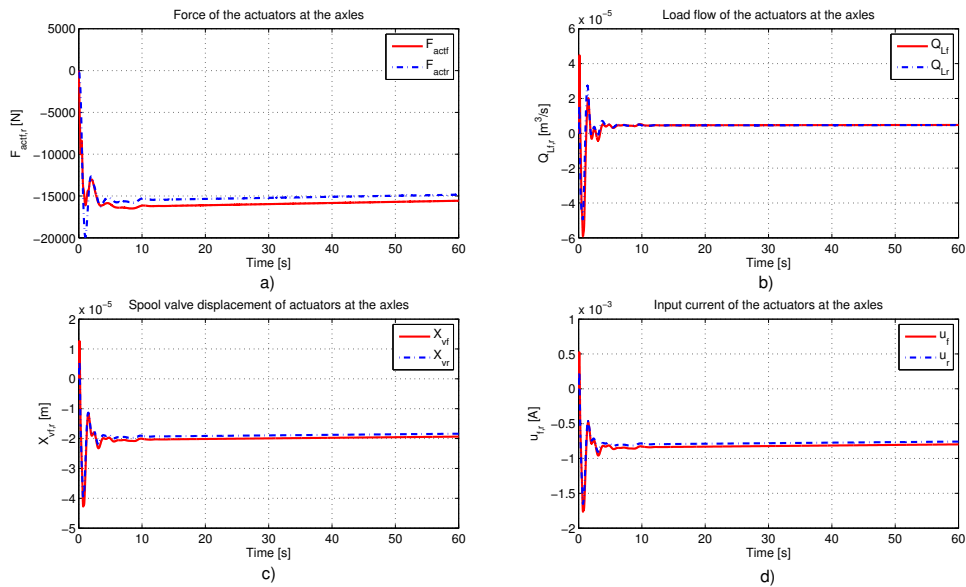


Figure 6.11: Unloaded tour bus: time response of the characteristic of the ESVH actuators.

characteristics are very far from the physical constraints of the ESVH actuator ($|F_{act}|_{max} = 120 \text{ kN}$, $|Q_L|_{max} = 2.2 \times 10^{-3} \text{ m}^3/\text{s}$, $|X_v|_{max} = 4.85 \times 10^{-4} \text{ m}$ and $|u|_{max} = 20 \text{ mA}$).

From the simulation results with the unloaded tour bus, we can see that the H_∞ active anti-roll bar controller improves the roll stability, and it always satisfies the physical constraints of the ESVH actuators at the two axles.

6.4.3 Simulation results in the case of the fully loaded tour bus (Cornering manoeuvre)

In this validation, the total weight of the tour bus is 9360 kg . The cornering manoeuvre with 180 deg of steering angle is used to evaluate the roll stability of the tour bus when it runs at 50 km/h . Even if the forward velocity at 50 km/h is not so high, this is still an emergency situation because the steering angle varies from 0 deg to 180 deg in just over 0.6 s as shown in Figure 6.13a. It is worth noting that the steering angle is kept the same in the two cases of the H_∞ active anti-roll bar and the passive anti-roll bar systems.

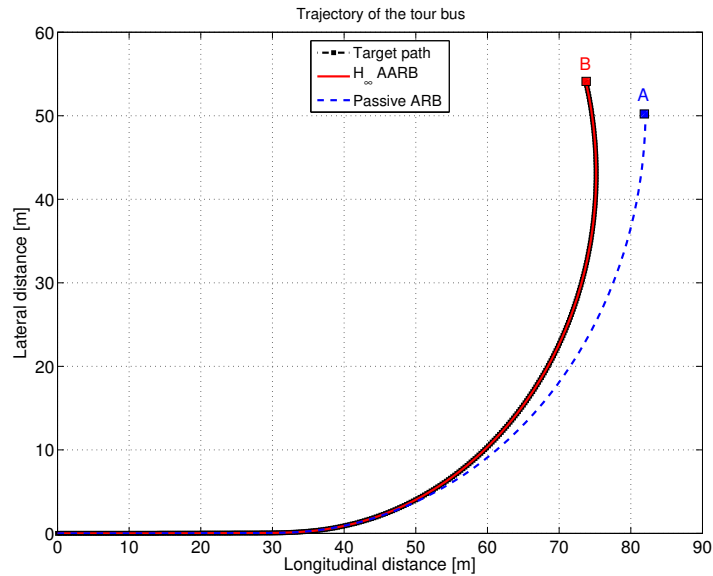


Figure 6.12: Trajectory of the tour bus in the cornering manoeuvre.

The trajectory of the tour bus in the cornering manoeuvre is shown in Figure 6.12. In the case of the H_∞ active anti-roll bar system, the vehicle always sticks to the target path (to point B). However, due to the left-front wheel lifting off the road from 2.8 s , the trajectory of the vehicle using the passive anti-roll bar system cannot follow the target path (to point A). Figure 6.13 shows the time response of (a) the steering angle, (b) the roll angle of sprung mass, and (c,d) the roll angle of the unsprung masses at the two axles, respectively. The comparison of the time response between the H_∞ active anti-roll bar and the passive anti-roll bar is summarized in Table 6.3. From Figure 6.13 and Table 6.3, we can see that in the case

Table 6.3: Time response comparison between the H_∞ active anti-roll bar and the passive anti-roll bar.

Time responses	ϕ [deg]	ϕ_{uf} [deg]	ϕ_{ur} [deg]
H_∞ AARB	2	1.3	1.8
Passive ARB	8	6.5	7.5

of the H_∞ active anti-roll bar control, the roll angle of the sprung and unsprung masses are significantly reduced, when compared to the passive anti-roll bar (the reductions are about 6 deg).

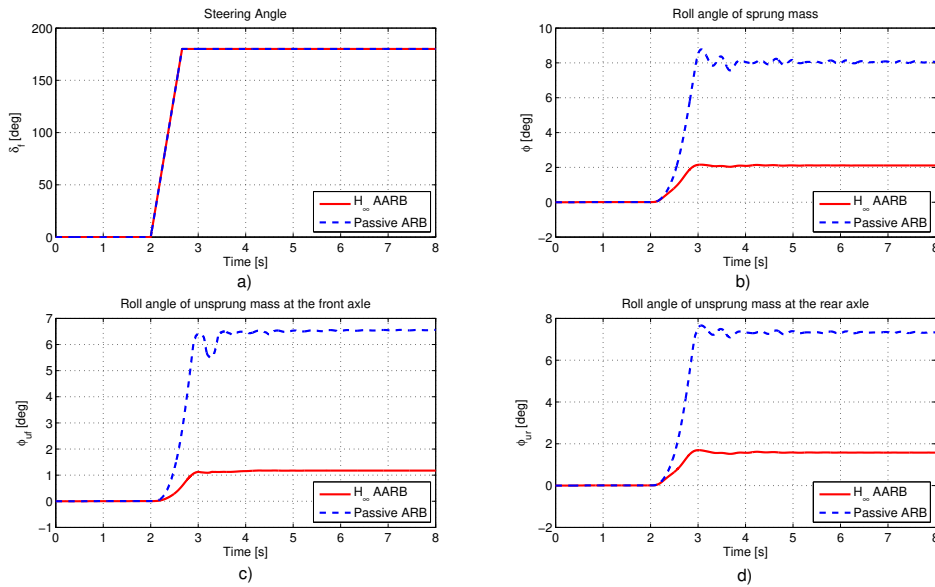


Figure 6.13: Fully loaded tour bus: time response of (a) steering angle, (b) roll angle of sprung mass, (c,d) roll angle of unsprung masses at the front/rear axles.

Figure 6.14 shows the time response of the tyre forces in the Z direction of all the wheels. We can see that in the case of the H_∞ active anti-roll bar controller, all the tyre forces are positive, which means that there is no wheel lift off the road. But in the case of the passive anti-roll bar, the left-front wheel lifts off from the road from 2.8 s (see Figure 6.14a). We can also see that the H_∞ active anti-roll bar control reduces the load transfer at both axles: the tyre force in the Z direction at the left-front wheel F_{zlf} is stable around 2000 N, the right-front wheel F_{zrf} is stable around 35000 N, the left-rear wheel F_{zlr} is stable around 18000 N and the right-rear wheel F_{zrr} is stable around 51000 N. So the H_∞ active anti-roll bar control makes the tyre forces in the Z direction quite stable for the whole time period. However, there are some oscillations in the passive anti-roll bar case. These results shows that the H_∞ active anti-roll bar control improves the roll stability of the fully loaded tour bus.

Figure 6.15 shows the time response of the characteristics of the ESVH actuators at both axles,

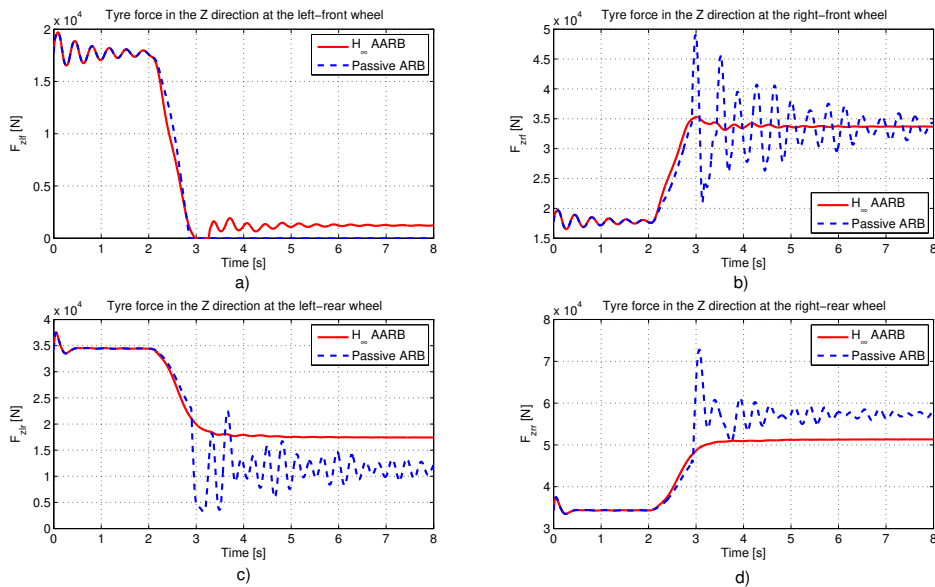


Figure 6.14: Fully loaded tour bus: time response of the tyre forces in the Z direction of (a) left-front wheel, (b) right-front wheel, (c) left-rear wheel, and (d) right-rear wheel.

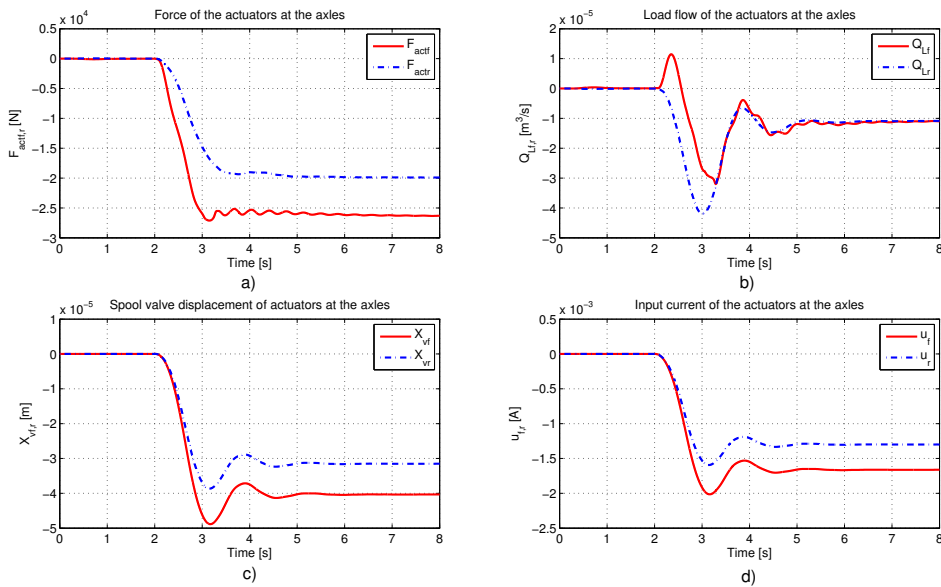


Figure 6.15: Fully loaded tour bus: time response of the characteristic of the ESVH actuators.

they are the (a) actuator forces, (b) the load flows, (c) the spool valve displacements and (d) the input currents. We can see that the maximum absolute value of the above characteristics are very far from the physical constraints of the ESVH actuator. Since the lateral load transfer at the front axle is higher than at the rear axle, so the ESVH actuator at the front axle needs more energy than at the rear one to prevent vehicle rollover.

From the simulation results shown in Figures 6.10 and 6.14, we can see that with the tour bus vehicle rollover will occur at the front axle before the rear axle. The reason is the influence of the position of the engine, because with all tour buses, the engine is usually mounted at the rear axle. Although the H_∞ active anti-roll bar control improves the roll stability of the tour bus in both cases of vehicle loading, this controller still has not any special focus on reducing the lateral load transfer at the front axle. This problem will be considered and improved by H_∞/LPV synthesis in Chapter 7.

6.5 Validation with the LCF truck

The LCF (Low Cab Forward) truck has been used in various configurations, including dump trucks, fire trucks, tow trucks, box trucks, crane/bucket trucks, flat beds and stake bodies. It uses two solid suspension systems at all axles, and the engine is mounted at the front of the vehicle. The single tyre is used for the front axle and the dual tyre for the rear axle. Two cases of vehicle loading will also be considered: unloaded and fully loaded.



Figure 6.16: LCF truck 2 axles (4×2) [*LCF-Truck*].

6.5.1 Parameters of the LCF truck (s-s, 4×2)

Figure 6.16 shows one LCF truck. As with the tour bus, in the unloaded state all of the parameters of the LCF truck can be easily determined from the vehicle configuration block in

TruckSim[®]. They are summarized in the Table 6.4, with a total weight of 5760 kg and 5 m length for the wheelbase.

Table 6.4: Parameters of the unloaded LCF truck.

Parameter	Value	Parameter	Value	Parameter	Value
m_s	4455 kg	b_f	30.9 $\frac{kN}{rad}$	I_{xx}	2284 kgm^2
$m_{u,f}$	570 kg	b_r	52.1 $\frac{kN}{rad}$	I_{zz}	34803 kgm^2
$m_{u,r}$	735 kg	k_{tf}	2019 $\frac{kNm}{rad}$	I_{xz}	1626 kgm^2
m	5760 kg	k_{tr}	3401 $\frac{kNm}{rad}$	h	1.2 m
$h_{u,f}$	0.51 m	k_f	515 $\frac{kNm}{rad}$	l_f	3.105 m
$h_{u,r}$	0.528 m	k_r	1215 $\frac{kNm}{rad}$	l_r	1.385 m
C_f	401 $\frac{kN}{rad}$	C_r	573 $\frac{kN}{rad}$	r	0.51 m

In the fully loaded state, we assume that the payload is a box, with a length of 3 m, height 1 m, width 2 m, with the center of gravity being $(-4.5m, 0m, 1.8m)$ from the origin. Figure 6.17 shows the payload, with the mass payload being $m_{sPayload}$ 6789 kg, height of the box center gravity from the ground $h_{Payload}$ 2.31 m, roll inertia ($I_{xxPayload}$) 2828.75 kgm^2 , pitch inertia ($I_{yyPayload}$) 5657.50 kgm^2 , yaw inertia ($I_{zzPayload}$) 7354.75 kgm^2 .

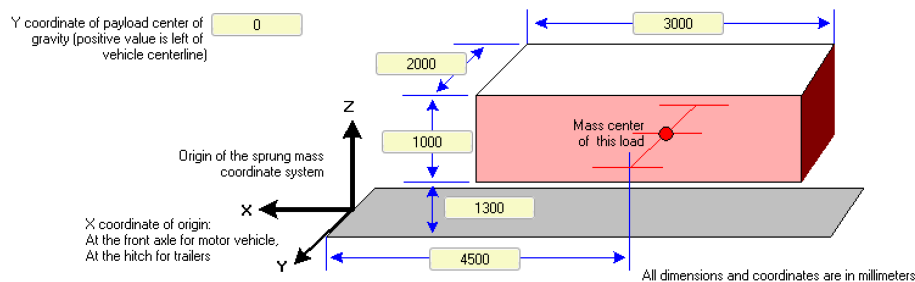


Figure 6.17: Payload of LCF truck.

6.5.2 Simulation results in the case of the unloaded LCF truck (Sine wave steering)

In this validation, the sine wave steering manoeuvre is used to evaluate roll stability of the LCF truck when it runs at 100 km/h. With this manoeuvre, the driver will change the steering wheel continuously in sine cycles, so the time response of the truck is also in the sine form. From figure 6.19a, the steering angle δ_f is the sine wave with the amplitude of 90 deg and a period of 4s, it is the same for the two cases. The trajectory of the LCF truck is shown in Figure 6.18. The trajectory of the vehicle in the case of the H_∞ active anti-roll bar control always follows the target path (to point B); meanwhile in the passive anti-roll bar case, it cannot stick to the target path (to point A).

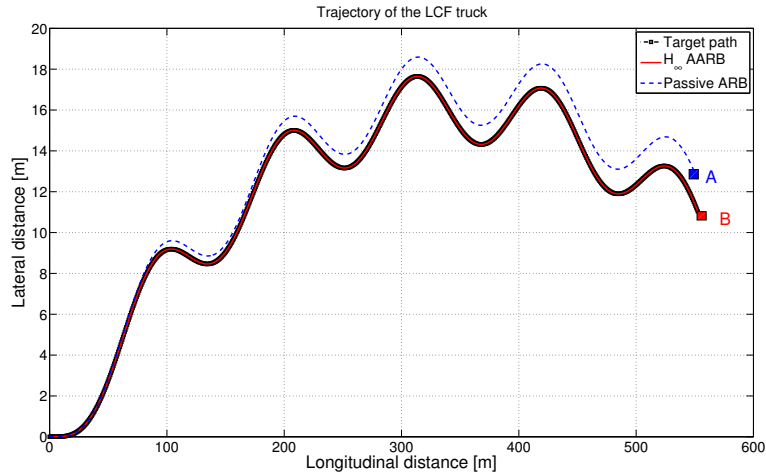


Figure 6.18: Trajectory of the LCF truck in the sine wave steering manoeuver.

Figures 6.19*b, c, d* show the time response of (b) the roll angle of the sprung mass, (c,d) the roll angle of the unsprung masses at the two axles, respectively. In the case of the H_∞ active anti-roll bar control, the roll angle of the sprung and unsprung masses are significantly reduced, when compared to the case of the passive anti-roll bar. The reduction of these signals is summarized in Table 6.5.

Table 6.5: Reduction of the signal magnitude compared to the passive anti-roll bar.

ϕ [deg]	ϕ_{uf} [deg]	ϕ_{ur} [deg]
1.5	1.4	0.7

Figure 6.20 shows the time response of the tyre forces in the Z direction of all the wheels. In the case of the H_∞ active anti-roll bar controller, all the tyre forces are positive, which means that there is no wheel lift off from the road. But in the case of the passive anti-roll bar, the two rear wheels lift off when the steering angle is at the peak of the sine wave.

In Figures 6.20*a, b* the amplitude of the tyre forces at the front axle for the H_∞ active anti-roll bar control are higher than those of the passive anti-roll bar. But In Figures 6.20*c, d* the amplitude of the tyre forces at the front axle for the H_∞ active anti-roll bar control are smaller than those of the passive anti-roll bar. This means that there is a load transfer between the two axles; this problem was also mentioned in the study of Professor David Cebon [Sampson and Cebon 2003b]. However, in general these results show that the H_∞ active anti-roll bar control improves roll stability of the unloaded LCF truck. The rollover risk is reduced by about 30% in the case of the H_∞ active anti-roll bar control, when compared to the passive anti-roll bar.

Figure 6.21 shows the time response of the characteristics of the ESVH actuators at the two axles, they are (a) the actuator forces, (b) the load flows, (c) the spool valve displacements

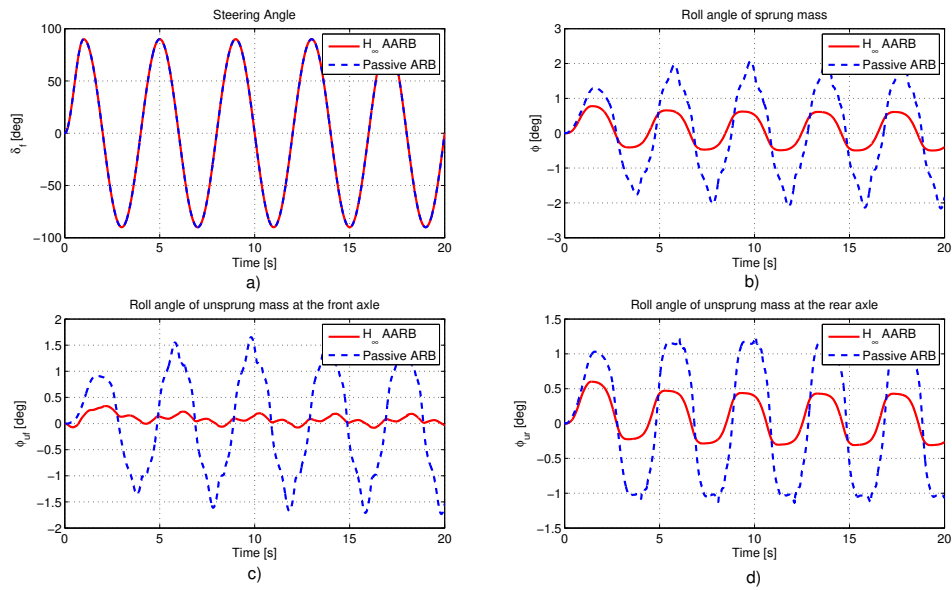


Figure 6.19: Unloaded LCF truck: time response of (a) steering angle, (b) roll angle of sprung mass, (c,d) roll angle of unsprung masses at the front/rear axles.

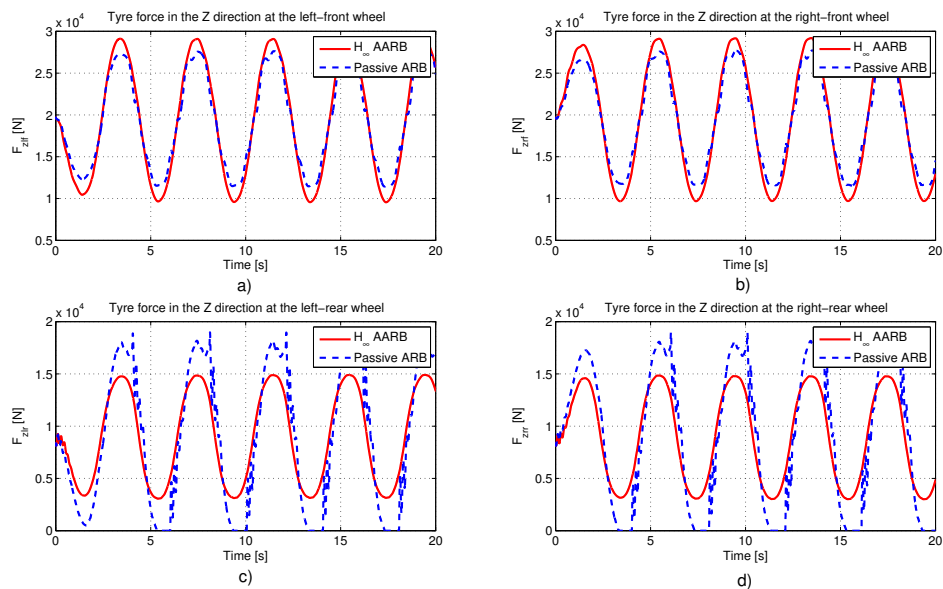


Figure 6.20: Unloaded LCF truck: time response of the tyre forces in the Z direction of (a) left-front wheel, (b) right-front wheel, (c) left-rear wheel, and (d) right-rear wheel.

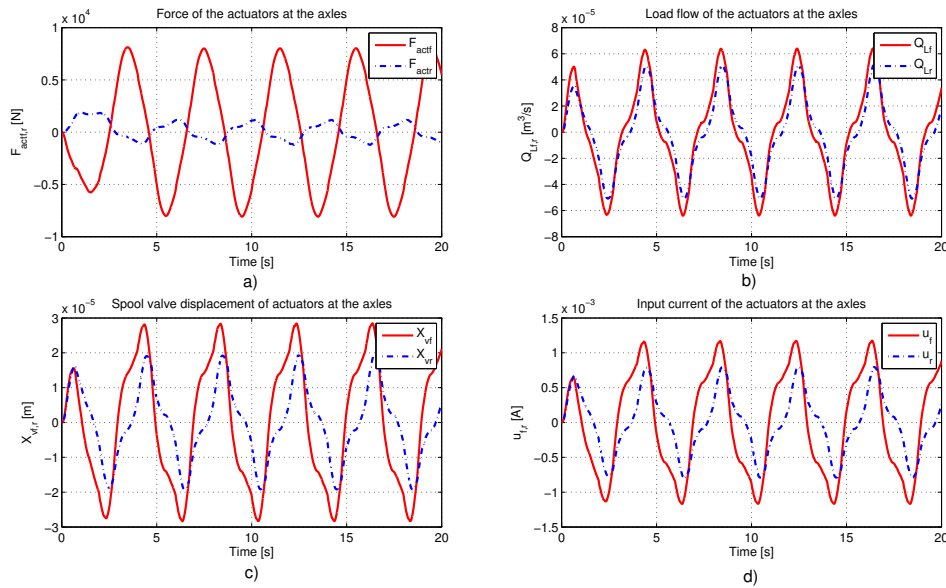


Figure 6.21: Unloaded LCF truck: time response of the characteristic of the ESVH actuators.

and (d) the input currents. The results also indicate that even if the LCF truck runs at 100 km/h , the maximum absolute value of the above characteristics are very far from the physical constraints of the ESVH actuator.

6.5.3 Simulation results in the case of the fully loaded LCF truck (Double lane change)

In this validation, the total weight of the fully loaded LCF truck is 12549 kg and the double lane change manoeuvre is used to evaluate its roll stability when it runs at 100 km/h . This represents the situation when the driver wishes to overtake another vehicle or to avoid an obstacle in an emergency situation.

Figure 6.22 shows the trajectory of the vehicle. In this manoeuvre with the goal of ensuring that the vehicle's trajectory sticks closely to the target path, the steering angle is controlled by the driver with the amplitude at about 100 deg as shown in Figure 6.23a.

Figures 6.23b, c, d show the time response of the roll angle of the sprung mass and the roll angle of the unsprung masses at the two axles, respectively. We can see that in the case of the H_∞ active anti-roll bar controller, the roll angle of the sprung and unsprung masses are significantly reduced when compared to the passive anti-roll bar (the reduction of the roll angle is about 20 deg for the sprung mass, 10 deg for the unsprung mass at the front, and 5 deg for the unsprung mass at the rear axle).

Figure 6.24 shows the time response of the tyre forces in the Z direction of all the wheels. In the case of the H_∞ active anti-roll bar controller, all the tyre forces are positive, which means that there is no wheel lift off the road. But in the case of the passive anti-roll bar, all the

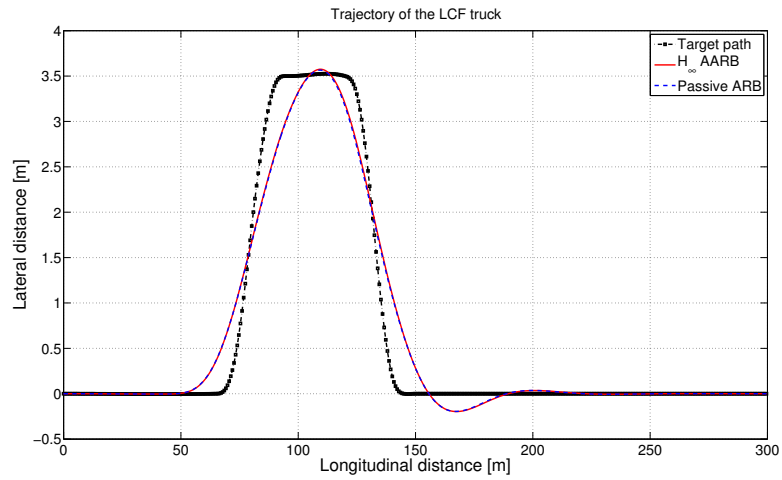


Figure 6.22: Trajectory of the LCF truck in the double lane change manoeuvre.

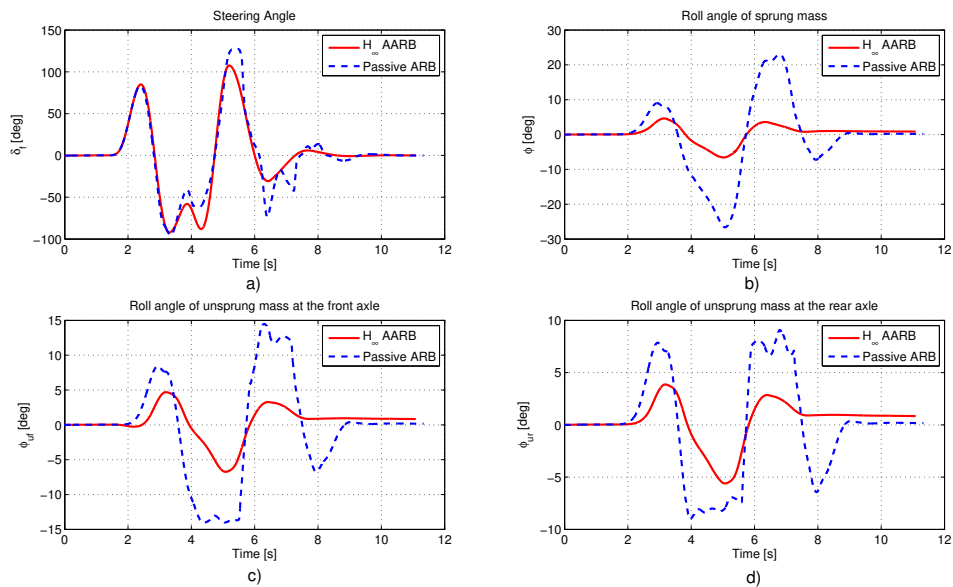


Figure 6.23: Fully loaded LCF truck: time response of (a) steering angle, (b) roll angle of sprung mass, (c,d) roll angle of the unsprung masses at the front/rear axles.

wheels lift off the road:

- The left-front wheel lifts off at $5.5s \div 7.2s$,
- The right-front wheel lifts off at $4s \div 5.5s$,
- The left-rear wheel lifts off at $3s$ and $5.8s \div 7.2s$,
- The right-rear wheel lifts off at $3.8s \div 5.5s$.

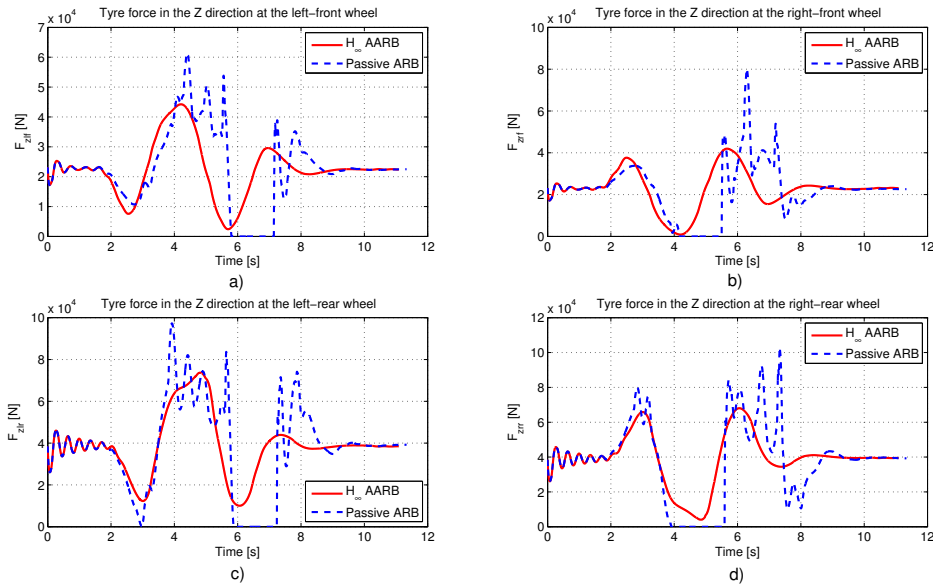


Figure 6.24: Fully loaded LCF truck: time response of the tyre forces in the Z direction of (a) left-front wheel, (b) right-front wheel, (c) left-rear wheel, and (d) right-rear wheel.

These simulation results in the double lane change manoeuvre, show that the H_∞ active anti-roll bar control improves the roll stability of the fully loaded LCF truck, compared to the passive anti-roll bar.

Figure 6.25 shows the time response of the characteristics of the ESVH actuators at the two axles, they are (a) the actuator forces, (b) the load flows, (c) the spool valve displacements and (d) the input currents. The maximum absolute value of the actuator forces is $|F_{act}|_{max} = 30 \text{ kN}$, load flows $|Q_L|_{max} = 0.8 \times 10^{-5} \text{ m}^3/\text{s}$, spool valve displacements $|X_v|_{max} = 1.7 \times 10^{-4} \text{ m}$ and input currents $|u|_{max} = 6.5 \text{ mA}$. These values are very far from the physical constraints of the ESVH actuator.

From the simulation results shown in Figures 6.20 and 6.24, we can see that vehicle rollover will occur at the rear axle before the front axle. The reason is that the rollover of a vehicle is affected by the suspension stiffness to load ratio, which is greater at the rear axle than at the front one. Therefore, vehicle rollover at the rear axle is the most important situation when we study the LCF truck.

From the simulation results shown in Figures 6.14 and 6.24, we can see that there are some

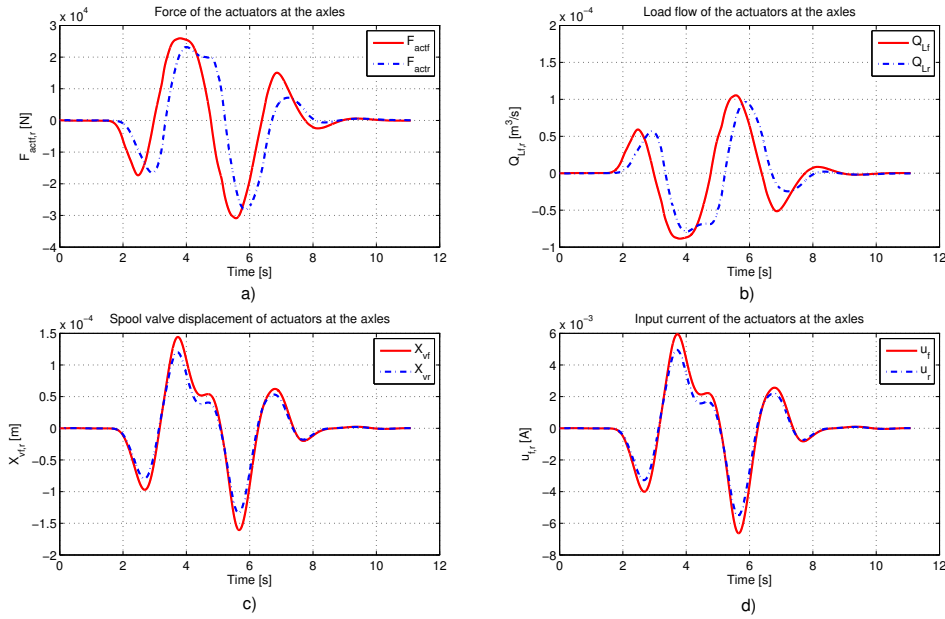


Figure 6.25: Fully loaded LCF truck: time response of the characteristic of the ESVH actuators.

oscillations appear on the tyre forces in the Z direction in the range up to 2s. This phenomenon occurs due to the vertical vibration when the vehicles move from static to dynamic states.

6.6 Conclusion

In this chapter, the validation of the H_∞ active anti-roll bar control by using the TruckSim[®] software is presented. The simulation results were obtained in collaboration with the Department of Control for Transportation and Vehicle Systems of the Budapest University of Technology and Economics, and the Computer and Automation Research Institute of the Hungarian Academy of Sciences, Hungary.

The co-simulation between Matlab[®]/Simulink and TruckSim[®] allows the synthesis of the H_∞ active anti-roll bar controller in the Matlab[®]/Simulink environment, and the use of the nonlinear high order vehicle model in TruckSim[®]. Specifically for this case, the outputs of TruckSim[®] (the lateral acceleration and roll rate of the sprung mass) are sent to the controller (as measurement signals) by using the H_∞ method. The outputs of the controller are the input currents of the ESVH actuators. The ESVH actuators generate the roll torques at the two axes and then they are inserted into the inputs of TruckSim[®].

According to the simulation results by using the nonlinear vehicle model in TruckSim[®], the rollover phenomenon of heavy vehicles is specified as follows:

- The bus: the vehicle rollover occurs at the front axle before at the rear axle (due to the

position of the engine);

- The truck: the vehicle rollover occurs at the rear axle before at the front axle (due to the suspension stiffness to load ratio).

The effect of the suspension stiffness to load ratio and the position of the engine mounted on the vehicle with respect to vehicle rollover performance will be considered by using the H_∞/LPV active anti-roll bar control synthesis in Chapter 7.

The simulation results in the four cases of the single unit heavy vehicle (4×2) (tour bus and LCF truck in unloaded and fully loaded states) with the different scenarios, showed that the H_∞ active anti-roll bar control drastically improved roll stability. Thanks to good simulation results obtained by using the nonlinear vehicle model in TruckSim[®], the validation of the H_∞ active anti-roll bar control in real-time will be of interest in the future.

Part III
Active anti-roll bar control: LPV
approach

This part includes two chapters and concentrates on the H_∞/LPV control synthesis for the active anti-roll bar system. In particular, this is the first time that the grid-based LPV approach and the LPVToolsTM toolbox are used for heavy vehicle dynamics. The main contents of this part are summarized as follows:

Chapter 7: Multivariable H_∞/LPV control for active anti-roll bar system

- We propose an LPV control-oriented integrated model of the vehicle with the forward velocity as a scheduling parameter.
- A MIMO H_∞/LPV controller is proposed, with three varying parameters: the forward velocity and the normalized load transfers at both axles. The controller design is performed by using parameter dependant weighting functions, which allows for vehicle performance adaptation to the risk of rollover.
- The simulation results in the frequency and time domains as well as the validation by using the TruckSim[®] software show that the H_∞/LPV active anti-roll bar controller drastically improves the vehicle roll stability, when compared to the passive anti-roll bar.

Chapter 8: Effect of oil leakage inside the servo-valve on the performance of an active anti-roll bar system

- The proposed fully integrated model (in Chapter 2) is used in this chapter. We consider that it is also an LPV model where the forward velocity is a varying parameter.
- The internal oil leakage inside the electronic servo-valve is analysed in detail. We evaluate the effect of this leakage on the performance of the open-loop and closed-loop systems. It is important to conclude that the existence of this leakage is necessary for the active anti-roll bar system of heavy vehicles. Thanks to this leakage, the active anti-roll bar system can act in a self-protection capacity when the controller fails.
- The survey results have shown that with the total flow pressure coefficient $K_P = [5 \times 10^{-15}, 4 \times 10^{-10}] \frac{m^5}{Ns}$, the two objectives of enhancing roll stability and the saturation of the actuators are simultaneously satisfied.
- The results of this chapter are the first step of fundamental study for further research into the fault tolerant control design on the active anti-roll bar system.

Multivariable H_∞/LPV control for active anti-roll bar system

Contents

7.1	Introduction	147
7.2	An LPV control-oriented model of a single unit heavy vehicle	148
7.3	Formulation of the H_∞/LPV control problem	150
7.3.1	Performance criteria	150
7.3.2	Performance specifications for the H_∞/LPV control design	150
7.3.3	The LPV generalized plant	151
7.4	Grid-based LPV approach for the active anti-roll bar system	152
7.5	Simulation results analysis	153
7.5.1	Analysis in the frequency domain	153
7.5.2	Analysis in the time domain	155
7.6	Validation of the H_∞/LPV active anti-roll bar control by using the TruckSim[®] simulation software	157
7.6.1	Validation with the tour bus (double lane change)	158
7.6.2	Validation with the LCF truck (sine wave steering)	160
7.7	Conclusion	162

7.1 Introduction

Linear Parameter Varying (LPV) systems arise naturally when modeling mechatronic systems such as pick-and-place robots, micro electro-mechanical systems and active vision systems, etc. Namely, most of these applications feature high-order coupled dynamics which are dominantly linear, but affected by time-varying parameters. To meet the tightening performance and higher accuracy demands from industry, identification and control design methodologies that account for these varying parameters, as well as uncertainty of the system dynamics, are becoming indispensable [Mohammadpour and Scherer 2012].

In order to design the LPV controller, three different kinds of approach are commonly used: Linear Fractional Transformations (LFT), Polytopic solution, Grid-based LPV [Sename, Gaspar, and Bokor 2013]. In the SLR team, we often use the Polytopic solution to synthesize the

LPV controller [Poussot-Vassal 2008], [Fergani 2014], [Nwesaty 2015], [Nguyen 2016]. This solution is a convex combination of the systems models defined at each vertex of a polytope given by the bounds of the scheduling parameters [Scherer, Gahinet, and Chilali 1997]. In this thesis, we use the grid-based LPV approach and the LPVToolsTM to design an LPV controller for the active anti-roll bar system of heavy vehicles. This is the first study on using this approach within the SLR team.

It is worth noting that a similar idea was used in [Gaspar, Bokor, and Szaszi 2004], [Gaspar, Bokor, and Szaszi 2005] for the yaw-roll model. The normalized load transfer at the rear axle was only considered in order to account for an actuator fault and to switch on braking actuations when critical situations occur. In those studies, the authors use the parameter dependent weighting function only for the lateral acceleration when the active brake system is activated. However, the weighting functions for the normalized load transfers at the two axles are chosen as a constant.

Based on the control-oriented integrated model presented in Chapter 2, this chapter proposes a MIMO H_∞/LPV controller, with three varying parameters (forward velocity and normalized load transfers at the two axles), designed using the grid-based LPV approach [Wu 1995]. Hence, the main contributions of this chapter can be summarized in the following points:

- Parameter dependant weighting functions are used to allow for performance adaptation to the rollover risk of heavy vehicles, characterized by the normalized load transfers at the two axles.
- The grid-based LPV approach is used to synthesize the H_∞/LPV controller depending on three varying parameters which are the forward velocity and the normalized load transfers at the two axles. It is the first time that the grid-based LPV approach is applied to heavy vehicle dynamics through the use of LPVToolsTM.
- The H_∞/LPV active anti-roll bar control is validated by using the TruckSim[®] simulation software with two different types of vehicle: a tour bus and a LCF (Low Cab Forward) truck, both fully loaded.
- The simulation results, in the frequency and time domains, show that the H_∞/LPV active anti-roll bar control is a realistic solution which drastically improves roll stability of a single unit heavy vehicle when compared to the passive anti-roll bar.

7.2 An LPV control-oriented model of a single unit heavy vehicle

In the control-oriented integrated model proposed in Chapter 2, by assuming that the right and left ESVH actuators are identical and symmetrically mounted at each axle, the characteristics of the two ESVH actuators do have the same magnitude and the opposite direction. Here the characteristics of the ESVH actuators on the right at the front axle, and on the right at the rear axle are considered. The diagram of the closed-loop system is shown in Figure 7.1.

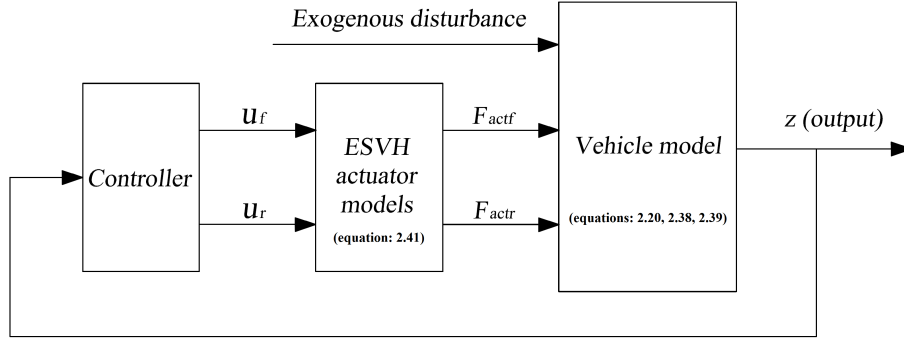


Figure 7.1: Diagram of the closed-loop system of the control-oriented integrated model.

We can see in (2.20)-(2.22) that the yaw-roll model depends on the forward velocity v and on the inverse of the forward velocity $\frac{1}{v}$. Moreover, when the vehicle is in motion, the forward velocity is one of the constantly changing parameters, and it depends on the driver and the motion condition of the vehicle. Here, the forward velocity v is chosen as a scheduling parameter.

Denoting $\rho_1 = v$, the control-oriented integrated model (2.42) is written in the state-space representation form as follows:

$$\dot{x} = A(\rho_1).x + B_1(\rho_1).w + B_2(\rho_1).u \quad (7.1)$$

where ρ_1 is a varying parameter. The matrices $A(\rho_1)$, $B_1(\rho_1)$, and $B_2(\rho_1)$ are expressed in the following form:

$$\begin{cases} A(\rho_1) = A_0 + A_1\rho_1 + A_2\frac{1}{\rho_1} \\ B_1(\rho_1) = B_{10} + B_{11}\rho_1 \\ B_2(\rho_1) = B_{20} + B_{21}\rho_1 \end{cases} \quad (7.2)$$

The state vector is:

$$x = \left[\beta \quad \dot{\psi} \quad \phi \quad \dot{\phi} \quad \phi_{uf} \quad \phi_{ur} \quad \Delta_{Pf} \quad X_{vf} \quad \Delta_{Pr} \quad X_{vr} \right]^T$$

The exogenous disturbance (steering angle) is:

$$w = \left[\delta_f \right]^T$$

and the control inputs (input currents):

$$u = \left[u_f \quad u_r \right]^T$$

The model (7.1) is transformed into a Linear Parameter Varying (LPV) model, whose state-space entries depend continuously on the time varying parameter vector $\rho_1(t)$. One characteristic of the LPV system is that it must be linear in the pair formed by the state vector (x), and the control input vector (u). The matrices $A(\rho_1)$, $B_1(\rho_1)$ and $B_2(\rho_1)$ are generally nonlinear functions of the scheduling vector ρ_1 .

Remark 7.1: *It is worth noting that $A(\rho_1)$ is not affine in ρ_1 since it includes ρ_1 and $\frac{1}{\rho_1}$. Therefore the classical polytopic approach cannot be used unless we consider two different parameters, which increases the conservatism.*

7.3 Formulation of the H_∞/LPV control problem

7.3.1 Performance criteria

As mentioned in Chapter 6, the tyre force (F_z) in the Z direction at the each wheel is considered to evaluate the vehicle rollover phenomenon. Rollover occurs when $F_z = 0$, and the wheel then starts to lift off the road. However the value of the tyre force (F_z) in the Z direction at each wheel is not easy to measure or estimate. In this chapter, this performance criterion is used when the H_∞/LPV active anti-roll bar control system is validated by using the TruckSim[®] simulation software.

For the yaw-roll model of a single unit heavy vehicle in Figure 2.6, the normalized load transfer $R_{f,r}$ (2.43) at the two axles is also used to evaluate the vehicle rollover, defined in [Gaspar, Bokor, and Szaszi 2004], [Yu, Guvenc, and Ozguner 2008], [Hsun-Hsuan, Rama, and Dennis 2012]. When the value of $R_{f,r}$ takes on the limit of ± 1 , the wheel in the inner bend lifts off the road, and rollover occurs.

According to the simulation results given in section 2.5.2.1, in the case of avoiding an obstacle in an emergency, the wheels at the rear axle lift off first for the truck, because the rollover of a vehicle is affected by the suspension stiffness to load ratio, which is greater at the rear axle than at the front one [Sampson 2000], [Gaspar, Bokor, and Szaszi 2004]. However the other effect to be considered in vehicle rollover is the distribution of the total load for the two axles. In the case of big buses, the engine is often mounted at the rear, so the wheels at the front axle usually lift off first. This is clearly shown by the simulation results with the passive anti-roll bar system installed on a bus in Chapter 6. Therefore it is generally necessary to consider the rollover risk at both axles of heavy vehicles.

Since such performance indices are key parameters to evaluate the risk of rollover, they are considered here as scheduling parameters of the LPV control, in order to provide a stable and smooth control action when reaching critical situations. To this aim, the parameter dependant weighting functions are used for the normalized load transfers at the two axles. We then define $\rho_2 = |R_f|$ and $\rho_3 = |R_r|$.

7.3.2 Performance specifications for the H_∞/LPV control design

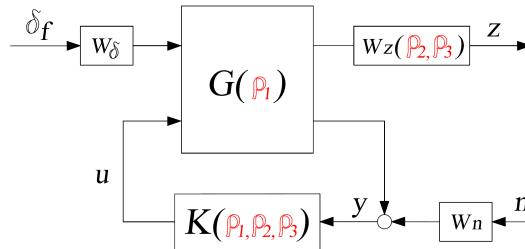


Figure 7.2: The closed-loop interconnection structure of the LPV active anti-roll bar control.

In this section the LPV control problem is presented for the active anti-roll bar system of heavy vehicles, using ESVH actuators. In Figure 7.2, the given H_∞/LPV control structure

includes the nominal model $G(\rho_1)$, the controller $K(\rho_1, \rho_2, \rho_3)$, the performance output z , the control input u , the measured output y , the measurement noise n . The steering angle δ_f is the disturbance signal, set by the driver. The weighting functions $W_\delta, W_z(\rho_{2,3}), W_n$ are presented thereafter, according to the considered performance objectives.

The weighting functions matrix W_z representing the performance output, is chosen as $W_z = \text{diag}[W_{zu}, W_{zR}]$. The purpose of the weighting functions is to keep the control inputs and normalized load transfers as small as possible over the desired frequency range up to 4rad/s , which represents the limited bandwidth of the driver [Gaspar, Bokor, and Szaszi 2004], [Sampson and Cebon 2003a]. As mentioned in Chapter 5, these weighting functions can be considered as penalty functions, that is, weights should be large in the frequency range where small signals are desired and small where larger performance outputs can be tolerated. The weighting function $W_{zu} = \text{diag}[W_{zuf}, W_{zur}]$ corresponds to the input currents at the front and rear axles. The reason for keeping the control signals small is to avoid the saturation of the actuator, and W_{zu} is selected as:

$$W_{zuf} = \frac{1}{0.4}; \quad W_{zur} = \frac{1}{0.4} \quad (7.3)$$

The weighting function $W_{zR} = \text{diag}[W_{zRf}, W_{zRr}]$ corresponds to the normalized load transfers at the front and rear axles, and is selected as:

$$W_{zRf} = \rho_2 \frac{\frac{s}{20} + 1}{\frac{s}{100} + 15}; \quad W_{zRr} = \rho_3 \frac{\frac{s}{20} + 1}{\frac{s}{100} + 15} \quad (7.4)$$

It is worth noting that the interest of parameter dependant weighting functions is to allow for the performance adaptation to the rollover risk of heavy vehicles. Indeed, the ESVH actuators will be tuned according to the varying parameters in order to meet the desired performance. For example, as far as the normalized load transfer at the front is concerned, when the varying parameter $\rho_2 \rightarrow 1$, the gain of the weighting function W_{zRf} is large, and therefore the normalized load transfer at the front will be penalized. In the same way, when ρ_3 is large, the normalized load transfer at the rear will be reduced.

The input scaling weight W_δ normalizes the steering angle to the maximum expected command. It is selected as $W_\delta = \pi/180$, which corresponds to a 1° steering angle command.

The weighting function W_n is selected as a diagonal matrix which accounts for sensor noise models in the control design. The noise weights are chosen as $0.01(m/s^2)$ for the lateral acceleration and $0.01(^\circ/sec)$ for the derivative of the roll angle $\dot{\phi}$ [Gaspar, Bokor, and Szaszi 2004].

7.3.3 The LPV generalized plant

According to Figure 7.2, the concatenation of the nonlinear model (7.1) with the performance weighting functions has a partitioned representation in the following way:

$$\begin{bmatrix} \dot{x}(t) \\ z(t) \\ y(t) \end{bmatrix} = \begin{bmatrix} A(\rho) & B_1(\rho) & B_2(\rho) \\ C_1(\rho) & D_{11}(\rho) & D_{12}(\rho) \\ C_2(\rho) & D_{21}(\rho) & D_{22}(\rho) \end{bmatrix} \begin{bmatrix} x(t) \\ w(t) \\ u(t) \end{bmatrix} \quad (7.5)$$

with the exogenous input $w(t) = [\delta_f \ n]^T$, the control input $u(t) = [u_f \ u_r]^T$, the measured output vector $y(t) = [a_y \ \dot{\phi}]^T$, and the performance output vector $z(t) = [u_f \ u_r \ R_f \ R_r]^T$.

It is worth noting that, in the LPV model of the active anti-roll bar system (7.5), the varying parameters $\rho = [\rho_1, \rho_2, \rho_3]$ are known in real time. Indeed the parameter $\rho_1 = v$ is measured directly, while the parameters $R_{f,r}$ (ρ_2 and ρ_3) can be calculated by using the measured roll angle of the unsprung masses $\phi_{u,f,r}$ [Gaspar, Bokor, and Szaszi 2004].

The control goal is to find an LPV controller $K(\rho)$ expressed in equation (3.33), which minimizes the induced \mathcal{L}_2 norm of the closed-loop LPV system $\sum_{CL}(\rho) = LFT(\sum(\rho), K(\rho))$ as in equation (3.36), with zero initial conditions.

7.4 Grid-based LPV approach for the active anti-roll bar system

Let us consider the LPV generalized plant (7.5). First, recall that several methods have arisen for representing the parameter dependence in LPV models, and then for designing the LPV controllers, such as: Linear Fractional Transformations (LFT), Polytopic solution, Linearizations on a gridded domain (grid-based LPV) [Hoffmann and Werner 2014]. As said in Chapter 3, the grid-based LPV models do not require any special dependence on the parameter vector and it is now available in the LPVToolsTM toolbox [Hjartarson, Seiler, and Packard 2015]. The solution for the LPV control design is presented in section 3.7.2.

In this study, the grid-based LPV approach and LPVToolsTM are used to synthesize the H_∞ /LPV active anti-roll bar control for heavy vehicles. It requires a gridded parameter space for the three varying parameters $\rho = [\rho_1, \rho_2, \rho_3]$. In the interconnection structure, the spacing of the grid points is selected on the basis of how well the H_∞ point designs perform for plants around the design point. The H_∞ controllers are synthesized for 10 grid points of the forward velocity in the range $\rho_1 = v = [40km/h, 130km/h]$ and 5 grid points of the normalized load transfers at the two axles in a range $\rho_2 = |R_f| = [0, 1]$, $\rho_3 = |R_r| = [0, 1]$, respectively.

In this work, we have chosen to design a controller that does not depend on the parameter derivatives (so the scalar basis functions (3.43) are constant). The following commands are used to make the grid points as well as the LPV controller synthesis by using LPVToolsTM:

```
rho1 = pgrid('rho1', linspace(40/3.6, 130/3.6, 10));
rho2 = pgrid('rho2', linspace(0, 1, 5));
rho3 = pgrid('rho3', linspace(0, 1, 5));
and [Klpv, normlpv] = lpvsyn(H, nmeas, ncont).
```

The weighting functions for both the performance and robustness specifications are considered unique for the whole grid. The optimal γ of the controller is obtained at $\gamma_{opt} = 0.2629$. The transfer function magnitude of the H_∞ /LPV active anti-roll bar controller is shown in Figure 7.3. The two inputs of the controller include the lateral acceleration a_y and the roll rate $\dot{\phi}$;

the two outputs of the controller are the input currents at the front axle u_f and at the rear u_r .

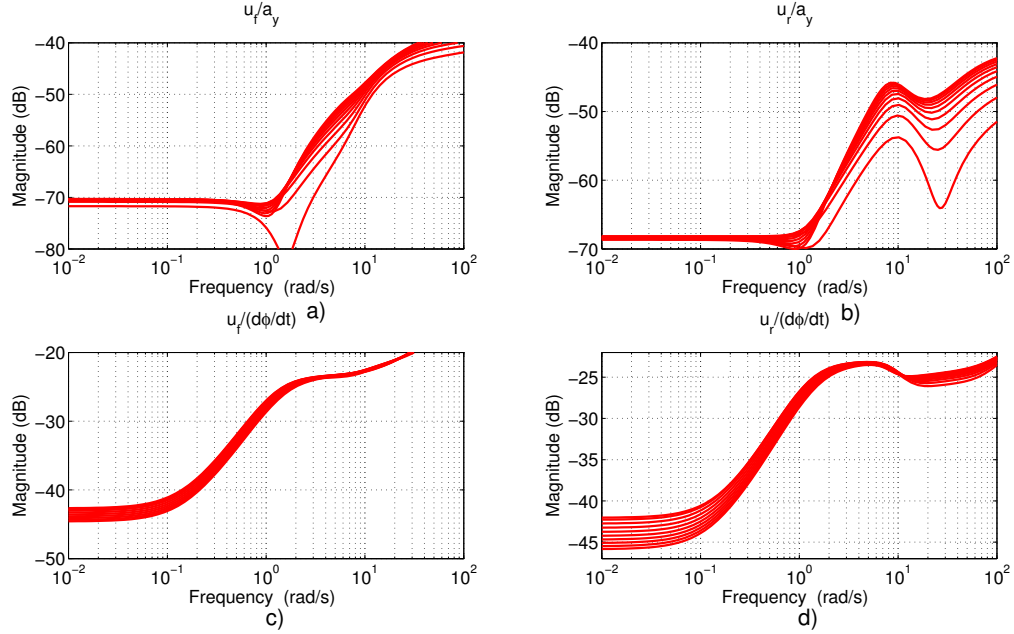


Figure 7.3: Transfer function magnitude of controller: from lateral acceleration to (a) input current at front axle $\frac{u_f}{a_y}$, (b) input current at rear axle $\frac{u_r}{a_y}$; from roll rate to (c) input current at front axle $\frac{u_f}{\dot{\phi}}$, (d) input current at rear axle $\frac{u_r}{\dot{\phi}}$.

The effect of the proposed H_∞/LPV active anti-roll bar controller to improve roll stability of heavy vehicles will be shown in the next sections.

7.5 Simulation results analysis

In this section, the simulation results for the single unit heavy vehicle using the four ESVH actuators with the H_∞/LPV controller are shown both in the frequency and time domains. The parameter values of the ESVH actuators and of the yaw-roll model are those given in Tables 2.1, 2.2.

7.5.1 Analysis in the frequency domain

Various closed-loop transfer functions of the LPV active anti-roll bar system on heavy vehicles are shown in this section. The main objective of the active anti-roll bar system is to reduce the normalized load transfer at each axle ($R_{f,r}$). To evaluate the effectiveness of the proposed H_∞/LPV active anti-roll bar controller, the two following cases will be considered:

- 1st case: the varying parameters are $\rho_1 = v = [40km/h, 130km/h]$, $\rho_{2,3} = 0.5$;
- 2nd case: the varying parameters are $\rho_{2,3} = [0, 1]$, $\rho_1 = v = 70 km/h$.

7.5.1.1 The 1st case: $\rho_1 = v = [40km/h, 130km/h]$ (10 grid points)

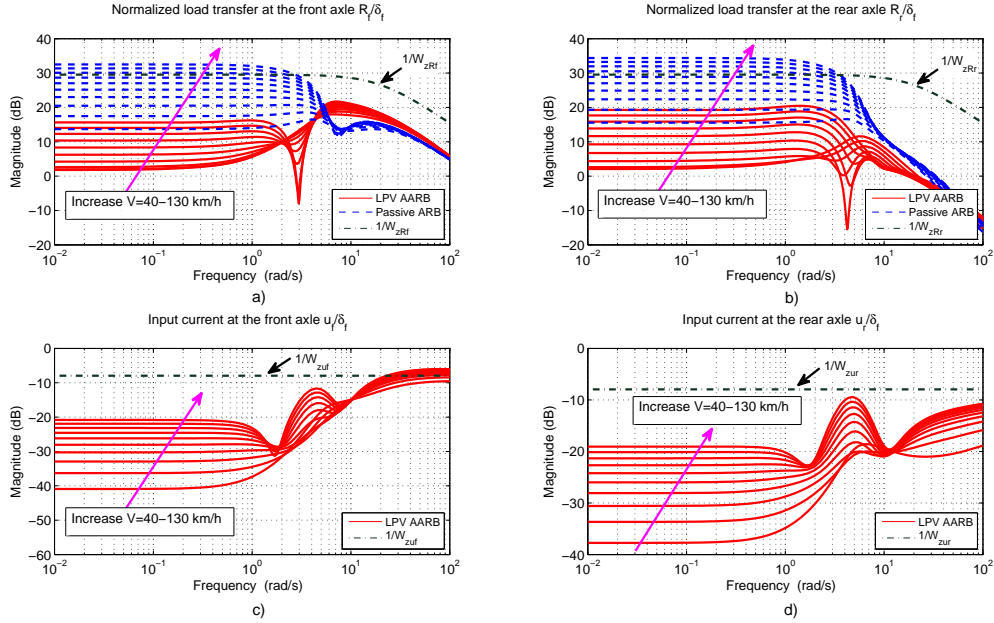


Figure 7.4: Transfer function magnitude of (a, b) the normalized load transfers $\frac{R_{f,r}}{\delta_f}$, (c, d) the input currents $\frac{u_{f,r}}{\delta_f}$ at the two axles.

We only consider the varying parameter $\rho_1 = v = [40km/h, 130km/h]$ with 10 grid points, while the varying parameters $\rho_{2,3}$ are kept constant at 0.5. Figure 7.4 shows respectively the transfer function of the normalized load transfers ($\frac{R_{f,r}}{\delta_f}$) and the input currents $\frac{u_{f,r}}{\delta_f}$ at the two axles, as well as the inverse of the weighting functions ($\frac{1}{W_{zRf}}, \frac{1}{W_{zRr}}, \frac{1}{W_{zuf}}, \frac{1}{W_{zur}}$). The reduction of the magnitude of transfer functions compared to the passive anti-roll bar at 40 km/h and 130 km/h is summarized in Table 7.1.

Table 7.1: Reduction of the magnitude of transfer functions compared with the passive anti-roll bar at 40 km/h and 130 km/h.

Transfer functions	$v = 40km/h$	$v = 130km/h$
$\frac{R_f}{\delta_f}$	11 dB [0, 4 rad/s]	18 dB [0, 5 rad/s]
$\frac{R_r}{\delta_f}$	14 dB [0, 10 rad/s]	16 dB [0, 10 rad/s]

As shown in Figures 7.4a,b and Table 7.1, the LPV active anti-roll bar system allows the reduction of the normalized load transfers (at the two axles) compared to the passive anti-roll bar in the frequency range to over 4 rad/s , which represents the limited bandwidth of the driver [Sampson and Cebon 2003a]. Figures 7.4c,d show the transfer function gains of the input currents at the front ($\frac{u_f}{\delta_f}$) and rear axles ($\frac{u_r}{\delta_f}$), respectively. When the forward velocity increases, the controller input currents ($u_{f,r}$) also increase. This indicates that the active anti-roll bar system requires more input current (i.e. energy) at higher forward velocities. Nonetheless, it remains in the allowed bound, which prevents from the actuator saturation.

7.5.1.2 The 2nd case: $\rho_{2,3} = [0, 1]$ (5 grid points)

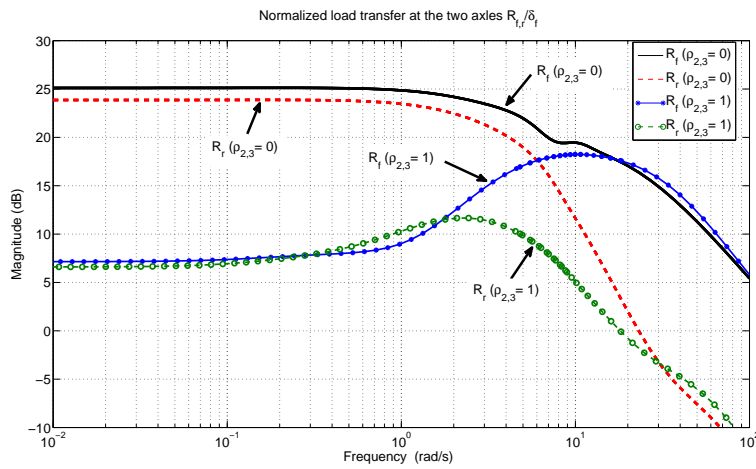


Figure 7.5: Transfer function magnitude of the normalized load transfers at the two axles $\frac{R_{f,r}}{\delta_f}$.

We consider the varying parameter $\rho_1 = v = 70 \text{ km/h}$, while the varying parameters $\rho_{2,3} = [0, 1]$ with 5 grid points for each parameter. Figure 7.5 shows the transfer function magnitude of the normalized load transfers at the two axles $\frac{R_{f,r}}{\delta_f}$ when the varying parameters $\rho_{2,3}$ are at the lower and upper bounds ($\rho_2 = 0, \rho_2 = 1$ and $\rho_3 = 0, \rho_3 = 1$).

As shown in Figure 7.5, when the values of $\rho_{2,3}$ increase, the normalized load transfers at the two axles decrease in the frequency range to over 4 rad/s . The reduction is about 19dB between $\rho_{2,3} = 0$ and $\rho_{2,3} = 1$.

The results above, indicate that the proposed H_∞/LPV controller (with the parameter dependent weighting functions, including the normalized load transfers at the two axles) provides for performance adaptation to the rollover risk of heavy vehicles.

7.5.2 Analysis in the time domain

In this section, some simulation results in the time domain are shown for two different situations: the passive anti-roll bar and the H_∞/LPV active anti-roll bar of the control-oriented

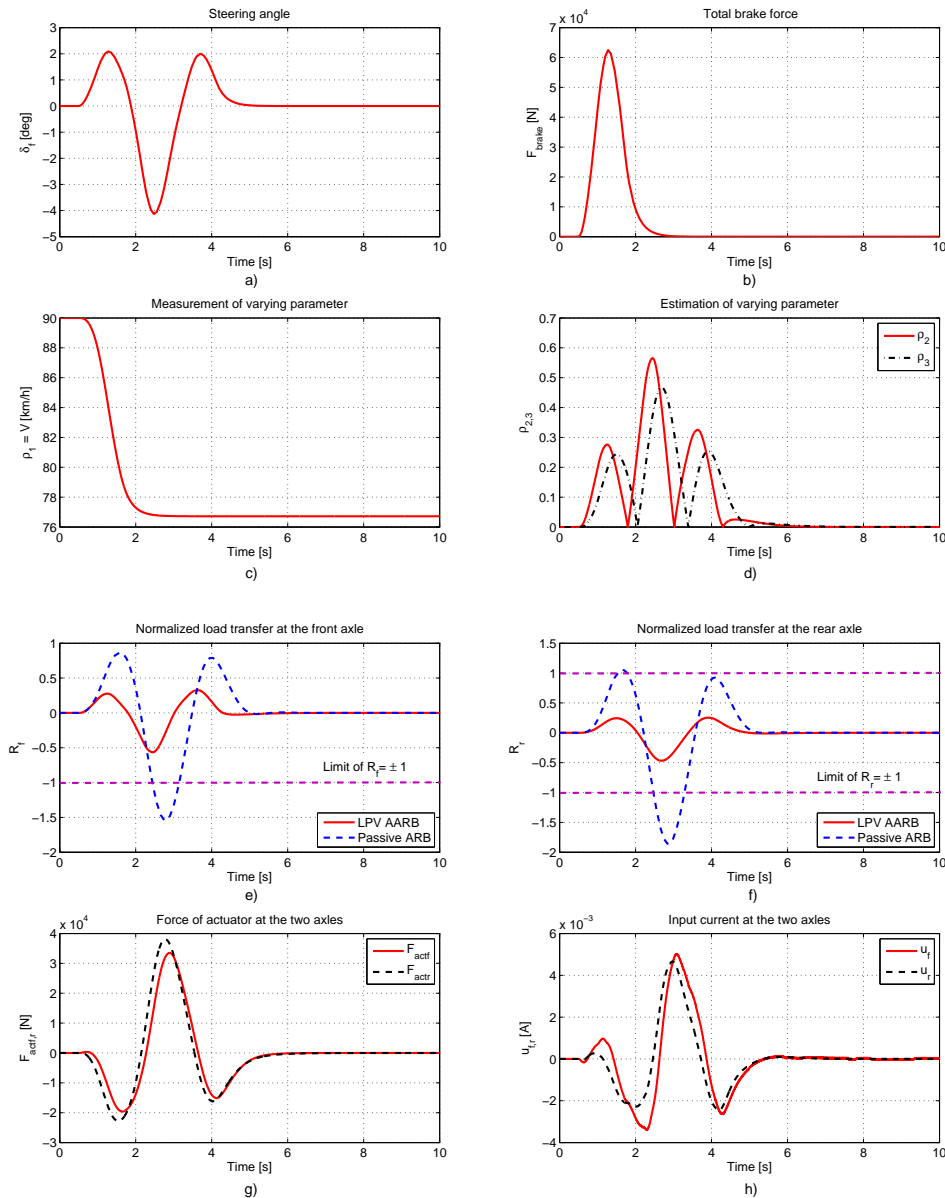


Figure 7.6: Time responses of a heavy vehicle in a double lane change manoeuvre to avoid an obstacle.

integrated model. The vehicle manoeuvre is a double lane change, which is a typical case to evaluate an obstacle avoidance in an emergency. The manoeuvre has a 2.5 m path deviation over 100 m. The steering angle δ_f is shown in Figure 7.6a.

To validate the proposed H_∞/LPV controller strategy for the active anti-roll bar system with three varying parameters $\rho_1 = v$, $\rho_2 = |R_f|$, $\rho_3 = |R_r|$, the following scenario is used:

- The initial forward velocity is 90 km/h, the vehicle runs on a dry road ($\mu = 1$). The

total rolling resistance and aerodynamic resistance forces are ignored.

- When the obstacle is detected, the driver reduces the throttle and brakes to reduce the forward velocity of the vehicle. The total brake force increases from 0.5s to 1.5s and then the driver releases the brake pedal, as shown in Figure 7.6b.

The differential equation for the forward velocity in the case of the braking situation is determined as in equation (7.6) [J.Y.Wong 2001], [Gaspar, Szabo, and Bokor 2005b].

$$m\dot{v} = - \sum_{i=1}^4 F_{bi} \quad (7.6)$$

where F_{bi} is the brake force at each wheel. Due to the brake force, the forward velocity reduces from 90 km/h to 76.5 km/h, as in Figure 7.6c.

Figures 7.6c, d show the variation of the varying parameters $\rho = [\rho_1, \rho_2, \rho_3]$. Figures 7.6e, f show the normalized load transfers at the two axles. We can see that in the case of the passive anti-roll bar system, the rollover does indeed occur at the two axles, but in the case of the H_∞/LPV active anti-roll bar control, the maximum absolute value of the normalized load transfers at the two axles are respectively 0.55 and 0.46. This indicates that the H_∞/LPV active anti-roll bar control does improve the roll stability of heavy vehicles when compared to the passive anti-roll bar. The force of the actuators as well as the input current at both axles are shown in Figure 7.6g, h.

The simulation results both in the frequency and time domains have shown the effectiveness of the H_∞/LPV active anti-roll bar controller synthesis, which considered the three varying parameters (the forward velocity and normalized load transfers at the two axles), when compared to the results of the passive anti-roll bar.

7.6 Validation of the H_∞/LPV active anti-roll bar control by using the TruckSim[®] simulation software

In the following validations, the author tested the proposed H_∞/LPV controller for the active anti-roll bar system with two different types of vehicle: the tour bus and the LCF (Low Cab Forward) truck using the solid suspension system, both vehicles fully loaded. The engine is mounted at the rear of the vehicle for the tour bus and at the front for the LCF truck. To evaluate the vehicle rollover, we consider the tyre force (F_z) in the Z direction at the each wheel (rollover occurs when $F_z = 0$). The author notes that the steering angle in the following section is the angle of the steering wheel, which is directly controlled by the driver. As mentioned in In Chapter 6, in the co-simulation between Matlab[®]/Simulink[®] and TruckSim[®], the steering angle is automatically changed to adapt with the vehicle trajectory. Here, the vehicle trajectories in the case of the passive anti-roll bar and of the active anti-roll bar will follow the target path, which fits the driver's wishes.

In Chapter 6, the TruckSim[®] simulation software was used to validate the H_∞ active anti-roll bar control. The two validations of this section are highlighted by the bold lettering (red color), and compared to those of Chapter 6 as shown in Table 7.2.

Table 7.2: Validation cases of the H_∞/LPV active anti-roll bar control by using co-simulation.

Scenario	Unloaded bus	Loaded bus	Unloaded truck	Loaded truck
Circular road test	Chapter 6	X	X	X
Cornering manoeuver	X	Chapter 6	X	X
Sine wave steering	X	X	Chapter 6	X 80 km/h
Double lane change	X	X 100 km/h	X	Chapter 6

7.6.1 Validation with the tour bus (double lane change)

Typically the buses are two axled vehicles (bus 2A) with a capacity of 45 passengers, as shown in Figure 6.5. In this validation, the total vehicle mass of the fully loaded tour bus is 10620 kg, the double lane change is used to evaluate the roll stability of the tour bus when it runs at 100 km/h, as shown in Figure 7.8a. This represents the situation when the driver wishes to overtake another vehicle. Figures 7.7, 7.8 show the time responses of the tour bus in the double lane change manoeuver with the solid line for the H_∞/LPV active anti-roll bar and the dashed line for the passive anti-roll bar.

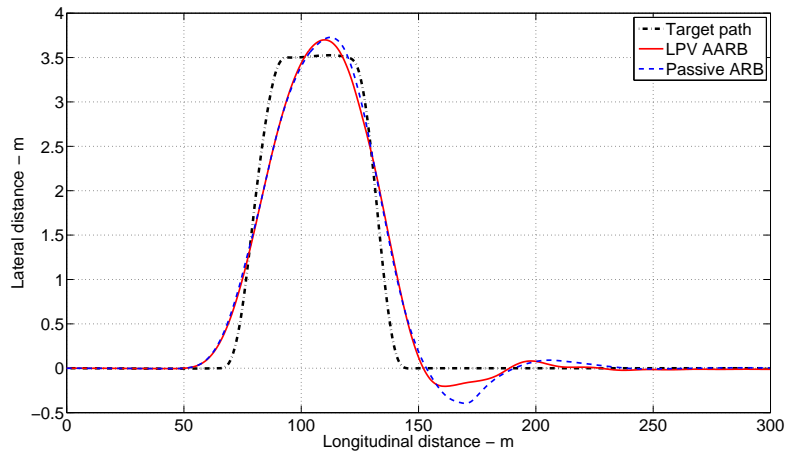


Figure 7.7: Trajectory of the tour bus in the double lane change manoeuver.

Figure 7.7 shows the trajectory of the tour bus in a double lane change manoeuver. We would like that, in ideal conditions, the center of the vehicle mass follows the target path. But in fact, the trajectory of the center of the vehicle mass of the real vehicle can not satisfy that (due to the impact of the suspension system, the wheelbase and the wheels lifting off from the road, etc). The trajectory of the vehicle in both cases of the H_∞/LPV active anti-roll bar and the passive anti-roll bar can only stick with the ideal target path.

Figure 7.8a shows the steering wheel angle controlled by the driver with the amplitude about 100 deg. To ensure the trajectory of the vehicle as in Figure 7.7, the driver generates the

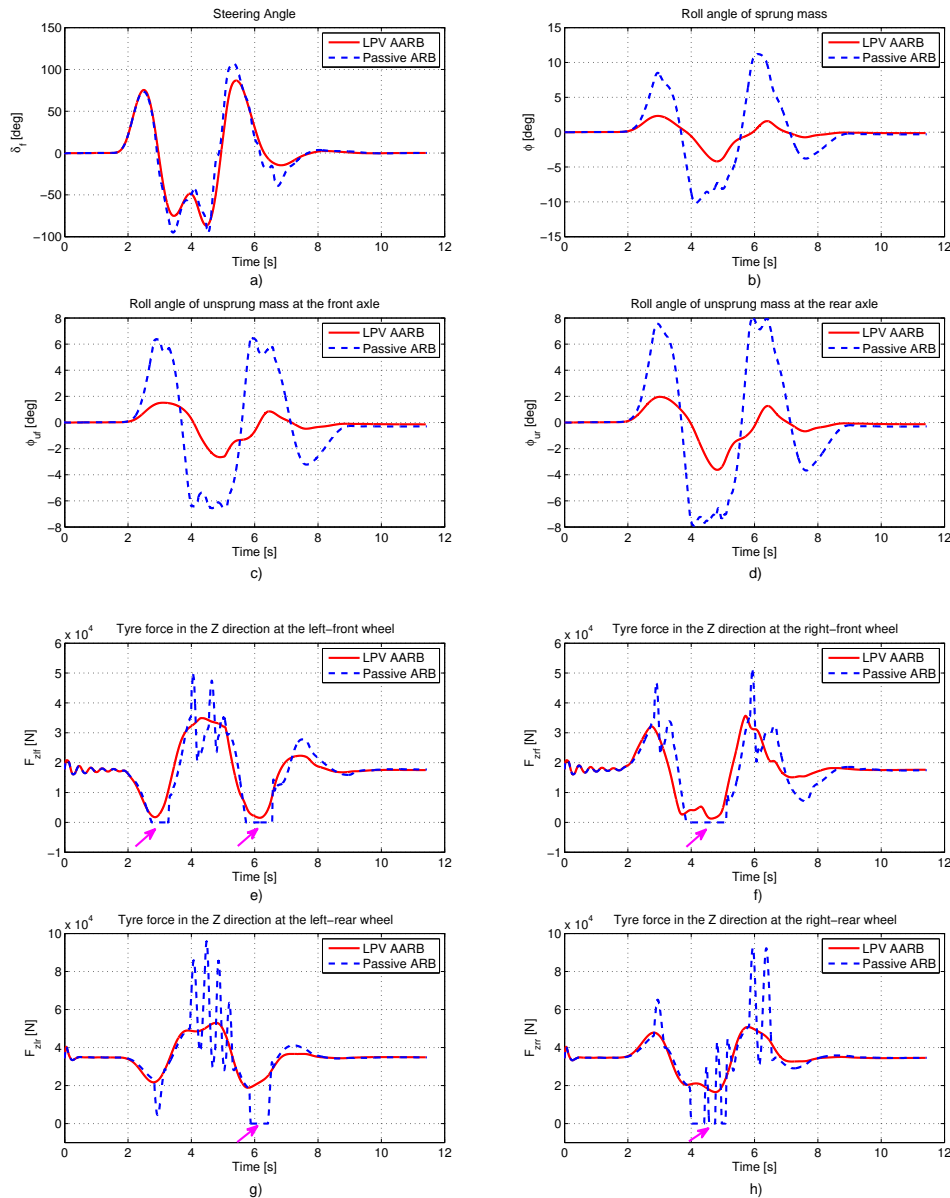


Figure 7.8: Time responses of the tour bus in the double lane change manoeuvre.

steering wheel angle difference between the H_∞/LPV active anti-roll bar and the passive anti-roll bar. We can easily see that the steering wheel angle of the H_∞/LPV active anti-roll bar is smoother than that of the passive anti-roll bar. Thus, with the H_∞/LPV active anti-roll bar, the driver is less tired and more capable to react than in the case of the passive anti-roll bar.

Figures 7.8b, c, d show the time response of the roll angle of the sprung mass and of the unsprung masses at both axles, respectively. We can see that with the H_∞/LPV active anti-roll bar controller, the roll angle of the sprung and unsprung masses are significantly reduced

when compared to the passive anti-roll bar (the reduction of the roll angle is about 6 *deg* for the sprung mass, 3 *deg* for the unsprung mass at the front and 4 *deg* for the unsprung mass at the rear axle).

Figures 7.8*e, f, g, h* show the time response of the tyre forces in the Z direction of all the wheels. In the case of the H_∞/LPV active anti-roll bar controller, all the tyre forces remain positive, which means that there is no wheel lift off the road. But in the case of the passive anti-roll bar, the left-front wheel lifts off at $2.6s \div 3.4s$ and $5.7s \div 6.5s$, the right-front wheel at $3.8s \div 5.3s$, the left-rear wheel at $5.8s \div 6.5s$, the right-rear wheel at $4s \div 5.5s$. These results show that the H_∞/LPV active anti-roll bar controller drastically improves the roll stability of the fully loaded tour bus.

7.6.2 Validation with the LCF truck (sine wave steering)

In this validation, the total vehicle mass of the fully loaded LCF truck is 12549 *kg* in Figure 6.16, a sine wave steering manoeuvre is used to evaluate roll stability of the LCF truck when it runs at 80 *km/h*, as shown in Figure 7.10*a*.

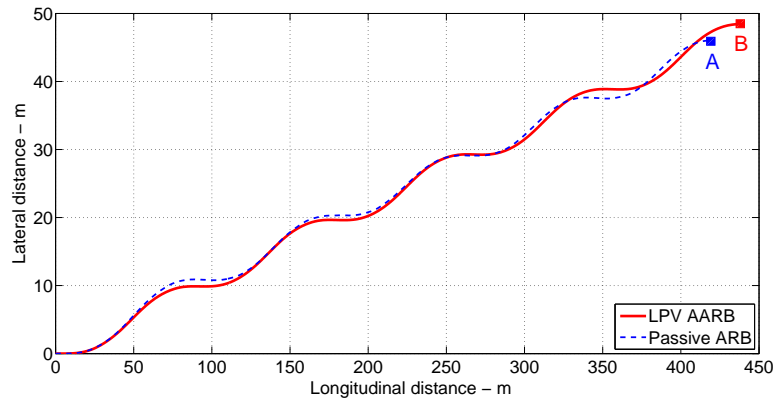


Figure 7.9: Trajectory of the truck in the sine wave manoeuvre.

Figures 7.9, 7.10 show the time response of the LCF truck. From figure 7.10*a*, the steering wheel angle δ_f is the sine wave with an amplitude of 90 *deg* and a period 4*s*. In this validation, the driver applies the same steering wheel angles for both the H_∞/LPV active anti-roll bar and the passive anti-roll bar. Figure 7.9 shows the trajectory of the LCF truck. We can see that even when the forward velocity is held constant at 80 *km/h* the LCF truck travels to point A in the case of the passive anti-roll bar, and to point B in the case of the H_∞/LPV active anti-roll bar. Since the wheels lift off the road with the passive anti-roll bar, some performance characteristics of the vehicle are lost.

Figures 7.10*b, c, d* show that in the case of the H_∞/LPV active anti-roll bar control, the roll angle of the sprung and unsprung masses are significantly reduced when compared to the passive anti-roll bar. The reduction of these signals is summarized in Table 7.3.

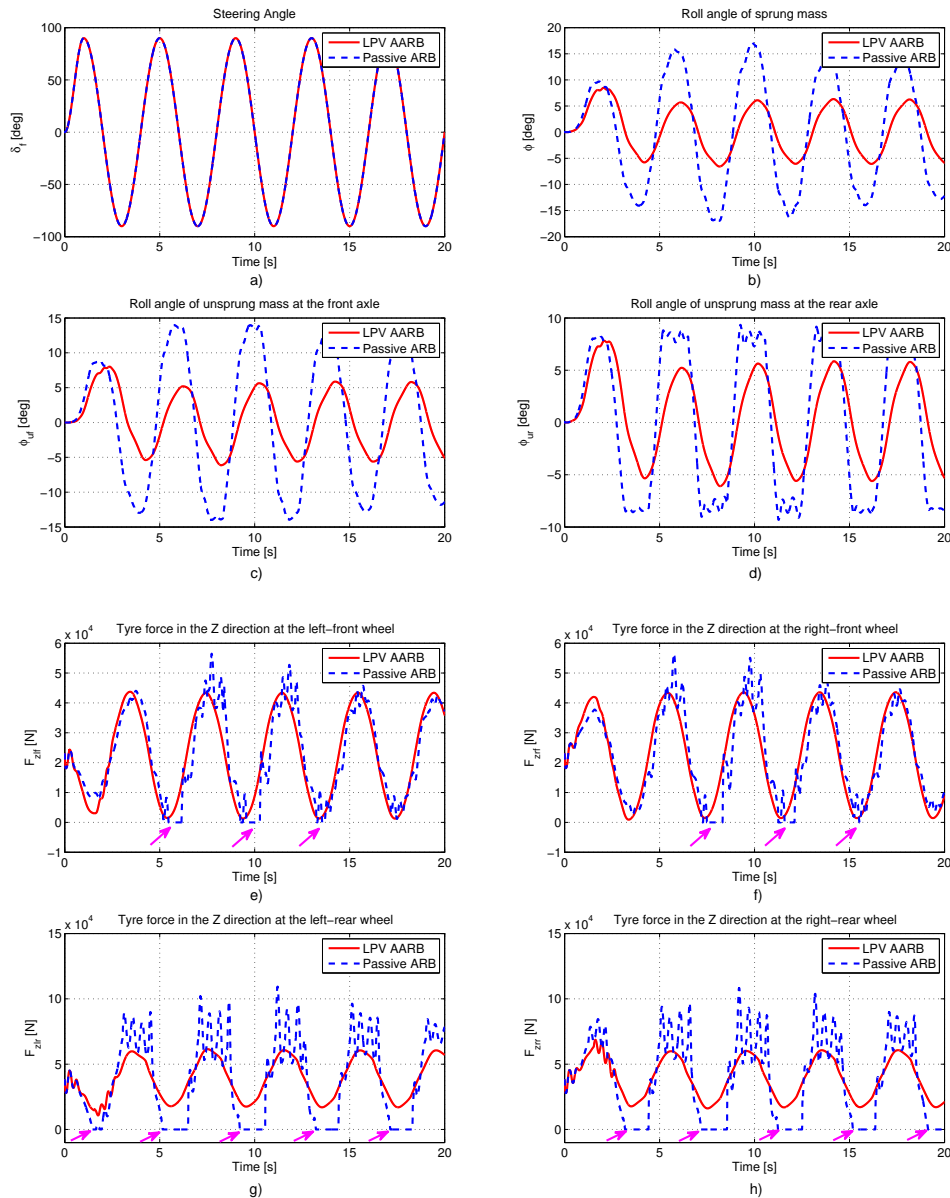


Figure 7.10: Time responses of the truck in the sine wave steering manoeuvre.

Figures 7.10e, f, g, h show the time response of the tyre forces in the Z direction of all the wheels. We can see that with the H_∞/LPV active anti-roll bar controller, all the tyre forces remain positive, which means that there is no wheel lift off the road. But in the case of the passive anti-roll bar, all the wheels at both two axles lift off. These results show that the LPV active anti-roll bar control improves roll stability in the case of the fully loaded LCF truck.

Table 7.3: Reduction of the signal magnitude compared with the passive case.

ϕ [deg]	ϕ_{uf} [deg]	ϕ_{ur} [deg]
10	8	3

7.7 Conclusion

In this chapter, the author considered the nonlinear model of a single unit heavy vehicle as an LPV model, with the forward velocity as a scheduling parameter. The H_∞/LPV active anti-roll bar controller is synthesized by using the grid-based LPV approach through LPVToolsTM. Three varying parameters are considered to schedule the H_∞/LPV controller: the forward velocity and the normalized load transfers at both axles. The H_∞/LPV design is performed using parameter dependant weighting functions which allow adaptation of the vehicle performance to the risk of rollover.

The simulation results in the frequency and time domains, as well as the validation by using the TruckSim[®] software, show that the H_∞/LPV active anti-roll bar controller drastically improves roll stability of the single unit heavy vehicle when compared to the passive anti-roll bar.

The simulation results for both the tour bus and LCF truck show a chaotic behavioural difference: for the tour bus, the wheels at the front axle lift off the road before the wheels at the rear axle (see Figure 7.8g, h). For the LCF truck, it is the opposite (see Figure 7.10g, h). So the rollover risk is not the same for all types of heavy vehicles. Therefore, the proposed H_∞/LPV controller, with the parameter dependent weighting functions including the normalized load transfers at both axles, allows adaptation of the vehicle performance against the risk of rollover for all types of heavy vehicles.

In the previous chapters, the ESVH actuators are considered with the nominal value of the total flow pressure coefficient $K_P = 4.2 \times 10^{-11} \frac{m^5}{Ns}$. However, the simulation results in Chapter 5 have pointed out that there are some effects of the internal oil leakage inside the electronic servo-valve on the characteristic of the closed-loop system. Therefore in the next chapter, this effect on the performance of the active anti roll bar system, when oil passes through the electronic servo-valve will be examined in details.

Effect of oil leakage inside the servo-valve on the performance of an active anti-roll bar system

Contents

8.1	Introduction	163
8.2	Internal leakage inside the electronic servo-valve	165
8.3	An LPV fully integrated model of a single unit heavy vehicle	167
8.4	Effect of the internal leakage inside the electronic servo-valve on the open-loop system	168
8.4.1	Neutral position of the spool valve	168
8.4.2	Effect of the internal leakage on the open-loop system	170
8.5	Effect of the internal leakage inside the electronic servo-valve on the closed-loop system	174
8.5.1	H_∞ /LPV control design for the fully integrated model	174
8.5.2	Simulation results analysis with the nominal value of the total flow pressure coefficient	176
8.5.3	Effect of the internal leakage on the performance of the H_∞ /LPV active anti-roll bar control system	181
8.6	Conclusion	185

8.1 Introduction

The Electronic Servo-Valve Hydraulic (ESVH) actuator is the most commonly used in the industrial sector and engineering practices. The ESVH actuator includes the main elements such as: (1) a servo regulator (controller), (2) a servo-valve, (3) an hydraulic cylinder, (4) a feedback position transducer and (5) a power supply, as shown in Figure 2.2. The dynamic response of the system mainly builds upon the frequency characteristics of the servo-valve and the load, but this overall quality of the servo control could be impaired by faults in the system. The fault usually includes the internal and external leakages [Milic, Situm, and Essert 2010], [Choux 2011]. The external leakage can be detected visually, so this leakage can be easily

perceived. Conversely, the internal leakage which occurs inside the hydraulic cylinder and the electronic servo-valve, cannot be detected easily, and therefore its detection is much more important. This internal leakage is caused by excessive wear of the piston seal or abrasion. This seal prevents leakage and closes the gap between the piston and the cylinder wall. The internal leakage inside the hydraulic cylinder can be detected when the actuator seal is almost completely destroyed [Choux 2011], [Kovari 2009]. Notice that, the internal leakage inside the servo-valve always exist for all the ESVH actuators, even if they are completely new [Rafa, Yahya, and Rawand 2009], [Kalyoncu and Haydim 2009].

In the literature, many studies have been dedicated to examine the internal leakage inside the electronic servo-valve of the ESVH actuator. In [Erylmaz and Wilson 2000], the authors combined the internal leakage and the orifice flows in an hydraulic servo-valve model. It indicated that with small spool valve displacements, the internal leakage flow between the spool valve and the body dominates the orifice flow through the valve. Kalyoncu *et al* [Kalyoncu and Haydim 2009] developed the mathematical model of the ESVH system considering the internal leakage within the electronic servo-valve. The simulation results showed that the leakage occurring during the small spool valve displacements does affect the mathematical model and position control of the system. By considering the internal leakage inside the electronic servo-valve, further improvements in the ESVH system performance is achieved. In [Has et al. 2014], [M. Wonohadidjojo, Kothapalli, and Y. Hassan 2013] and [Rahmat et al. 2011], the authors proposed the position controller for the ESVH system. The proposed scheme has the ability to improve the position tracking performance of the actuator in the presence of friction and internal leakage inside the electronic servo-valve.

In this chapter, by ignoring the external leakage and the internal leakage inside the hydraulic cylinder, the author is only interested in the effects of the internal leakage inside the electronic servo-valve on the performance of the active anti-roll bar system of heavy vehicles. Hence, the main contributions can be summarized in the following points:

- The internal leakage inside the electronic servo-valve is analysed in detail and characterized by the total flow pressure coefficient. Thanks to this leakage, it is important that the active anti-roll bar system can act in a self-protection capacity when the controller fails.
- An H_∞/LPV active anti-roll bar controller for the fully integrated model is synthesized by using the grid-based LPV approach [Wu 1995]. Here, the forward velocity is considered as the varying parameter to adapt to the different types of heavy vehicle movements.
- The simulation results indicate that the internal leakage inside the electronic servo-valve drastically affects the characteristics of the closed-loop system. The two main objectives (enhancing roll stability and avoiding the saturation of the actuators) are simultaneously satisfied when the total flow pressure coefficient K_P is chosen in the interval $[5 \times 10^{-15}, 4 \times 10^{-10}] \frac{m^5}{Ns}$.
- This analysis is the basis for further studies of the fault tolerant control and fault accommodation on the active anti-roll bar system of heavy vehicles using the ESVH actuators in order to improve the performance of the active anti-roll bar system.

8.2 Internal leakage inside the electronic servo-valve

In Chapter 2, the internal leakage inside the electronic servo-valve is linearized by the total flow pressure coefficient K_P to model the ESVH actuator. In this section, to further clarify this leakage, the structure and nonlinear characteristics of the servo-valve will be considered in detail.

At small spool valve displacements, the leakage load flow between the spool valve and body of the servo-valve dominates the orifice load flow through the valve. In precision positioning applications, where the servo-valve operates around the null region, this load flow, if ignored, may severely degrade the performance of a conventional servo hydraulic design [Erylmaz and Wilson 2000], [M. Wonohadidjojo, Kothapalli, and Y. Hassan 2013].

Here, we consider an accurate model of the leakage load flow [Erylmaz and Wilson 2000], by making a smooth transition between the leakage load flow and the orifice load flow, which would likely improve the precision of the ESVH system design and performance. The model used is a nonlinear servo-valve model that accurately captures the servo-valve leakage behavior over the whole range of the spool valve displacement. The leakage behavior is modelled as a turbulent load flow with a load flow area inversely proportional to the overlap between the spool valve areas and the servo-valve orifices.

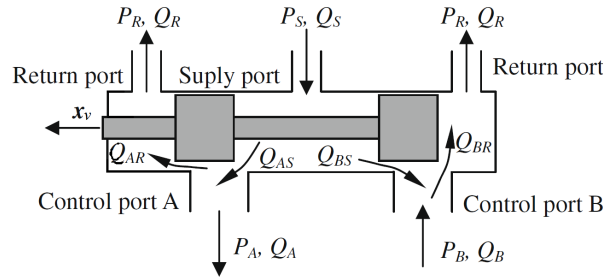


Figure 8.1: Servo-valve configuration [Erylmaz and Wilson 2000].

Figure 8.1 depicts a servo-valve configuration. This servo-valve consists of two control ports (A, B) with variable orifices which regulate the load flows. The load flow through the control ports of the servo-valve are expressed in equation (8.1), and the load flow at the supply and return ports are represented in equation (8.2).

$$Q_A = Q_{AS} - Q_{AR} \quad \text{and} \quad Q_B = Q_{BR} - Q_{BS} \quad (8.1)$$

$$Q_S = Q_{AS} + Q_{BS} \quad \text{and} \quad Q_R = Q_{AR} + Q_{BR} \quad (8.2)$$

By combining the load flow relations in equations (8.1) and (8.2), the supply port load flow in terms of the load flows at the control and return ports is defined as follows:

$$Q_S = Q_R + (Q_A - Q_B) \quad (8.3)$$

The nonlinear load flow relations for the control port **A** are given by the following equations

[Kalyoncu and Haydim 2009]:

$$Q_{AS} = K_{AS} \sqrt{P_S - P_A} \cdot \begin{cases} x_0 + x_v & , \quad x_v \geq 0 \\ x_0^2(x_0 - k_{AS}x_v)^{-1} & , \quad x_v < 0 \end{cases} \quad (8.4)$$

$$Q_{AR} = K_{AR} \sqrt{P_A - P_R} \cdot \begin{cases} x_0^2(x_0 + k_{AR}x_v)^{-1} & , \quad x_v \geq 0 \\ x_0 - x_v & , \quad x_v < 0 \end{cases} \quad (8.5)$$

The nonlinear load flow relations for the control port **B** are given as follows [Kalyoncu and Haydim 2009]:

$$Q_{BS} = K_{BS} \sqrt{P_S - P_B} \cdot \begin{cases} x_0^2(x_0 + k_{BS}x_v)^{-1} & , \quad x_v \geq 0 \\ x_0 - x_v & , \quad x_v < 0 \end{cases} \quad (8.6)$$

$$Q_{BR} = K_{BR} \sqrt{P_B - P_R} \cdot \begin{cases} x_0 + x_v & , \quad x_v \geq 0 \\ x_0^2(x_0 - k_{BR}x_v)^{-1} & , \quad x_v < 0 \end{cases} \quad (8.7)$$

where x_0 is equivalent to a spool valve displacement that would result in the same amount of the load flow in a non-leaking servo-valve as the load flow in a leaking servo-valve with a centred spool. Namely, the equivalent orifice opening x_0 is assumed to be the same for matched servo-valve ports. For a symmetric servo-valve with matched control ports, it can be considered as:

$$K_x = K_{AS} = K_{AR} = K_{BS} = K_{BR} \quad (8.8)$$

$$K_P = k_{AS} = k_{AR} = k_{BS} = k_{BR} \quad (8.9)$$

where K_P is the leakage coefficient (total flow pressure coefficient), K_x is the servo-valve flow gain. For any servo-valve, the servo-valve leakage parameters (K_x, x_0, K_P) can be determined from readily available manufacturer data for a symmetric servo-valve with matched ports.

When the **control ports (A, B) are blocked**, the total supply load flow Q_S representing the internal leakage load flow, can be expressed as follows [M. Wonohadidjojo, Kothapalli, and Y. Hassan 2013]:

$$Q_S = 2K_x(P_S - P_R)^2(x_0 + |x_v|)(1 + f(x_v))^2 \quad (8.10)$$

where

$$f(x_v) = \left[1 + \frac{|x_v|}{x_0}\right]^2 + \left[1 + K_P \frac{|x_v|}{x_0}\right]^2 \quad (8.11)$$

Figure 8.2 shows a typical leakage load flow curve. It has a maximum at the neutral spool valve position and decreases rapidly with the valve stroke.

Equations (8.10), (8.11) and Figure 8.2 indicate that the internal leakage always exists for any electronic servo-valve, whenever there is a pressure difference $\Delta P = P_S - P_R$. In the next section, the internal leakage inside the electronic servo-valve (when the spool valve is at the neutral position) will be considered in the absence of the input current entering the active anti-roll bar system. Additionally the effect on the closed-loop system will be investigated by using an H_∞/LPV controller.

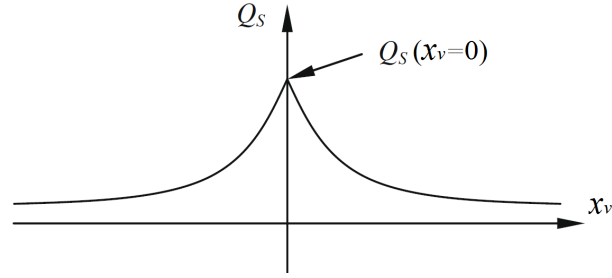


Figure 8.2: Typical servo-valve leakage flow rate curve [Kalyoncu and Haydim 2009].

8.3 An LPV fully integrated model of a single unit heavy vehicle

The fully integrated model proposed in Chapter 2, includes four ESVH actuators in combination with a yaw-roll model of a single unit heavy vehicle. The symbols and parameters of the fully integrated model are given in Tables 2.1 and 2.2. Figure 8.3 shows the diagram of the closed-loop system of the fully integrated model.

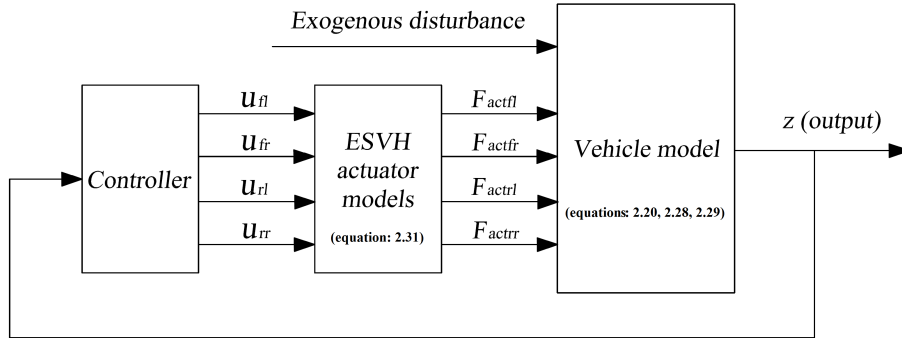


Figure 8.3: Diagram of the closed-loop system of the fully integrated model.

The vehicle motion equations are characterized by some nonlinear parameters, such as the tyre, damper and spring coefficients, etc. However, the forward velocity is one of the constantly changing parameters; normally it depends on the driver and on the motion condition of the vehicle. Here, by considering the forward velocity as a scheduling parameter ($\rho = v$), the fully integrated model given in equation (2.32) can be written in the LPV state-space representation form as follows:

$$\dot{x} = A(\rho).x + B_1(\rho).w + B_2(\rho).u \quad (8.12)$$

where the state vector is:

$$x = [\beta \quad \dot{\psi} \quad \phi \quad \dot{\phi} \quad \phi_{uf} \quad \phi_{ur} \quad \Delta_{Pfl} \quad X_{vfl} \quad \Delta_{Pfr} \quad X_{vfr} \quad \Delta_{Prl} \quad X_{vrl} \quad \Delta_{Prr} \quad X_{vrr}]^T$$

The exogenous disturbance (steering angle) is:

$$w = [\delta_f]^T$$

and the control inputs (input currents):

$$u = [u_{fl} \quad u_{fr} \quad u_{rl} \quad u_{rr}]^T$$

The model (8.12) is transformed into a Linear Parameter Varying (LPV) model, whose state space entries depend continuously on a time varying parameter vector ρ . Here, the matrices $A(\rho)$, $B_1(\rho)$ and $B_2(\rho)$ are generally nonlinear functions of the scheduling vector.

Remark 8.1: The matrices A , B_1 and B_2 are shown in Appendix A.

8.4 Effect of the internal leakage inside the electronic servo-valve on the open-loop system

The Electronic Servo-Valve Hydraulic (ESVH) actuator is used for the active anti-roll bar system in the proposed fully integrated model. This actuator is not the same as with the active damper which is often used for the active system in cars, such as an active or semi-active suspension system, because the piston of the hydraulic cylinder is solid. From Figure 2.5 and Table 2.1 we can see that the total leakage coefficient of the hydraulic cylinder is zero, which means that oil cannot pass through the contact surfaces between the cylinder and piston of the hydraulic cylinder.

The problem we want to tackle is: **What happens, if when the vehicle is running, the active anti-roll bar system suddenly stops working?** The reasons may be due to broken wiring from the controller to the servo-valve, or the controller is not working, etc. In this situation, the spool valve of the servo-valve is at the neutral position, but the suspension roll angles always exist due to the effect of the lateral inertia force. If there is no internal oil leakage inside the electronic servo valve, the oil cannot pass between the two chambers of the hydraulic cylinder, therefore the movement of the piston inside the hydraulic cylinder is impossible. This leads to the sprung mass and unsprung mass becoming one block and the role of the suspension will be removed, which would lead to a dangerous situation for the vehicle. In this section, we will give an answer to the above question by investigating the internal leakage inside the electronic servo-valve when the spool valve is at the neutral position.

8.4.1 Neutral position of the spool valve

In section 8.2, it was indicated that the internal leakage always exists for any electronic servo-valve. It has a maximum at the neutral spool valve position when the two control ports are blocked.

To evaluate the effect of the internal leakage inside the electronic servo-valve on an ESVH actuator, let us consider the servo-valve structural characteristics illustrated in section 2.2.1. Due to the orifices of the servo-valve being symmetrically matched, from equation (2.5), at the neutral position of the spool valve, the areas of the 1st and 2nd orifices are equal and defined as follows:

$$A_1(0) = A_2(0) = A_0 \tag{8.13}$$

In this case, the load flow through the ESVH actuator in equation (2.9) is as follows:

$$Q_L = C_d A_0 \sqrt{\frac{1}{\rho} (P_s - \Delta P)} - C_d A_0 \sqrt{\frac{1}{\rho} (P_s + \Delta P)} \quad (8.14)$$



Figure 8.4: The three-land-four-way spool valve [Merritt 1967].

Considering equation (8.14) and Figure 8.4, there are three cases of interest for the differential pressure between the two chambers of the hydraulic cylinder as follows:

- If $P_1 < P_2$, then $\Delta P < 0$ and $Q_L > 0$. This means that the direction of the load flow is in the same direction with the direction as illustrated in Figure 8.4.
- If $P_1 = P_2$, then $\Delta P = 0$ and $Q_L = 0$. This means that there is no the load flow though the actuator.
- If $P_1 > P_2$, then $\Delta P > 0$ and $Q_L < 0$. This means that the direction of the load flow will reverse with the direction as illustrated in Figure 8.4.

Thus, although the spool valve is at the neutral position, thanks to the internal leakage inside the electronic servo-valve, the oil can still pass from the higher pressure chamber to the lower pressure chamber of the hydraulic cylinder with a certain level. This allows the piston to move inside the hydraulic cylinder. Therefore when the active anti-roll bar system suddenly stops working, the sprung and unsprung masses will not be blocked. This can be called the self-protection capacity of the active anti-roll bar system when the controller does not work. To clarify this issue, in the next section the author considers the absence of the input currents from the controller to the ESVH actuators and it is compared with the two cases of the passive and "without anti-roll bar".

8.4.2 Effect of the internal leakage on the open-loop system

In this section, the effect of the internal leakage inside the servo-valve on the vehicle behavior in the frequency and time domains will be assessed by using the proposed fully integrated model. The parameter values of the ESVH actuators and the yaw-roll model are detailed in Tables 2.1 and 2.2. The forward velocity is constant at 70 km/h . Here, we compare the three following cases:

- **First case: "Open-loop system"** is defined when the ESVH actuators are installed in the vehicle but there is no input current entering these actuators (i.e the faulty case);
- **Second case: "Passive anti-roll bar"** is determined in Chapter 2. This is typical of the modern vehicles;
- **Third case: "Without anti-roll bar"**, this is the case where heavy vehicles do not have any anti-roll bar system.

8.4.2.1 Effect of the internal leakage inside the servo-valve in the frequency domain

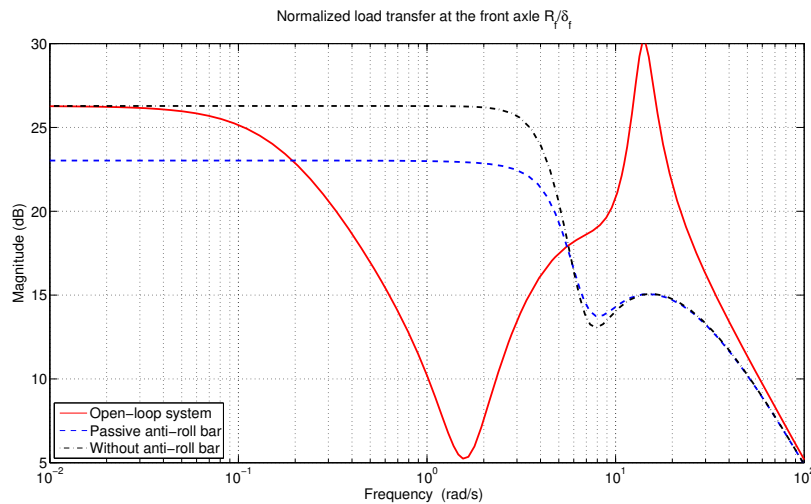


Figure 8.5: The transfer function magnitude of the normalized load transfer ($\frac{R_f}{\delta_f}$) at the front axle.

In the active anti-roll bar system of heavy vehicles, the frequency response up to 4 rad/s is considered to represent the limited bandwidth of the driver [Gaspar, Szabo, and Bokor 2005a]. Figures 8.5 and 8.6 show the comparison of the transfer function magnitude of the normalized load transfer at both axles, for three cases: (1) open-loop system (continued line), (2) passive anti-roll bar (dash line) and (3) without anti-roll bar (dash-dot line). We can see that in the

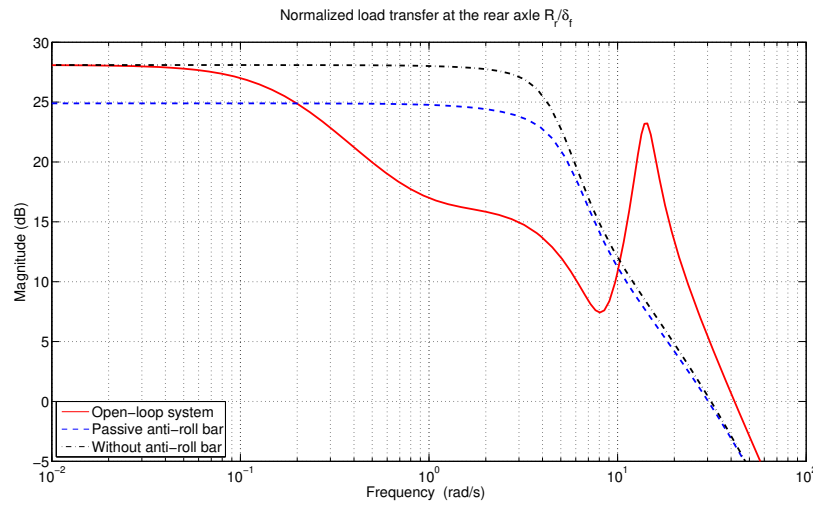


Figure 8.6: Transfer function magnitude of normalized load transfer ($\frac{R_r}{\delta_f}$) at the rear axle.

case of the passive anti-roll bar, the normalized load transfers at the two axles are reduced by about $3.5dB$ in the frequency range to over $4 rad/s$, compared to the case without anti-roll bar.

In the case of the open-loop system, there are two frequency ranges of interest:

- **The frequency range from $0.1 rad/s$ to over $4 rad/s$:** the normalized load transfers at both axles are reduced significantly, compared with the case without anti-roll bar. Hence, these reductions show that even if the controller does not work (no input currents entering to the ESVH actuators), thanks to the internal leakage inside the servo-valve, the active anti-roll bar system still has a positive effect on improving the roll stability of heavy vehicles.
- **The frequency range less than $0.1 rad/s$ (the steady state manoeuvre):** the open-loop system can not change the roll stability of heavy vehicles, compared with the case without anti-roll bar.

In the next section we will consider the heavy vehicle behaviour in the steady state manoeuvre case (the frequency range less than $0.1 rad/s$).

8.4.2.2 Effect of the internal leakage inside the servo-valve in the time domain

To survey the effect of the internal leakage inside the servo-valve in the steady state manoeuvre, we consider that the steering angle is in a step signal from $0.5s$ to $2.5s$ and then remains constant at $2.5 deg$ [Gaspar, Bokor, and Szaszi 2004], as showed in the Figure 8.8a. The vehicle's trajectory is shown in Figure 8.7.

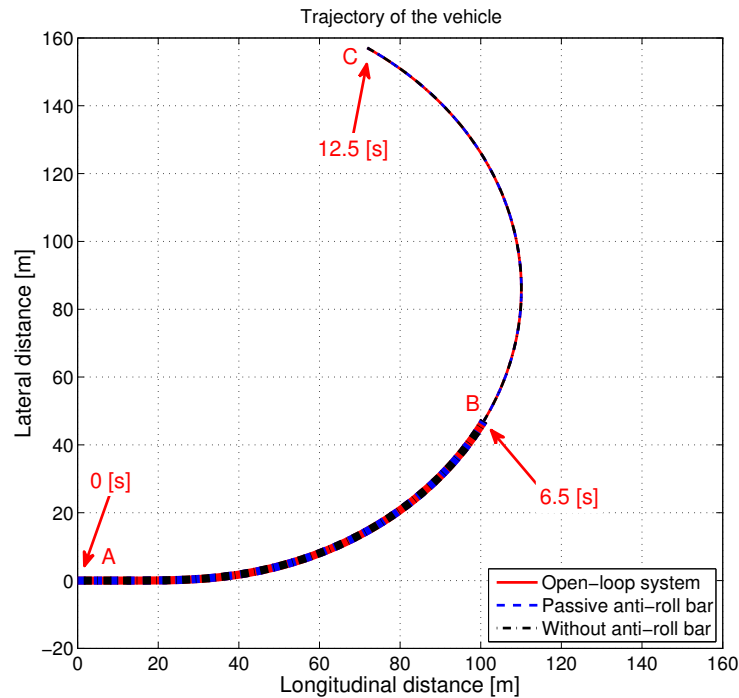


Figure 8.7: Trajectory of the vehicle.

Figures 8.8 shows the time response of the roll angles of the sprung mass, the normalized load transfers, differential pressures inside the hydraulic cylinder and load flows of the oil through the servo-valve at both axles. From 0.5s, the driver starts to change the steering angle. Due to the impact of the inertial force, the roll angles of the suspension are altered and they generate the relative displacement of the piston and cylinder inside each hydraulic cylinder. This increases the differential pressure up to 2.5s, and the oil also starts to flow through the servo-valve. But from 2.5s, the inertial force is held constant and the impact of the internal leakage inside the servo-valve makes the differential pressure rapidly drop up to 35s; then there is no more differential pressure inside the hydraulic cylinder and the oil will not pass through the servo-valve. This greatly affects the roll stability of the vehicle.

Figures 8.8c, d show the normalized load transfers at the two axles. They indicate that from 0.5s the normalized load transfers at both axles start to increase. The normalized load transfers in the open-loop system case will intersect that of the passive anti-roll bar case at 6.5s (point B in Figure 8.7). In the open-loop system case, at 12.5s the normalized load transfer at the rear axle equals 1 ($R_r = 1$) and at this time, rollover will occur (point C in Figure 8.7). Additionally the time response of the heavy vehicle as well as of the ESVH actuators on the right at the front and rear axles in the case of the open-loop system are synthesised in Table 8.1.

Due to the constant forward velocity of 70 km/h, at 6.5s the vehicle will travel the distance (S) of 126m (from point A to point B in Figure 8.7) and at 12.5s the distance travelled would be 243m (from point A to point C in Figure 8.7). Although at 12.5s the rollover will occur

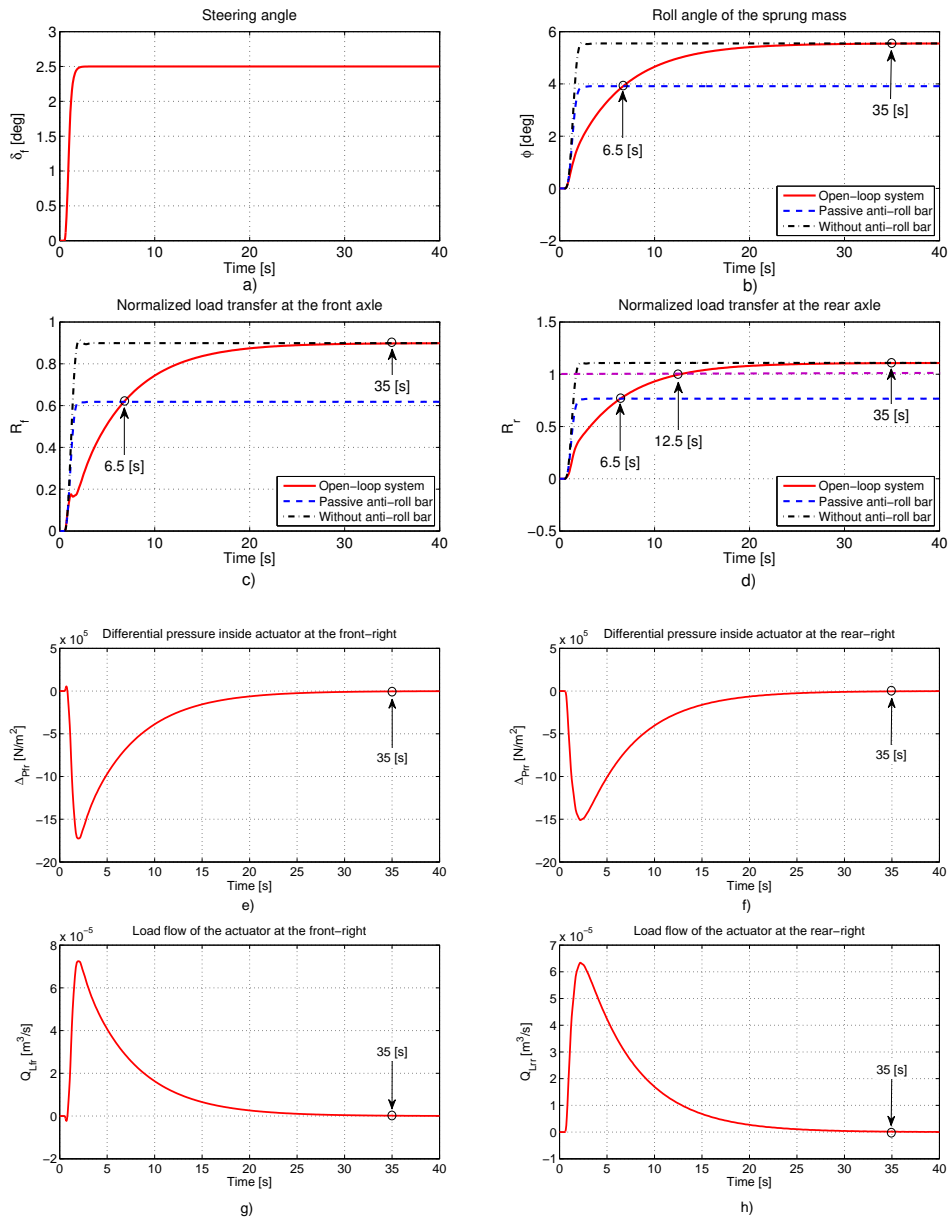


Figure 8.8: Time responses of the heavy vehicle and the actuators in the case of the steady state manoeuvre.

($R_r = 1$), but in fact with the distance of 243m the driver usually will have some impacts on the steering angle to accommodate the vehicle's trajectory or there is the effect of the road on the front wheels. This will allow the open-loop system to improve the roll stability by the internal leakage inside the servo-valve in the frequency range of $[0.1, 4] \text{ rad/s}$. Therefore even in the steady state manoeuvre, roll stability of the vehicle is always guaranteed in practice.

From the analysis and simulation results in the frequency and time domains shown above

Table 8.1: Synthesis of the time response in the steady state manoeuver.

Time (s)	0.5	2.5	6.5	12.5	35
$\delta_f(deg)$	0	2.5	2.5	2.5	2.5
$\Delta P_{fr}(\times 10^5 N/m^2)$	0	-17	-8	-2.5	0
$Q_{Lfr}(\times 10^{-5} N/m^2)$	0	7	3	1	0
R_f	0	0.3	0.6	0.8	0.9
$\Delta P_{rr}(\times 10^5 N/m^2)$	0	-15	-8	-2.5	0
$Q_{Lrr}(\times 10^{-5} N/m^2)$	0	6.3	3.5	1	0
R_r	0	0.4	0.8	1 (rollover)	1.1
$S(m)$	9.7	49	126	243	680

we have answers to the previous questions about roll stability of the vehicle when the active anti-roll bar system suddenly fails. We can confirm that the installation of the active anti-roll system using ESVH actuators does not reduce the operational performance of the vehicle for every situation.

Survey results also indicate that:

- If the total flow pressure coefficient K_P is less than $2.2 \times 10^{-16} \frac{m^5}{Ns}$, the role of the internal leakage inside the servo-valve will be ignored. The oil cannot move between the two chambers of the hydraulic cylinder and the movement of the piston inside the hydraulic cylinder is impossible. In this case, the sprung mass and unsprung mass will become one block. This is a dangerous situation for heavy vehicles.
- If the total flow pressure coefficient K_P is higher than $5.2 \times 10^{-10} \frac{m^5}{Ns}$, the internal leakage inside the servo-valve does not produce any effect on roll stability. Therefore the vehicle behavior will be the same as in the case without anti-roll bar.

8.5 Effect of the internal leakage inside the electronic servo-valve on the closed-loop system

8.5.1 H_∞/LPV control design for the fully integrated model

The aim is to design the control so that the active anti-roll bars are operating all the time, thus improving roll stability. Roll stability is achieved by limiting the lateral load transfers to below the levels required for wheel lift-off. In order to describe the control objective, the nonlinear model (8.12) has a partitioned representation in the following way:

$$\begin{bmatrix} \dot{x}(t) \\ z(t) \\ y(t) \end{bmatrix} = \begin{bmatrix} A(\rho) & B_1(\rho) & B_2(\rho) \\ C_1(\rho) & D_{11}(\rho) & D_{12}(\rho) \\ C_2(\rho) & D_{21}(\rho) & D_{22}(\rho) \end{bmatrix} \begin{bmatrix} x(t) \\ w(t) \\ u(t) \end{bmatrix} \quad (8.15)$$

with the exogenous input $w(t) = [\delta_f]$, the control input $u(t) = [u_{fl} \ u_{fr} \ u_{rl} \ u_{rr}]^T$, the performance output vector $z(t) = [u_{fl} \ u_{fr} \ u_{rl} \ u_{rr} \ R_f \ R_r]^T$ and the measured output vector $y(t) = [a_y \ \dot{\phi}]^T$. Here, the lateral acceleration is defined as follows: $a_y = v\dot{\beta} + v\dot{\psi} - h\ddot{\phi}$ [Hsun-Hsuan, Rama, and Dennis 2012], [Gaspar, Szabo, and Bokor 2005a].

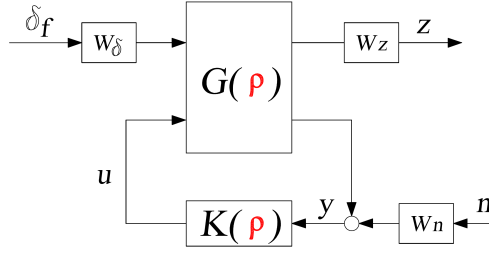


Figure 8.9: The closed-loop interconnection structure of the fully integrated model.

In Figure 8.9, the closed-loop system includes the feedback structure of the nominal model $G(\rho)$, the controller $K(\rho)$, the weighting functions and the performance objectives. In this diagram, u is the control input, y the measured output, n the measurement noise and z the performance output. The steering angle δ_f is the disturbance signal set by the driver. The weighting functions W_δ, W_n, W_z are respectively characterized for the steering angle, sensor noise and performance output. Similar to the H_∞/LPV synthesis in Chapter 7, the weighting functions W_δ and W_n are chosen as in Table 8.2.

The weighting function W_z represents the performance output and is chosen as a diagonal matrix $W_z = \text{diag}[W_{zu}, W_{zR}]$. The weighting function $W_{zu} = \text{diag}[W_{zu1}, W_{zu2}, W_{zu3}, W_{zu4}]$ is adapted to the four input currents entering the four ESVH actuators. The weighting function $W_{zR} = \text{diag}[W_{zRf}, W_{zRr}]$, corresponds to the normalized load transfers at the front and rear axles. The elements of the weighting function W_z are selected in Table 8.2.

Table 8.2: The weighting functions of the H_∞/LPV synthesis for the fully integrated model.

W_δ	W_{n1}	W_{n2}	W_{zu1}	W_{zu2}	W_{zu3}	W_{zu4}	W_{zRf}	W_{zRr}
$\frac{\pi}{180}$	0.01	0.01	$\frac{1}{0.4}$	$\frac{1}{0.4}$	$\frac{1}{0.4}$	$\frac{1}{0.4}$	$\frac{\frac{s}{20}+2}{\frac{s}{100}+15}$	$\frac{\frac{s}{20}+2}{\frac{s}{100}+15}$

In the LPV model of an active anti-roll bar system (8.15), the forward velocity v is selected as the varying parameter $\rho = v$ which can be measured directly by the sensors. The quadratic LPV γ -performance problem is to choose the parameter-varying control matrices $A_K(\rho), B_K(\rho), C_K(\rho), D_K(\rho)$ in such a way that the resulting closed-loop system is quadratically stable and the induced \mathcal{L}_2 norm from w to z is less than γ . The structure of the LPV

controller $K(\rho)$ is defined as follows:

$$\begin{bmatrix} \dot{x}_K(t) \\ u(t) \end{bmatrix} = \begin{bmatrix} A_K(\rho) & B_K(\rho) \\ C_K(\rho) & D_K(\rho) \end{bmatrix} \begin{bmatrix} x_K(t) \\ y(t) \end{bmatrix} \quad (8.16)$$

where $A_K(\rho)$, $B_K(\rho)$, $C_K(\rho)$, $D_K(\rho)$ are continuous bounded matrix functions.

For the interconnection structure shown in Figure 8.9, the H_∞ controllers are synthesized for 10 values of the forward velocity v in the range $[30, \dots, 130]$ km/h . The spacing of the grid points is based upon how well the H_∞ point design performs for the plant around the design point.

At all the grid points, the proposed weighting functions are applied to the entire grid parameter space and the effect of the scheduling parameter is ignored. In the H_∞ control design, the γ iteration results in an optimal γ value and an optimal controller. However, if the weighting functions were changed, another optimal γ and another optimal controller would be gained. The following commands are used to make the grid points as well as the LPV controller synthesis by using LPVTools™:

```
rho = pgrid('rho', linspace(30/3.6, 130/3.6, 10));
and [Klpv, normlpv] = lpvsyn(H, nmeas, ncont).
```

The optimal γ of the controller is: $\gamma_{opt} = normlpv = 0.8096$.

Figures 8.10, 8.11 show the transfer function magnitude of the H_∞/LPV active anti-roll bar controller, with two inputs (the lateral acceleration a_y , the roll rate $\dot{\phi}$) and the four outputs (the input currents entering the ESVH actuators at the front-left u_{fl} , at the front-right u_{fr} , at the rear-left u_{rl} , at the rear-right u_{rr}). We can see that, due to the ESVH actuators at each axle being identical and symmetrical, the transfer functions of the H_∞/LPV controller from the inputs to the outputs have the same magnitude at the front and rear axles.

8.5.2 Simulation results analysis with the nominal value of the total flow pressure coefficient

In this section, the simulation results of the fully integrated model with the H_∞/LPV controller are shown in both frequency and time domains. The nominal value of the total flow pressure coefficient is $K_P = 4.2 \times 10^{-11} \text{ m}^5/(Ns)$. The parameters values of the ESVH actuators and of the yaw-roll model are those given in Tables 2.1 and 2.2.

8.5.2.1 Analysis in the frequency domain

The main objective of the active anti-roll bar system is to reduce the normalized load transfers at all axles. Figures 8.12 shows the transfer function magnitude of the normalized load transfers and input currents of the ESVH actuators on the right at both axles. The varying parameter $\rho = v$ is considered in the interval $[30, 130]$ km/h . Figures 8.12a,b indicates that in the case of the H_∞/LPV active anti-roll bar control, the normalized load transfers at the two axles are significantly reduced when compared to the passive anti-roll bar. This reduction

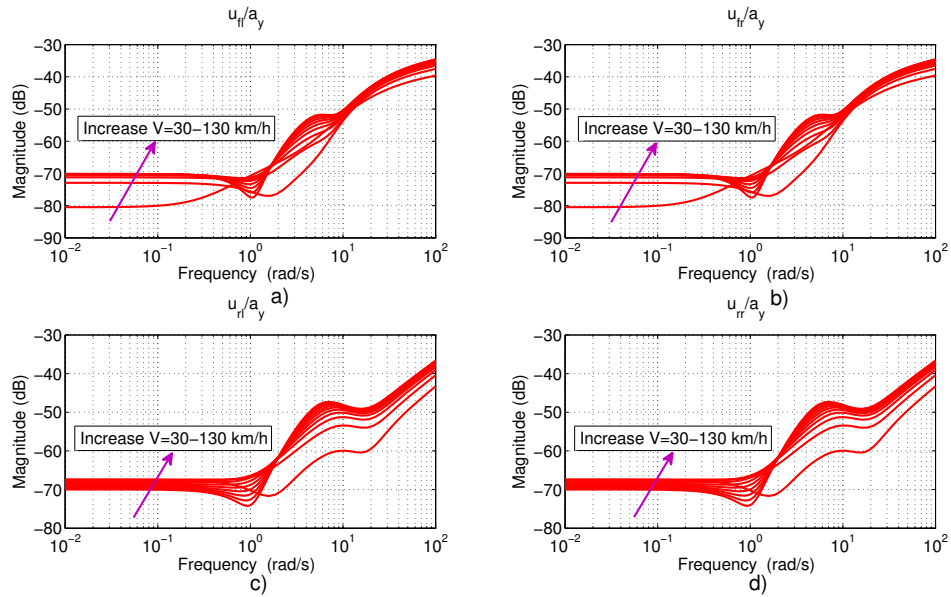


Figure 8.10: Transfer function magnitude of controller: from lateral acceleration to (a) input current at front-left $\frac{u_{fl}}{a_y}$, (b) input current at front-right $\frac{u_{fr}}{a_y}$, (c) input current at rear-left $\frac{u_{rl}}{a_y}$, (d) input current at rear-right $\frac{u_{rr}}{a_y}$.

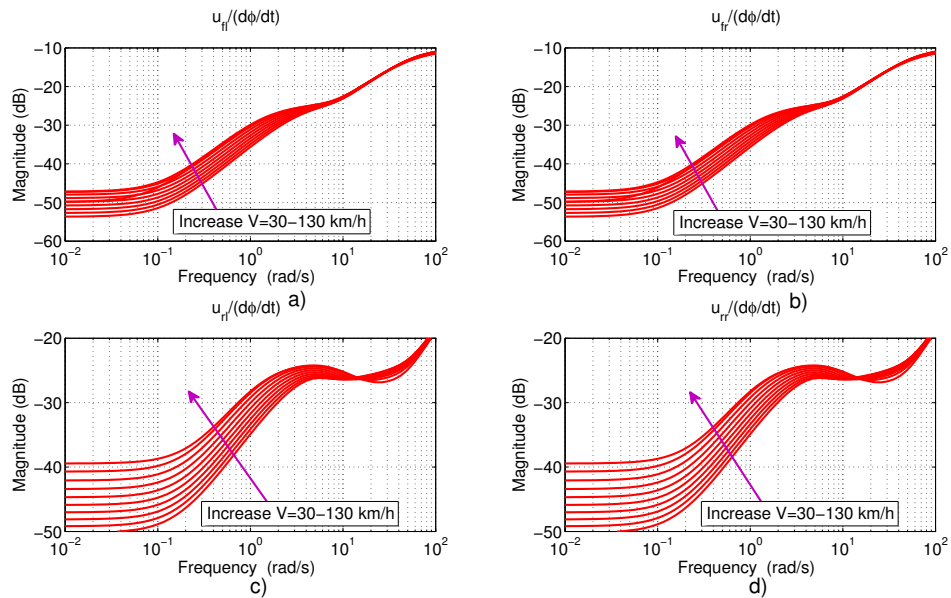


Figure 8.11: Transfer function magnitude of controller: from roll rate to (a) input current at front-left $\frac{u_{fl}}{\phi}$, (b) input current at front-right $\frac{u_{fr}}{\phi}$, (c) input current at rear-left $\frac{u_{rl}}{\phi}$, (d) input current at rear-right $\frac{u_{rr}}{\phi}$.

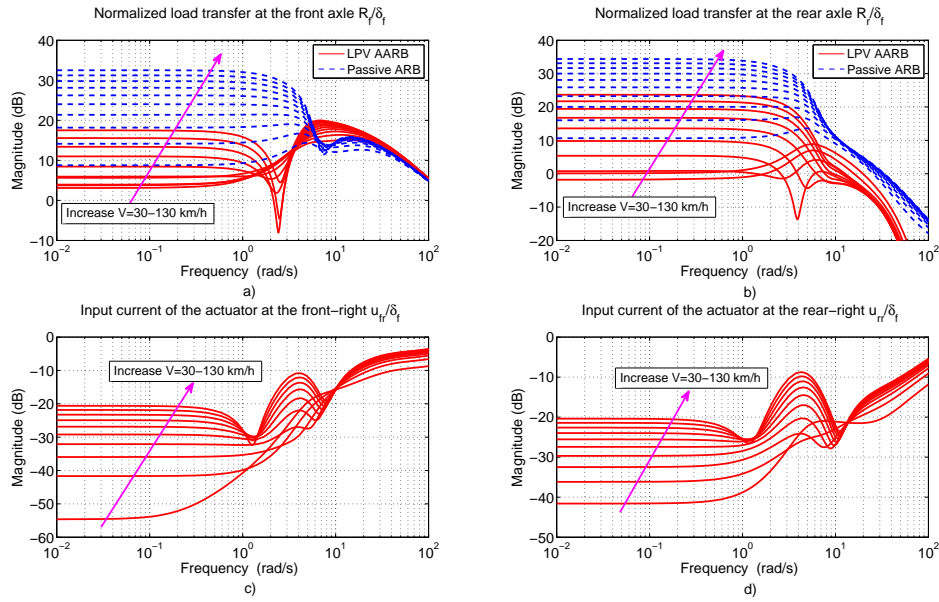


Figure 8.12: Transfer function magnitude of (a, b) the normalized load transfers at the two axles $\frac{R_{f,r}}{\delta_f}$, (c, d) the input currents of the ESVH actuators at the front-right $\frac{u_{fr}}{\delta_f}$ and at the rear-right $\frac{u_{rr}}{\delta_f}$.

is achieved in the frequency range to over 4 rad/s , which represents the limited bandwidth of the driver [Sampson and Cebon 2003a]. Therefore, we can confirm that the H_∞/LPV active anti-roll bar control improves roll stability of heavy vehicles in reducing the rollover risk in all of the desired forward velocity range.

Figures 8.12c, d show the transfer functions magnitude of the input currents on the right at the front axle ($\frac{u_{fr}}{\delta_f}$) and at the rear axle ($\frac{u_{rr}}{\delta_f}$), respectively. When the forward velocity increases, the controller input currents ($u_{fr,rr}$) also increase. This indicates that the active anti-roll bar system requires more input current (i.e. energy) at high forward velocity than at low forward velocity.

8.5.2.2 Analysis in the time domain

In this section, the simulation results of the single unit heavy vehicle in the time domain are shown in the steady state manoeuvre. The steering angle (a step signal) is shown in Figure 8.8a and the forward velocity is held constant at 70 km/h .

Figure 8.13 shows the normalized load transfers and suspension roll angles at the two axles in comparison between the H_∞/LPV active anti-roll bar control and the passive anti-roll bar. The H_∞/LPV active anti-roll bar control reduces the normalized load transfers by about 60%, compared to the passive anti-roll bar. On the other hand, when compared with Figures 8.8c, d, it indicates that the H_∞/LPV active anti-roll bar control system has provided a stabilisation

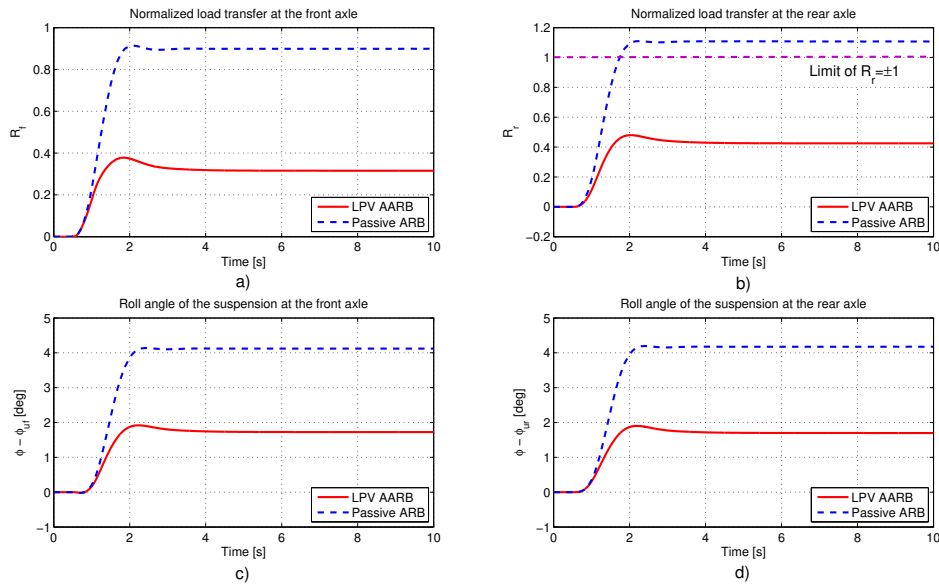


Figure 8.13: The normalized load transfers and roll angle of the suspensions in the steady state manoeuver.

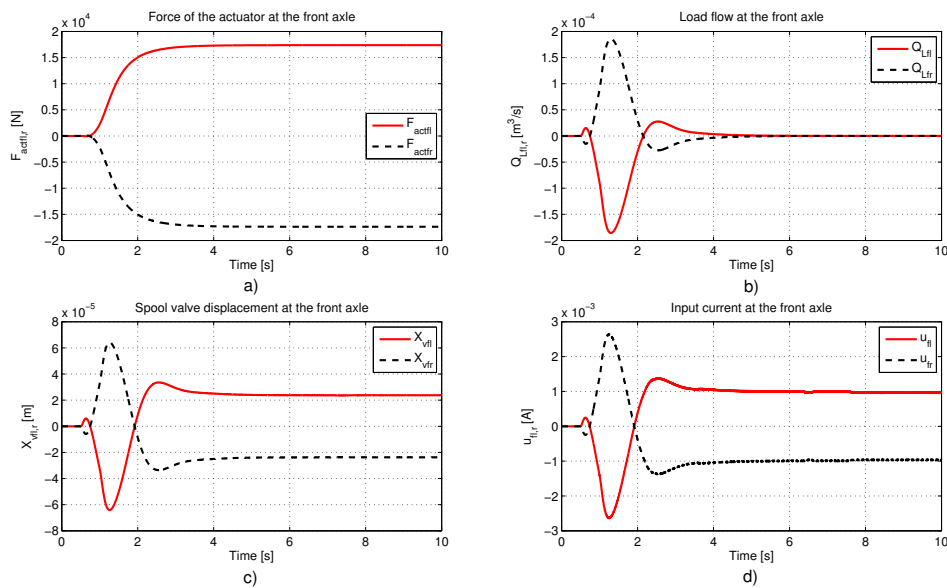


Figure 8.14: The characteristics of the ESVH actuators at the front axle.

of the normalized load transfers in the steady state manoeuver. Indeed in the case of the H_∞/LPV active anti-roll bar control, the normalized load transfers at both axles increase with the increase of the steering angle from 0.5s to 2s, and then they are kept stable at 0.32 for the front axle, and 0.42 for the rear axle. Meanwhile, in the open-loop system, these values

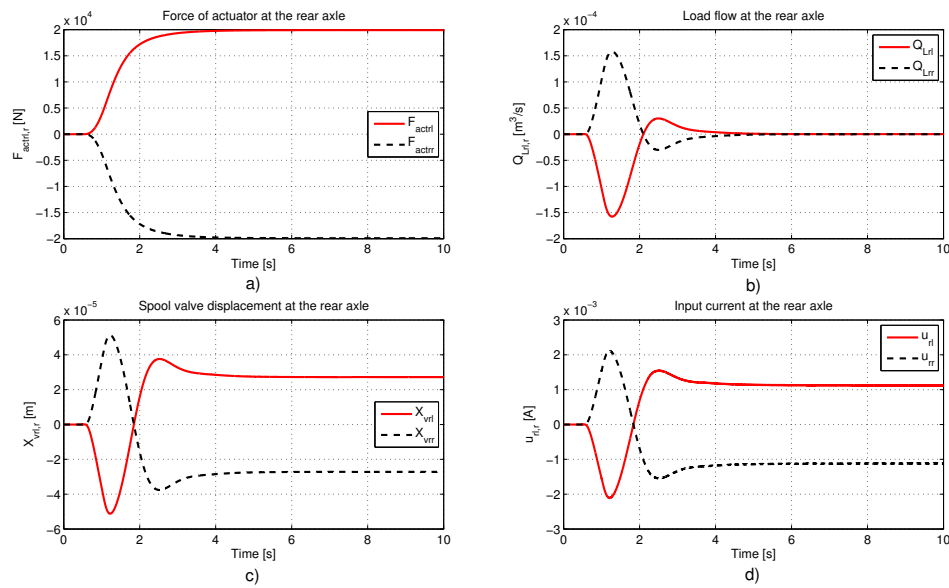


Figure 8.15: The characteristics of the ESVH actuators at the rear axle.

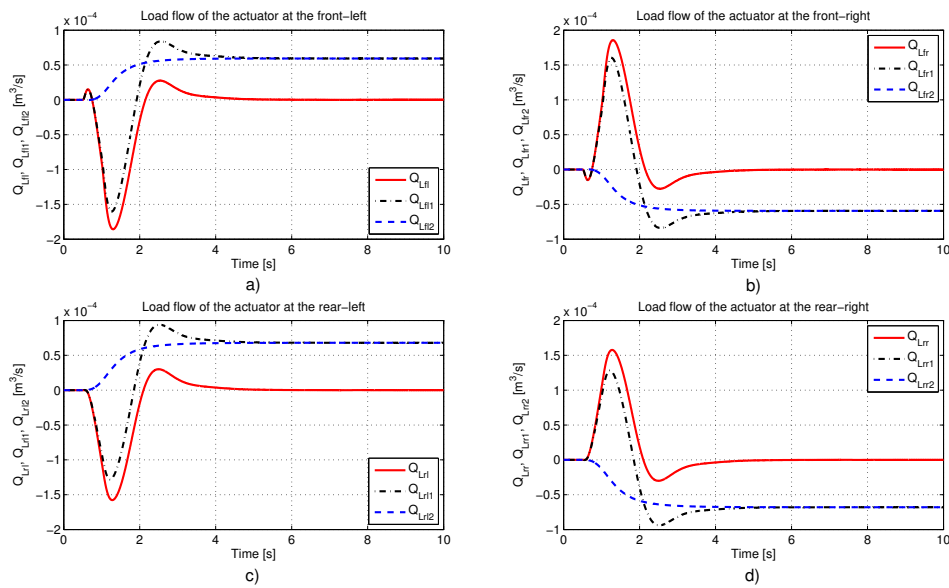


Figure 8.16: The load flow of the four ESVH actuators in the steady state manoeuvre.

increase constantly and they reach stability at 35s, then the vehicle shows the same results as the case without anti-roll bar.

Figures 8.14 and 8.15 show the characteristics of the four ESVH actuators of the fully integrated model. If the right and left ESVH actuators are identical and symmetrically mounted

at each axle, then the characteristics of the two ESVH actuators do have the same magnitude and the opposite direction. This reinforces the results in Appendix B and equations (2.33) - (2.36) of the control-oriented integrated model of a single unit heavy vehicle, shown in section 2.4.2.

As mentioned in section 2.2.1, the load flow through the hydraulic cylinder (Q_L) includes:

- **The first part** ($Q_{L1} = K_x X_v$) is the orifice load flow through the servo-valve and is adjusted by the movement of the spool valve displacement X_v ,
- **The second part** ($Q_{L2} = K_P \Delta P$) is the internal leakage load flow inside the electronic servo-valve, which passes through the contact surface between the spool valve and the body of the servo-valve

Therefore, the actual load flow between the two chambers of the ESVH actuator is as follows:

$$Q_L = Q_{L1} - Q_{L2} \quad (8.17)$$

The analysis in Figure 8.16 is the detail of the load flow of the four ESVH actuators. Here, the first part Q_{L1} is shown in the dash-dot line, the second part Q_{L2} in the dash line and the actual load flow between the two chambers of the ESVH actuator in the solid line. We can see that in the case of the H_∞/LPV active anti-roll bar control system, due to the displacement of the spool valve (shown in Figures 8.14c and 8.15c), the orifice load flows through the servo-valve $Q_{L1} = K_x X_v$ are balanced with the oil leakage inside the electronic servo-valve $Q_{L2} = K_P \Delta P$. Therefore the actual load flow between the two chambers of the ESVH actuator Q_L becomes zero in the steady state manoeuver.

The simulation results in the frequency and time domains, allow to conclude that with the nominal value of the total flow of pressure coefficient ($K_{PNominal} = 4.2 \times 10^{-11} \frac{m^5}{Ns}$), the proposed H_∞/LPV active anti-roll bar control system can guarantee the objective of improving the roll stability of heavy vehicles. It is obtained by creating a balance between the load flows generated by the controller with that of the oil leakage. However, in practice, the total flow of pressure coefficient K_P often changes depending on the working conditions and the life of the ESVH actuator. In the next section, we will consider the effect of the internal leakage inside the electronic servo-valve on the proposed H_∞/LPV active anti-roll bar control of the fully integrated model.

8.5.3 Effect of the internal leakage on the performance of the H_∞/LPV active anti-roll bar control system

To assess the influence of the internal leakage inside electronic servo-valve on the performance of the proposed H_∞/LPV active anti-roll bar control system, three cases of the total flow pressure coefficient (K_P) are considered and detailed as follows:

- First case: The 1st H_∞/LPV active anti-roll bar control system with the **nominal value** of the total flow pressure coefficient, $K_{PNominal} = 4.2 \times 10^{-11} \frac{m^5}{Ns}$.

- Second case: The 2nd H_∞/LPV active anti-roll bar control system with the **low** total flow pressure coefficient, $K_{PLow} = 5 \times 10^{-13} \frac{m^5}{Ns}$, (small internal oil leakage).
- Third case: The 3rd H_∞/LPV active anti-roll bar control system with the **high** total flow pressure coefficient, $K_{PHight} = 1 \times 10^{-8} \frac{m^5}{Ns}$, (high internal oil leakage).

The three cases of the H_∞/LPV active anti-roll bar control systems presented above will be compared with the passive anti-roll bar case.

8.5.3.1 Analysis in the frequency domain

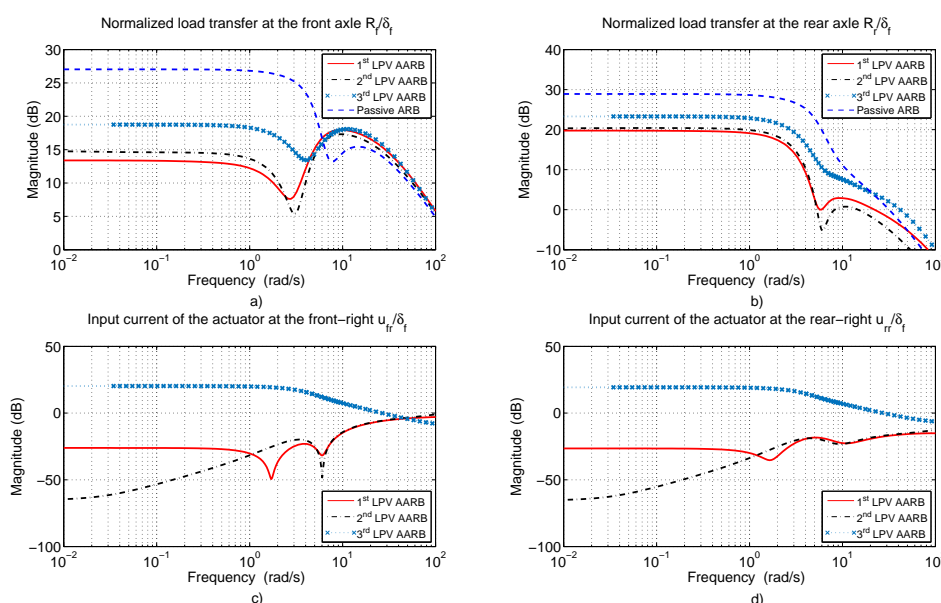


Figure 8.17: The transfer function magnitude of (a, b) the normalized load transfers at the two axles $\frac{R_{f,r}}{\delta_f}$, (c, d) the input currents of the actuators at the front-right $\frac{u_{fr}}{\delta_f}$ and at the rear-right $\frac{u_{rr}}{\delta_f}$.

In this section, we consider the forward velocity at 90 km/h. As mentioned above, the main objective of the active anti-roll bar system is to reduce the normalized load transfers at all the axles. But we need also to pay attention to the actuator's saturation.

Figure 8.17 shows the transfer function magnitude of the normalized load transfers and input currents on the right at both axles. When the total flow pressure coefficient is low (K_{PLow}), the internal leakage inside the electronic servo-valve is small, so the 2nd H_∞/LPV active anti-roll bar control system needs lower input current. In the high total flow pressure coefficient case (K_{PHight}), the internal leakage inside the electronic servo-valve is high, so the 3rd H_∞/LPV active anti-roll bar control system needs a huge input current, without having the ability to greatly improve the roll stability of heavy vehicles compared to the nominal case ($K_{PNominal}$). The simulation results indicate that, if the total flow pressure coefficient (K_P) is greater

than $3 \times 10^{-8} \frac{m^5}{Ns}$, the H_∞/LPV active anti-roll bar control system does not provide any improvement in the roll stability of heavy vehicles, despite the input current being very high. Indeed in these cases, the orifice load flow through the servo-valve generated by the movement of the spool valve cannot adapt to the oil leakage inside the electronic servo-valve.

8.5.3.2 Analysis in the time domain

In this section, some simulation results in the time domain are shown for four different cases: the three H_∞/LPV active anti-roll bar control systems and the passive anti-roll bar. The vehicle manoeuvre is a double lane change to overtake. The steering angle δ_f is shown in Figure 8.18a.

The following scenario is used to evaluate the effect of the internal leakage inside the electronic servo-valve on the closed-loop system with the varying parameter $\rho = v$:

- The initial forward velocity is 80 km/h, the vehicle is running on a dry road ($\mu = 1$).
- When the driver wishes to overtake another vehicle, the driver will increase the throttle, so the total tractive force will increase from 0.5s to 2s in order to increase the forward velocity from 80 km/h up to 108 km/h. By ignoring the total rolling resistance and aerodynamic resistance forces, the forward velocity is kept constant at 108 km/h. At 6s the driver starts to brake to reduce the forward velocity of the vehicle to 90 km/h as shown in Figure 8.18b. The total brake force will increase from 6s to 6.8s and then the driver will reduce the pressure on the brake pedal. The total tractive and braking forces are shown in Figures 8.18c, d.

The differential equation for the forward velocity is determined as [J.Y.Wong 2001]:

$$m\dot{v} = \sum_{i=1}^2 F_{ti} - \sum_{i=1}^4 F_{bi} \tag{8.18}$$

where F_{ti} is the tractive force at each wheel drive, F_{bi} the braking force at each wheel. Figures 8.18e, f show the normalized load transfers at both axles. In the cases of the three H_∞/LPV active anti-roll bar controllers, roll stability of the heavy vehicle is greatly improved, compared to the passive anti-roll bar (this is perfectly consistent with the results on the frequency domain). Figures 8.18g, h show the input currents at both axles. To create a good efficiency for roll stability (shown in Figures 8.18e, f) in the case of the 3rd H_∞/LPV active anti-roll bar controller with the high total flow pressure coefficient (K_{PHigh}), one needs a huge input current (reaches 362 [mA] for the front axle, 382 [mA] for the rear axle), this value largely exceeds the limit allowed 20 [mA] [Rafa, Yahya, and Rawand 2009]. Whereas in the cases of the 2nd H_∞/LPV controller with the low total flow pressure coefficient (K_{PLow}) and of the 1st H_∞/LPV controller with the nominal total flow pressure coefficient ($K_{PNominal}$), the maximum input currents required are less than 5 [mA]. The maximum absolute value of the normalized load transfers and the input currents are summarized in Table 8.3.

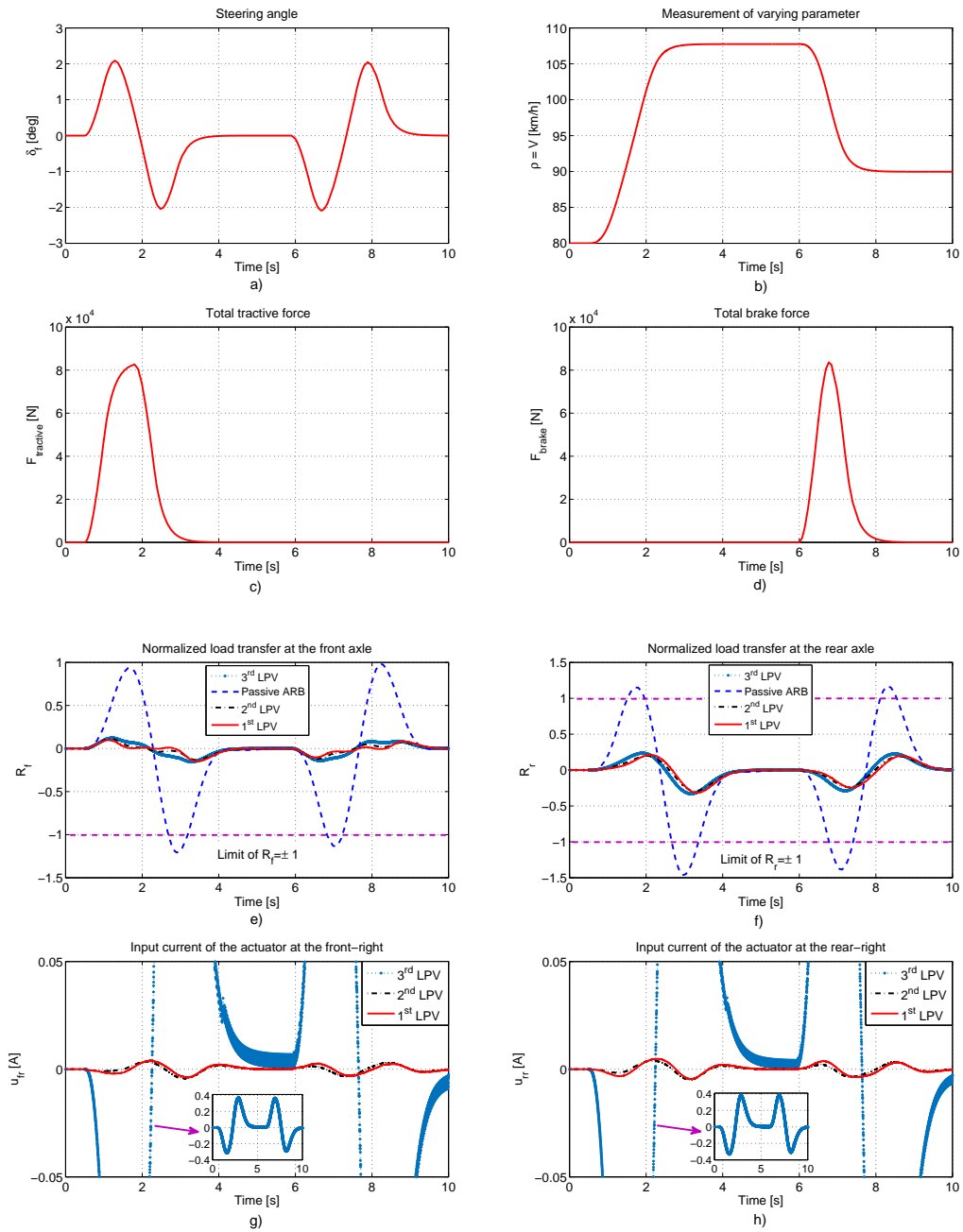


Figure 8.18: Time responses of a single unit heavy vehicle in a double lane change manoeuvre to overtake.

As mentioned in the control objective, the main objective of the active anti-roll bar system is to improve roll stability, and vehicle rollover will occur if the normalized load transfer takes on the limit of ± 1 [Sampson and Cebon 2003b]. However, it is also necessary to avoid the actuators' saturation, with $20 [mA]$ being the maximum absolute value of the input current

Table 8.3: Maximum absolute value of the signals in the double lane change manoeuvre to overtake.

Anti-roll bar system	$ R_f _{max}$	$ R_r _{max}$	$ u_{fr} _{max}$ [mA]	$ u_{rr} _{max}$ [mA]
1 st H_∞/LPV	0.149	0.317	4	4.7
2 nd H_∞/LPV	0.132	0.294	3.5	4
3 rd H_∞/LPV	0.153	0.329	362	382
Passive	1.207 (rollover)	1.46 (rollover)	0	0

recommended by [Rafa, Yahya, and Rawand 2009]. The survey results in both the frequency and time domains have shown that, to satisfy simultaneously the two goals of enhancing roll stability and avoiding the saturation of the actuators, the total flow pressure coefficient has to be kept in the range of $K_P = [5 \times 10^{-15}, 4 \times 10^{-10}] \frac{m^5}{Ns}$.

8.6 Conclusion

In this chapter, to evaluate the effect of the internal leakage inside the electronic servo-valve on the active anti-roll bar system of heavy vehicles, the author used the fully integrated model including four ESVH actuators (two at the front and two at the rear axles) on a linear single unit heavy vehicle yaw-roll model. The nonlinear model of a single unit heavy vehicle is considered as a LPV model, where the forward velocity is considered as a scheduling parameter. The H_∞/LPV active anti-roll bar controller is synthesized in order to improve roll stability of heavy vehicles. The effect of the internal leakage inside the electronic servo-valve on the open-loop and closed-loop systems is analysed in detail. The survey results have shown that with the total flow pressure coefficient $K_P = [5 \times 10^{-15}, 4 \times 10^{-10}] \frac{m^5}{Ns}$, the two objectives of enhancing roll stability and avoiding the saturation of the actuators are simultaneously satisfied.

In actual use, the total flow pressure coefficient K_P will decline over time, because it depends on the quality of the contact surfaces between the spool valve and the body of the servo-valve. From the simulation results by using the H_∞ active anti-roll bar controller in Chapter 5 and the H_∞/LPV active anti-roll bar controller in this chapter, we can confirm that the internal leakage inside the electronic servo-valve will affect the performance quality of the active anti-roll bar system of heavy vehicles. Therefore an LPV approach for fault tolerant control design will be also an interesting area for further research.

Part IV
Future direction and General
conclusions

This part presents the last two chapters, with the main contents introducing the possible future research directions using the active braking system in order to prevent vehicle rollover and the general conclusions of this thesis. They are summarized as follows:

Chapter 9: Future direction to prevent vehicle rollover by using active braking system

- An H_∞/LPV active braking system is proposed in combination with the passive suspension system with the aim of preventing the vehicle rollover phenomenon.
- By considering the "Braking monitor" concept, the H_∞/LPV controllers allow the active braking system to be activated only when the vehicle comes close to a dangerous situation.
- The simulation results in comparison between the three H_∞/LPV control designs and the passive suspension show that the second H_∞/LPV active braking control design can satisfy simultaneously the adaptation to vehicle rollover in an emergency situation, with lower braking forces, and improved handling performance of the vehicle.
- This constitutes the preliminary research results of this approach and it also opens up some interesting research initiatives for the future.

Chapter 10: General conclusions and Perspectives

- One gives a summary of the main contributions of the thesis obtained during three years in terms of vehicle modelling, control methodologies, application, vehicle rollover prevention, handling performance and actuator's fault.
- Some general perspectives are outlined on possible further research directions in active anti-roll bar as well as active roll control systems.

Future direction to prevent vehicle rollover by using active braking system

Contents

9.1	Introduction	189
9.2	The LPV model of a single unit heavy vehicle using an active braking system	191
9.3	The H_∞/LPV synthesis for an active braking system	193
9.3.1	The H_∞/LPV control design	193
9.3.2	The solution of the H_∞/LPV control problem	194
9.3.3	Simulation results analysis in the frequency domain	194
9.4	Analysis in the time domain	197
9.4.1	Braking monitor	197
9.4.2	Simulation results analysis in the time domain	199
9.5	Conclusion	202

9.1 Introduction

Active Braking System (ABS) is the general concept of controlled braking on vehicles, such as Electronic Brake System (EBS), Anti-lock Braking System (ABS), Advanced Emergency Braking System (AEBS), Autonomous Emergency Braking (AEB) [Gabriel and Donal 2002], [D'alfio, Morgando, and Sorniotti 2006]. The active braking system was introduced to the automotive industry in the 1950s with the objective to improve braking performance. For a long time, the hydraulic brake systems dominated the market, however the main disadvantage is the noticeable oscillation of the wheel slip around a reference value. Today, electromechanical actuators are becoming common and will most probably replace totally hydraulic brakes in the near future, along with the development of X-by-wire technology. These actuators allow the application of a smoother and continuous braking action on the brake pads [Balamili, Köse, and Anlaş 2007]. The evolution of braking systems in the automotive field is well described in Figure 9.1. We can see that, since electronics have been integrated into vehicles, the advances in the development of active vehicle control systems have been inextricably linked to advances in sensors and actuators technology [Savaresi and Tanelli 2010]. The United Nations Economic

Commission for Europe (UNECE) has made active braking system mandatory in all new heavy vehicles manufactured from 2013. Using this system, a reduction in accidents of 27% which accounts to eight thousand lives per year will be expected.

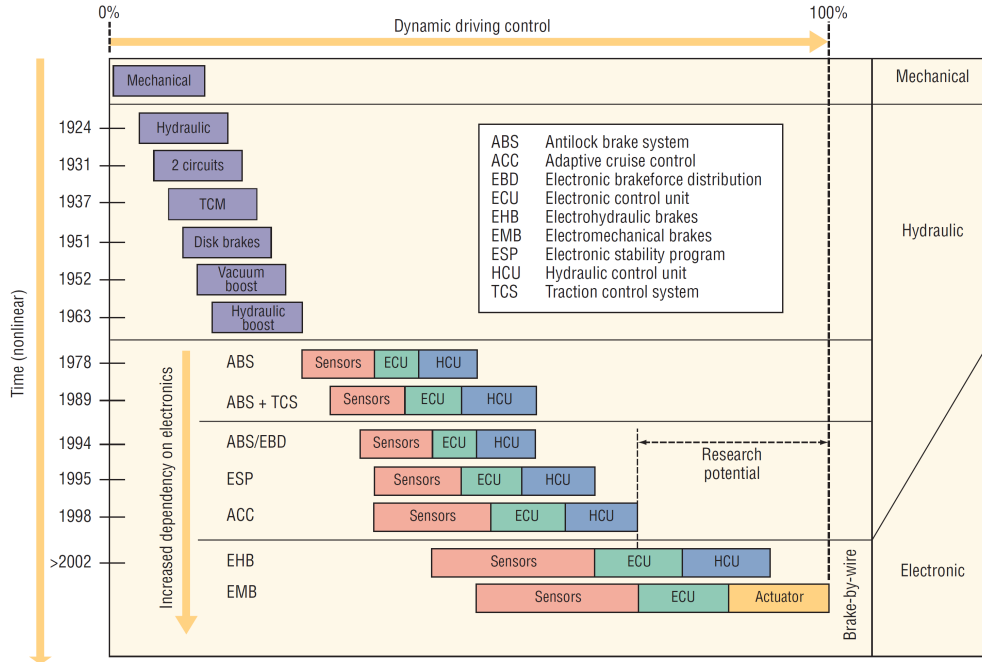


Figure 9.1: The evolution of braking systems [Savaresi and Tanelli 2010].

As explained in the previous chapters, the rollover of a vehicle starts when the tyre-road contact force on one of the inner curve-side wheels becomes zero. This situation has to be detected or measured; however, a force transducer for measuring the vertical wheel load is not available or feasible. The pair of forces responsible for vehicle rollover arises from the high lateral inertial force and its counterpart on the road, which is generated by the tyre, the lateral force component. If the centre of gravity point position is high, the resulting moment is also large and can result in rollover. From this, it can be seen that just by means of the controlled suspension, the prevention of rollover is not possible since it cannot reduce the lateral tyre force component, the only effect is to keep the vehicle body perpendicular to the road, thus eliminating the rolling torque of the gravitational force [Palkovics, Semsey, and Gerum 1999], [Morrison and Cebon 2017].

In the previous chapters, the active anti-roll bar system is presented as a good solution to improve roll stability of heavy vehicles. In practice, the passive suspension can maintain roll stability during normal vehicle behavior. Therefore it is not necessary that the active anti roll bar system is always operating, because it requires energy. A combined control structure between the active anti-roll bar system and the active braking system was proposed in [Gaspar, Bokor, and Szaszi 2004]. The best part of this solution is that, in a normal driving situation, only the active anti-roll bar system is working and the active braking system is only activated when the vehicle comes close to a rollover situation.

Based on the idea in [Gaspar, Bokor, and Szaszi 2004], here the author would like to present preliminary research results on the active braking system with the aim of preventing the vehicle rollover phenomenon. The active braking system is combined with the passive anti-roll bar system (the passive suspension system). In normal situations the active braking system is in "off" mode, but when the normalized load transfer at the rear axle reaches the limitation of ± 0.75 the active braking system will be activated. This approach is also being promoted by worldwide truck manufacturers, such as Volvo trucks.

9.2 The LPV model of a single unit heavy vehicle using an active braking system

The yaw-roll model of a single unit heavy vehicle for studying the active anti-roll bar system is presented in Chapter 2. Here, this model is suitably modified for the active braking system by using the yaw moment control M_z as shown in Figure 9.2 [Gaspar, Bokor, and Szaszi 2005]. The parameters and variables of the yaw-roll model are detailed in Table 2.2. The motion differential equations are formalized as follows:

$$\left\{ \begin{array}{l} mv(\dot{\beta} + \dot{\psi}) - m_s h \ddot{\phi} = F_{yf} + F_{yr} \\ -I_{xz} \ddot{\phi} + I_{zz} \ddot{\psi} = F_{yf} l_f - F_{yr} l_r + M_z \\ (I_{xx} + m_s h^2) \ddot{\phi} - I_{xz} \ddot{\psi} = m_s g h \phi + m_s v h (\dot{\beta} + \dot{\psi}) - k_f (\phi - \phi_{uf}) \\ \quad - b_f (\dot{\phi} - \dot{\phi}_{uf}) + M_{ARf} - k_r (\phi - \phi_{ur}) - b_r (\dot{\phi} - \dot{\phi}_{ur}) + M_{ARr} \\ -r F_{yf} = m_{uf} v (r - h_{uf}) (\dot{\beta} + \dot{\psi}) + m_{uf} g h_{uf} \phi_{uf} - k_{uf} \phi_{uf} \\ \quad + k_f (\phi - \phi_{uf}) + b_f (\dot{\phi} - \dot{\phi}_{uf}) + M_{ARf} \\ -r F_{yr} = m_{ur} v (r - h_{ur}) (\dot{\beta} + \dot{\psi}) - m_{ur} g h_{ur} \phi_{ur} - k_{ur} \phi_{ur} \\ \quad + k_r (\phi - \phi_{ur}) + b_r (\dot{\phi} - \dot{\phi}_{ur}) + M_{ARr} \end{array} \right. \quad (9.1)$$

where the lateral tyre forces $F_{yf,r}$ and the moment of the passive anti-roll bar system impacts the unsprung and sprung masses $M_{ARf,r}$ are defined in equations (2.21), (2.26) and (2.27).

M_z , the yaw moment control generated by the active braking system, depends linearly on the difference between the left and right braking forces ΔF_b as follows:

$$M_z = l_w \Delta F_b \quad (9.2)$$

where ΔF_b is defined by [Gaspar, Bokor, and Szaszi 2004]:

$$\Delta F_b = (F_{b,rr} + r_1 F_{b,fr}) - (F_{b,rl} + r_2 F_{b,fl}) \quad (9.3)$$

Here $F_{b,fl}$, $F_{b,fr}$, $F_{b,rl}$ and $F_{b,rr}$ are the longitudinal braking forces at each wheel. In our case it is assumed that the braking forces are equal at the front and rear wheels on each side, so $F_{b,fl} = F_{b,rl}$, $F_{b,fr} = F_{b,rr}$. The difference between the left and right braking forces in equation (9.3) is rewritten with the braking forces at the rear axle as follows:

$$\Delta F_b = F_{b,rr} (1 + r_1) - F_{b,rl} (1 + r_2) \quad (9.4)$$

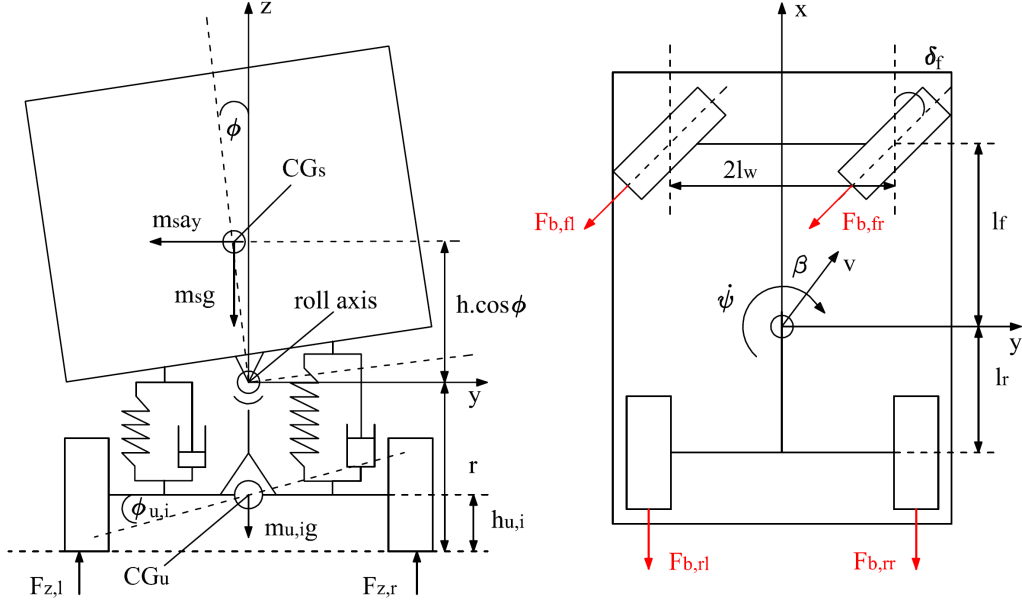


Figure 9.2: Yaw-Roll model of a single unit heavy vehicle [Gaspar, Bokor, and Szaszi 2004].

where r_1, r_2 are defined as:

$$\begin{cases} r_1 = \frac{\sqrt{l_f^2 + l_w^2}}{l_w} \sin(\tau - \delta_f) \\ r_2 = \frac{\sqrt{l_f^2 + l_w^2}}{l_w} \sin(\tau + \delta_f) \\ \tau = \arctan\left(\frac{l_w}{l_f}\right) \end{cases} \quad (9.5)$$

It can be assumed that the steering angle (δ_f) is small during stable driving conditions, so r_1 and r_2 are approximately equal to 1. Hence the driving throttle is constant during a lateral manoeuvre and the forward velocity depends only on the brake forces. The differential equation of the forward velocity is:

$$m\dot{v} = -F_{b,fl} - F_{b,fr} - F_{b,rl} - F_{b,rr} = -2F_{b,rr} - 2F_{b,rl} \quad (9.6)$$

The motion differential equations (9.1)-(9.6) can be rewritten in the LPV state-space representation with the forward velocity as the varying parameter ($\rho_1 = v$) as follows:

$$\dot{x} = A(\rho_1).x + B_1(\rho_1).w + B_2(\rho_1).u \quad (9.7)$$

with the state vector $x = [\beta \ \dot{\psi} \ \phi \ \dot{\phi} \ \phi_{uf} \ \phi_{ur} \ v]^T$, the exogenous disturbance $w = [\delta_f]^T$, and the control input $u = [M_z]^T$.

9.3 The H_∞/LPV synthesis for an active braking system

9.3.1 The H_∞/LPV control design

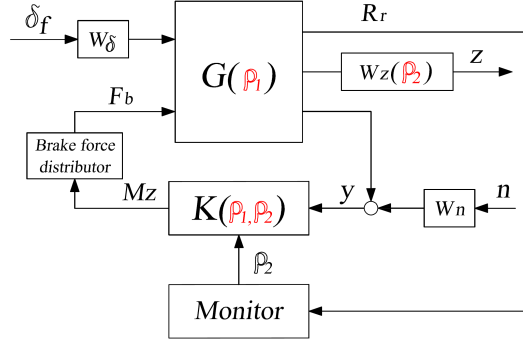


Figure 9.3: The closed-loop interconnection structure of the active braking system.

In this section, the H_∞/LPV control design is presented for the active braking system in heavy vehicles to prevent rollover in emergency situations. In Figure 9.3 the H_∞/LPV control structure includes the nominal model $G(\rho_1)$, the controller $K(\rho_1, \rho_2)$, the performance output z , the control input u , the measured output y , and the measurement noise n . δ_f is the steering angle (disturbance signal), set by the driver. The measured output is $y = [a_y, \phi]$. The weighting functions W_δ , W_n are selected according to the methods used in Chapter 7.

The parameter dependent weighting function W_z represents the performance output and is chosen as $W_z = \text{diag}[W_{zMz}, W_{zay}]$. The purpose of this weighting function is to keep the yaw moment M_z and the lateral acceleration a_y as small as possible over the desired frequency range to over 4 rad/s , which represents the limited bandwidth of the driver [Gaspar, Bokor, and Szaszi 2004], [Sampson and Cebon 2003a]. The weighting function W_{zMz} , chosen to avoid the saturation of the braking system, is selected as follows:

$$W_{zMz} = \frac{1}{12000} \quad (9.8)$$

In an emergency situation, the vehicle leans out of the centreline due to the effect of the inertial force. The weighting function W_{zay} is used to reduce the lateral acceleration by decreasing the lateral tyre force, and it is selected as follows:

$$W_{zay} = \rho_2 \frac{0.5s + 2}{0.1s + 100} \quad (9.9)$$

The author would like to stress that the interest of the parameter dependent weighting function is to allow for the vehicle performance adaptation to the risk of rollover. In the case of a truck avoiding an obstacle in an emergency, the wheels at the rear axle lift off first [Sampson and Cebon 2003a], because the rollover of the vehicle is affected by the suspension stiffness to load ratio. For that reason, the varying parameter is defined as $\rho_2 = f(|R_r|)$. As far as the normalized load transfer at the rear axle R_r is concerned, when the varying parameter ρ_2 increases, the gain of the weighting function W_{zay} is large, and therefore the lateral acceleration will be penalized.

9.3.2 The solution of the H_∞/LPV control problem

According to Figure 9.3, the concatenation of the nonlinear model (9.7) with the performance weighting functions has a partitioned representation in the following form:

$$\begin{bmatrix} \dot{x}(t) \\ z(t) \\ y(t) \end{bmatrix} = \begin{bmatrix} A(\rho) & B_1(\rho) & B_2(\rho) \\ C_1(\rho) & D_{11}(\rho) & D_{12}(\rho) \\ C_2(\rho) & D_{21}(\rho) & D_{22}(\rho) \end{bmatrix} \begin{bmatrix} x(t) \\ w(t) \\ u(t) \end{bmatrix} \quad (9.10)$$

where the exogenous input $w(t) = [\delta_f \quad n]^T$, the control input $u(t) = [M_z]^T$, the measured output vector $y(t) = [a_y \quad \dot{\phi}]^T$, and the performance output vector $z(t) = [M_z \quad a_y]^T$. The LPV model of the active braking system (9.10) uses the varying parameters $\rho = [\rho_1, \rho_2]$, which are known in real time. As explained in the previous chapters, the parameter $\rho_1 = v$ is measured directly, while the parameter $\rho_2 = f(|R_r|)$ can be calculated by using the measured roll angle of the unsprung mass at the rear axle ϕ_{ur} .

In this chapter, we also use the grid-based LPV approach and the LPVToolsTM presented in Chapter 3 to synthesize the H_∞/LPV active braking control system. It requires a gridded parameter space for the two varying parameters $\rho = [\rho_1, \rho_2]$. The H_∞ controllers are synthesized for 10 grid points of the forward velocity in the range $\rho_1 = v = [40km/h, 130km/h]$ and 5 grid points of the normalized load transfer at the rear axle in a range $\rho_2 = f(|R_r|) = [0, 1]$. The grid points and the LPV controller synthesis using LPVToolsTM are expressed by the following commands::

```
rho1 = pgrid('rho1', linspace(40/3.6, 130/3.6, 10));
rho2 = pgrid('rho2', linspace(0, 1, 5));
and [Klpv, normlpv] = lpvsyn(H, nmeas, ncont).
```

9.3.3 Simulation results analysis in the frequency domain

The parameters of the yaw-roll model of a single unit heavy vehicle are detailed in Table 2.2. The H_∞/LPV active braking control design was proposed by using the parameter dependent weighting function W_{zay} . To evaluate the effectiveness of the active braking system on the prevention of vehicle rollover in the frequency domain, the two following cases will be considered as:

- **1st case:** the varying parameters $\rho_1 = v$ vary from 40 km/h to 130 km/h and $\rho_2 = 0.8$;
- **2nd case:** the varying parameters $\rho_2 = [0, 0.8, 1]$ vary and $\rho_1 = v = 80$ km/h.

9.3.3.1 1st case: the varying parameters $\rho_1 = v$ vary from 40 km/h to 130 km/h and $\rho_2 = 0.8$

Vehicle rollover often occurs when the forward velocity is higher than 60 km/h. Therefore, in this case, the author considers the varying parameter of the forward velocity $\rho_1 = v$ from 40

km/h to $130 km/h$, while the varying parameter ρ_2 is kept constant at 0.8 .

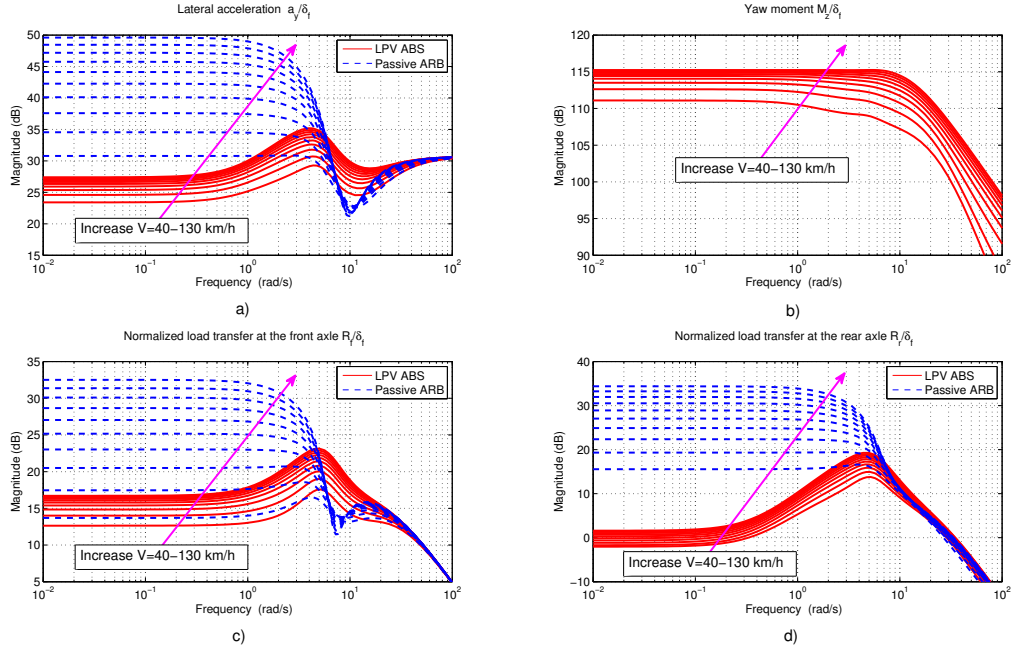


Figure 9.4: 1st case: transfer function magnitude of (a) the lateral acceleration $\frac{a_y}{\delta_f}$, (b) the yaw moment $\frac{M_z}{\delta_f}$, (c, d) the normalized load transfers $\frac{R_{f,r}}{\delta_f}$ at the two axles.

The objective of the H_∞/LPV active braking control design is to prevent vehicle rollover in an emergency situation with the considered frequency range to over $4 rad/s$ [Sampson and Cebon 2003b]. Figure 9.4 shows the transfer function magnitude of (a) the lateral acceleration, (b) the yaw moment, and (c, d) the normalized load transfers at the two axles. We can see that the H_∞/LPV active braking control system reduces significantly the lateral acceleration and the normalized load transfers in the specified frequency range. By penalizing the lateral acceleration, the lateral tyre forces are reduced, therefore the normalized load transfers are also reduced. Figures 9.4c, d also show that in the case of the H_∞/LPV active braking control system the normalized load transfers are maintained with a stability of around $15 dB$ for the front axle and $0 dB$ for the rear axle, even if the forward velocity changes in a wide range from $40 km/h$ to $130 km/h$. It indicates that the H_∞/LPV active braking control system can generate a roll stability that is quite in balance with the indicated forward velocities.

9.3.3.2 2nd case: the varying parameters $\rho_2 = [0, 0.8, 1]$ vary and $\rho_1 = v = 80 km/h$

In this case, the forward velocity is kept constant at $\rho_1 = v = 80 km/h$, while the varying parameter ρ_2 is surveyed at the three values: $\rho_2 = 0$, $\rho_2 = 0.8$, $\rho_2 = 1.0$. The reason to choose these values is the use of a "braking monitor" for the active braking system as expressed in

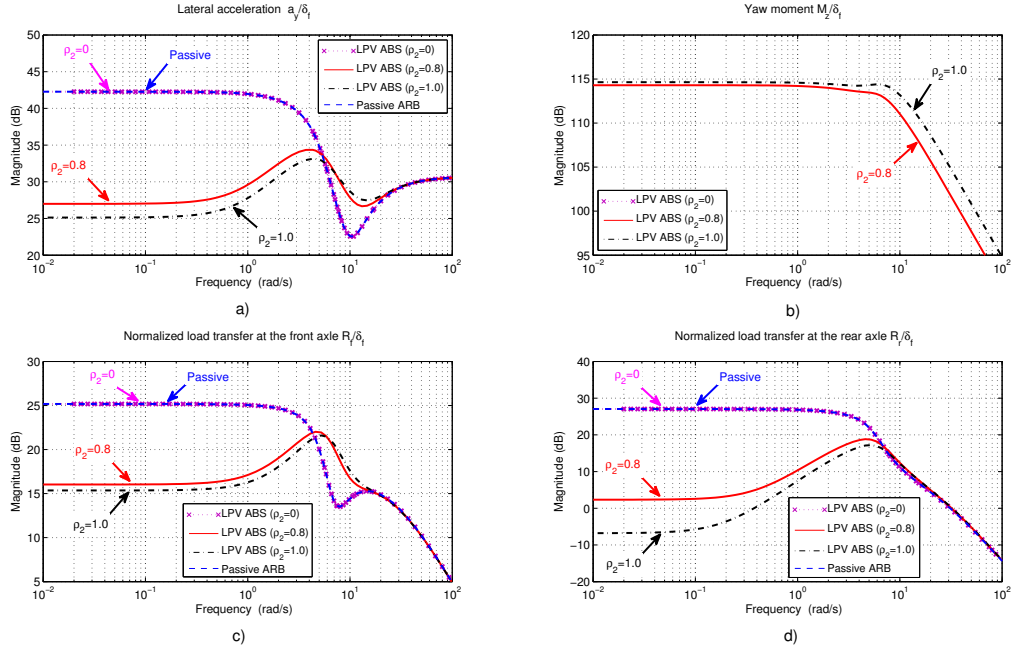


Figure 9.5: 2nd case: transfer function magnitude of (a) the lateral acceleration $\frac{a_y}{\delta_f}$, (b) the yaw moment $\frac{M_z}{\delta_f}$, (c, d) the normalized load transfers $\frac{R_{f,r}}{\delta_f}$ at the two axles.

equation (9.11). The active braking system will be activated when the maximum absolute value of the normalized load transfer at the rear axle $|R_r|$ equals 0.75. And then, the varying parameter ρ_2 increases as fast as possible to adapt to preventing vehicle rollover. When the normalized load transfer at the rear axle reaches 0.8, the varying parameter ρ_2 is $|R_r|$, the objective of this choice is to reduce the effect of the switching point. So the H_∞/LPV active braking control system will satisfy simultaneously the two objectives which are the prevention of vehicle rollover and increased stability at the smooth switching point.

Figure 9.5 shows the simulation results in the frequency domain of the lateral acceleration, the yaw moment, as well as the normalized load transfers at the two axles. They show clearly the effect of the varying parameter ρ_2 to prevent vehicle rollover in the frequency range to over 4 rad/s. When the varying parameter ρ_2 increases, the lateral acceleration and the normalized load transfers at the two axles decrease, which means that the active braking system can adapt to the rollover situation by increasing ρ_2 . The reduction of the transfer function magnitude of the lateral acceleration and the normalized load transfers when $\rho_2 = [0, 0.8, 1]$, compared to the passive anti-roll bar, is summarized as in Table 9.1. However, Figure 9.5b indicates that when the varying parameter ρ_2 increases, the transfer function magnitude of the yaw moment $\frac{M_z}{\delta_f}$ also increases.

The simulation results in the frequency domain have shown that the proposed H_∞/LPV active braking control system is able to prevent vehicle rollover in an emergency situation.

Table 9.1: Reduction of the magnitude of the transfer functions compared to the passive anti-roll bar system.

Transfer functions	$\rho_2 = 0$	$\rho_2 = 0.8$	$\rho_2 = 1$
$\frac{a_y}{\delta_f}$	0	16 dB	18 dB
$\frac{R_f}{\delta_f}$	0	9 dB	10 dB
$\frac{R_r}{\delta_f}$	0	25 dB	34 dB

9.4 Analysis in the time domain

The proposed H_∞/LPV active braking control design aims to prevent vehicle rollover; the varying parameter ρ_2 is changed according the absolute value of the normalized load transfer at the rear axle ($\rho_2 = f(|R_r|)$). However, due to the active braking system effects on reducing the vehicle performance characteristics, the concept of a "Braking monitor" is considered in this section.

9.4.1 Braking monitor

The braking monitor makes use of the varying parameter $\rho_2 = f(|R_r|)$. In the following, three H_∞/LPV active braking control designs are considered and explained. We would like to emphasize that the first and second control designs are the new contributions of this thesis, while the third control design is repeated here with the purpose to highlight the advantages of the second control design.

- **First control design** ($1^{st}H_\infty/LPVABS$): the varying parameter ρ_2 is chosen as $\rho_2 = |R_r|$. In this case the active braking system always operates even when the lateral acceleration is small. This case is unrealistic, because when the active braking system is in use, it will reduce the various vehicle performance characteristics, which are highlighted by the increased energy consumption, the reduced longevity of the engine, the increased wear of the tyres and the brake actuators. In order to satisfy simultaneously the vehicle performance and prevention of vehicle rollover in the emergency situation, the second case is proposed to fit better with the real world application.
- **Second control design** ($2^{nd}H_\infty/LPVABS$): vehicle rollover often occurs when the lateral acceleration reaches around 0.5 g [Palkovics, Semsey, and Gerum 1999]. So the active braking system should only be activated when the vehicle reaches the critical rollover situation to reduce the lateral acceleration. The objective of the braking monitor is to allow the active braking system to react when the normalized load transfer at the rear axle reaches the criteria of rollover ± 1 . The varying parameter ρ_2 is chosen as

follows:

$$\rho_2 = \begin{cases} 0 & \text{when } |R_r| \leq R_{Crit}^1 \\ |R_r| \frac{|R_r| - R_{Crit}^1}{R_{Crit}^2 - R_{Crit}^1} & \text{when } R_{Crit}^1 < |R_r| < R_{Crit}^2 \\ |R_r| & \text{when } |R_r| \geq R_{Crit}^2 \end{cases} \quad (9.11)$$

The values of R_{Crit}^1 and R_{Crit}^2 are chosen so that they respond to the emergency situation, satisfying the time delay of the braking system and limiting the influence of the switch point. Here, the author proposes $R_{Crit}^1 = 0.75$ and $R_{Crit}^2 = 0.8$.

- **Third control design ($3^{rd}H_\infty/LPVABS$):** In [Gaspar, Bokor, and Szaszi 2004], the authors proposed a combined control structure between the active anti-roll bar system and the active braking system, in order to prevent vehicle rollover. The main idea is that the active anti-roll bar system is used all the time to prevent the rollover. The active braking system is only activated when the vehicle comes close to the rollover situation; in a normal driving situation, the braking part of the control should not be activated. Therefore, the varying parameter ρ_2 was chosen as follows:

$$\rho_2 = \begin{cases} 0 & \text{when } |R_r| \leq R_1 \\ 2 \frac{|R_r| - R_1}{R_2 - R_1} & \text{when } R_1 < |R_r| < R_2 \\ 2 & \text{when } |R_r| \geq R_2 \end{cases} \quad (9.12)$$

where $R_1 = 0.85$ and $R_2 = 0.95$ [Gaspar, Bokor, and Szaszi 2004]. This idea has been proven to be good for the combination between the active anti-roll bar system and the active braking system.

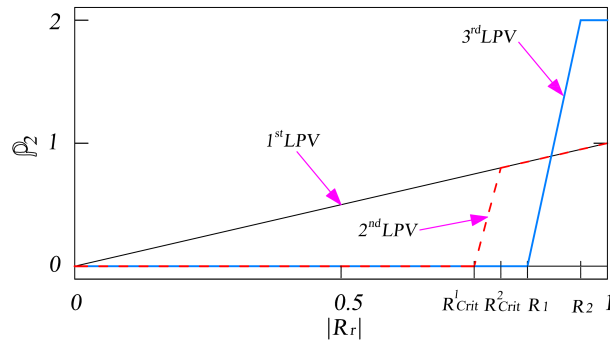


Figure 9.6: Varying parameter $\rho_2 = f(|R_r|)$.

Figure 9.6 shows the behavior of the varying parameter ρ_2 to better understand the differences between the three proposed control designs. In the next sections, the simulation results in the time domain will be used to evaluate these three control designs, and we would like to emphasize the effectiveness of the second control design.

9.4.2 Simulation results analysis in the time domain

In this section, we use the yaw-roll model of a single unit heavy vehicle shown in section 9.2. The effectiveness of the three H_∞/LPV active braking control designs is considered in terms of the three following criteria:

- Roll stability and vehicle rollover: roll angle of the sprung mass, lateral acceleration, normalized load transfers and the suspension roll angles at both axles,
- Value of the brake forces,
- Vehicle handling performance: phase plane $\beta - \dot{\beta}$, stability index λ .

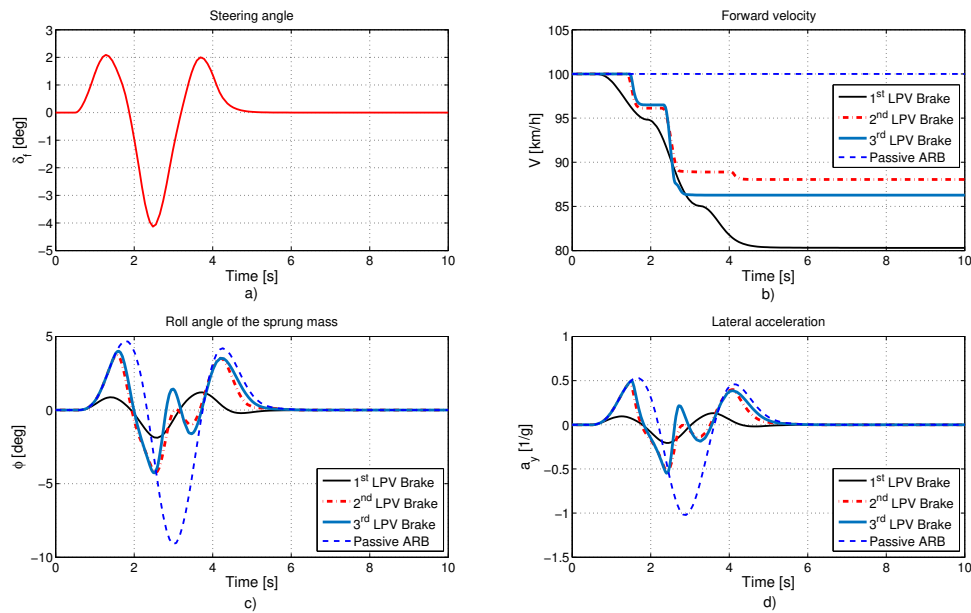


Figure 9.7: Time responses of (a) the steering angle δ_f , (b) forward velocity v , (c) roll angle of the sprung mass ϕ and (d) lateral acceleration a_y .

The simulation results in the frequency domain show that the H_∞/LPV active braking control design with the two varying parameters $\rho_1 = v$ and $\rho_2 = f(|R_r|)$ significantly reduces the normalized load transfer in the frequency range to over 4 rad/s . As mentioned in section 9.4.1, the first H_∞/LPV design operates continuously even when the vehicle is not in an emergency situation, which is not realistic for a real world application. The goal to design the second and third H_∞/LPV designs is that, once the vehicle enters into a dangerous situation, the active braking system is activated. In this section, the braking monitor with the varying parameter ρ_2 will be considered. The simulation results are compared between the three H_∞/LPV designs and the passive anti-roll bar. The double lane change manoeuvre to avoid an obstacle is used in this scenario, with the steering angle as shown in Figure 9.7a.

Figures 9.7 and 9.8 show the time response of the single unit heavy vehicle. The initial forward velocity is 100 km/h as in Figure 9.7b. In the case of the passive anti-roll bar, the forward velocity is kept constant at 100 km/h because there is no reason to reduce it. In the case of the first H_∞/LPV design, the forward velocity reduces continuously by 19 km/h from 0.5s to 6s. However, in the cases of the second and third H_∞/LPV designs, the forward velocity only decreases when the normalized load transfer at the rear axle reaches its limitation. The reductions are 12 km/h for the second H_∞/LPV and 14 km/h for the third H_∞/LPV designs.

Figure 9.8a shows the normalized load transfer at the front axle R_f . In the case of the second H_∞/LPV design, the normalized load transfer at the front axle reaches -1 at 2.5s but it is -1.07 for the third H_∞/LPV design. This means that with the second H_∞/LPV design the vehicle can avoid rollover. Figure 9.8b shows the normalized load transfer at the rear axle R_r . The normalized load transfer at the rear axle in the case of the second H_∞/LPV design is always less than that of the third H_∞/LPV design. Additionally, in the case of the passive anti-roll bar, the normalized load transfers at the two axles exceed the limitation of ± 1 . So the use of the passive anti-roll bar in this scenario is not enough to prevent vehicle rollover. The simulation results indicate that, due to the braking monitor, the active braking system can be activated when the vehicle comes close to the rollover situation. In the normal situation, the vehicle can manoeuvre as in the case of the passive anti-roll bar. Therefore, the lateral acceleration a_y in the case of the second H_∞/LPV design is kept to less than the limitation of 0.5g [Palkovics, Semsey, and Gerum 1999] as shown in Figure 9.7d. The maximum absolute value of the roll angle of sprung mass, lateral acceleration, suspension roll angles and normalized load transfers at both axles are listed in Table 9.2 for the three cases of the H_∞/LPV designs and the passive anti-roll bar. From Figures 9.7 and 9.8, we can see that **the second H_∞/LPV design behaves better than does the third H_∞/LPV design in term of avoiding vehicle rollover.**

Table 9.2: The maximum absolute value of the signals.

Signals	Passive anti-roll bar	1 st H_∞/LPV	2 nd H_∞/LPV	3 rd H_∞/LPV
$ \phi _{max}[deg]$	9.02	1.88	4.23	4.27
$ a_y _{max}[1/g]$	1.02	0.21	0.50	0.55
$ R_f _{max}$	1.54	0.57	1	1.07
$ R_r _{max}$	1.88	0.20	0.79	0.86
$ \phi - \phi_{uf} _{max}[deg]$	7.06	1.07	2.75	2.62
$ \phi - \phi_{ur} _{max}[deg]$	6.9	1.68	3.62	3.84

Figures 9.9a, b show the time response of the wheel braking forces at the rear axle. The braking forces in the case of the second H_∞/LPV design is 75% and 56%, compared to the third H_∞/LPV design.

The vehicle handling performance is analysed in Figure 9.9c, d by using the phase plane $\beta - \dot{\beta}$ and the stability index λ given in equation (4.6). We can see that the handling performance

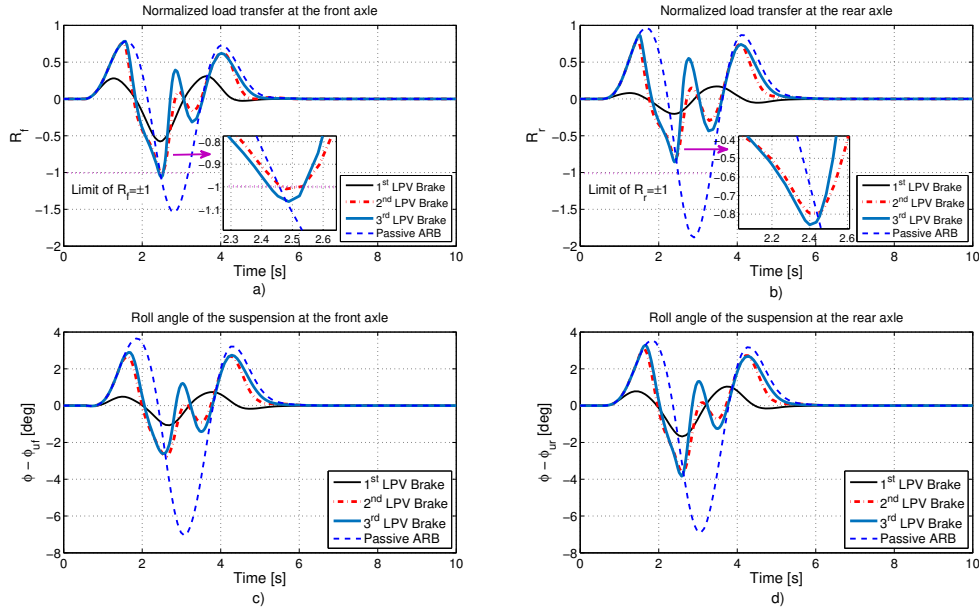


Figure 9.8: Time responses of the (a, b) normalized load transfers $R_{f,r}$ and (c, d) roll angle of the suspensions $\phi - \phi_{ur}$ at the two axes.

is not satisfied for the passive anti-roll bar and the third H_∞/LPV designs. However, for the second H_∞/LPV design, the trajectory of the phase plane $\beta - \dot{\beta}$ is in the stability region boundaries and the stability index λ is still inside the limitation of 1.

The simulation results in the time domain indicate that:

- The first H_∞/LPV active braking control design can provide improvements to roll stability, but it also reduces the vehicle performance. Therefore, it is not realistic for a real world application. So we will not use this approach in our further studies.
- The third H_∞/LPV active braking control design can adapt to the vehicle rollover in an emergency situation. The active braking system is only activated when the normalized load transfer at the rear axle reaches 0.85. Due to the fact that the time to rollover is usually very fast, to avoid vehicle rollover, the active braking control design provides huge braking forces but this will reduce the vehicle handling performance. Therefore, the proposition of this control design is only satisfactory in the case of the combined control structure between the active anti-roll bar system and the active braking system as proved in [Gaspar, Bokor, and Szaszi 2004]. It is not good enough for the combination between the active braking system and the passive suspension.
- The second H_∞/LPV active braking control design satisfies simultaneously the adaptation of vehicle rollover in an emergency situation, with low braking forces and improved handling performance of the vehicle. Therefore, in order to avoid vehicle rollover, this approach could be used in further studies on the active braking system.

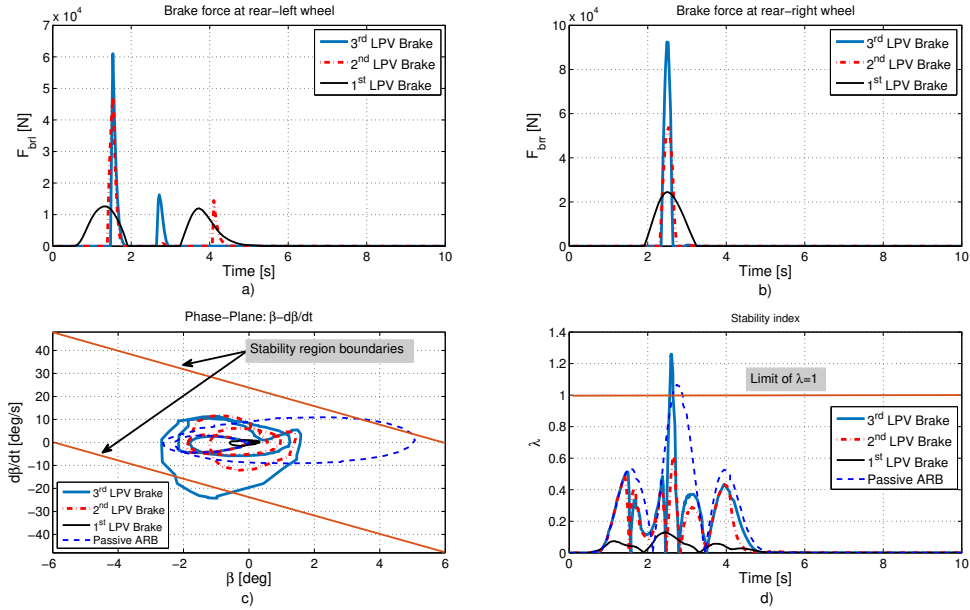


Figure 9.9: Time responses of the (a) brake force at the rear-left wheel $F_{br,l}$, (b) braking force at the rear-right wheel $F_{br,r}$, (c) phase - plane: $\beta - \dot{\beta}$ and (d) stability index λ .

9.5 Conclusion

This chapter proposed first preliminary results on the combination of the active braking system and the passive anti-roll bar system for a single unit heavy vehicle. The H_∞/LPV active braking controller is synthesized to adapt to vehicle rollover. The active braking system is only activated when the vehicle comes close to a dangerous situation. These initial results open the following research directions:

- In this study the vehicle model is quite simple: since we assume that the braking forces are equal at the front and rear wheels of each side, the control signal used here is the yaw moment M_z . Therefore, this approach should be explored in a full braking model.
- The time at which the active braking system starts to be activated is very important and it directly affects the quality of the system. This timing is closely linked to the "Time-To-Rollover (TTR)" concept [Chen and Peng 2001], [Yu, Guvenc, and Ozguner 2008]. If the active braking system can combine with the brake warning system, it would be a good solution for preventing vehicle rollover.
- The validation of the proposed H_∞/LPV active braking control design by using TruckSim[®] software would be an interesting area for the further studies.

General conclusions and Perspectives

10.1 General conclusions

This thesis has been dedicated to solving the problem of how to improve the roll stability of heavy vehicles. This is mainly achieved through the active anti-roll bar system, which is an interesting approach from both academic and industrial points of view. The results of this thesis has been presented in 4 parts and 10 chapters. In summary, the main contributions of the thesis are as follows:

In terms of modelling:

- A full model of the ESVH actuator is considered, where the input current is the control signal and the output signal is the actuator force (Chapter 2);
- The integrated model is proposed by combining the yaw-roll model of a single unit heavy vehicle with the ESVH actuators. Depending on the completeness of the model, one gets two forms: the fully integrated model and the control-oriented model (Chapter 2).

In terms of control methodologies:

- An active anti-roll bar controller was developed within the LQR approach, taking into account the normalized load transfer and input current limitations (Chapter 4);
- The conventional H_∞ control was designed for the active anti-roll bar system. The robustness analysis in the frequency domain using the μ -tool and a weighting function optimization procedure using genetic algorithms for the H_∞ control was also considered (Chapter 5);
- Multivariable H_∞/LPV controllers are synthesized by using the LPV ToolsTM toolbox. The varying weighting function approach is used to allow the active system to response as quickly as possible to the vehicle rollover behavior (Chapters 7, 8, 9).

In terms of application:

- The co-simulation between Matlab[®]/Simulink and TruckSim[®] software is developed. Here the two basic types of heavy vehicles considered are a truck and a bus that have been carefully scrutinized in various situations (Chapter 6);

- The validation of the H_∞ and H_∞/LPV control methods by using the TruckSim[®] software has proven the effectiveness of the active anti-roll bar system in improving roll stability of heavy vehicles (Chapters 6, 7);
- Using the LPVTools[™] toolbox for synthesizing controllers is extremely useful. In this thesis, the LPVTools[™] toolbox was first used for heavy vehicle dynamics (Chapters 3, 7, 8, 9).

In terms of preventing vehicle rollover:

- The active anti-roll bar system is used for the purpose of improving the vehicle roll stability. However, the H_∞/LPV controller using the varying weighting functions, it can create dynamic effects so that the active anti-roll bar system can respond to the rollover behavior when the vehicle reaches a critical situation (Chapter 7);
- The active braking system is also one effective solution to prevent vehicle rollover. It is activated when the vehicle comes close to a rollover situation (Chapter 9).

In terms of handling performance:

- In this thesis, the phase plane $\beta - \dot{\beta}$ and the stability index λ are used to evaluate the handling performance. The results have proven that the active anti-roll bar system can improve both roll stability and handling performance (Chapter 4);
- For the active braking system, the time when the system is activated will greatly affect the handling performance. In the active braking control design, the prevention of vehicle rollover and improved handling performance are required at the same time (Chapter 9).

In terms of the actuator's fault:

- This thesis has confirmed that the internal oil leakage inside the electronic servo-valve always exists, even when the ESVH actuator is completely new, and has a direct influence on the performance of the open-loop and closed-loop systems (Chapters 2, 8);
- The survey results have shown that, with the total flow pressure coefficient $K_P = [5 \times 10^{-15}, 4 \times 10^{-10}] \frac{m^5}{Ns}$, the two objectives of enhancing roll stability and the saturation of the actuators are simultaneously satisfied (Chapter 8).

Here, the author would like to emphasize that developing and perfecting the model for the active anti-roll bar system by combining the yaw-roll model and the ESVH actuators is an important step. It revived the direction studied by professors David Cebon and Peter Gaspar in the late 1990s and early 2000s.

10.2 Perspectives

During the thesis, many interesting points have been explored. Among others, according to the author, the following additional items also seem to be of great interest and in the future could be continued and developed further:

Short-term perspectives:

- **Vehicle model:** Enhancing the vehicle model with a higher nonlinear level (such as nonlinear suspension system, flexible frame model, etc.) to build robust controllers w.r.t. crucial nonlinearities that affect the control performance. It also would be necessary to consider the effect of the active anti-roll bar system on the vertical motion of the vehicle.
- **Actuator model:** There are many types of actuators that can be used for the active anti-roll bar system, but most of them have nonlinear characteristics (including the ESVH actuator used in this thesis). Therefore, the evaluation of the effectiveness of the control methods on the nonlinear actuator model will result in more accurate results.
- **TruckSim[®] software:** Although all the vehicle parameters can be easily determined from the vehicle configuration block in TruckSim[®] software (given in Chapter 6), simulation results show that it is necessary to perform the parametric identification problem. This is expected to be more accurate and fully adaptable to the yaw-roll model.
- **Fault tolerant control:** As mentioned in Chapter 8, the internal oil leakage is a permanent feature for every ESVH actuator, even if it is absolutely new. This leakage has a significant effect on the performance of the active anti-roll bar system, therefore the fault tolerant control solution should be investigated for this system [Choux 2011].

Long-term perspectives:

- **Active braking system:** For a driver, to have maximum control over a vehicle, it is very important, for the braking system, to be in correct working order. Anti-lock Braking Systems (ABS), Electronic Braking Systems (EBS) and Electronic Stability Programs (ESP) all help in preventing vehicle rollover, as they can automatically adjust the braking pattern for each wheel, possibly giving the driver greater control. The combined effects of ABS, EBS, ESP, yaw rate sensors and steering angle sensors could apply corrective action to assume greater control from the driver and reduce the risk of rollover.
- **Long combination vehicles:** The number of accidents associated with the long combination vehicles always accounts for the largest proportion of deaths. With the large loading capacity and bulky size, improving roll stability of this type of vehicle should be a priority. Nowadays, for long combination vehicles, companies such as Volvo often use the ESP system to prevent the rollover phenomenon. However, the active anti-roll bar system should also be considered as a promising solution.

- **Global chassis control:** The control systems for heavy vehicles are more and more developed, such as active braking systems, active steering systems, active suspension systems, active anti-roll bar systems, etc. However, they can not operate independently, and they always have a mutual impact and influence. Therefore, the concept of a "Global chassis control" should be studied in more detail.

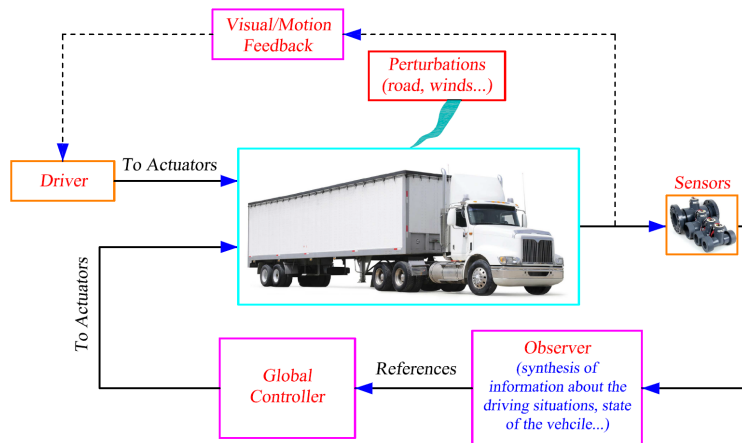


Figure 10.1: Global chassis control.

- **Real world application:** In this thesis, the active anti-roll bar system has proven to be effective in improving roll stability of heavy vehicles. Therefore, the survey and evaluation in real vehicle testing will be of great interest in the future.



(a)



(b)

Figure 10.2: Real example of the application of the active anti-roll bar system on heavy vehicles [Cambridge Vehicle Dynamics Consortium].

Matrices of the fully integrated model

The matrices A^f , B_1^f , and B_2^f in the state equation

From the equations (2.20), (2.31), the state equation for the fully integrated model can be written in the following form:

$$\dot{x} = E_f^{-1} A_0^f .x + E_f^{-1} B_{01}^f .w + E_f^{-1} B_{02}^f .u \quad (\text{A.1})$$

where the state vector:

$$x = [\beta \quad \dot{\psi} \quad \phi \quad \dot{\phi} \quad \phi_{uf} \quad \phi_{ur} \quad \Delta_{Pfl} \quad X_{vfl} \quad \Delta_{Pfr} \quad X_{vfr} \quad \Delta_{Prl} \quad X_{vrl} \quad \Delta_{Prr} \quad X_{vrr}]^T$$

the exogenous disturbance: $w = [\delta_f]^T$, the control inputs: $u = [u_{fl} \quad u_{fr} \quad u_{rl} \quad u_{rr}]^T$

The state equation for the fully integrated model in the *LTI* state-space representation (2.32) as:

$$\dot{x} = A^f .x + B_1^f .w + B_2^f .u \quad (\text{A.2})$$

From (A.1) and (A.2) the matrices $A^f = E_f^{-1} A_0^f$, $B_1^f = E_f^{-1} B_{01}^f$ and $B_2^f = E_f^{-1} B_{02}^f$. Some notations are used as:

$$Y_{\beta f} = -\mu .C_f, \quad Y_{\dot{\psi} f} = -\mu . \frac{l_f .C_f}{v}, \quad Y_{\beta r} = -\mu .C_r, \quad Y_{\dot{\psi} r} = \mu . \frac{l_r .C_r}{v}$$

$$Y_{\beta} = Y_{\beta f} + Y_{\beta r} = -\mu .(C_f + C_r), \quad Y_{\dot{\psi}} = Y_{\dot{\psi} f} + Y_{\dot{\psi} r} = \mu . \left(\frac{C_r .l_r - C_f .l_f}{v} \right), \quad Y_{\delta} = \mu .C_f$$

$$N_{\beta} = \mu .(l_r .C_r - l_f .C_f), \quad N_{\dot{\psi}} = -\mu . \left(\frac{l_f^2 .C_f + l_r^2 .C_r}{v} \right), \quad N_{\delta} = \mu .l_f .C_f$$

So, the matrices B_{01}^f , B_{02}^f , E and A_0^f are given as:

$$B_{01}^f = \begin{bmatrix} Y_{\delta} \\ N_{\delta} \\ 0 \\ rY_{\delta} \\ 0 \\ 0 \\ 0 \\ 0 \\ 0 \\ 0 \\ 0 \\ 0 \\ 0 \\ 0 \\ 0 \\ 0 \\ 0 \\ 0 \\ 0 \\ 0 \end{bmatrix} \quad B_{02}^f = \begin{bmatrix} 0 & 0 & 0 & 0 \\ 0 & 0 & 0 & 0 \\ 0 & 0 & 0 & 0 \\ 0 & 0 & 0 & 0 \\ 0 & 0 & 0 & 0 \\ 0 & 0 & 0 & 0 \\ 0 & 0 & 0 & 0 \\ 0 & 0 & 0 & 0 \\ \frac{K_v}{\tau} & 0 & 0 & 0 \\ 0 & 0 & 0 & 0 \\ 0 & \frac{K_v}{\tau} & 0 & 0 \\ 0 & 0 & 0 & 0 \\ 0 & 0 & 0 & 0 \\ 0 & 0 & \frac{K_v}{\tau} & 0 \\ 0 & 0 & 0 & 0 \\ 0 & 0 & 0 & 0 \\ 0 & 0 & 0 & \frac{K_v}{\tau} \end{bmatrix}$$

Characteristics of the ESVH actuators in the fully integrated model

The characteristics of interest of the ESVH actuators include:

- Forces: $F_{actfl}, F_{actfr}, F_{actrl}, F_{actrr}$
- Load flows: $Q_{Lfl}, Q_{Lfr}, Q_{Lrl}, Q_{Lrrr}$;
- Spool valve displacements: $X_{vfl}, X_{vfr}, X_{vrl}, X_{vrr}$;
- Input currents: $u_{fl}, u_{fr}, u_{rl}, u_{rr}$.

The LQR control method is used to evaluate the characteristics of the ESVH actuators in the fully integrated model, with the diagram of the closed-loop system shown in Figure B.1.

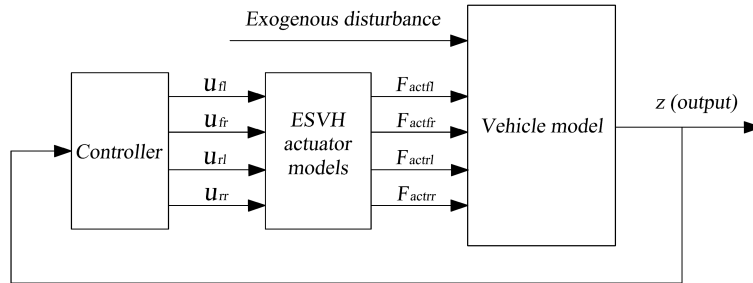


Figure B.1: Closed-loop system using a LQR active anti-roll bar controller.

Here, the performance index J of the LQR active anti-roll bar controller is selected as follows:

$$J = \int_0^{\infty} (\rho_1 \phi^2 + \rho_2 R_f^2 + \rho_3 R_r^2 + \rho_4 (\phi - \phi_{uf})^2 + \rho_5 (\phi - \phi_{ur})^2 + R_{ufl} u_{fl}^2 + R_{ufr} u_{fr}^2 + R_{url} u_{rl}^2 + R_{urr} u_{rr}^2) dt$$

where $\rho_1 = \rho_4 = \rho_5 = R_{ufl} = R_{ufr} = R_{url} = R_{urr} = 1, \rho_2 = \rho_3 = 100$.

Figure B.2 and Figure B.3 show the characteristics of the ESVH actuators at the two axles in the frequency domain. Figure B.4 and Figure B.5 are concerned with the time domain simulation for the fully integrated model using the LQR active anti-roll bar controller.

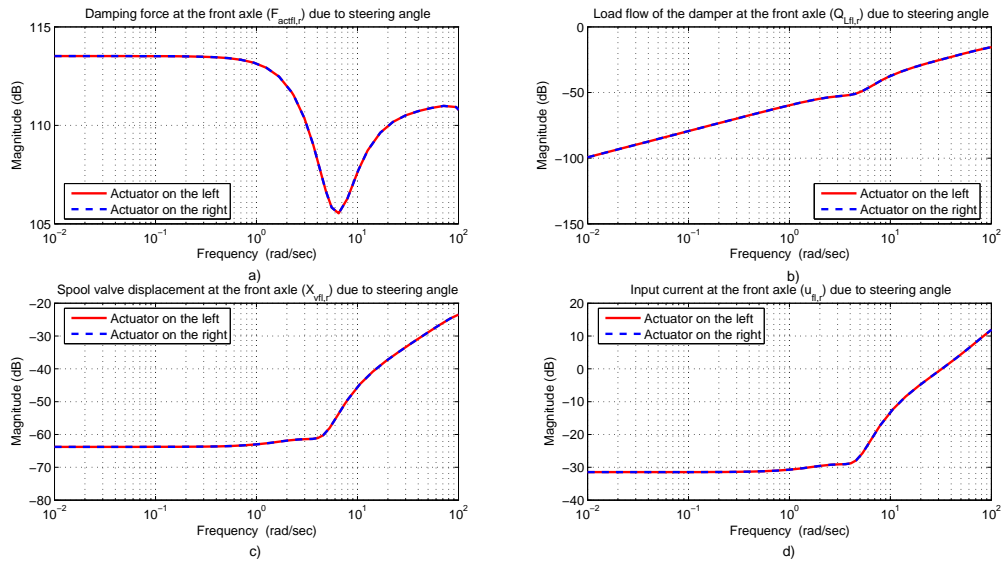


Figure B.2: Frequency responses of the characteristics of the ESVH actuators at the front axle.

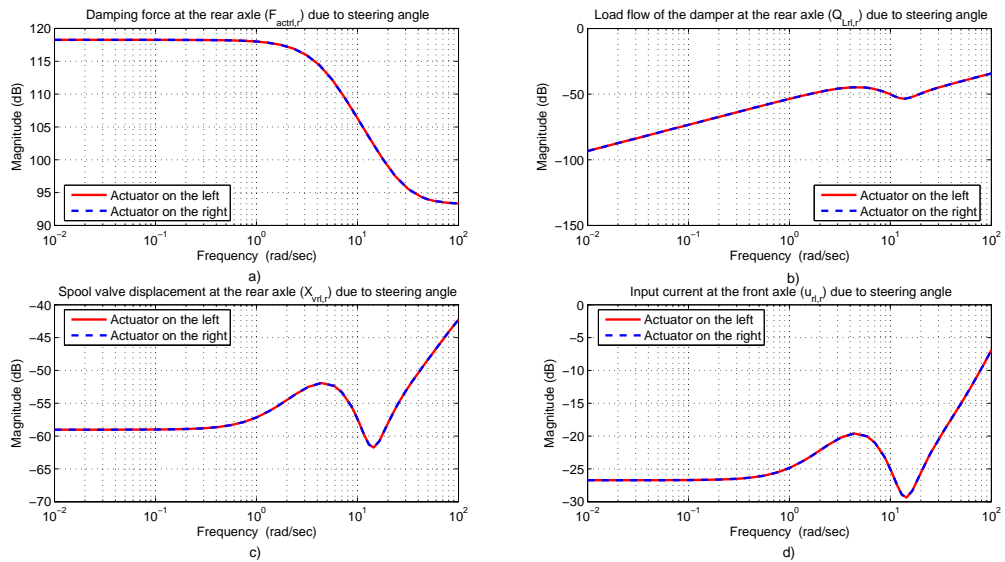


Figure B.3: Frequency responses of the characteristics of the ESVH actuators at the rear axle.

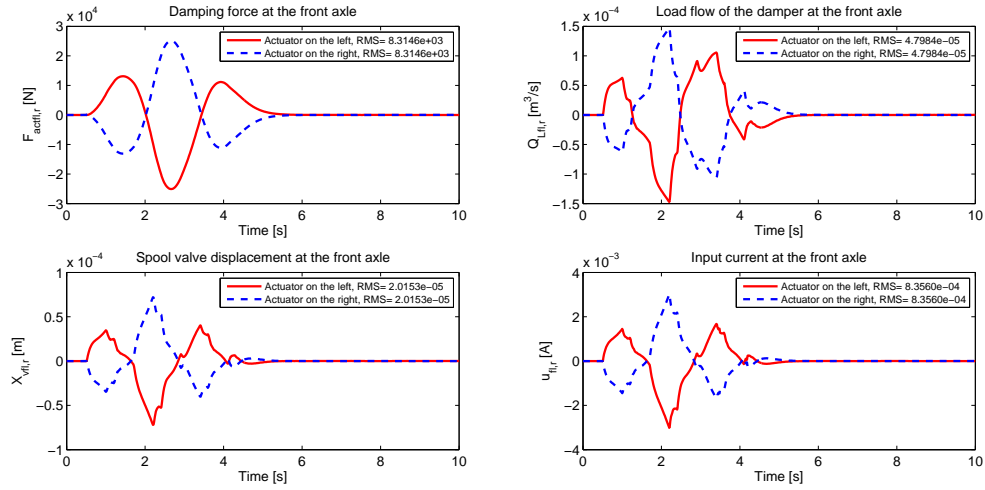


Figure B.4: Time responses of the characteristics of the ESVH actuators at the front axle.

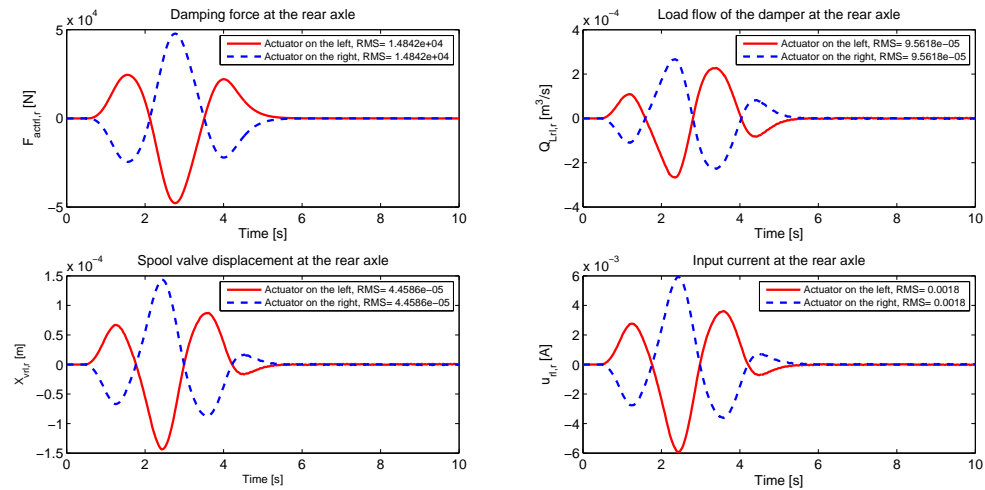


Figure B.5: Time responses of the characteristics of the ESVH actuators at the rear axle.

Matrices of the control-oriented integrated model

The matrices A^c , B_1^c , and B_2^c in the state equation

From the equations (2.20), (2.41), the state equation for the control-oriented integrated model can be written in the following form:

$$\dot{x} = E_c^{-1}A_0^c.x + E_c^{-1}B_{01}^c.w + E_c^{-1}B_{02}^c.u \quad (C.1)$$

where the state vector:

$$x = [\beta \quad \dot{\psi} \quad \phi \quad \dot{\phi} \quad \phi_{uf} \quad \phi_{ur} \quad \Delta_{Pf} \quad X_{vf} \quad \Delta_{Pr} \quad X_{vr}]^T$$

the exogenous disturbance: $w = [\delta_f]^T$, the control inputs: $u = [u_f \quad u_r]^T$

The state equation for the full integrated model in the *LTI* state-space representation (2.42) as:

$$\dot{x} = A^c.x + B_1^c.w + B_2^c.u \quad (C.2)$$

From (C.1) and (C.2) the matrices $A^c = E_c^{-1}A_0^c$, $B_1^c = E_c^{-1}B_{01}^c$ and $B_2^c = E_c^{-1}B_{02}^c$. Some notations are given in Appendix A, so the matrices E_c , A_0^c , B_{01}^c and B_{02}^c as:

$$E_c = \begin{bmatrix} m.v & 0 & 0 & -m_s.h & 0 & 0 & 0 & 0 & 0 & 0 & 0 \\ 0 & I_{zz} & 0 & -I_{xz} & 0 & 0 & 0 & 0 & 0 & 0 & 0 \\ -m_s.v.h & -I_{xz} & 0 & I_{xx} + m_s.h^2 & -b_f & -b_r & 0 & 0 & 0 & 0 & 0 \\ -m_{uf}.v.(r - h_{uf}) & 0 & 0 & 0 & b_f & 0 & 0 & 0 & 0 & 0 & 0 \\ -m_{ur}.v.(r - h_{ur}) & 0 & 0 & 0 & 0 & b_r & 0 & 0 & 0 & 0 & 0 \\ 0 & 0 & 1 & 0 & 0 & 0 & 0 & 0 & 0 & 0 & 0 \\ 0 & 0 & 0 & 0 & -A_{P^{lact}} & 0 & \frac{V_f}{4\beta_e} & 0 & 0 & 0 & 0 \\ 0 & 0 & 0 & 0 & 0 & 0 & 0 & 1 & 0 & 0 & 0 \\ 0 & 0 & 0 & 0 & 0 & -A_{P^{lact}} & 0 & 0 & \frac{V_r}{4\beta_e} & 0 & 0 \\ 0 & 0 & 0 & 0 & 0 & 0 & 0 & 0 & 0 & 0 & 1 \end{bmatrix};$$

Matrices \mathcal{Q} , \mathcal{R} of the performance index J

The performance index J in equation 3.18 is:

$$J = \int_0^{\infty} (x^T \mathcal{Q}x + u^T \mathcal{R}u) dt \quad (\text{D.1})$$

where \mathcal{Q} and \mathcal{R} are positive definite weighting matrices.

The performance index J for the LQR active anti-roll bar control of heavy vehicles is expressed as follows:

$$J = \int_0^{\infty} (\rho_1 \phi^2 + \rho_2 R_f^2 + \rho_3 R_r^2 + \rho_4 (\phi - \phi_{uf})^2 + \rho_5 (\phi - \phi_{ur})^2 + R_{uf} u_f^2 + R_{ur} u_r^2) dt \quad (\text{D.2})$$

where $\rho_1, \rho_2, \rho_3, \rho_4, \rho_5, R_{uf}$ and R_{ur} are the weighting parameters.

The matrix \mathcal{Q} is defined as:

$$\mathcal{Q} = \begin{bmatrix} 0 & 0 & 0 & 0 & 0 & 0 & 0 & 0 & 0 & 0 & 0 \\ 0 & 0 & 0 & 0 & 0 & 0 & 0 & 0 & 0 & 0 & 0 \\ 0 & 0 & \rho_1 + \rho_4 + \rho_5 & 0 & -\rho_4 & -\rho_5 & 0 & 0 & 0 & 0 & 0 \\ 0 & 0 & 0 & 0 & 0 & 0 & 0 & 0 & 0 & 0 & 0 \\ 0 & 0 & -\rho_4 & 0 & \rho_2 \left(\frac{2k_{uf}}{l_w m_f g}\right)^2 + \rho_4 & 0 & 0 & 0 & 0 & 0 & 0 \\ 0 & 0 & -\rho_5 & 0 & 0 & \rho_3 \left(\frac{2k_{ur}}{l_w m_r g}\right)^2 + \rho_5 & 0 & 0 & 0 & 0 & 0 \\ 0 & 0 & 0 & 0 & 0 & 0 & 0 & 0 & 0 & 0 & 0 \\ 0 & 0 & 0 & 0 & 0 & 0 & 0 & 0 & 0 & 0 & 0 \\ 0 & 0 & 0 & 0 & 0 & 0 & 0 & 0 & 0 & 0 & 0 \\ 0 & 0 & 0 & 0 & 0 & 0 & 0 & 0 & 0 & 0 & 0 \end{bmatrix}$$

The matrix \mathcal{R} is defined as:

$$\mathcal{R} = \begin{bmatrix} R_{uf} & 0 \\ 0 & R_{ur} \end{bmatrix}$$

However, in the Matlab the performance index J penalizes the state variables and the inputs, thus it has the standard form as:

$$J = \int_0^{\infty} (x^T \mathcal{Q}x + u^T \mathcal{R}u + 2x^T \mathcal{N}u) dt \quad (\text{D.3})$$

So in the real work by using Matlab, we have to choose the matrix \mathcal{N} as follows:

$$\mathcal{N} = \begin{bmatrix} 0 & 0 \\ 0 & 0 \\ 0 & 0 \\ 0 & 0 \\ 0 & 0 \\ 0 & 0 \\ 0 & 0 \\ 0 & 0 \\ 0 & 0 \\ 0 & 0 \end{bmatrix}$$

The command for the LQR control in Matlab as follows: $[K, S, e] = lqr(A, B, Q, R, N)$.

Bibliography

- Alfaro-Cid, E., E.W. McGookin, and D.J. Murray-Smith (2008). “Optimisation of the weighting functions of an H_∞ controller using genetic algorithms and structured genetic algorithms.” In: *International Journal of Systems Science* 39.4, pp. 335–347 (cit. on p. 103).
- Amin M. ; Hudha, Khisbullah; Abd Kadir Zulkiffli; Amer Noor Hafizah (2015). “Skyhook control for 7 DOF ride model of armored vehicle due to road disturbance.” In: *IEEE Asian Control Conference - 10th ASCC 2015*. Kota Kinabalu, Malaysia (cit. on p. 19).
- Apkarian, P. and R. J. Adams (1998). “Advanced gain-scheduling techniques for uncertain systems.” In: *IEEE Transactions on Control Systems Technology* 6.1, pp. 21–32 (cit. on pp. 50, 52).
- Apkarian, P. and P. Gahinet (1995). “A Convex Characterization of Gain-Scheduled H_∞ Controllers.” In: *IEEE Transactions on Automatic Control* 40.5, pp. 853–864 (cit. on pp. 50, 65).
- Aubouet, Sébastien (2010). “Modélisation et commande de suspensions semi-actives SOBEN.” PhD thesis. Institut National Polytechnique de Grenoble, France (cit. on pp. xv, 1).
- Babesse, S. and D. Ameddah (2014). “Enhanced Active Anti-roll Control of a Single Unit Heavy Vehicle Using Neuronal Network.” In: *2nd Intl’ Conference on Advances in Engineering Sciences and Applied Mathematics*. Istanbul, Turkey (cit. on p. 19).
- Balamili, S. Çağlar, İ. Emre Köse, and Günay Anlaş (2007). “Robust control of anti-lock brake system.” In: *Vehicle System Dynamics: International Journal of Vehicle Mechanics and Mobility* 45.3, pp. 217–232 (cit. on p. 189).
- Baogialai. <http://www.baogialai.com.vn/channel/1601/201306/thua-thien-hue-xe-o-to-dau-keo-do-deo-nhanh-lat-vang-50-met-2241264/> (cit. on p. 10).
- Becker, Gregory (1993). “Quadratic Stability and Performance of Linear Parameter Dependent Systems.” PhD thesis. University of California at Berkeley, USA (cit. on p. 65).
- Besselmann, T., J. Lofberg, and M. Morari (2012). “Explicit MPC for LPV Systems: Stability and Optimality.” In: *IEEE Transactions on Automatic Control* 57.9, pp. 2322–2332 (cit. on p. 52).
- Bharane, Pravin et al. (2014). “Design, Analysis and Optimization of Anti-Roll Bar.” In: *Journal of Engineering Research and Applications* 4.9, pp. 137–140 (cit. on p. 43).
- Boada, M.J.L. et al. (2007). “Active roll control using reinforcement learning for a single unit heavy vehicle.” In: *12th IFToMM World Congress*. Besancon, France (cit. on pp. 11, 21, 22, 28).
- Cambridge Vehicle Dynamics Consortium. http://www.arnaudmiege.co.uk/images/CVDC_experimental_vehicle.html (cit. on p. 206).
- Carcruising. <http://www.carcruising.com/watch-video-cement-truck-rollover-terrifying-angle/> (cit. on p. 10).
- Chen, Bo-Chiuan and Hwei Peng (2001). “Differential-Braking-Based Rollover Prevention for Sport Utility Vehicles with Human-in-the-loop Evaluations.” In: *Vehicle System Dynamics: International Journal of Vehicle Mechanics and Mobility* 36.4, pp. 359–389 (cit. on pp. 10, 202).

- Choux, Martin (2011). “Nonlinear, Adaptive and Fault-Tolerant Control for Electro Hydraulic Servo Systems.” PhD thesis. Technical University of Denmark, Denmark (cit. on pp. xxx, 163, 164, 205).
- Christopher, B. Winkler and D. Ervin Robert (1999). *Rollover of Heavy Commercial Vehicles*. UMTRI-99-19. Transportation Research Institute, The University of Michigan, US (cit. on p. 16).
- Christopher, B. Winkler et al. (2000). *Rollover of Heavy Commercial Vehicles*. SAE International (cit. on p. 18).
- Cole, David J. (2001). “Fundamental Issues in Suspension Design for Heavy Road Vehicles.” In: *Vehicle System Dynamics: International Journal of Vehicle Mechanics and Mobility* 35.4-5, pp. 319–360 (cit. on pp. 19, 21, 28).
- D’alfio, N., A. Morgando, and A. Sorniotti (2006). “Electro-hydraulic brake systems: design and test through hardware-in-the-loop simulation.” In: *Vehicle System Dynamics: International Journal of Vehicle Mechanics and Mobility* 44.0, pp. 378–392 (cit. on p. 189).
- Das, I. and J. E. Dennis (1997). “A closer look at drawbacks of minimizing weighted sums of objectives for Pareto set generation in multicriteria optimization problems.” In: *Structural and Multidisciplinary Optimization* 14.1, pp. 63–69 (cit. on p. 69).
- Davis, Lawrence (1991). *Handbook of genetic algorithms*. Van Nostrand Reinhold (cit. on p. 70).
- Do, Anh Lam (2011). “Approche LPV pour la commande robuste de la dynamique des véhicules : amélioration conjointe du confort et de la sécurité.” PhD thesis. Institut National Polytechnique de Grenoble, France (cit. on pp. xv, 1, 69, 103).
- Do, Lam Anh et al. (2011). “Multi-objective optimization by genetic algorithms in H_∞ /LPV control of semi-active suspension.” In: *IFAC World Congress - 18th IFAC WC 2011*. Italy (cit. on p. 103).
- Dorling, Richard (1996). “Integrated Control of Road Vehicle Dynamics.” PhD thesis. University of Cambridge, UK (cit. on p. 20).
- Doyle, John, Bruce Francis, and Allen Tannenbaum (1990). *Feedback Control Theory*. Macmillan (cit. on pp. 50, 54).
- Edwards, Nicholas (2011). *Vehicle Roll-over*. Society of Operations Engineers (cit. on p. 11).
- Ehrgott, Matthias (2005). *Multicriteria optimization. 2nd*. Springer (cit. on pp. 50, 69).
- Erylmaz, B. and B. Wilson (2000). “Combining leakage and orifice flows in a hydraulic servovalve model.” In: *Journal of Dynamic Systems Measurement Control* 122.3, pp. 576–579 (cit. on pp. 164, 165).
- Evgenikos, Petros et al. (2016). “Characteristics and Causes of Heavy Goods Vehicles and Buses Accidents in Europe.” In: *Transportation Research Procedia* 14, pp. 2158–2167 (cit. on pp. 9, 10).
- Fergani, Soheib (2014). “Robust Multivariable Control for vehicle dynamics.” PhD thesis. Institut National Polytechnique de Grenoble, France (cit. on p. 148).
- Fergani, Soheib et al. (2016). “LPV/ H_∞ suspension robust control adaptation of the dynamical lateral load transfers based on a differential algebraic estimation approach.” In: *IFAC Symposium on Advances in Automotive Control - 8th AAC 2016*. Sweden (cit. on p. 91).

- Fossum, Timothy V. and Gilbert N. Lewis (1981). “A Mathematical Model for Trailer–Truck Jackknifing.” In: *Society for Industrial and Applied Mathematics* 23.1, pp. 95–99 (cit. on p. 12).
- Gabriel, Leen and Heffernan Donal (2002). “Expanding Automotive Electronic Systems.” In: *Computer* 35.1, pp. 88–93 (cit. on p. 189).
- Gaspar, Peter, Jozsef Bokor, and Istvan Szaszi (2004). “The Design of a Combined Control Structure to Prevent the Rollover of Heavy Vehicles.” In: *European Journal of Control* 10.2, pp. 148–162 (cit. on pp. xv, 1, 20–22, 24, 25, 28, 34, 42, 45, 64, 66, 75, 81, 83, 86, 96, 98, 99, 101, 109, 118, 131, 148, 150–152, 171, 190–193, 198, 201).
- (2005). “Reconfigurable control structure to prevent the rollover of heavy vehicles.” In: *Control Engineering Practice* 13.6, pp. 699–711 (cit. on pp. 20, 22, 28, 35, 87, 96, 148, 191).
- Gaspar, Peter, Zoltan Szabo, and Jozsef Bokor (2005a). “Prediction based combined control to prevent the rollover of heavy vehicles.” In: *Proceedings of the 13th Mediterranean Conference on Control and Automation*. Limassol, Cyprus (cit. on pp. 64, 170, 175).
- (2005b). “The Design of an Integrated Control System in Heavy Vehicles Based on an LPV Method.” In: *Proceedings of the 44th IEEE Conference on Decision and Control, and the European Control Conference*. Seville, Spain (cit. on pp. xv, 1, 64, 157).
- Goldberg, David E. (1989). *Genetic Algorithms in Search, Optimization and Machine Learning*. 1st. Addison-Wesley Longman (cit. on p. 70).
- Has, Zulfatman et al. (2014). “Robust Position Tracking Control of an Electro-Hydraulic Actuator in the Presence of Friction and Internal Leakage.” In: *Arabian Journal for Science and Engineering* 39.4, pp. 2965–2978 (cit. on pp. 29, 164).
- Hecker, Simon (2014). “Generating structured LPV-models with maximized validity region.” In: *IFAC World Congress - 19th IFAC WC 2014*. Cape Town, South Africa (cit. on p. 67).
- Henk, Smakman (2000). “Functional integration of slip control with active suspension for improved lateral vehicle dynamics.” PhD thesis. Delft University of Technology, The Netherlands (cit. on p. 91).
- Hjartarson, Arnar, Peter Seiler, and Gary J. Balas (2013). “LPV aeroservoelastic control using the LPVTools toolbox.” In: *AIAA Atmospheric Flight Mechanics*. United States (cit. on pp. 50, 65, 68).
- Hjartarson, Arnar, Peter Seiler, and Andrew Packard (2015). “LPVTools: A Toolbox for Modeling, Analysis, and Synthesis of Parameter Varying Control Systems.” In: *First IFAC Workshop on Linear Parameter Varying Systems*. France (cit. on pp. 65, 66, 68, 152).
- Hoffmann, Christian and Herbert Werner (2014). “Complexity of Implementation and Synthesis in Linear Parameter-Varying Control.” In: *IFAC World Congress - 19th IFAC WC 2014*. Cape Town, South Africa (cit. on pp. 65, 152).
- Holland, John H. (1975). *Adaptation in natural and artificial systems: an introductory analysis with applications to biology, control, and artificial intelligence*. Ann Arbor: University of Michigan Press (cit. on pp. 50, 70).
- Hsun-Hsuan, Huang, K.Yedavalli Rama, and A. Guenther Dennis (2012). “Active roll control for rollover prevention of heavy articulated vehicles with multiple-rollover-index minimisation.” In: *Vehicle System Dynamics: International Journal of Vehicle Mechanics and Mobility* 50.3, pp. 471–493 (cit. on pp. 20, 42, 131, 150, 175).

- Hu, Jiankun, Christian Bohn, and H.R. Wu (2000). "Systematic H_∞ weighting function selection and its application to the real-time control of a vertical take-off aircraft." In: *Control Engineering Practice* 8, pp. 241–252 (cit. on p. 102).
- Ieluzzi, Michele, Patrizio Turco, and Mauro Montiglio (2006). "Development of a heavy truck semi-active suspension control." In: *Control Engineering Practice* 14.3, pp. 305–312 (cit. on p. 19).
- Imine Hocine; Benallegue, Abdelaziz; Madani Tarek; Srairi Salim (2014). "Rollover Risk Prediction of Heavy Vehicle Using High-Order Sliding-Mode Observer: Experimental Results." In: *IEEE Transactions on Vehicular Technology* 63.6, pp. 2533–2543 (cit. on p. 19).
- Imine, H. and M. Djemaï (2016). "Switched control for reducing impact of vertical forces on road and heavy vehicle rollover avoidance." In: *IEEE Transactions on Vehicular Technology* 65.6, pp. 4044–4052 (cit. on p. 19).
- Imine, H., L. M. Fridman, and T. Madani (2012). "Steering Control for Rollover Avoidance of Heavy Vehicles." In: *IEEE Transactions on Vehicular Technology* 61.8, pp. 3499–3509 (cit. on p. 19).
- Jackknifing*. <http://part380.com/blog/category/dot-101/page/2/> (cit. on p. 12).
- Junjie, He (2005). "Integrated vehicle dynamics control using active steering, driveline and braking." PhD thesis. The University of Leeds, UK (cit. on p. 91).
- Junjie, He and D A Crolla (2006). "Coordination of active steering, driveline, and braking for integrated vehicle dynamics control." In: *Proceedings of the Institution of Mechanical Engineers Part D Journal of Automobile Engineering* 220.10, pp. 1401–1420 (cit. on p. 91).
- J.Y.Wong (2001). *Theory of ground vehicles*. 3rd ed. John Wiley & Sons (cit. on pp. 157, 183).
- Kahrobaeian, A. and Y. A. R. I. Mohamed (2013). "Direct Single-Loop μ -Synthesis Voltage Control for Suppression of Multiple Resonances in Microgrids with Power-Factor Correction Capacitors." In: *IEEE Transactions on Smart Grid* 4.2, pp. 1151–1161 (cit. on p. 112).
- Kalyoncu, Mete and Mustafa Haydim (2009). "Mathematical modelling and fuzzy logic based position control of an electrohydraulic servosystem with internal leakage." In: *Mechatronics* 19.6, pp. 847–858 (cit. on pp. 29, 164, 166, 167).
- Knipling, P.R. (2007). *The domain of truck and bus safety research*. Transportation Research Circular, No. E-C117. Transportation Research Board, National Research Council, Washington DC, US (cit. on p. 9).
- Kovari, Attila (2009). "Influence of cylinder leakage on dynamic behavior of electrohydraulic servo system." In: *IEEE - 7th International Symposium on Intelligent Systems and Informatics*. Subotica, Serbia (cit. on p. 164).
- Lam, Q.L., A.I. Bratcu, and D. Riu (2016). "Robustness Analysis of Primary Frequency H_∞ Control in Stand-alone Microgrids with Storage Units." In: *IFAC Workshop on Control of Transmission and Distribution Smart Grids - CTDSG 2016*. Prague, Czech Republic (cit. on p. 112).
- LCF-Truck*. <http://jingletruck.com/2006-ford-lcf-16ft-43932> (cit. on p. 136).
- Lee Shihao; Kasahara, Misawa; Mori Yasuchika (2013). "Roll Damping Control of a Heavy Vehicle under the Strong Crosswind." In: *IFAC Symposium on Advances in Automotive Control - 7th AAC 2013*. Tokyo, Japan (cit. on p. 19).
- Lin, Ching-Fang (1994a). *Advanced Control Systems Design*. Prentice Hall, USA (cit. on p. 77).

- Lin, R. C. (1994b). “An Investigation of Active Roll Control for Heavy Vehicle Suspensions.” PhD thesis. University of Cambridge, UK (cit. on p. 78).
- Lin, R. C, D Cebon, and D J Cole (1996). “Optimal roll control of a single-unit lorry.” In: *Proceedings of the Institution of Mechanical Engineers Part D Journal of Automobile Engineering* 210.14, pp. 45–55 (cit. on p. 78).
- M. Wonohadidjojo, Daniel, Ganesh Kothapalli, and Mohammed Y. Hassan (2013). “Position control of electro-hydraulic actuator system using fuzzy logic controller optimized by particle swarm optimization.” In: *International Journal of Automation and Computing* 10.3, pp. 181–193 (cit. on pp. 164–166).
- Marcos, Andres and Gary J. Balas (2004). “Development of Linear-Parameter-Varying Models for Aircraft.” In: *Journal of Guidance, Control, and Dynamics* 27.2, pp. 218–228 (cit. on pp. 65, 67).
- Marler, R.T. and J.S. Arora (2004). “Survey of multi-objective optimization methods for engineering.” In: *Structural and Multidisciplinary Optimization* 26, pp. 369–395 (cit. on pp. 69, 70).
- Mechanical Simulation Corporation*. <https://www.carsim.com/downloads/pdf> (cit. on p. 124).
- Merritt, H.E. (1967). *Hydraulic control systems*. John Wiley & Sons (cit. on pp. 30, 31, 169).
- Miège, A. and D. Cebon (2002). “Design and implementation of an active roll control system for heavy vehicles.” In: *6th International Symposium on Advanced Vehicle Control, AVEC 2002*. Hiroshima, Japan (cit. on pp. 10, 21, 28, 33, 38, 41).
- (2005a). “Active roll control of an experimental articulated vehicle.” In: *Proceedings of the Institution of Mechanical Engineers Part D Journal of Automobile Engineering* 219.6, pp. 791–806 (cit. on p. 20).
- (2005b). “Optimal roll control of an articulated vehicle: theory and model validation.” In: *Vehicle System Dynamics: International Journal of Vehicle Mechanics and Mobility* 43.12, pp. 867–884 (cit. on pp. 20, 21, 78, 131).
- Miège, Arnaud J.P. (2000). “Development of Active Anti-Roll Control for Heavy Vehicles.” PhD thesis. University of Cambridge, UK (cit. on pp. 21, 28, 32).
- Milic, Vladimir, Zeljko Situm, and Mario Essert (2010). “Robust H_∞ position control synthesis of an electro-hydraulic servo system.” In: *ISA Transactions* 49.4, pp. 535–542 (cit. on p. 163).
- Mohammadpour, J. and C. Scherer (2012). *Control of Linear Parameter Varying Systems with Applications*. Springer (cit. on p. 147).
- Morrison, G. and D. Cebon (2017). “Combined emergency braking and turning of articulated heavy vehicles.” In: *Vehicle System Dynamics: International Journal of Vehicle Mechanics and Mobility* 55.5, pp. 725–749 (cit. on p. 190).
- Nguyen, Manh Quan (2016). “LPV approaches for modelling and control of vehicle dynamics: application to a small car pilot plant with ER dampers.” PhD thesis. Institut National Polytechnique de Grenoble, France (cit. on pp. xv, 1, 148).
- NHTSA*. <https://crashstats.nhtsa.dot.gov/Api/Public/ViewPublication/812150> (cit. on p. 10).

- Nwesaty, Waleed (2015). “*LPV/H_∞ control design of on-board energy management systems for electric vehicles.*” PhD thesis. Institut National Polytechnique de Grenoble, France (cit. on pp. xv, 1, 103, 148).
- Odenthal, D., T. Bunte, and J. Ackermann (1999). “Nonlinear steering and braking control for vehicle rollover avoidance.” In: *European Control Conference*. Germany (cit. on p. 19).
- Packard, Andy (1994). “Gain scheduling via linear fractional transformations.” In: *Systems and Control Letters* 22.2, pp. 79–92 (cit. on p. 65).
- Palkovics, Laszlo, Akos Semsey, and Eduard Gerum (1999). “Roll-Over Prevention System for Commercial Vehicles - Additional Sensorless Function of the Electronic Brake System.” In: *Vehicle System Dynamics: International Journal of Vehicle Mechanics and Mobility* 32.4-5, pp. 285–297 (cit. on pp. 190, 197, 200).
- Poussot-Vassal, Charles (2008). “Commande Robuste LPV Multivariable de Châssis Automobile.” PhD thesis. Institut National Polytechnique de Grenoble, France (cit. on pp. xv, 1, 148).
- Rafa, A. Baldawi, A. Faraj Yahya, and E. J. Talabani Rawand (2009). “A Study on the Effects of Servo-valve Lap on the Performance of a Closed - Loop Electrohydraulic Position Control System.” In: *Al-Rafidain Engineering* 17.5, pp. 1–14 (cit. on pp. 24, 29, 33, 75, 81, 88, 118, 164, 183, 185).
- Rahmat, M. F. et al. (2011). “Modeling and controller design of an industrial hydraulic actuator system in the presence of friction and internal leakage.” In: *International Journal of the Physical Sciences* 6.14, pp. 3502–3517 (cit. on p. 164).
- Renn, Jyh-Chyang and Tsung-Han Wu (2007). “Modeling and control of a new 1/4T servo-hydraulic vehicle active suspension system.” In: *Journal of Marine Science and Technology* 15.3, pp. 265–272 (cit. on p. 29).
- Rugh, W. J. (1990). “Analytical Framework for Gain Scheduling.” In: *Proceedings of the American Control Conference*. California, United States (cit. on p. 52).
- Rydberg, Karl-Erik (2016). *Hydraulic Servo Systems: Dynamic Properties and Control*. Linköping: Linköping University Electronic Press (cit. on p. 31).
- SAE (1996). *Spring Design Manual*. 2nd ed. SAE International (cit. on p. 43).
- Sampson, D. and D. Cebon (1998). “An Investigation of Roll Control System Design for Articulated Heavy Vehicles.” In: *4th International symposium on Advanced Vehicle Control, AVEC1998*. Nagoya, Japan (cit. on pp. 20, 21, 78).
- (2003a). “Achievable roll stability of heavy road vehicles.” In: *Proceedings of the Institution of Mechanical Engineers, Part D: Journal of Automobile Engineering*. Vol. 217. United Kingdom, pp. 269–287 (cit. on pp. 21, 78, 131, 151, 155, 178, 193).
- Sampson, David and David Cebon (2003b). “Active Roll Control of Single Unit Heavy Road Vehicles.” In: *Vehicle System Dynamics: International Journal of Vehicle Mechanics and Mobility* 40.4, pp. 229–270 (cit. on pp. 45, 81, 131, 138, 184, 195).
- Sampson, David John Matthew (2000). “Active Roll Control of Articulated Heavy Vehicles.” PhD thesis. University of Cambridge, UK (cit. on pp. 13, 14, 16, 19–22, 24, 28, 45, 75, 87, 89, 99, 109, 118, 150).
- Savaresi, Sergio and Mara Tanelli (2010). *Active Braking Control Systems Design for Vehicles*. Springer (cit. on pp. 189, 190).

- Scherer, C., P. Gahinet, and M. Chilali (1997). “Multiobjective output-feedback control via LMI optimization.” In: *IEEE Transactions on Automatic Control* 42.7, pp. 896–911 (cit. on pp. 50, 61, 62, 65, 148).
- Schwartz, SH. and SA. Fleming (2007). *Motor Carrier Safety: A statistical approach will better identify commercial carriers that pose high crash risks than does the current federal approach*. USA Publication GAO-07-585. US Government Accountability Office, Washington DC, US (cit. on p. 9).
- Segel, L. and M. A. Dorgham (1987). *The mechanics of heavy-duty trucks and truck combinations*. International Association for Vehicle Design (cit. on p. 17).
- Sename, Olivier and Luc Dugard (2003). “Robust H_∞ control of quarter-car semi-active suspensions.” In: *European Control Conference (ECC)*. Cambridge, UK, pp. 3112–3117 (cit. on p. 112).
- Sename, Olivier, Peter Gaspar, and Jozsef Bokor (2013). *Robust Control and Linear Parameter Varying Approaches: Application to Vehicle Dynamics*. Springer (cit. on pp. 91, 147).
- Shamma, J. S. and M. Athans (1990). “Analysis of gain scheduled control for nonlinear plants.” In: *IEEE Transactions on Automatic Control* 35.8, pp. 898–907 (cit. on p. 52).
- Skogestad, Sigurd and Ian Postlethwaite (2001). *Multivariable Feedback Control. 2nd*. John Wiley & Sons (cit. on pp. 57, 59, 102).
- (2005). *Multivariable Feedback Control: Analysis and Design*. John Wiley & Sons (cit. on p. 112).
- Topac, M. Murat, H. Eren Enginar, and N. Sefa Kuralay (2011). “Reduction of stress concentration at the corner bends of the anti-roll bar by using parametric of optimisation.” In: *Mathematical and Computational Applications* 16.1, pp. 148–158 (cit. on pp. 42, 44).
- Tour-bus*. <https://www.grenoble-congres.com/fr/catalogue/activite/navette-grenoble-aeroport-geneve-gva-632985/> (cit. on p. 128).
- Vu, VanTan et al. (2016). “Active anti-roll bar control using electronic servo-valve hydraulic damper on single unit heavy vehicle.” In: *IFAC Symposium on Advances in Automotive Control - 8th AAC 2016*. Norrköping, Sweden (cit. on p. 35).
- Wang, Yi et al. (2016). “Model Order Reduction of Aeroservoelastic Model of Flexible Aircraft.” In: *57th Structures Structural Dynamics and Materials Conference*. California, United States (cit. on p. 65).
- Wu, Fen (1995). “Control of linear parameter varying systems.” PhD thesis. University of California at Berkeley, USA (cit. on pp. 50, 53, 64–66, 148, 164).
- (2001). “A generalized LPV system analysis and control synthesis framework.” In: *International Journal of Control* 74.7, pp. 745–759 (cit. on pp. 52, 64–66).
- Wu, Fen et al. (1996). “Induced L2-norm control for LPV systems with bounded parameter variation rates.” In: *International Journal of Robust and Nonlinear Control* 6.9-10, pp. 983–998 (cit. on pp. 64–66).
- Yu, H., L. Guvenc, and U. Ozguner (2008). “Heavy duty vehicle rollover detection and active roll control.” In: *Vehicle System Dynamics: International Journal of Vehicle Mechanics and Mobility* 46.6, pp. 451–470 (cit. on pp. 10, 19, 21, 22, 28, 78, 131, 150, 202).
- Yu, Zhixin. et al. (2010). “Anti-Rollover Control Algorithm for Heavy Semi-Trailer Based on LQG.” In: *Proceedings of the 2010 IEEE International Conference on Information and Automation*. Harbin, China (cit. on p. 19).

- Zhou, Kemin, John C. Doyle, and Keith Glover (1996). *Robust and Optimal Control*. Prentice-Hall (cit. on pp. 54, 58, 59).
- Zulkarnain, Noraishikin et al. (2012). "Application of an Active Anti-roll Bar System for Enhancing Vehicle Ride and Handling." In: *2012 IEEE Colloquium on Humanities, Science & Engineering Research*. Kota Kinabalu, Sabah, Malaysia (cit. on pp. 19, 47).

Résumé — La stabilité en roulis des véhicules est un problème de sécurité très critique, en particulier pour les poids lourds. Actuellement, la plupart des poids lourds sont équipés de systèmes de barres anti-roulis passifs. Malheureusement ceux-ci ne sont pas capables, en général, de surmonter les situations critiques. Cette thèse se concentre sur les systèmes de barres anti-roulis actifs, qui constituent l’approche la plus communément utilisée pour améliorer la stabilité en roulis des poids lourds.

Le travail de recherche de cette thèse est divisé en trois parties principales. Dans la première partie, un modèle intégré est développé, comprenant quatre actionneurs hydrauliques commandés par des servo-valves, associés à un modèle linéaire lacet-roulis de poids lourd. Dans la deuxième partie, le système anti-roulis actif est développé suivant deux méthodologies de contrôle dans le cadre LTI: LQR et H_∞ . Dans la troisième partie, une approche LPV, basée sur le maillage, est utilisée pour synthétiser le contrôleur H_∞/LPV de barre anti-roulis actif avec des fonctions de pondération dépendant de paramètres variants, à l’aide du progiciel LPVToolsTM.

Les résultats de simulation dans les domaines fréquentiel et temporel, ainsi que la validation avec le logiciel de simulation TruckSim[®], montrent que les systèmes de barres anti-roulis actifs sont une solution réaliste et efficace qui améliore considérablement la stabilité en roulis des poids lourds par rapport aux systèmes de barres anti-roulis passifs.

Mots clés : Dynamique des véhicules, Poids lourds, Système de barre anti-roulis actif, commande LQR, commande H_∞ , commande LPV, Stabilité en roulis.

Abstract — Vehicle rollover is a very serious problem for the safety of heavy vehicles. Most modern heavy vehicles are equipped with passive anti-roll bars, however they may be not sufficient to overcome critical situations. This thesis focuses on the active anti-roll bar system, which is the most common method used to improve roll stability of heavy vehicles.

The thesis research work is divided into three main parts. In the first part, an integrated model is proposed with four electronic servo-valve hydraulic actuators mounted in a linear yaw-roll model of a single unit heavy vehicle. In the second part, the active anti-roll bar system uses two control approaches in the LTI framework: LQR, H_∞ . In the third part, the grid-based LPV approach is used to synthesize the H_∞/LPV active anti-roll bar controller with parameter dependant weighting functions, by using LPVToolsTM.

The simulation results, in the frequency and time domains, as well as the validation by using the TruckSim[®] simulation software, show that the active anti-roll bar control is a realistic and efficient solution which drastically improves roll stability of a single unit heavy vehicle, compared to the passive anti-roll bar.

Keywords: Vehicle dynamics, Heavy vehicles, Active anti-roll bar system, LQR control, H_∞ control, LPV control, Roll stability, Rollover.